THE GEOCHEMISTRY OF A MEDIUM PRESSURE GRANULITE TERRAIN AT SOUTHERN EYRE PENINSULA, AUSTRALIA.

by

Graham M. Bradley

Thesis submitted for the degree of
Doctor of Philosophy, in the
Australian National University, Canberra.

December, 1972.

The data, arguments and conclusions presented in this thesis are my own except where acknowledgements are made.

Signed 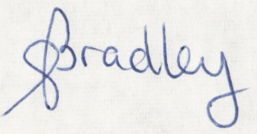

(G.M. Bradley)

ABSTRACT

Acid and basic rocks at southern Eyre Peninsula were subjected to temperatures of 800-950°C and pressures of 7-9 kb during granulite facies metamorphism. The metamorphism occurred at relatively deep crustal levels (20-26 km), and the geothermal gradients active were moderately high (35-45C°/km).

The metamorphosed acid gneisses consist of a sedimentary sequence with some granodioritic intrusive batholiths. The acid gneisses were intruded by continental tholeiite dykes prior to, and during, the granulite facies metamorphism. Charnockite batholiths were also intruded during the metamorphism. The metasediments consist of arkosic greywackes with minor intercalations of dolomite and graphitic impure dolomites. The metasediments represent continental and/or continental shelf sediments. The tectonic history of the sediments involved deep burial, deformation and metamorphism in the lower crust.

Many of the acid gneisses are depleted in K, Rb, Cs, Sr, Th, U and Li, and have high K/Rb ratios. Several gneisses are depleted in Ba and Pb, and some garnet-gneisses are enriched in Fe, Mg, Mn, Sc, V, Cr, Co, Ni, heavy REE and Y. Many of the metasedimentary gneisses have REE patterns fractionated relative to sedimentary abundances. The enrichment of K, Rb, Cs, Ba, Sr, Pb, Th, U, Li and light REE in the anatectic pegmatites is consistent with the depletion of these elements in the acid gneisses.

A proposed anatectic fractionation model predicts the observed depletion of K, Rb and Cs, and fractionation of REE. The model predicts enrichment of heavy REE in garnet-gneisses, and depletion of REE with generation of positive Eu anomalies in garnet-free quartzo-feldspathic gneisses. The presence of minor zircon and/or apatite suppresses REE fractionation in quartzo-feldspathic gneisses. The model predicts enrichment of Sr, and enrichment or depletion of Ba. The fractionation model explains many of the geochemical features of the acid gneisses, but cannot explain the depletion of Sr.

Dehydration fractionation of the basic rocks depleted K, Rb and Ba, and increased K/Rb ratios. Rehydration (retrogression) of the basic rocks commonly resulted in the reverse effect. The granulite facies metamorphism caused depletion and extensive redistribution of Cu in the basic rocks, minor depletion of average Si and Sr, limited redistribution of K, Rb, Ba, Ca, Na, U and Li. Ti, Al, Fe, Mn, Mg, P, Ga, Th, Pb, Zr, Nb, REE, Y, Sc, V, Co, Ni, Cr and Zn were apparently immobile during metamorphism of the basic rocks.

Pyroxene granulite "subfacies", hornblende granulite "subfacies" and amphibolite facies basic rocks are closely associated at Eyre Peninsula. The different facies and "subfacies" appear to have crystallised at similar total pressures and temperatures, but at different equilibrium water pressures and silica activities.

Granulite facies and amphibolite facies mineral assemblages can coexist over a very wide P-T field, and are usually closely associated in metamorphic terrains. This common association is not the result of retrogression at lower temperatures (although some of the amphibolite facies rocks may have crystallised at lower temperatures). There is no unique P-T field of granulite facies metamorphism, and amphibolite facies rocks are entirely eliminated only at the most extreme temperatures of metamorphism producing granulite facies rocks.

The metamorphic facies concept, applied in the descriptive mineralogical sense, has limited absolute pressure-temperature significance. Pressure and temperature may be determined from the mineralogical facies of a rock, only if chemical composition, and variables such as equilibrium water pressure, oxygen fugacity and silica activity are taken into account.

CONTENTS

Page

Page

LIST OF TABLES

APPENDIX TABLES

LIST OF FIGURES

CHAPTER 1

INTRODUCTION

1.1 THESIS OBJECTIVES

Heat-flow data for continental crust comprised of Archaean rocks indicate upward concentration of radioactive elements (Hyndman, et al., 1968). The heat-flow data stimulated interest in crustal fractionation and the processes active during deep-seated metamorphism, especially in medium- to high-pressure granulites. Heier and co-workers (1965-1971), Sheraton (1970) and Sighinolfi (1969-1971) postulated depletion of deep continental crust in Si, K, Rb, Pb, Th, U, Cs and Li, and enrichment in Fe, Mg, Mn, Ca, Ba, Sr, Zr, Nb and Y. The fractionation was attributed to removal of fluids and anatectic melts produced during the high grade metamorphism. This thesis is concerned with dehydration and anatectic aspects of the crustal fractionation hypothesis. This involves use of a computed fractionation model and examination of the chemical composition of a granulite metamorphic terrain. The southern Eyre Peninsula granulite terrain was selected for study because previous petrological work (Tilley, 1921a) indicated metamorphism within the medium-pressure granulite field of Green & Ringwood (1967a). Thus, the terrain is suitable for study of the postulated effects of crustal fractionation.

The current usage of the metamorphic facies concept is unsatisfactory and confused. Metamorphic facies are used to designate specific P-T fields of metamorphism, and to describe specific sets of mineral assemblages in rocks of different compositions repeatedly associated in space and time. Petrographic assignment of rocks to metamorphic facies solely on a mineralogical basis may result in facies with very little pressure-temperature significance because critical factors such as Fe/Mg, silica activity, fluid composition and oxygen fugacity cannot be taken into account.

This thesis makes a critical evaluation of the current concept of metamorphic facies with specific reference to the amphibolite and granulite facies, and the status of "retrogressive" metamorphism, an almost universal feature of granulite facies metamorphism.

The term "granulite" will be used in this thesis to denote rocks formed at extreme temperatures of regional metamorphism (but at pressures below the eclogite stability field), and characterised by anhydrous mineral assemblages or hydrous assemblages in which amphiboles and/or biotite-phlogopite micas have partly decomposed to yield anhydrous products containing orthopyroxene. Granulites in which amphibole and/or mica remained stable will be termed "hornblende granulites", and those in which all hydrous minerals decomposed will be termed "pyroxene granulites". The presence of orthopyroxene in basic rocks will be assumed diagnostic of granulites. (The usage of "granulite" in the textural sense, to describe metamorphic rocks with sub-equigranular polyhedral mineral grains is now less common and highly confusing: White, 1971).

1.2 FIELD GEOLOGY

The region studied is at the southern tip of Eyre Peninsula, South Australia (figure 1.1). The metamorphic age of the Precambrian basement rocks is 1780 ± 120 million years (Compston & Arriens, 1968). Previous studies (Tilley 1921, a,b&c; Glaessner & Parkin, 1957; and Johns, 1961) indicate that the metamorphic basement is divisible into two broad groups (figure 1.1). The first, the Flinders Group, is characterised by relatively uniform composition; and the second, the Hutchison Group, contains rocks of extremely varied compositions. The Flinders Group is dominantly composed of massive charnockites, augen gneisses and granitic gneisses. The group also contains basic granulites and amphibolites, metabasalt dykes and abundant pegmatites. The second, the Hutchison Group, contains banded garnet-gneisses, banded charnockites, graphitic calc-silicate gneisses, graphite-carbonate rocks, forsterite marbles, dolomites, basic granulites, amphibolites and

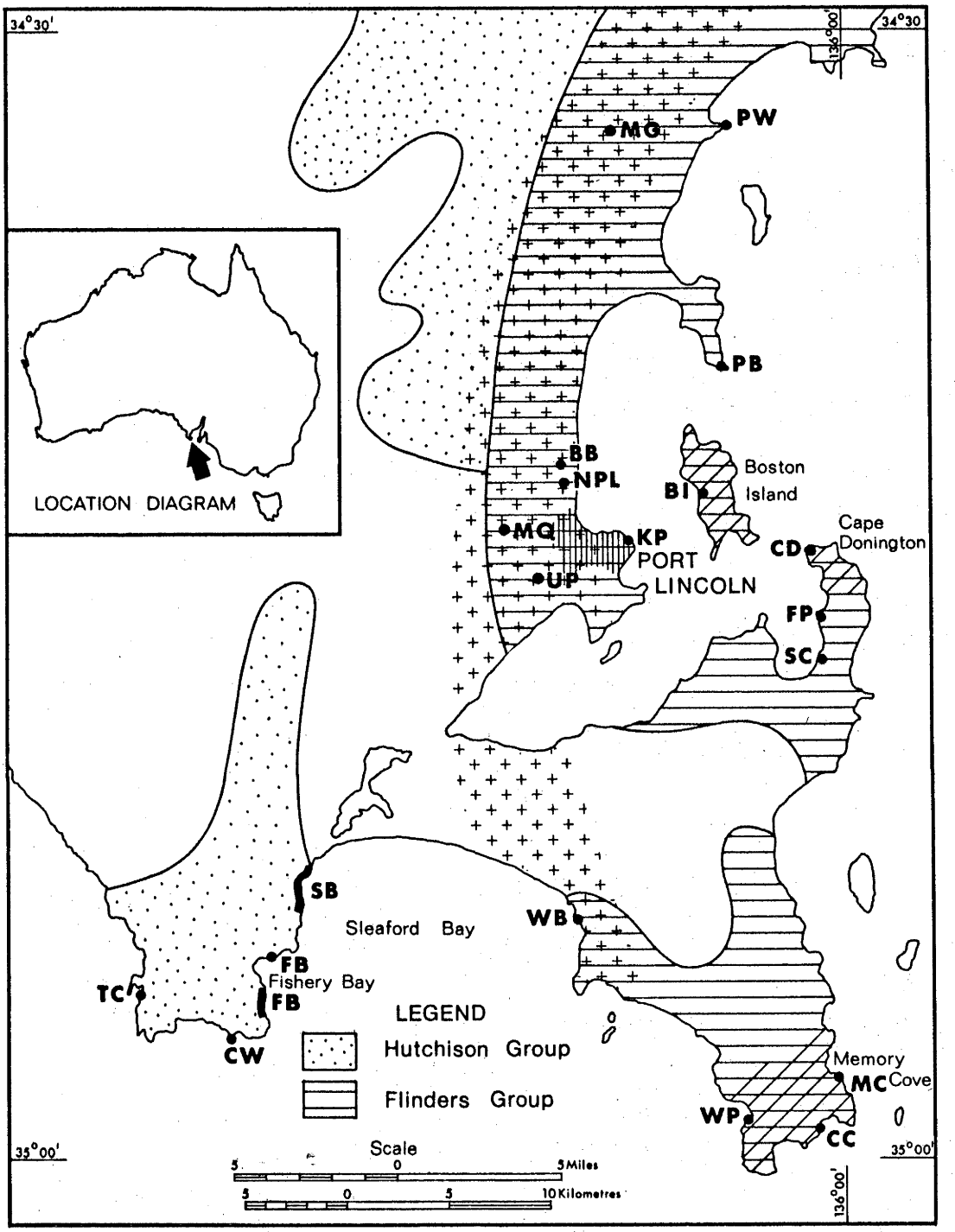

FIGURE 1.1 : LOCATION OF THE SOUTHERN EYRE PENINSULA METAMORPHIC TERRAIN.

The diagonal hatching marks areas of massive intrusive charnockite : the area marked with crosses contains only amphibolite facies rocks, whereas granulites and/or retrogressed granulites occur at all other locations sampled; SB, FB, etc., mark sample locations (appendix A); the regional geology is from Whitten & Risley (1968).

abundant pegmatites. The banded appearance and compositional variation of the Hutchison Group suggest a metasedimentary origin, whereas the massive uniform appearance of the Flinders Group suggests an igneous origin.

The charnockites are characterised by dark grey, bluish-grey or green colour and include both massive and banded varieties. In contrast, the granitic gneisses and garnet-gneisses are light-coloured. The granitic gneisses are white to light grey, and the garnet-gneisses are white to very pale bluish-grey with sporadically distributed pink to mauve garnets. The basic rocks include grey to greyish-black granulites, black amphibolites and greyish-black to black metabasalts. The pegmatites are distinguishable from surrounding acid gneisses by coarser grain size, lighter colour and absence of gneissosity. The pegmatites range from very coarse-grained K-feldspar-quartz pegmatites (feldspar crystals up to ½ metre across) through coarse-grained K-feldspar-quartz ± plagioclase pegmatites (figure 1.2) to medium-grained pegmatites commonly gradational into surrounding acid gneisses. (Detailed mineralogy and petrology of the rock types and individual samples are presented in appendix A.)

The coarse-grained feldspar pegmatites are unfoliated, and cut across the gneissic foliation, compositional banding and basic inclusions in adjacent rocks (e.g. figure 1.2). The medium-grained hornblende pegmatites are characterised by coarse euhedral to subhedral prismatic hornblende. The hornblende pegmatites are unfoliated or weakly foliated, and may be discordant or broadly concordant with the regional gneissosity. The hornblende pegmatites are commonly associated with and disrupt basic inclusions, intruding fractures and boudinaged "necks" in the basic rocks. The hornblende pegmatites grade imperceptibly into surrounding acid gneisses.

The contacts between metabasalts and host acid gneiss are sharply defined in all cases. The contacts between basic pyroxene granulites or amphibolites and acid gneisses range

Figure 1.2: Coarse K-feldspar + quartz ± plagioclase pegmatite (portion of 70-1212) transecting gneissosity in and islanding blocks of banded garnet-gneiss (69-944).

Figure 1.3: Sharply defined contact between boudinaged basic rock (retrogressed granulite: 69-791) and granitic gneiss (69-1170).

Figure 1.4: Gradational migmatitic contact between basic rock (amphibolite: 69-1178) and granite gneiss (69-1170). (Photo was taken about 5 metres from 1.3).

from sharply defined (figure 1.3) to gradational migmatitic contacts (figure 1.4). Migmatitic contacts are commonly characteristic of the more extensive "reaction zones" (chapter 5). Coarse-grained amphibolites, and rehydrated basic granulites are commonly associated with intrusion and disruption of the basic inclusions by pegmatites.

CHAPTER 2

BASIC ROCKS

2.1 FIELD APPEARANCE

The basic rocks occur as dykes, layers or boudins in the acid gneisses. The partly recrystallised metabasalts are commonly discordant with the foliation in the acid gneisses, and are relatively undeformed. The competely recrystallised basic rocks (granulites and amphibolites) are concordant with the acid gneiss foliation and are commonly deformed and boudinaged (e.g. figure 1.3). The granulites are characterised in the handspecimen by grey to greyish-black colour, in contrast to the black amphibolites. Many of the recrystallised basic rocks are disrupted by intrusion of pegmatites.

2.2 MINERALOGY

The completely recrystallised basic rocks are dominantly composed of plagioclase, orthopyroxene, clinopyroxene, hornblende, biotite and quartz (appendix A). Hornblende and biotite are absent in the pyroxene granulites. Orthopyroxene is absent and clinopyroxene may be absent in the amphibolites. The metabasalts contain relict igneous olivine and/or pyroxenes partly recrystallised to granulite metamorphic assemblages (appendix A). Primary igneous olivine, and delicate zoning and hourglass structures in primary igneous pyroxene are preserved within rims of recrystallisation products. The metabasalts were intruded during the granulite facies metamorphism, but later than the more deformed and recrystallised granulites and amphibolites. Several "pyroxenites" contain coarse pyroxene prisms with abundant exsolution lamellae. These pyroxenes may also be primary igneous pyroxenes.

The pyroxenes in the basic granulites and amphibolites are moderately Al-rich. The clinopyroxenes have low Na, and usually contain no jadeite-component. The hornblendes contain high Ti and low octahedral Al. The mineralogy of

the basic granulites and amphibolites is discussed in detail in chapter 7.

2.3 SAMPLING

Alteration and metamorphism of basalts may cause extreme redistribution of major elements (Vallance, 1965, 1967; Smith, 1968). Such studies were directed at obviously altered compositions, and included many originally glassy samples which were susceptible to alteration. Samples selected for trace element geochemical studies are generally free from obvious alteration veins and patches, and avoid most altered compositions. Selection criteria for high grade metabasalts are less obvious, although original alteration patches should be preserved in patchy metamorphic mineral distribution.

The basic rocks sampled in this study are uniform in composition and texture, and it is believed that major element redistribution was limited.

2.4 EFFECTS OF ALTERATION

Na, Ca, K, Si, Rb, Ba, Cs, Sr, Pb, Zn and Cu are mobile during alteration and metamorphism (Vallance, 1965, 1967; Smith, 1968; Hart, 1969; Cann, 1970; Hart & Nalwark, 1970; Hermann & Wedepohl, 1970; Haynes, 1972; Philpotts & Schnetzler, 1969). Haynes (1972) concluded that during alteration of continental tholeiites Na was increased significantly, Sr and Cu were decreased significantly, and Si, Ca, K, Ba, Rb, Zn and Pb were redistributed without significant enrichment or depletion. Hermann & Wedepohl (1970) noted increased Na and decreased Ca and Si in continental tholeiites. Sea-water alteration of basalts generally increases K, Rb and Cs, and occasionally decreases Ca and Sr (Hart, 1969; Philpotts & Schnetzler, 1969; Hart & Nalwark, 1970; Hart *et al.*, 1970; Cann, 1970; Matthews, 1971). In some cases K may be leached (Hart & Nalwark, 1970). Nagasawa & Schnetzler (1971) observed significant increases and decreases in Ba, and suggested that light REE (especially La and Ce) may

also be affected. No other major geochemical changes in sea-floor basalts were observed during alteration and metamorphism up to amphibolite facies.

Many elements behave as fixed components in all but the most extreme alteration. Haynes (1972) showed that Ti, Al, Ga, Fe, Mn, Mg, V, Ni, Zr, Nb, Hf, P, Th and Y are nearly unaffected by hot-spring alteration and low-grade (prehnite-pumpellyite) metamorphism of continental tholeiites. Cann (1970) and Pearce & Cann (1971) concluded that Ti, Zr, Nb and Y are unaffected by even severe secondary processes. The highly significant mutual correlations between these elements are preserved after alteration, but correlations between Ti, Zr, Nb, Y and mobile elements are greatly reduced or destroyed. Frey et al., (1968), Hermann & Wedepohl (1970) and Haynes (1972) established that REE are immobile. Identification of the original basalt type can only be achieved with confidence by comparison of immobile elements in the metamorphosed basalts and suites of basalts whose origin is known.

2.5 VARIATION OF BASALT CHEMISTRY WITH GEOLOGICAL AGE

The metabasalts at Eyre Peninsula are about 1,780 million years old (metamorphic age) and the completely recrystallised granulitic and amphibolitic basic rocks are probably older. It is possible that the compositions of such basalts could be significantly different from more recent magmas. Hart et al. (1970) and White et al., (1971) pointed out the close similarity between Archaean greenstones (about 3 billion years old) and modern island arc low-K tholeiites. They concluded that no significant changes in basalt geochemistry had occurred since the Archaean. Slight differences observed in the Archaean basalts compared with modern island arc tholeiites include lower Si, K, Ba and Sr (Hart et al., 1970; White et al., 1971; Jakeš & White, 1971) and higher Fe/Mg (Glikson, 1971; Jakeš & White, 1971). The differences are small and (excepting Fe/Mg) occur in elements mobile during alteration. Significant changes in basalt chemistry since the Archaean have not yet been demonstrated.

2.6 EYRE PENINSULA BASIC ROCKS

Major and trace element geochemistry and C.I.P.W. norms of the basalts and metamorphosed basic equivalents are summarised in appendix C.

2.6.1 Basalt Classification

All but three of the basic rocks plot within the tholeiite field in the silica-alkalis plot (figure 2.1). The three rocks plotting in the alkali basalt field (above the boundary line of Irvine & Baragar) include a basic xenolith (69-790) from a charnockite batholith, an amphibolite (69-794) and a strongly rehydrated pyroxenite (69-788). Evidence is presented in chapter 7 for addition of K during rehydration ("retrogression") of these rocks. All the rocks plotting near the boundaries of Irvine & Baragar (1971) and Macdonald & Katsura (1964) are amphibolites or partly rehydrated granulites, but evidence of addition of K, Rb and Ba during rehydration was obvious in only two (69-782 and 69-1352). All Eyre Peninsula basic rocks free of obvious alteration by reaction with pegmatitic fluids rich in alkalis plot within the tholeiitic basalt field of Irvine & Baragar (1971). Comparative geochemistry was therefore restricted to tholeiitic basalts.

2.6.2 Varieties of Eyre Peninsula Basalts

Two varieties of basaltic rocks or metamorphosed equivalents occur: (1) the common tholeiitic basalts; and (2) the much less abundant picritic tholeiites or "pyroxenites". The two types are separated by a compositional discontinuity of about 5% Al_2O_3, 500 ppm Cr and 70 ppm Ni. All other elements grade continuously from one type to the other. Basic rocks with K_2O up to 1% have low Rb (1-60 ppm) and Ba (20-250 ppm), whereas those with high K_2O (2.6-3.9%) have proportionally higher Rb (80-280 ppm) and Ba (400-760 ppm). The higher K, Rb and Ba of the latter group is considered due to alteration during metamorphism and samples with $K_2O > 1.5\%$ have been excluded from averages for the purpose of K, Rb and Ba. Loss-free

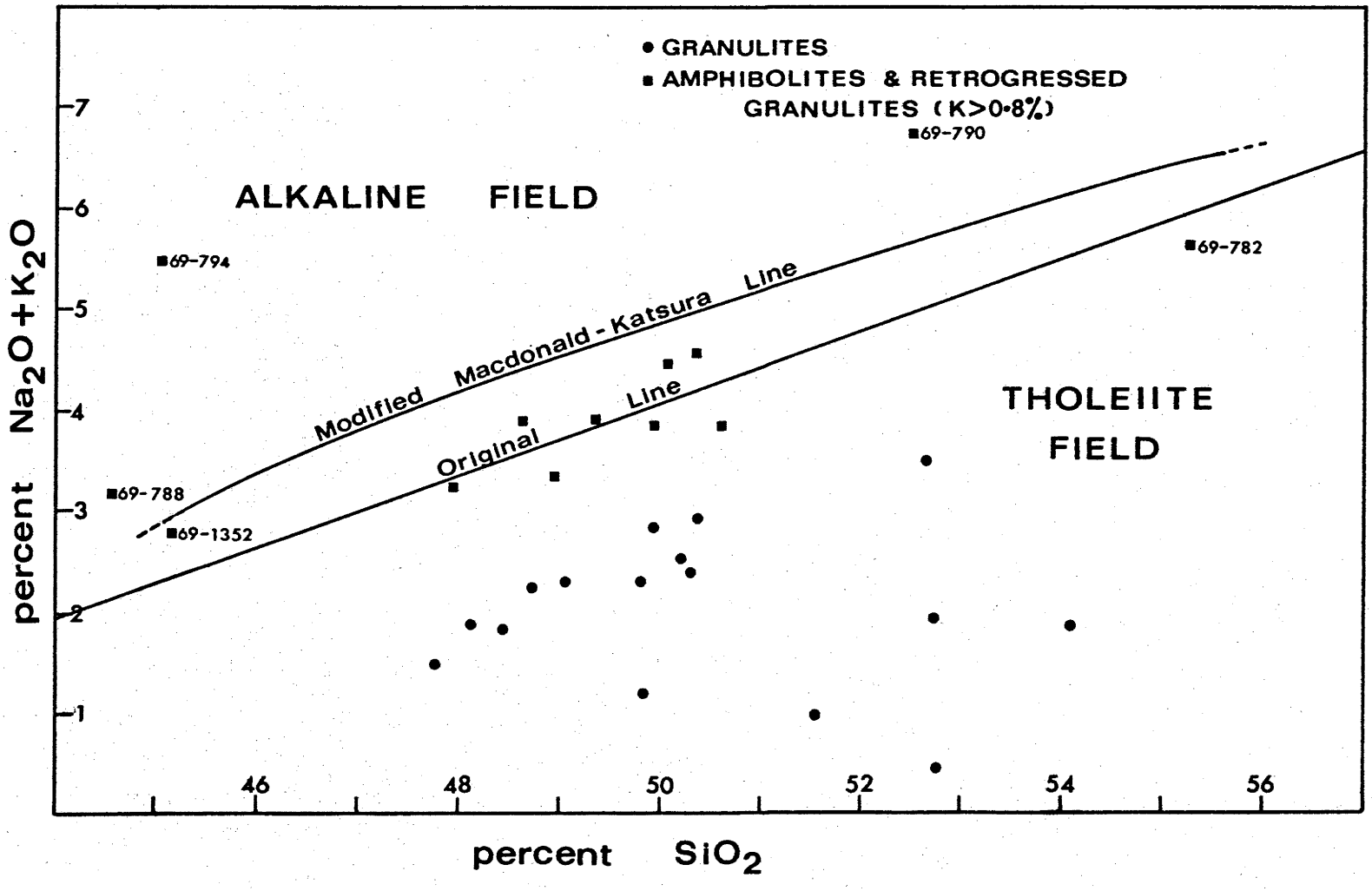

FIGURE 2.1 : MACDONALD-KATSURA SILICA-ALKALIS PLOT FOR THE BASIC ROCKS.

The modified Macdonald-Katsura line is from Irvine & Baragar (1971) and the original line is from Macdonald & Katsura (1964). Loss-free Eyre Peninsula data has been plotted.

averages of the tholeiites and picritic tholeiites are compared with average basalts from oceanic, island arc and continental environments in table 2.1.

The normative compositions of the basalts may have been significantly altered by oxidation or reduction during metamorphism, or by addition of K during reaction with pegmatites. The weight % Fe_2O_3/FeO of one of the least metamorphosed basalts (69-739) is 0.22. Norms were recalculated with the Fe_2O_3/FeO ratios arbitrarily adjusted to 0.2 ($\sim$0.22) to correct the worst effects of oxidation and reduction. Samples in which K had been increased were recalculated with adjusted K_2O values of 0.6% (the average K_2O of the basalts excluding high-K altered samples). C.I.P.W. norms of the basalts with corrected and uncorrected oxidation states and K_2O are presented in appendix C. Silica-saturated and silica-undersaturated basalts occur in approximately equal proportions. Note that some basalts are nepheline-normative: this is attributed to silica depletion and/or alkali enrichment during alteration. Some quartz-normative rocks may be due to silica enrichment during alteration.

2.6.3 Identification of Basalt Type

The initial basalt type may be identified by immobile element contents, especially Ti, Zr, Y, Nb and REE.

2.6.3.1 Rare Earth Elements (REE)

REE patterns are normalised to chondritic abundances, and Y in partial patterns is plotted at the Ho position (appendix D). The REE patterns (figures 2.2, 2.3 and 2.4) range from relatively weakly fractionated patterns (69-775 and 69-1351: chondrite normalised La/Yb 2.0 and 1.7 respectively), to patterns moderately enriched in light REE (69-1366 and 69-788: chondrite normalised La/Yb 11.4 and 11 respectively). Three rocks have moderately pronounced negative europium anomalies (69-1366, 69-756 and 69-782: chondrite-normalised Eu/Eu* 0.53, 0.68 and 0.76

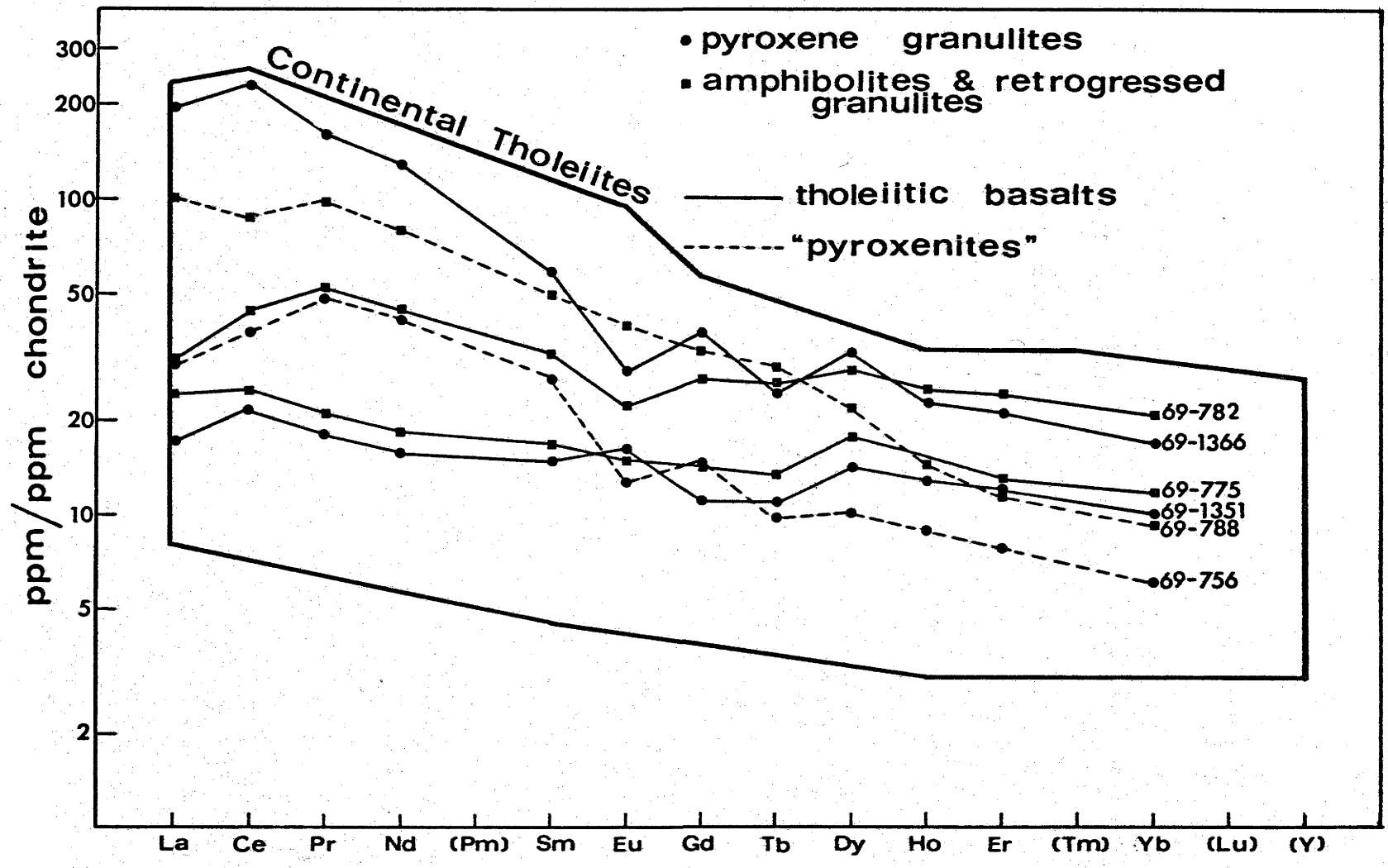

FIGURE 2.2 : COMPARISON OF THE CONTINENTAL THOLEIITE RARE EARTH ELEMENT FIELD AND RARE EARTH PATTERNS FOR SIX BASIC ROCKS.

The continental tholeiite field is the composite of dyke and lava fields in figure 2.5.

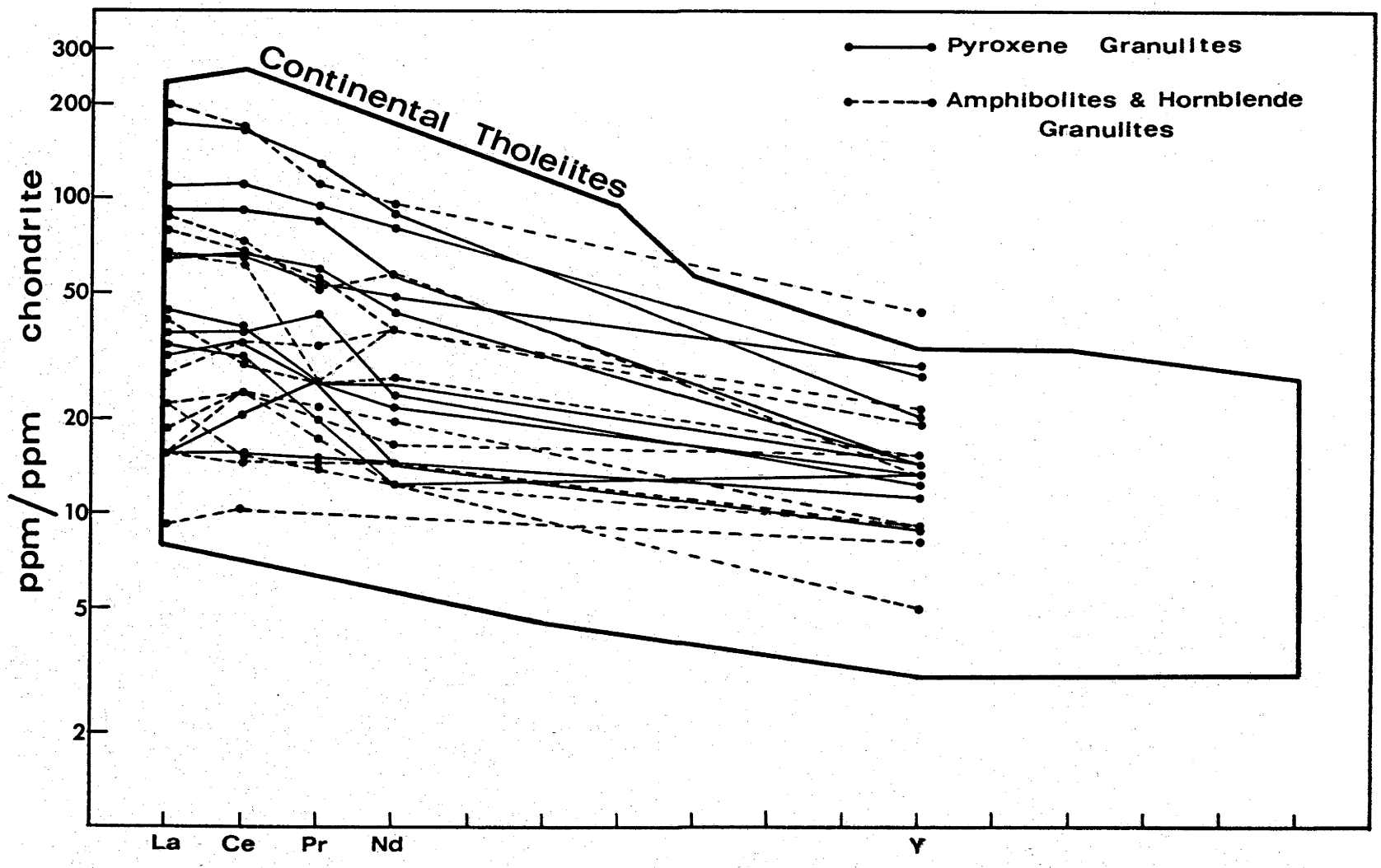

FIGURE 2.3 : COMPARISON OF THE CONTINENTAL THOLEIITE RARE EARTH ELEMENT FIELD AND PARTIAL RARE EARTH PATTERNS FOR THE THOLEIITIC BASALTS.

The continental tholeiite field is the composite of dyke and lava fields in figure 2.5.

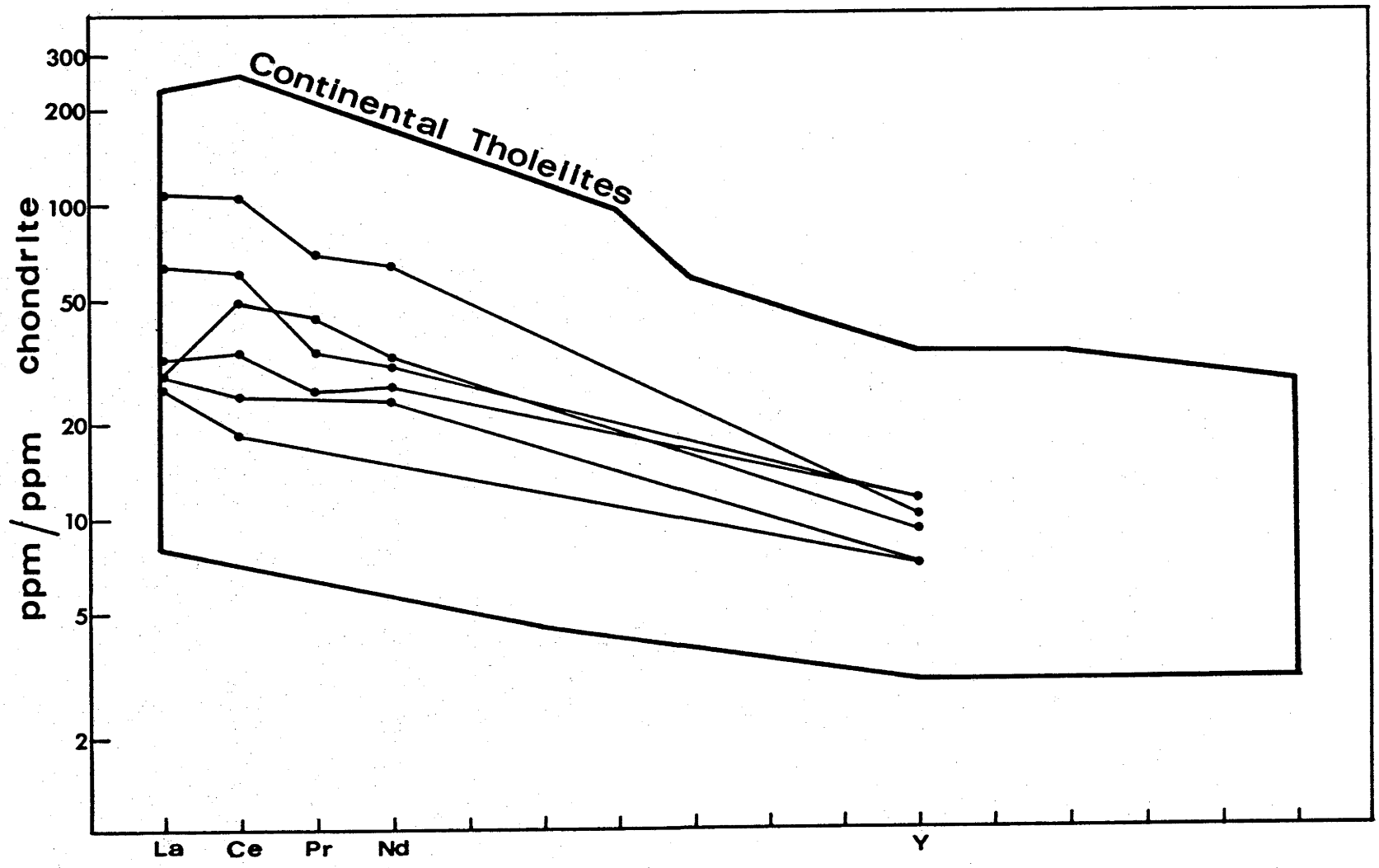

FIGURE 2.4 : COMPARISON OF THE CONTINENTAL THOLEIITE RARE EARTH ELEMENT FIELD AND PARTIAL RARE EARTH PATTERNS FOR THE "PYROXENITES" OR PICRITIC THOLEIITES.

The continental tholeiite field is the composite of dyke and lava fields in figure 2.5.

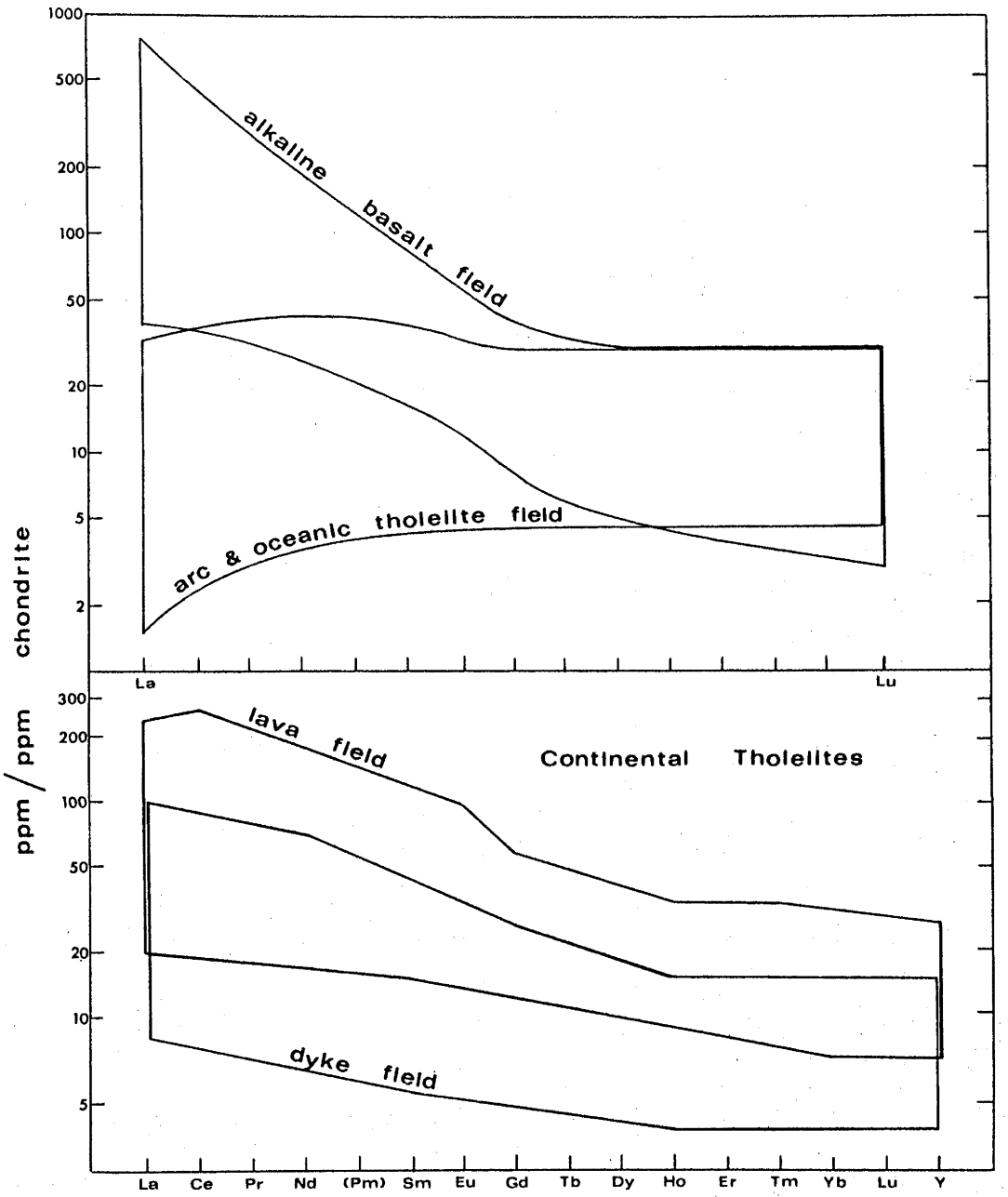

FIGURE 2.5 : COMPARISON OF THE RARE EARTH ELEMENT FIELDS FOR ALKALI BASALTS, ISLAND ARC & OCEANIC THOLEIITES, AND CONTINENTAL THOLEIITE LAVAS & DYKES.

The alkali basalt field includes nephelinites, phonolites and trachytes and was compiled from the data of Hubbard (1969), Schilling & Winchester (1969), Wedepohl (1970) and Zielsinski & Frey (1970). The composite island arc and oceanic tholeiite field was compiled from Hubbard (1969) and Jakeš & Gill (1970). The continental tholeiite lava field was compiled from Frey et al., (1968), Osawa & Coles (1970) and Hermann & Wedepohl (1970). The continental tholeiite dyke field was compiled from Frey et al., (1968), Ragland et al., (1970) and Haynes (1972).

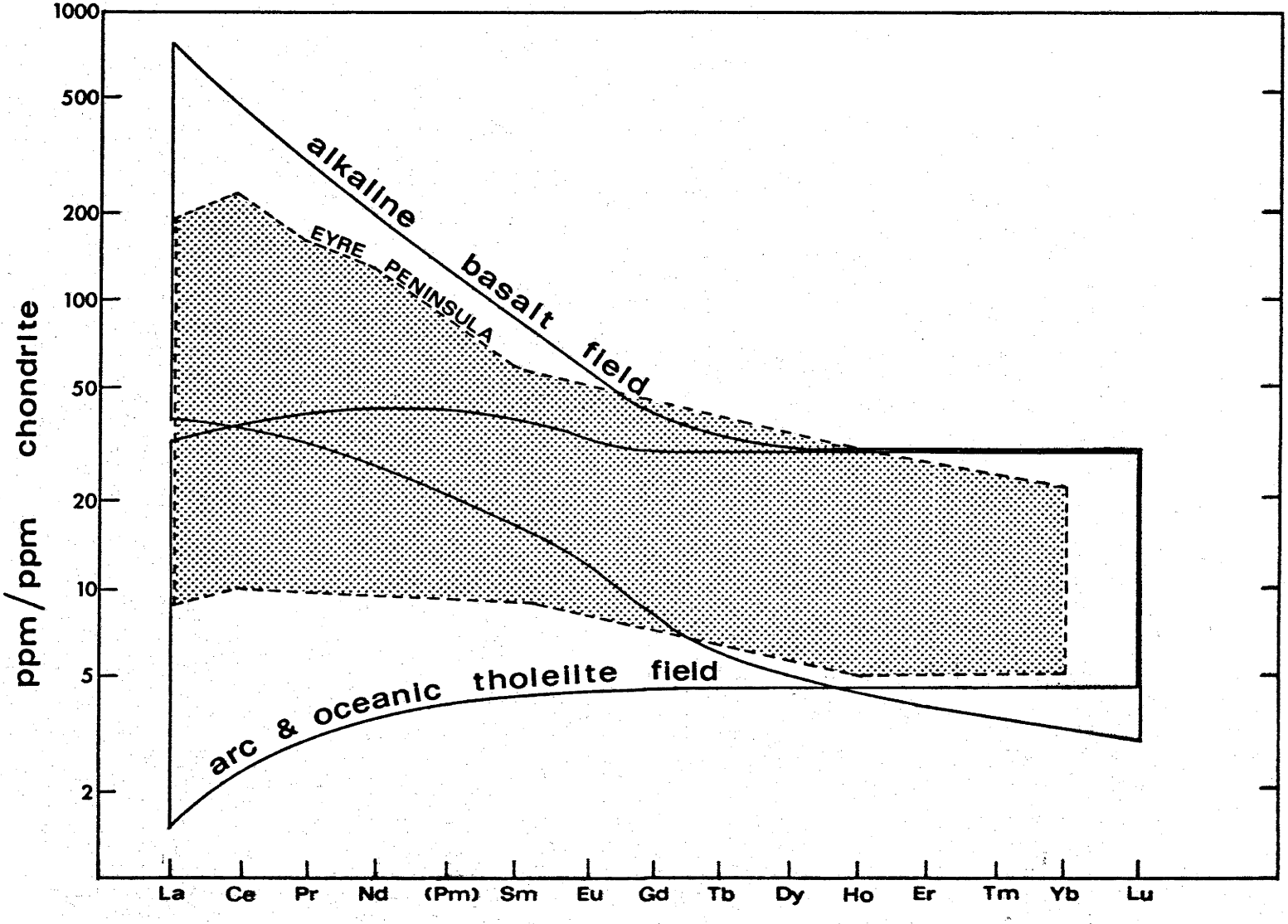

FIGURE 2.6 : COMPARISON OF THE ALKALI BASALT AND ISLAND ARC & OCEANIC THOLEIITE RARE EARTH ELEMENT FIELDS WITH THE COMPOSITE RARE EARTH ELEMENT FIELD (STIPPLED) FOR ALL EYRE PENINSULA BASIC ROCKS.

The basalt fields are from figure 2.5.

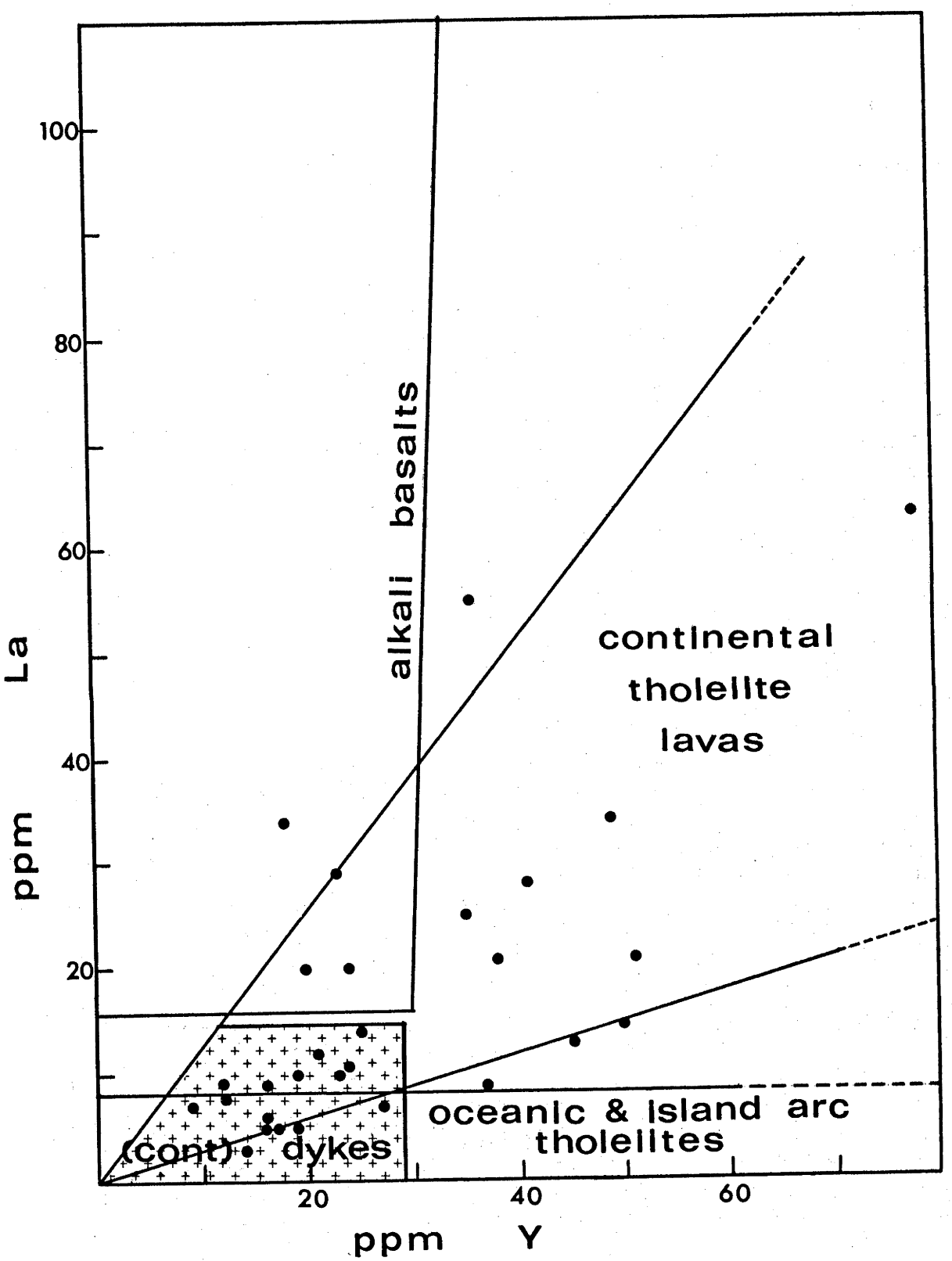

FIGURE 2.7 : La-Y PLOT FOR THE BASIC ROCKS.

The alkali basalt, continental tholeiite lava, continental tholeiite dyke (marked with crosses) and oceanic and island arc tholeiite fields were transferred from the corresponding La-Yb fields of Haynes (1972) using the chondrite abundance ratio of Y/Yb ≈ 10 and assuming minimal fractionation between Y(=Ho) and Yb.

respectively). The six samples selected for complete REE analysis (figure 2.2) cover most of the REE range shown by the partial patterns (figures 2.3 and 2.4) and should be representative of the basalt group. There are no significant differences between REE in the "pyroxenites" and the tholeiitic basalts. There are no consistent differences between pyroxene granulite and amphibolite REE patterns suggesting that REE are probably immobile in basic rocks even during granulite metamorphism. Amphibolites and hornblende granulites cover similar fields to the pyroxene granulites and have similar patterns.

The REE fields for alkali basalts, continental tholeiite lavas and dykes and oceanic/island arc tholeiites are plotted in figure 2.5. The basic rocks plot entirely within the continental tholeiite field (lava + dyke) with the exception of one sample (69-794) with slightly higher heavy REE (figure 2.3). The REE in the basic rocks plot within the upper two-thirds of the dyke field and all of the lava field. The basic rocks do not fit wholly within the alkali basalt or the island arc/ocean-floor tholeiite fields (figure 2.6). The basic rocks form a continuum from the continental lava to the continental dyke field in the La-Y plot (figure 2.7), but plot between the alkali basalt and oceanic/arc tholeiite fields.

The REE data indicate that the Eyre Peninsula basic rocks were originally continental tholeiites. The gradation of the basic rocks from the continental tholeiite dyke field into the lava field may be a characteristic of their deep crustal origin.

2.6.3.2 Titanium-Zirconium-Yttrium

The TiO_2-Zr plot (figure 2.8) indicates that the basic rocks are not island arc tholeiites. All except three of the basic rocks plot within the ocean-ridge tholeiite field. Two of the three basic rocks plot considerably outside the ocean-ridge field. The basic rocks plot within the continental tholeiite field with the exception of two plotting slightly below the dyke field. The TiO_2-Zr plot

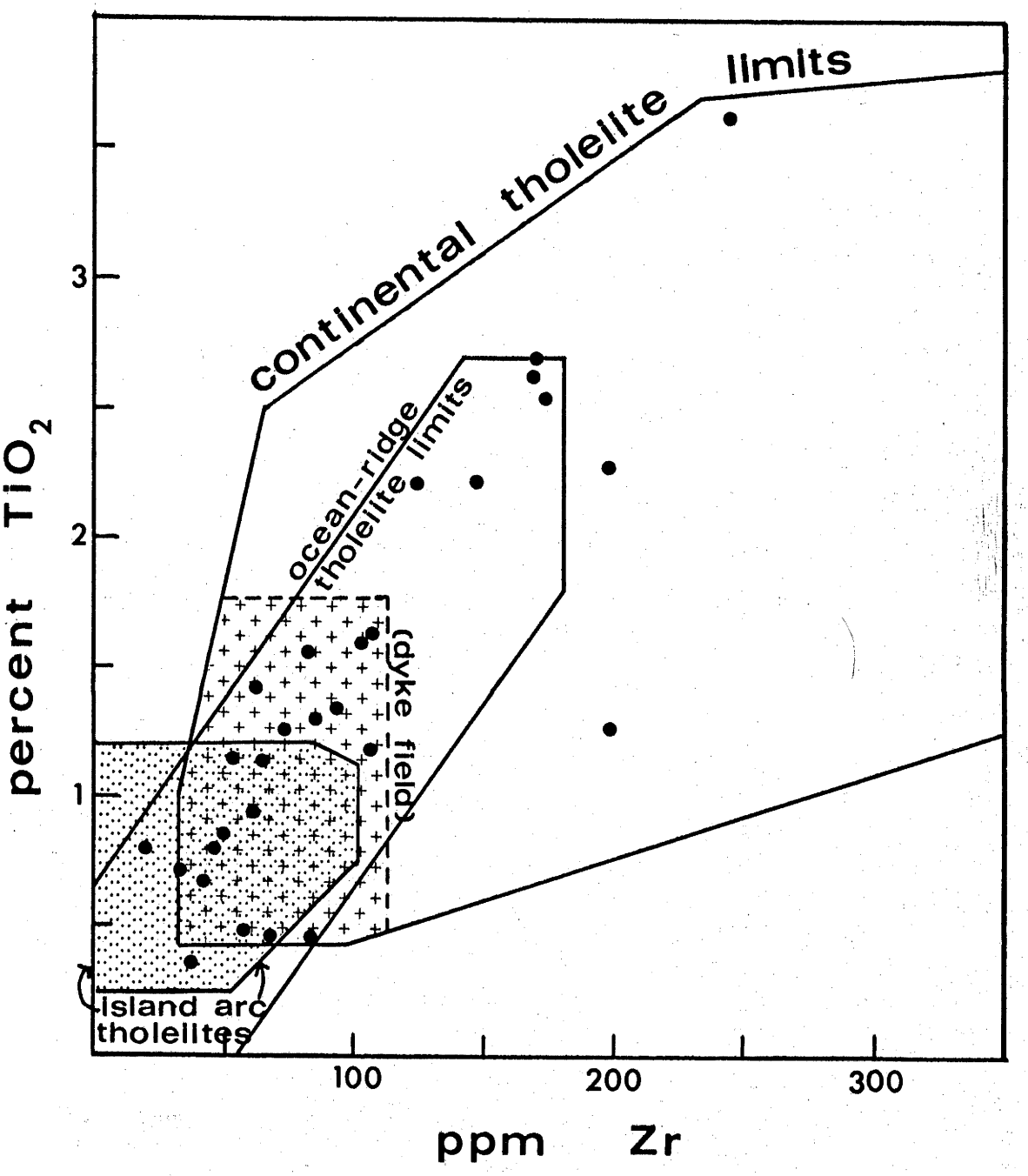

FIGURE 2.8 : TiO_2 - Zr PLOT FOR THE BASIC ROCKS.

The ocean-ridge tholeiite field was compiled from Hubbard (1969) and Pearce & Cann (1971). The island arc tholeiite field (stippled) is from Haynes (1972). The fields for continental tholeiite lavas and continental tholeiite dykes (marked with crosses) were compiled from references cited in table 2.1.

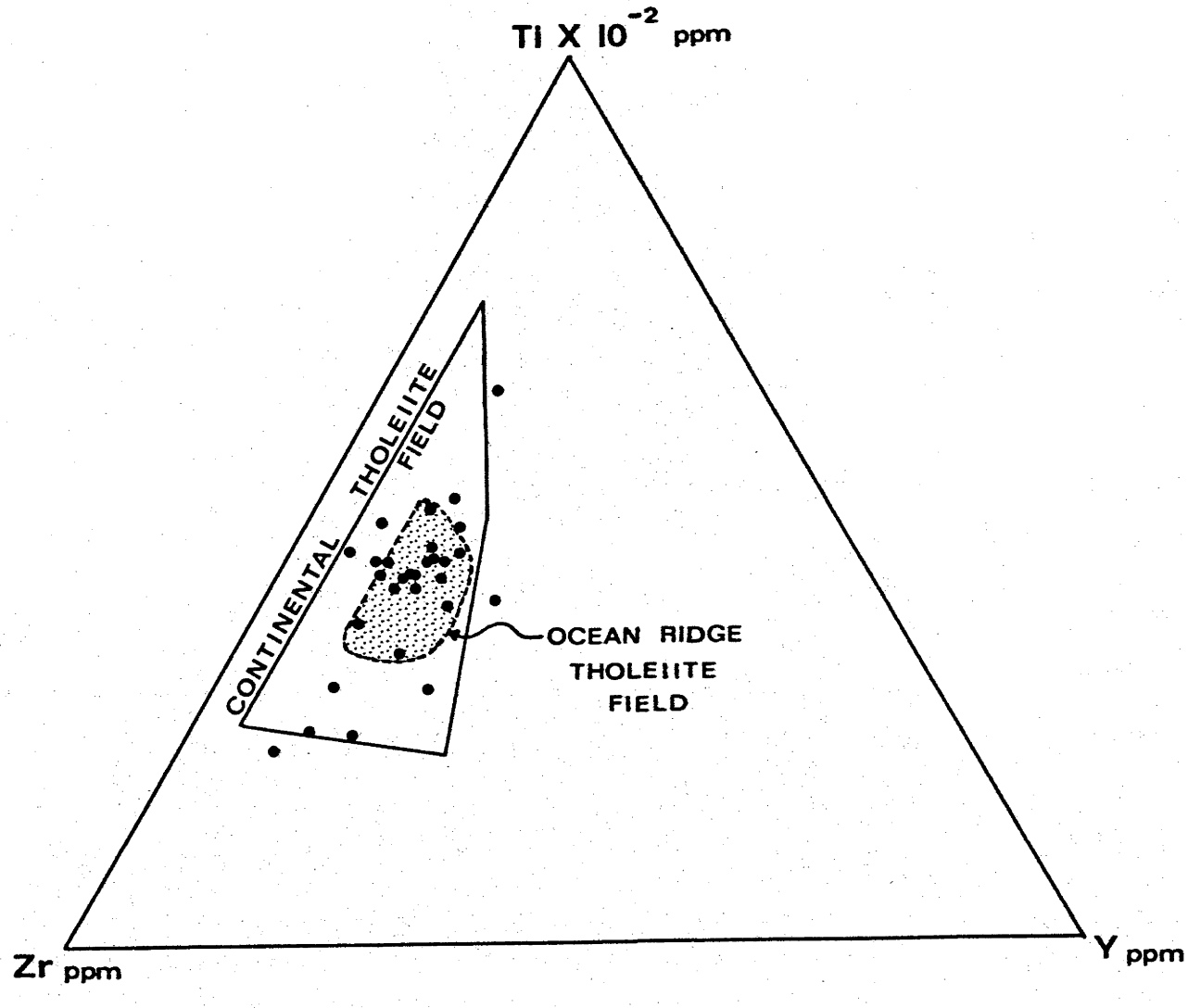

FIGURE 2.9 : Ti-Zr-Y PLOT FOR THE BASIC ROCKS.

The ocean-ridge tholeiite field (stippled) is from Pearce & Cann (1971), and the continental tholeiite field was compiled from references cited in table 2.1.

suggests that the basic rocks are either ocean-ridge tholeiites or continental tholeiites transitional to lava and dyke types. However, the association of the basic rocks with large quantities of dominantly potassic acid gneisses makes an ocean-ridge origin unlikely.

The Ti-Zr-Y plot (figure 2.9) demonstrates that the basic rocks are continental tholeiites and not ocean-ridge tholeiites. Many of the basic rocks plot outside the more restricted ocean-ridge tholeiite field.

2.6.3.3 Conclusion

The combination of REE, Y, Ti and Zr abundances identify the basic rocks at Eyre Peninsula as continental tholeiites. Quartz-normative and olivine-normative tholeiites are present, but, due to silica mobility during alteration and metamorphism, this may not reflect original compositional variation.

2.6.4 Geochemistry of The Tholeiitic Basalts

2.6.4.1 Immobile Elements

The average Eyre Peninsula tholeiite is compared in table 2.1 with other basalt averages. Ti is closest to the oceanic tholeiite and continental tholeiite (3), higher than the island arc tholeiite or continental tholeiites (5) and (6), and lower than continental tholeiite (4) (*). Zr is very close to the oceanic tholeiite, slightly higher than the island arc tholeiite and continental tholeiites (3), (5) and (6), and much lower than the continental tholeiite (4) (*). (* Note: the main difference between continental tholeiite averages (3) and (4) is the inclusion in the latter of a suite of high Zr-Nb-Ti basalts from Baja California and New Mexico - pers. comm. D. Haynes.) La is very close to the average continental basalt (3) and too high for the island arc tholeiite. Y is approximately the same as oceanic and continental tholeiites (3), (4) and (5) but higher than the island arc tholeiites. Such comparison of individual elements does not discriminate as efficiently as methods used

TABLE 2.1

AVERAGE THOLEIITES AND EYRE PENINSULA BASICS

	Oceanic		Island Arc		Continental Basalt		Continental Lava		Continental Dyke I		Continental Dyke II		Eyre Peninsula Basalt		Eyre Peninsula Pyroxenite	
	(1)	R/2	(2)	R/2	(3)	R/2	(4)	S.D.	(5)	R/2	(6)	S.D.		S.D.		S.D.
SiO_2	49.8	0.9	51.9	0.4	51.3	4.2	50.8	1.8	51.3	2.3	51.8	1.8	49.9	2.0	49.5	4.2
TiO_2	1.7	0.7	0.9	0.2	1.6	1.3	2.5	0.5	1.1	0.6	1.0	0.5	1.5	0.8	1.1	0.9
Al_2O_3	15.7	0.9	16.7	1.1	15.0	2.3	14.2	1.3	15.2	0.3	15.2	0.8	14.6	1.1	6.1	1.8
*FeO	10.0	2.2	10.1	1.0	11.4	2.6	12.2	2.7	11.7	1.7	10.2	—	12.9	3.2	14.0	3.9
MnO	0.2	—	0.2	0.05	0.2	0.05	0.2	0.03	0.2	—	0.2	—	0.2	0.3	0.2	0.04
MgO	7.7	1.4	6.1	0.8	7.2	3.8	6.0	1.1	8.0	2.2	8.2	1.6	6.7	1.3	18.7	3.1
CaO	11.2	0.7	10.3	1.4	9.8	1.8	8.8	0.8	9.8	1.8	10.5	0.6	10.5	1.4	7.7	3.1
Na_2O	2.6	0.4	2.7	0.7	2.4	0.8	2.8	0.5	2.2	0.3	2.1	0.5	2.3	0.7	0.9	0.3
K_2O	0.3	0.3	0.5	0.2	0.8	0.7	1.2	0.4	0.5	0.2	0.6	0.3	0.6	0.4	0.5	0.3
P_2O_5	0.2	—	0.2	0.1	0.3	0.3	0.4	0.1	0.2	—	0.2	—	0.2	0.2	0.1	0.1
Total	99.4		99.6		100.0		99.1		100.2		100.0		99.4		98.8	
Rb	4	4	9	4	21	13	35	14	17	7	22		16	16	21	16
Ba	59	75	139	60	209	32	541	209	180	238	373		103	78	128	72
Sr	183	58	268	150	153	38	509	219	148	32	220		118	47	92	23
Ga	—	—	12	3	23	7	19	2	—	—	—		18	6	9	2
Th	0.5	0.3	0.4	0.1	2.7	1.4	2.3	3.0	—	—	2.0		3	4	1.2	1.3
U	0.2	0.1	0.3	0.1	0.8	0.5	0.5	—	—	—	0.5		0.5	0.7	0.5	0.4
Pb	—	—	7	3	10	—	—	—	—	—	10		12	6	9	4
Zr	104	81	82	37	82	24	226	126	80	22	90		101	63	88	42
Nb	7	9	—	—	—	—	33	34	—	—	—		8	6	13	16
La	—	—	9	6	16	7	—	—	—	—	—		18	16	15	11
Ce	—	—	21	15	—	—	—	—	—	—	—		42	35	38	25
Y	33	10	20	8	26	6	37	17	33	18	—		30	16	16	3
Sc	—	—	29	1	37	4	—	—	—	—	—		38	6	31	8
V	—	—	262	45	276	39	262	82	303	130	290		277	55	171	50
Cr	297	—	114	60	255	369	178	106	320	336	266		186	131	1622	936
Co	32	—	29	4	48	16	49	—	56	7	37		38	11	82	14
Ni	110	13	60	33	119	137	97	48	144	137	158		77	41	657	302
Cu	82	—	111	47	94	17	103	79	94	17	98	20	56	55	64	72
Zn	—	—	77	3	98	29	110	10	98	29	87	10	122	38	152	71
Li	—	—	—	—	13	5	—	—	16	3	—		18**		18***	
K/Rb of average	623		461		316		285		244		226		311		197	
Average K/Rb			—		—				—		—		487	305		

Notes: *total iron as FeO
**nine samples
***one sample

R/2: one half maximum range of area averages used in grand average. S.D.: standard deviation.

Data compiled as follows:

oceanic tholeiite: White et al (1971), Heier et al (1965), Compston et al (1968), Gliksom (1971), Cann (1970), Hart et al (1970), Jakes & Gill (1970), Pearce & Cann (1971); island arc tholeiitte: Jakes & Gill (1970), Pearce & Cann (1971), White et al (1971), Lowder & Carmichael (1970), Gill (1970); continental tholeiite dyke I: Rivalenti & Sighinolfi (1970), Weigand & Ragland (1970); continental tholeiite dyke II & lava (samples with less than 53½% silica): Haynes (1972); continental basalt (dykes in I plus lavas as follows): Waters (1961), Cox & Hornung (1966), Cox et al (1967), Poldervaart (1955), Heier & Adams (1964), Osawa & Goles (1970), Compston et al (1968), Clark et al (1966), Aoki (1967), Heier et al (1965).
(area averages for silica less than 54% were obtained, then grand averages of these calculated)

in 2.6.3. However, graphical comparison of ranges of elements shown by the basalts (figure 2.10) shows the consistent overlap of Ti, La, Y and Zr in the Eyre Peninsula tholeiites with the continental tholeiites. Ti, Zr and Y in the basic rocks also overlap with the oceanic tholeiite. The island arc tholeiites have consistently lower Ti, Zr, La and Y than the Eyre Peninsula tholeiites.

Elements correlating significantly (table 2.2) with Ti, Zr, Y (also representing heavy REE) and La, Ce (representing light REE) are: Pb, Th, Nb, V, Co, (Sc) (99.9% confidence level); Si, Fe(III), Fe(II), Mg, Na, P, Ba, (Sc) (99.5% confidence level) (Sc is borderline to 99.9% and 99.5%). These elements may also be used for identification of basalt type. All of these elements except Ba, Si and Na are immobile during alteration and metamorphism. The significant correlation of Ba, Si and Na with immobile elements indicates restricted mobility of Ba, Si and Na during alteration and metamorphism.

The immobile elements in the Eyre Peninsula tholeiites which correlate with Ti, Zr, Nb, REE and Y will now be examined (table 2.1). Th is close to the average continental tholeiite basalt (3), lava (4) and dyke (6), but significantly higher than the oceanic and island arc tholeiites. Pb is close to continental basalt (3) and dyke (6) but is significantly higher than the island arc tholeiite. Nb is much too low for continental tholeiite lava (4) (* see note near the beginning of 2.6.4.1), but close to the oceanic tholeiite. Sc is very close to continental tholeiite lava (3) but significantly higher than the island arc tholeiite. V is close to island arc tholeiite and continental tholeiites (3), (4) and (6) but slightly lower than continental tholeiite dyke (5). Co is close to continental tholeiite dyke (6), only slightly higher than the oceanic and island arc tholeiites and only slightly lower than continental tholeiites (3) and (4), but significantly lower than (5). Total Fe is close to continental tholeiites (3), (4) and (5) but considerably higher than continental tholeiite dyke (6), and oceanic and island arc tholeiites. Mg is closest to the

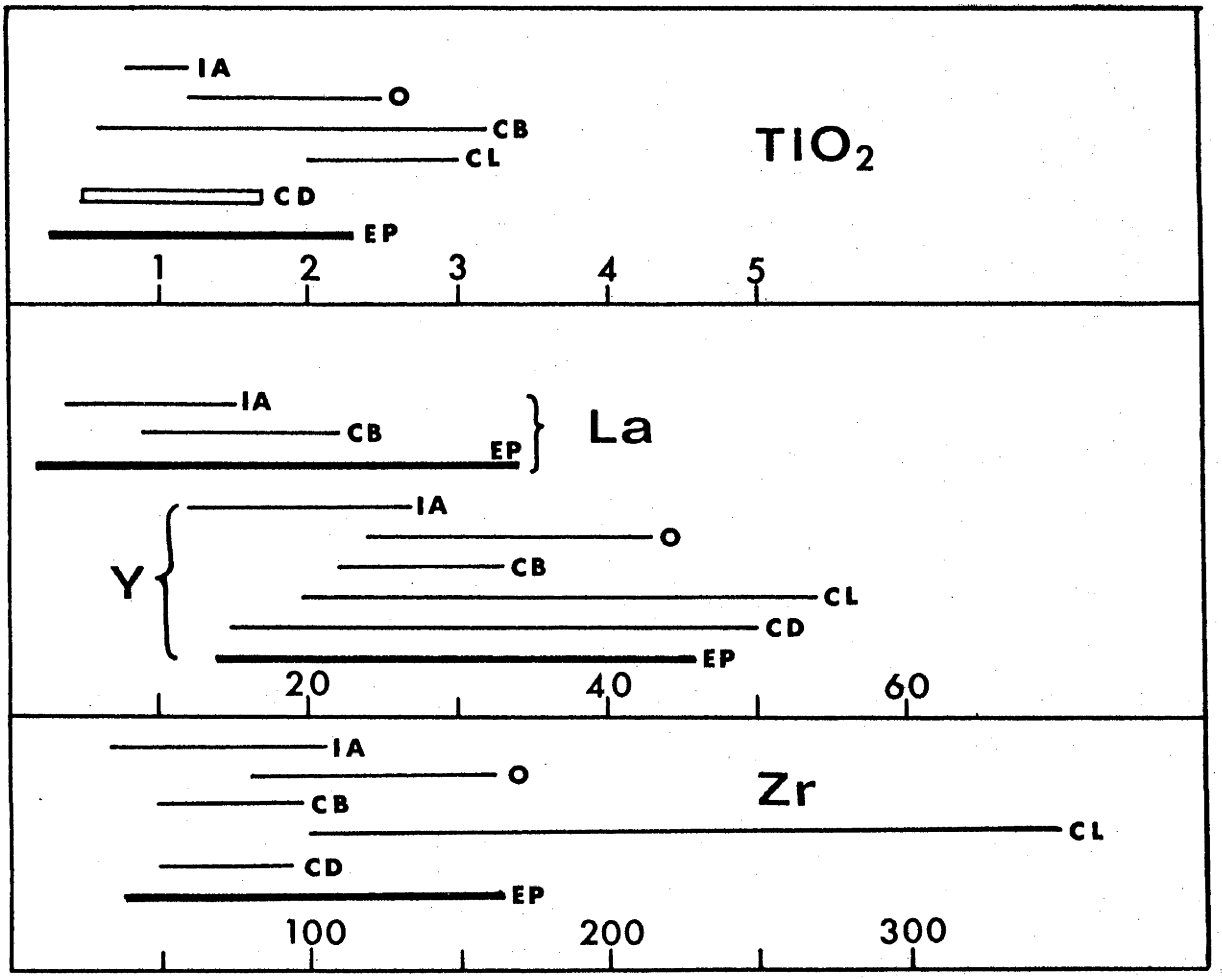

FIGURE 2.10 : COMPARISON OF THE RANGES OF TiO_2, La, Y and Zr IN EYRE PENINSULA THOLEIITIC BASALTS WITH THOSE IN THOLEIITES FROM VARIOUS ENVIRONMENTS.

The limits of the "ranges" are given by addition/subtraction of one standard deviation (S.D.) or "range/2" (R/2) to/from the average values (table 2.1). IA = island arc tholeiites; O = oceanic tholeiites; CB, CL & CD = continental tholeiite basalts, lavas and dykes respectively; EP = Eyre Peninsula tholeiitic basalts.

TABLE 2.2

CORRELATION COEFFICIENT MATRIX
EYRE PENINSULA BASICS (LOSS FREE)

99.9% confidence level 0.57
99.5% confidence level 0.45

(N.B. decimal points omitted)

SiO_2																
-536	TiO_2															
-374	548	Fe_2O_3														
-268	555	030	FeO													
-145	-336	-144	163	MgO												
256	-112	-106	-496	-689	Na_2O											
-173	511	044	453	-277	-064	P_2O_5										
-206	480	263	245	006	-058	246	Ba									
016	277	021	-103	-417	586	135	448	Pb								
-078	334	033	052	-314	348	451	211	609	La							
-054	321	017	055	-299	295	470	190	565	993	Ce						
058	330	091	-068	-467	521	267	140	691	902	884	Y					
113	024	187	-030	-166	-215	047	-354	-391	-487	-463	-401	Sc				
-286	589	422	213	-486	-013	230	-115	-165	-201	-207	-112	565	V			
-202	-323	015	112	885	-577	-376	056	-415	-453	-461	-571	-102	-440	Co		
114	144	068	-159	-318	504	102	129	609	874	863	926	-578	-303	-391	Zr	
-430	630	495	292	-044	-063	304	583	408	609	609	502	-480	-033	-022	545	Nb
217	-015	-022	-327	-323	568	019	118	609	822	812	873	-588	-376	-393	969	432	Th

island arc and continental tholeiites (3) and (4), slightly lower than the oceanic tholeiite and considerably lower than continental tholeiite dykes (5) and (6). P is close to all tholeiites except continental tholeiite (4) which is higher. The Eyre Peninsula tholeiites exhibit maximum similarity to the continental tholeiite basalt (3) (which includes both lavas and dykes), and are also very similar to the continental tholeiite dyke (6).

Graphical comparison of the ranges of the preceding elements in the Eyre Peninsula tholeiites with the tholeiite types (figure 2.11) shows complete overlap with the continental tholeiites for total Fe, Sc, V and Th. Co is significantly lower than the continental tholeiite dykes but overlaps with the lower part of the continental basalt range. Mg is in the lower part of the continental tholeiite range and covers the island arc and oceanic tholeiite fields. V completely overlaps the island arc and oceanic tholeiite fields. Sc in the island arc tholeiites is below the basic rocks. Total Fe, Th and Co in the island arc and oceanic tholeiites fall in the lower range of the Eyre Peninsula tholeiites.

Al, Ga and Mn in the Eyre Peninsula tholeiites are close to the average continental tholeiites, and were probably immobile during metamorphism. Cr and Ni in the continental tholeiites cover a wide range and are generally higher than in the Eyre Peninsula tholeiites (figure 2.11) and table 2.1). Inclusion of the high-Ni and high-Cr pyroxenites would result in the overall Eyre Peninsula average and range corresponding much more closely to the continental tholeiites. Cr and Ni were probably immobile during metamorphism, but this cannot be demonstrated with the present data.

The immobile element geochemistry of the Eyre Peninsula tholeiites is significantly different from that of the island arc tholeiites. The relatively small volume of Eyre Peninsula tholeiites and the large volume of associated dominantly potassic acid rocks ($Na_2O/K_2O < 1$) are unlikely

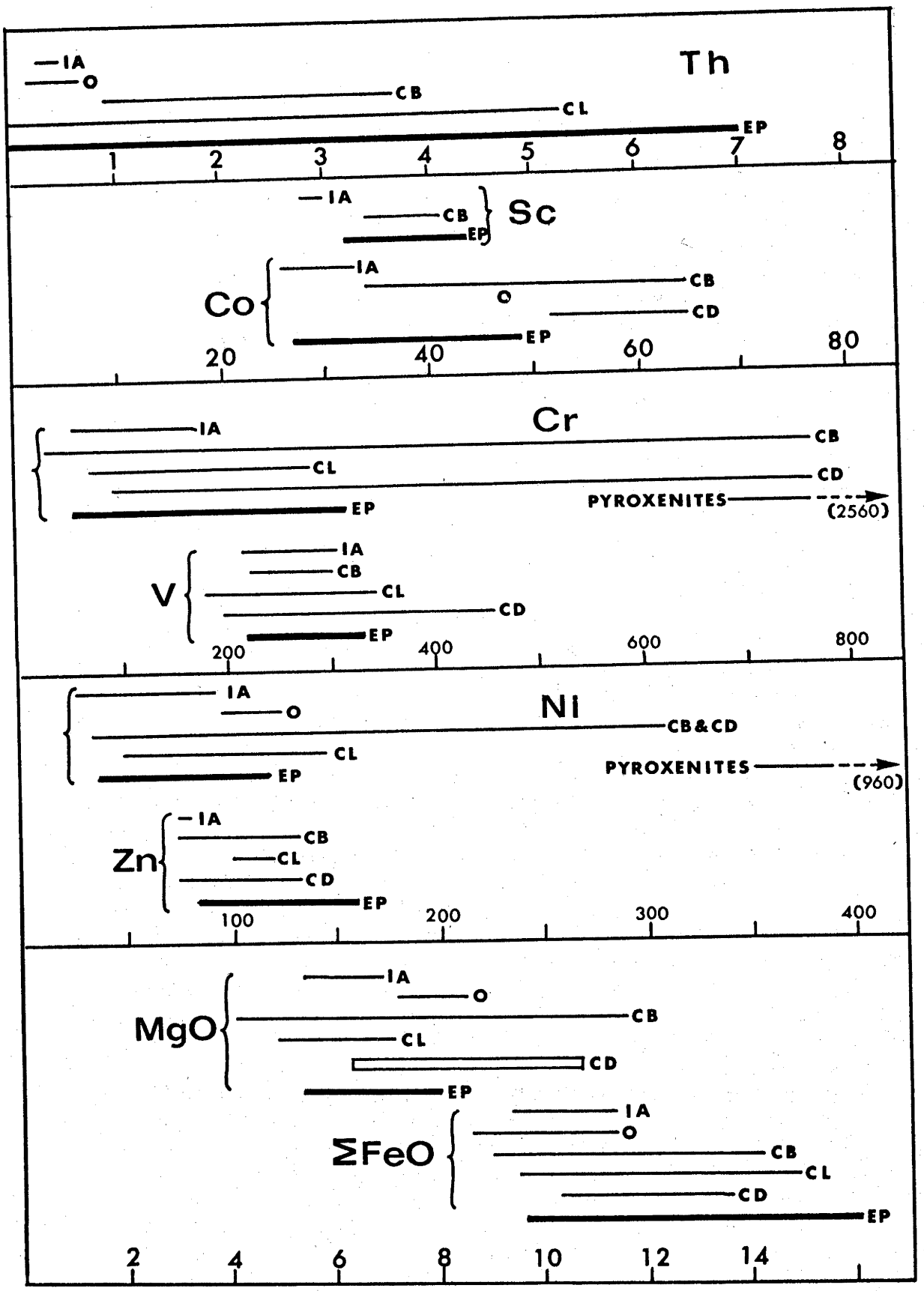

FIGURE 2.11 : COMPARISON OF THE RANGES OF Th, Sc, Co, Cr, V, Ni, Zn, MgO AND TOTAL FeO IN EYRE PENINSULA THOLEIITIC BASALTS WITH THOSE IN THOLEIITES FROM VARIOUS ENVIRONMENTS.

(Explanation as for figure 2.10 except that Cr and Ni for the Eyre Peninsula "pyroxenites" or picritic tholeiites are also shown).

in an island arc environment, which is typified by very abundant tholeiites and sodic acid volcanics ($Na_2O/K_2O > 1$) (Jakeš & Gill, 1970). The inert element geochemistry of the Eyre Peninsula tholeiites is significantly different from the oceanic and island arc tholeiites, and very similar to the continental tholeiites, with affinities to both lavas and dykes.

2.6.4.2 Mobile Elements

Limited mobility of Si, Ba and Na is indicated by the significant correlation of these elements with immobile elements (2.6.4.1). Limited mobility of Si and Ba is common, but Na is frequently increased significantly during alteration and metamorphism (2.4). Si, Ba and Na in the Eyre Peninsula tholeiites are compared with other tholeiites in table 2.1. Na is very close to continental tholeiites (3), (5) and (6) and only slightly lower than continental tholeiite (4), oceanic and island arc tholeiites. Si is slightly lower than the continental tholeiites. Ba is considerably lower than the continental tholeiites. The close correspondence of Na in the Eyre Peninsula tholeiites with unaltered continental tholeiites indicates that Na was not significantly affected during alteration and metamorphism. Si appears to be slightly depleted. Pronounced depletion of Ba is unlikely because correlation with immobile elements (Ti and Nb) has not been destroyed (cf. Cann, 1970). Ba correlates strongly with K and Rb (appendix F), and K, Rb and Ba were either consistently leached coherently (cf. Cann, 1970), or the correlation reflects the initial geochemistry. Although K and Rb are mobile elements, their abundances in the Eyre Peninsula tholeiites are very similar to continental tholeiites (3), (5) and (6) (table 2.1 and figure 2.12). The correlation of Ba with inert elements, and with K and Rb, coupled with the closeness of K and Rb to unaltered tholeiite averages, suggest that Ba was not significantly altered. The low Ba may be a relatively unaltered primary geochemical feature. Sr in the basic rocks is slightly lower than in continental tholeiites (3) and (5) and considerably lower than in (4) and (6) (table 2.1 and figure 2.12). Sr has been depleted or was initially

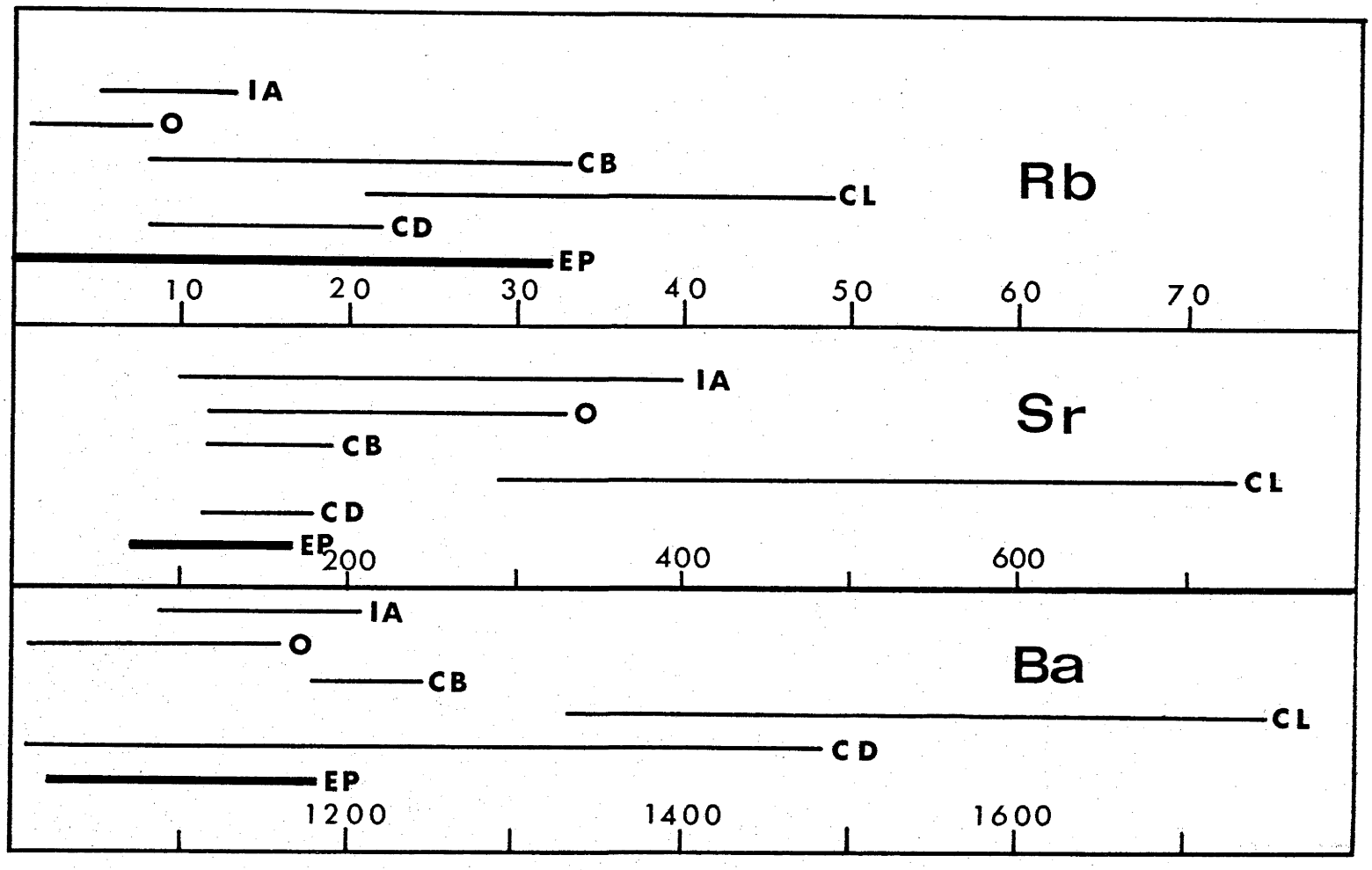

FIGURE 2.12 : COMPARISON OF THE RANGES OF Rb, Sr AND Ba IN EYRE PENINSULA THOLEIITIC BASALTS WITH THOSE IN THOLEIITES FROM VARIOUS ENVIRONMENTS.

(Explanation as for figure 2.10).

low. Strong positive correlations exist in unaltered ocean floor basalts between Sr and Zr, Nb, K, Ti (Cann, 1970). In altered basalts the correlation of Sr with Zr and Ti is destroyed, and greatly reduced with Nb and K. Sr in the Eyre Peninsula tholeiites does not correlate with inert elements. This may be a primary geochemical feature or may suggest alteration of Sr. Haynes (1972) demonstrated extensive Sr depletion accompanying Na enrichment. Similar alteration should destroy correlation of Sr with inert elements, and may cause negative correlation of Sr with Na. A significant positive correlation exists between Na and Sr (appendix F). Sr depletion must have been relatively uniform and small (certainly not much more than 50 ppm), or the low Sr is a primary feature. Li and Zn are slightly higher than in the continental tholeiite averages (table 2.1 and figure 2.11). U is comparable in all the basalt averages. Cu in the Eyre Peninsula tholeiites is depleted by an average of 40-50 ppm (table 2.1) and irregularly redistributed (figure 2.13). Four samples collected within close proximity (69-785, 69-786, 69-788 and 69-1352) have Cu contents respectively of 21, 27, 196 and 1 ppm: both depleted and enriched specimens are present. Cu mobilised from the basic rocks was partly retained in some cases in sulphide-bearing reaction zones at acid gneiss contacts (chapter 5), or was disseminated as sulphides in neighbouring acid gneisses which may contain up to 50 ppm Cu (chapter 3). Ca commonly exhibits great mobility during alteration, but is very close in the basic rocks to continental tholeiite averages (3), (5) and (6). The similarity to unaltered tholeiites and the small standard deviation of Ca (table 2.1) suggest limited redistribution of Ca.

2.6.4.3 Effects of Alteration and Metamorphism

Alteration and metamorphism of the Eyre Peninsula basic rocks resulted in extensive depletion and redistribution of Cu, relatively small depletion of Si and Sr (?) and limited redistribution of K, Rb, Ba, Li, Ca, Na and U. The metamorphism had no demonstrable effects on Ti, Al, Fe, Mn, Mg, P, Ga, Th, Pb, Zr, Nb, REE, Y, Sc, V, Co, Ni (?), Cr (?)

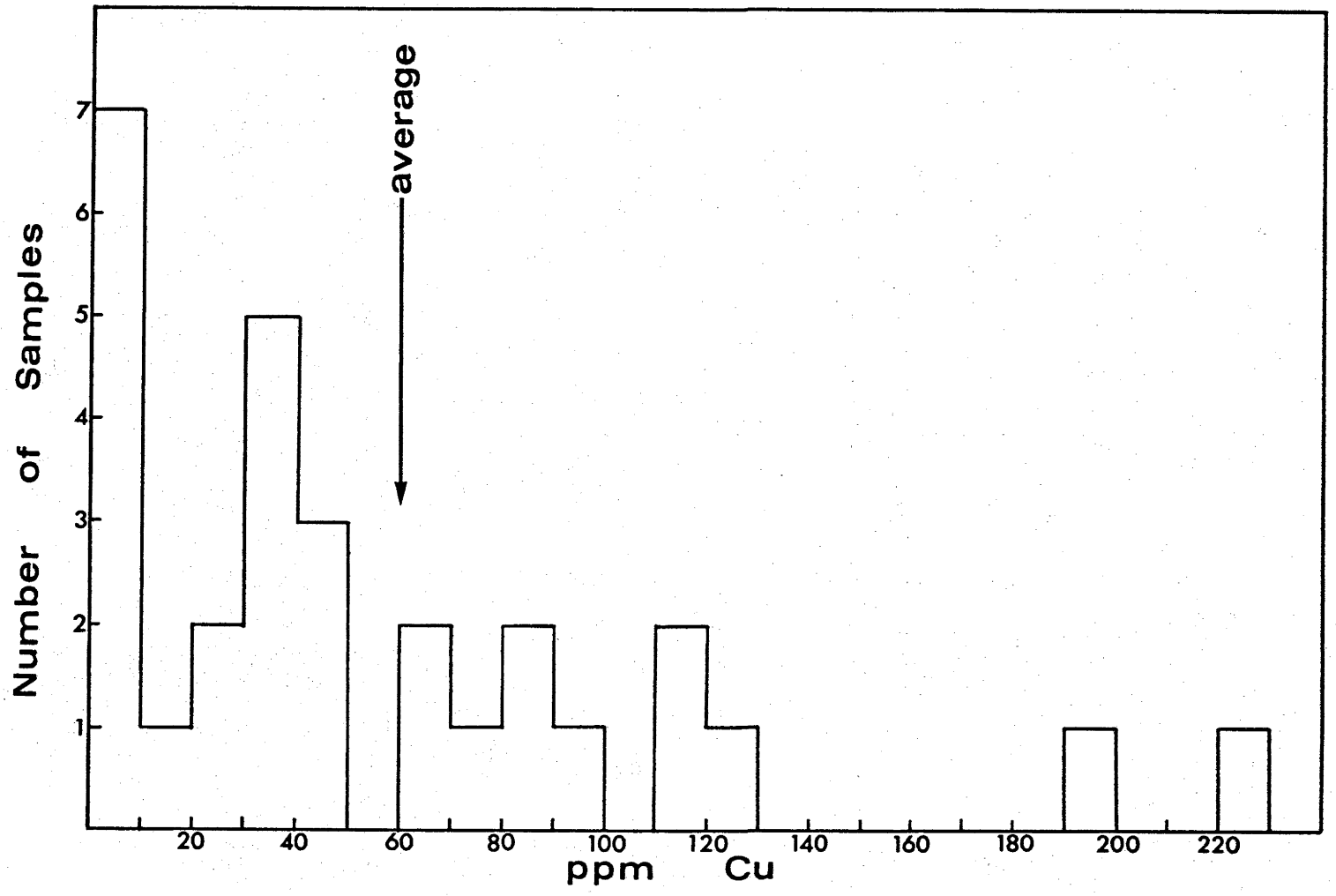

FIGURE 2.13 : HISTOGRAM FOR COPPER CONCENTRATIONS IN THE BASIC ROCKS, SHOWING ENRICHED AND DEPLETED SAMPLES.

and Zn (?). The low Ba and possibly the low Sr in the Eyre Peninsula tholeiites appear to be primary geochemical features.

2.6.5 Geochemistry of the Pyroxenites

The "pyroxenites" or picritic tholeiites are characterised by lower Al, Ca and Na, and higher Mg/Fe Fe, Mg, Ni, Co, Cr and Zn than the tholeiitic basalts (table 2.1 and appendix C). The pyroxenites are compared in table 2.3 with olivine-rich picritic tholeiites from Baffin Bay, a picritic tholeiite accumulate from the Palisades Sill and an Archaean pyroxenite. The main differences between Baffin Bay lava averages (1), (2) and (3) are decreasing normative olivine (about 48%, 28% and 8% respecitvely), and increasing plagioclase (about 24%, 34% and 44%) and clinopyroxene (15%, 19% and 24%).

The concentrations of the immobile elements Zr, Y, Ti, P, Mg, Ni and Cr in the Eyre Peninsula pyroxenites and the Baffin Bay tholeiites are very similar. However, the mobile elements K, Rb and Ba are higher and Sr lower in the pyroxenites. If the Eyre Peninsula pyroxenites are equivalent to picritic magmas like the Baffin Bay tholeiites, they should be closest to the Baffin Bay average (2), which has similar Mg. However, Si, Fe and K are significantly higher and Al, Ca and Na significantly lower. The lower Na, Ca and Al, and higher Si and Fe in the pyroxenites can be explained by higher orthopyroxene and lower plagioclase (and, perhaps, lower clinopyroxene and olivine). Crystal fractionation of olivine tholeiite at 9kb and 13.5kb (table 2.4) satisfactorily accounts for the compositions of three of the pyroxenites as crystal-enriched accumulates, (69-739, 69-788 and 69-1352) and approximately accounts for a fourth (69-756). The crystal accumulates for the last three (table 2.4) are rich in orthopyroxene, and the other two pyroxenites (69-785 and 69-786) are rich in normative orthopyroxene (62% and 53%: appendix C) suggesting that the pyroxenites <u>are</u> orthopyroxene-rich picritic tholeiites. The coarse pyroxene prisms with exsolution lamellae commonly observed in the pyroxenites are probably

TABLE 2.3

COMPARISON OF PYROXENITES WITH PICRITIC THOLEIITES

		Eyre Peninsula Pyroxenite		Baffin Bay Tholeiites			Picritic Tholeiite	Archean Pyroxenite	
			S.D.	(1)	(2)	(3)			S.D.
	SiO_2	49.5	4.2	44.4	45.7	48.0	49.0	50.2	2.4
	TiO_2	1.1	0.9	1.0	1.0	1.3	0.8	0.5	0.2
	Al_2O_3	6.1	1.8	7.6	10.9	13.7	9.5	7.4	1.2
total	FeO*	14.0	3.9	11.5	10.8	10.4	13.7	10.6	1.2
	MnO	0.2	0.04	0.2	0.2	0.2	0.1	0.2	0.05
	MgO	18.7	3.1	26.7	19.6	11.8	17.7	21.3	2.5
	CaO	7.7	3.1	7.2	9.8	12.0	7.1	8.7	1.5
	Na_2O	0.9	0.3	1.1	1.2	1.8	1.6	1.0	1.2
	K_2O	0.5	0.3	0.2	0.1	0.2	0.4	0.03	0.02
	P_2O_5	0.1	0.1	0.1	0.1	0.1	0.1		
	Total	98.8		100.0	99.4	99.5	100.0	99.93	
	Rb	21	16	4	2	4			
	Ba	128	72	72	53	78			
	Sr	92	23	198	191	229			
	Ga	9	2	12	16	19			
	Zr	88	42	70	67	84			
	Y	16	3	15	18	24			
	Cr	1622	936	1700	1900	815		3400**	
	Ni	657	302	1630	995	360		470**	
	Cu	64	72	80	123	144			
	Zn	152	71	72	68	63			

* total Fe as FeO
** one sample only
S.D is standard deviation

Data Compiled as Follows:

Baffin Bay data from Clark (1970): average (1) is Clark's picritic basalt (2), average (2) is average of Clark's (3) & (4), average (3) is average of Clark's (5) & (6); Archaean pyroxenite - average of picritic basalts, pyroxenites and basaltic komatiites with MgO greater than 15% (McCall & Leishman 1971); picritic tholeiite - Palisades sill (Turner & Verhoogen 1960 p215).

TABLE 2.4

COMPARISON OF PYROXENITES WITH COMPUTED CRYSTAL ACCUMULATES

FRACTIONATION OF OLIVINE THOLEIITE

	9 kb Fractionation						13.5 kb Fractionation	
	69-739		69-788		69-1352		69-756	
	Actual	Calculated	Actual	Calculated	Actual	Calculated	Actual	Calculated
SiO_2	47.7	46.7	44.5	44.4	45.2	45.2	52.8	51.4
Al_2O_3	8.3	9.4	6.2	8.9	7.3	9.2	2.9	10.8
FeO	8.9	11.3	12.2	11.7	12.8	11.8	9.4	8.2
MgO	24.2	24.5	16.8	16.9	16.9	17.2	20.4	22.0
CaO	6.5	7.2	8.2	5.7	7.9	5.9	13.1	8.2
Mg.No.	83	79	69	72	68	72	82	83
	COMPOSITIONS OF THE ACCUMULATES							
Parent Melt	—	66%	—	47%	—	49%	—	49%
Olivine	—	27%	—	—	—	—	—	—
Orthopyroxene	—	7%	—	53%	—	51%	—	26%
Clinopyroxene	—	—	—	—	—	—	—	25%

Parent olivine tholeiite melt and compositions of olivine, orthopyroxenes and clinopyroxenes used are from Green & Ringwood (1967b).

primary igneous pyroxenes which survived the metamorphism without recrystallisation. The compositions of the pyroxenites (excluding 69-739) can be explained by fractionation of olivine tholeiite involving orthopyroxene ± clinopyroxene, but no olivine. This indicates fractionation at pressures greater than about 13 kb (Green & Ringwood, 1967b). The pyroxenite involving olivine fractionation (69-739) fractionated at lower pressures (probably 9-12 kb). The crystal fractionation probably occurred prior to intrusion of the pyroxenites. It is highly unlikely that the large accumulation of crystals occurred in situ because the pyroxenites occur in relatively small dyke-like bodies less than several metres wide.

The Eyre Peninsula pyroxenites are very similar to the Palisades sill picritic tholeiite (table 2.3); except that Na and Al are slightly lower, and Mg slightly higher. The Eyre Peninsula pyroxenites are also similar in composition to the "pyroxenites" or basaltic komatiites associated with Archaean greenstone belts. A composite of Archaean picritic tholeiites (MgO > 15%) and basaltic komatiites from Kalgoorlie is similar to the average Eyre Peninsula pyroxenite (table 2.3) except that the pyroxenite has higher Ti, total Fe and lower Mg, and higher Fe/Mg ratio. The trace element data given for one Kalgoorlie "pyroxenite" is broadly similar. The overall similarity, however, is coincidental, since the Kalgoorlie greenstones are probably island arc tholeiites.

CHAPTER 3

ACID GNEISSES

3.1 THE HIGH-POTASSIUM GARNET-FREE CHARNOCKITES

(Samples analysed: 69-789, 69-954, 69-956, 69-1372: appendix C.)

3.1.1 Field Appearance

This group appears homogeneous in the field in that there is total absence of compositional banding. The rocks are generally of massive appearance (although some have poorly defined gneissic foliation) with coarser feldspar crystals set in a finer grained matrix. Pegmatites and migmatitic veinlets are absent. The charnockites are characterised by dark bluish-grey or grey colour in the handspecimen.

3.1.2 Mineralogy

The high-K charnockites are dominantly composed of quartz, plagioclase and orthoclase with lesser amounts of orthopyroxene, hornblende and biotite (appendix A). The hornblende and biotite occur as discrete grains, and moulded upon or intergrown with the orthopyroxene. Hornblende and biotite are absent in some of the charnockites. No minerals from the charnockites were analysed.

3.1.3 Geochemistry

Samples collected along approximately 6 km. of coastline and representing at least 10 sq. km. of this rock type (diagonal shading near Memory Cove in figure 1.1) show restricted variation of major and trace element compositions (table 3.2, figure 3.9 and appendix C). The observed variation is systematic: smooth changes are observed in major and trace elements with increasing silica (figures 3.1 and 3.2). Decreases in element concentrations cannot be accounted for by simple silica dilution, and must be the result of igneous processes. The relative uniformity of

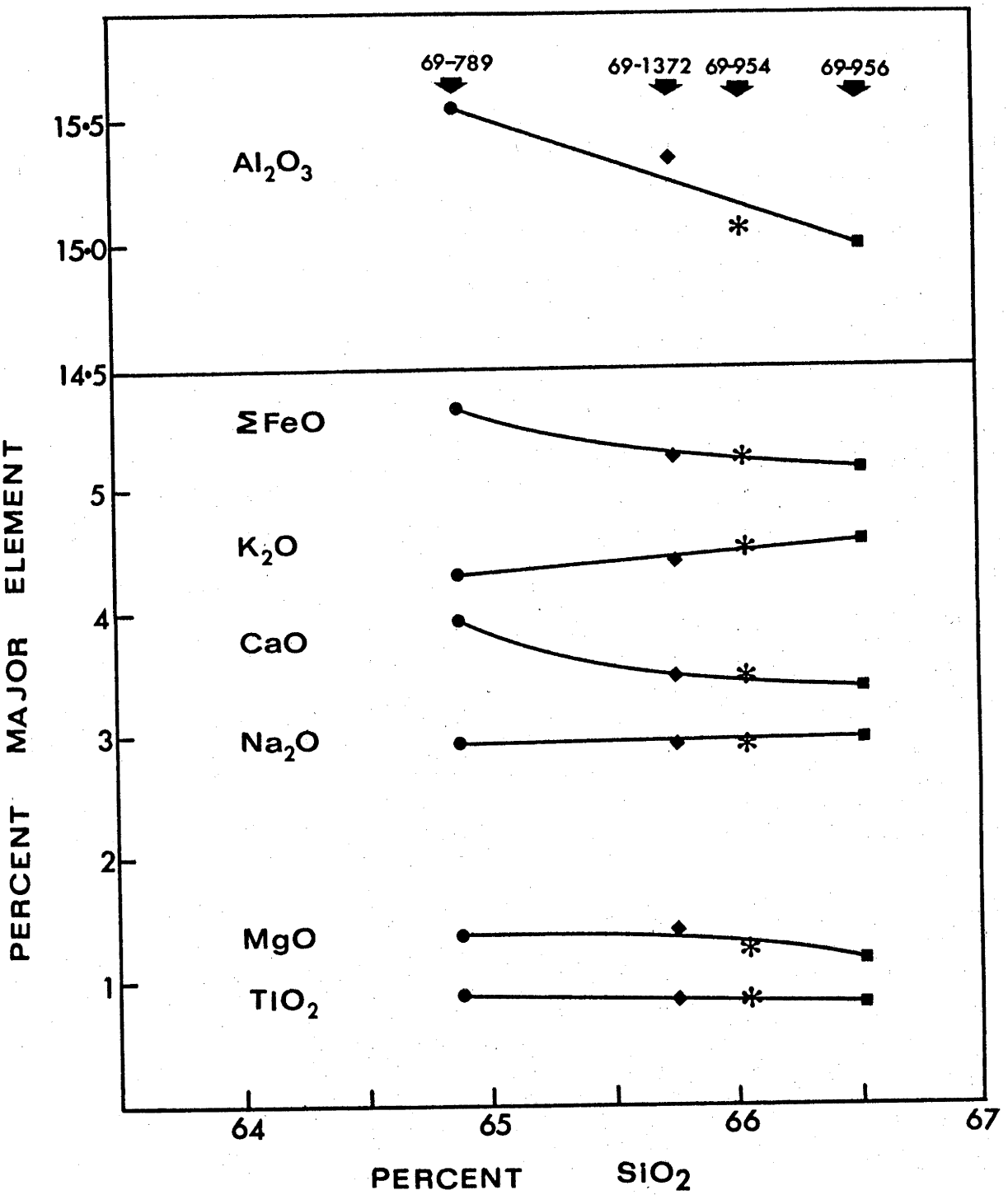

FIGURE 3.1 : SMOOTH VARIATION OF MAJOR ELEMENTS IN THE HIGH-K GARNET-FREE CHARNOCKITES.

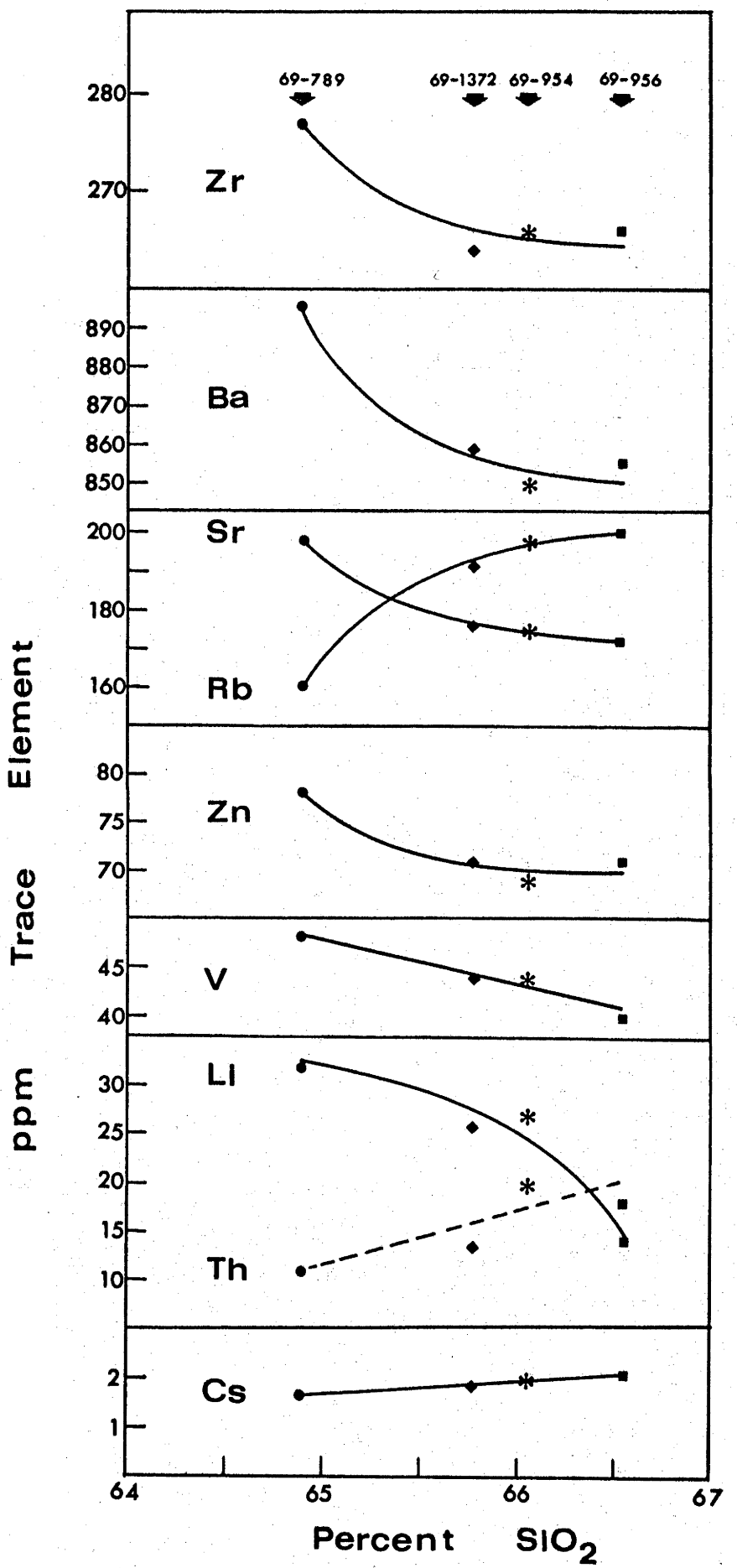

FIGURE 3.2 : SMOOTH VARIATION OF TRACE ELEMENTS IN THE HIGH-K GARNET-FREE CHARNOCKITES.

major element compositions and smooth variation of major and trace elements over such a large area suggest a batholithic origin. Increasing Si is accompanied by increases in K, Rb, Cs and Th, and decreases in Al, total Fe, Ca, Ba, Sr, Zr, V, Zn and Li; Na increases slightly, Ni increases irregularly; Ti, Mg and Cr decrease slightly, Ga, Pb, Nb, Y, Sc, Cu, U, Pr and Nd (last 2 are XRF values) show small but erratic variation. Although REE determined by X-ray fluorescence spectroscopy show no systematic variation, REE determined by the more sensitive mass spectrometer technique (figure 3.3) show the more fractionated sample (69-956: chondrite-normalised La/Yb = 9.7) (see appendix D) has a pattern richer in light and poorer in heavy REE than the less fractionated sample (69-1372: chondrite-normalised La/Yb = 6.2). The more fractionated rock also has a slightly more pronounced negative europium anomaly (chondrite-normalised Eu/Eu* 0.67 cf. 0.75). Further evidence for an igneous origin are the smooth decreases in K/Rb, K/Cs and Ba/Rb, and increase in K/Ba with increasing silica (table 3.1).

The charnockites are close in major element chemistry to the average granodiorite (table 3.2) except that average SiO_2 is $\sim$ 1% lower, MgO $\sim$ ½% lower, Na_2O and Al_2O_3 $\sim$ ½% higher, K_2O and total FeO $\sim$ 1% higher. Ti, Mn, Ca and P are quite close to the average granodiorite. The trace element chemistry is also very similar to the average granodiorite: Rb and Pb in the charnockites are slightly higher, but K/Rb and K/Pb ratios of the averages are nearly identical ($\sim$200 and $\sim$1300 repectively); Ba, Ga, Th, U, Sc, Co, Ni, Cu, Zn, Li and Cs are very similar to the granodiorite average, although Th is slightly higher and U, Cs slightly lower in the charnockite yielding a higher Th/U ratio (7.6 cf. 4 for average granodiorite), and considerably higher K/Cs and Rb/Cs (17,800 cf. 9,130; and 90 cf. 45 respectively). Zr is slightly higher in the charnockites (268 cf. 224 ppm) and Nb is slightly lower (15 cf. 20 ppm) resulting in higher Zr/Nb (18 cf. 11). Light REE and Y are about 20% higher in the charnockites and Cr slighly lower (23 cf. 35 ppm). However, all the preceding elements are well

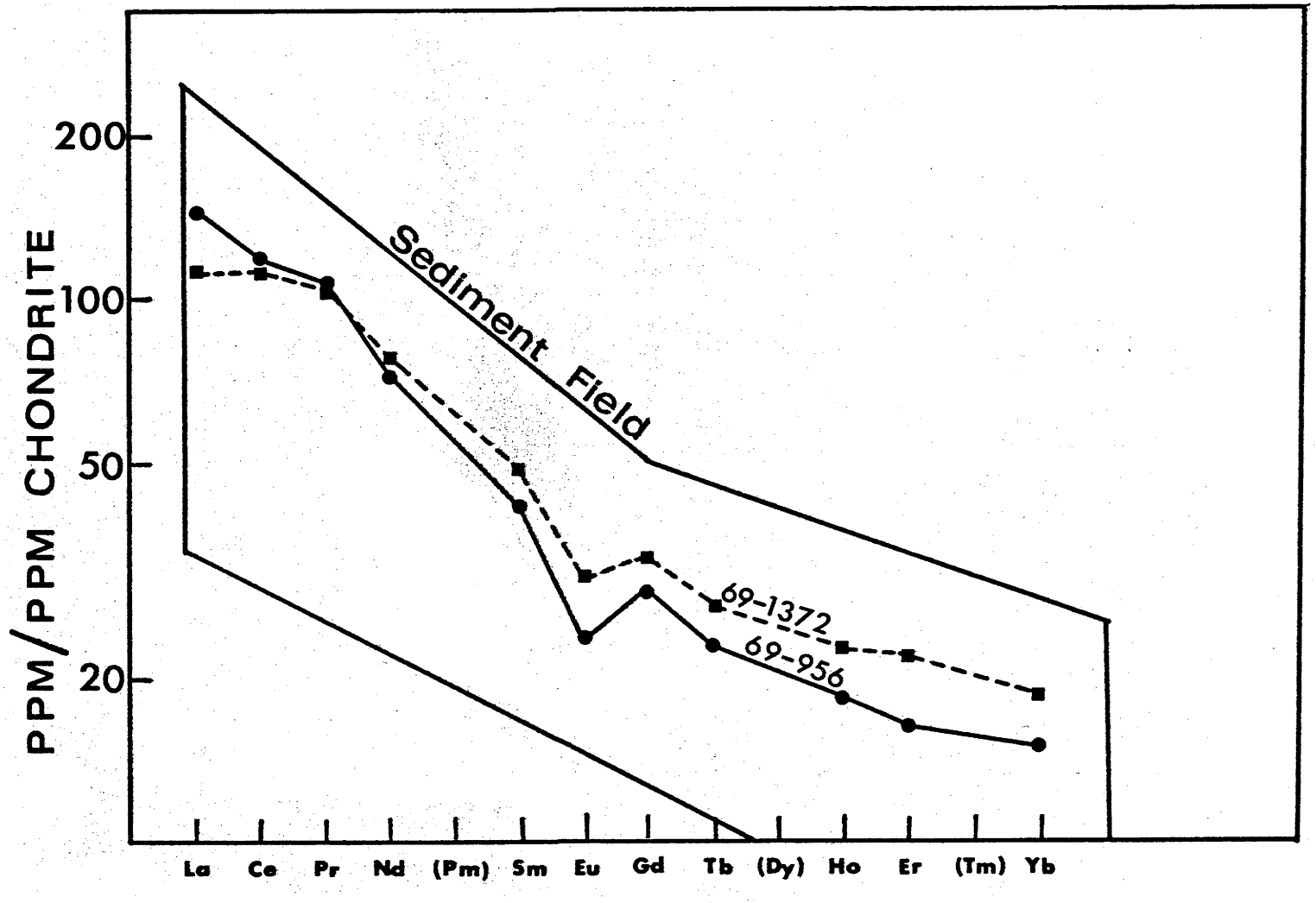

FIGURE 3.3 : RARE EARTH ELEMENT PATTERNS OF TWO HIGH-K GARNET-FREE CHARNOCKITES.

TABLE 3.1

HIGH-POTASSIUM CHARNOCKITES

——— Increasing Silica ———→

	69-789	69-1372	69-954	69-956
K/Rb	223	191	190	188
K/Csx10^{-3}	21.1	19.3	18.8	17.9
Ba/Rb	5.6	4.5	4.3	4.3
K/Ba	40.2	42.8	44.2	44.0

TABLE 3.2

COMPARISON OF AVERAGE GRANODIORITE AND HIGH-K CHARNOCKITE

	Average Granodiorite		Average of 4 High-K Garnet-Free Charnockites	
	(1)	R/2	(2)	S.D.
SiO_2	66.7	1.6	65.8	0.7
TiO_2	0.7	0.4	0.8	0.03
Al_2O_3	15.6	0.7	15.1	0.3
*total FeO	4.3	0.5	5.3	0.2
MnO	0.1	---	0.1	0.01
MgO	1.9	0.3	1.3	0.1
CaO	3.4	0.8	3.6	0.3
Na_2O	3.4	0.6	2.9	0.02
K_2O	3.3	0.7	4.5	0.1
P_2O_5	0.3	0.1	0.3	0.02
Total	99.7		99.7	
Rb	134	83	188	18
Ba	893	525	865	20
Sr	525	384	181	12
Ga	20	3	18	1
Th	12	4	16	4
U	3	0.6	2.1	0.3
Pb	22	7	27	0.5
Zr	224	95	268	6
Nb	20	---	15	0.5
La	46	6	53	2
Ce	88	7	113	3
Y	30	8	36	1
Sc	16	5	14	1
V	70	16	44	3
Cr	35	14	23	1
Co	11	4	10	3
Ni	16	7	12	4
Cu	22	8	24	2
Zn	60	---	72	4
Li	27	8	25	8
Cs	3	2	1.9	0.2
Hf	2	---	7.2**	---
***K/Rb	204		199	
K/Pb	1250		1380	

*total iron as FeO
**average of two
***ratios are calculated from averages.

Notes: (1) Granodiorite data compiled as follows: Turekian & Wedepohl (1961), Taylor (1962), Kolbe & Taylor (1966b), de Albequerque (1971), Poldervaart (1955), Condie & Lo (1971), Clark et al (1966); (2) R/2: ½ max. range of averages used in grand average; (3) S.D.: standard deviation.

within, and near the middle of the granodiorite range. The one exception is Sr which is low in the charnockites (181 cf. 525 ppm for average granodiorite) but within the lower part of the expected granodiorite range. Low Sr (90 - 130 ppm) is characteristic of early sodic Archaean granites (Glikson, 1971), but not characteristic of Archaean potassic granites. The low Sr may be a regional geochemical peculiarity at Eyre Peninsula.

The absence of migmatites and pegmatites associated with the high-K charnockites can be explained by crystallisation of a batholith with low water content, or by metamorphism of a crystalline batholith with minor water content. The high-K charnockites do not contain normative corundum and probably crystallised from melts poor in water (Luth et al., 1964). The batholith was probably metamorphosed to a minor extent subsequent to magma crystallisation.

The high-K charnockites plot close to the average adamellite and granodiorite in Q-Ab-Or and Ab-Or-An plots, and within the Q-Ab-Or field of plutonic melts with total Q+Ab+Or+An greater than 80% (figures 3.5, 3.6 and 3.7). The normative Q+Ab+Or (69-73%) and Q+Ab+Or+An (85-88%) in the charnockites are nearly identical to the corresponding values for the average granodiorite (71% and 86% respectively), stressing the similarity of the two. The high-potassium garnet-free charnockites are not minimum melts (figures 3.5, 3.6 and 3.7) but plot within the granodioritic-granitic melt and have acid plutonic melt compositions.

The water contents of the charnockites (0.2 - 0.4%) suggest an initial melt water content of 1 - 3% after allowing for loss of some water to possible high level pegmatites not represented at the present level of erosion and as fluid phase into the surrounding metamorphic gneisses. The amount of hornblende and/or biotite moulded upon orthopyroxene (appendix A) is usually minor and may represent primary igneous or secondary metamorphic crystallisation. In the latter case water may have been added to the

charnockites from the surrounding gneisses, and the water content after magmatic crystallisation would have been even lower than 0.2 - 0.4%, and the melt water content perhaps lower than 3%. Assuming water contents as high as 4% results in liquidus temperatures of approximately 900°C (chapter 8) at pressures of 7 - 9 kb acting during metamorphism (chapter 6); or if water contents of 2% or 1% are assumed the liquidus temperatures would be approximately 1,000° and 1,100°C respectively. Temperatures of ∿ 900°C are consistent with metamorphic conditions estimated in chapter 6, suggesting ∿ 4% water in the melt.

Available data indicates that the high-potassium garnet-free charnockites are part of a water-undersaturated intrusive batholith. The charnockites were not modified significantly by metamorphism, and the weak to moderate gneissic foliation may have developed during late magmatic crystallisation.

3.2 THE GARNET-SYMPLECTITE CHARNOCKITES

(Samples analysed: 69-746, 69-938, 69-1378, 69-1381: appendix C.)

3.2.1 Field Appearance

The garnet-symplectite charnockites occur in a band greater than several 100 metres wide adjacent to the graphitic calc-silicates, and were sampled along approximately 1 km. strike length. The group is characterised by the presence of garnet in massive dark-green charnockite containing coarse feldspars in a finer grained matrix. (Garnet occurs in the other charnockites only in "reaction zones" adjacent to basic inclusions: chapter 5). Pegmatites are commonly associated with the garnet-symplectite charnockites. The charnockites are characterised in the handspecimen by very dark green colour.

3.2.2 Mineralogy

The garnet-symplectite charnockites are dominantly composed of quartz, plagioclase and orthoclase with lesser

amounts of garnet, orthopyroxene, clinopyroxene and hornblende (appendix A). The garnet occurs as separate euhedral to subhedral grains, or as garnet-quartz symplectitic intergrowths occurring between orthopyroxene, clinopyroxene, hornblende or magnetite/ilmenite and plagioclase or orthoclase feldspars. Hornblende occurs as discrete grains and intergrown with orthopyroxene.

One garnet analysed is extremely rich in Fe and poor in Sc, V, Cr, Co and Ni (table 3.3) reflecting the composition of the host gneiss. The garnet is dominantly almandine-grossular with moderate andradite-content. Enrichment of garnet-bearing gneisses in Y and heavy REE during anatectic fractionation (chapter 8) is emphasised by the efficient concentration of Y (= heavy REE) in the garnet.

3.2.3 Geochemistry

Major element compositions are broadly similar to the high-K garnet-free charnockites (table 3.4) although average SiO_2 is much higher ($\sim$ 4%), Al_2O_3 much lower ($\sim$ 2½%), and CaO and MgO lower ($\sim$ 1%). Also more variation occurs in major elements (especially in silica and iron) in the garnet-symplectite charnockites than in the high-K charnockites (table 3.5, figure 3.9 and appendix C). However, trace element compositions are nearly completely different: Ba, Zr, Y, K/Rb and Zr/Nb are considerably higher in the garnet-symplectite charnockites, and Rb, Sr, Th, U, Sc, V, Cr, Co, Ni, Cu and Li are considerably lower.

The observed variation in geochemistry in the garnet-symplectite charnockites is erratic and cannot be correlated with silica. To illustrate this, some of the elements showing smooth variation with respect to silica in the high-K charnockites (3.1.3) are plotted in figure 3.4 using the same relative vertical and horizontal scales for Rb, Sr, Zn but reduced vertical scale for Zr, Ba: the variation with silica for these elements, as well as for K, La, Ce, Y and Th is erratic. The large irregular variation in composition over such relatively small distances together with

TABLE 3.3

GARNET FROM GARNET-SYMPLECTITE CHARNOCKITE (69-1381)

SiO_2	39.55
TiO_2	0.04
Al_2O_3	19.51
Fe_2O_3	2.84
FeO	28.46
MnO	1.34
MgO	0.64
CaO	7.71
Na_2O	nd
K_2O	0.07
*Y_2O_3	0.09
Total	100.25

Mole % of End Members	
Pyrope	2.8
Almandine	69.7
Grossular	14.8
Spessartine	3.3
Andradite	9.4

Sc	29
Co	11
Cu	13
Ba	9
Y	670

nd = not determined;

trace elements not detected by emission spectroscopy: V, Cr, Ni, Sr and La.

TABLE 3.4

COMPARISON OF AVERAGE COMPOSITION OF HIGH-K AND GARNET-SYMPLECTITE CHARNOCKITES

	High-K Garnet-Free Charnockites	Garnet-Symplectite Charnockites
SiO_2	65.8	69.9
TiO_2	0.8	0.6
Al_2O_3	15.1	12.8
*total FeO	5.3	5.8
MnO	0.1	0.1
MgO	1.3	0.3
CaO	3.6	2.6
Na_2O	2.9	2.8
K_2O	4.5	4.2
P_2O_5	0.3	0.2
Rb	188	91
Ba	865	977
Sr	181	132
Th	16	10
U	2.1	0.5
Zr	268	532
Nb	15	16
Y	36	62
Sc	14	9
V	44	3
Cr	23	< 1
Co	10	< 3
Ni	12	< 1
Cu	24	4
Zn	72	78
Li	25	5
K/Rb	198	387
Zr/Nb	17.9	33.3

*Total iron as FeO

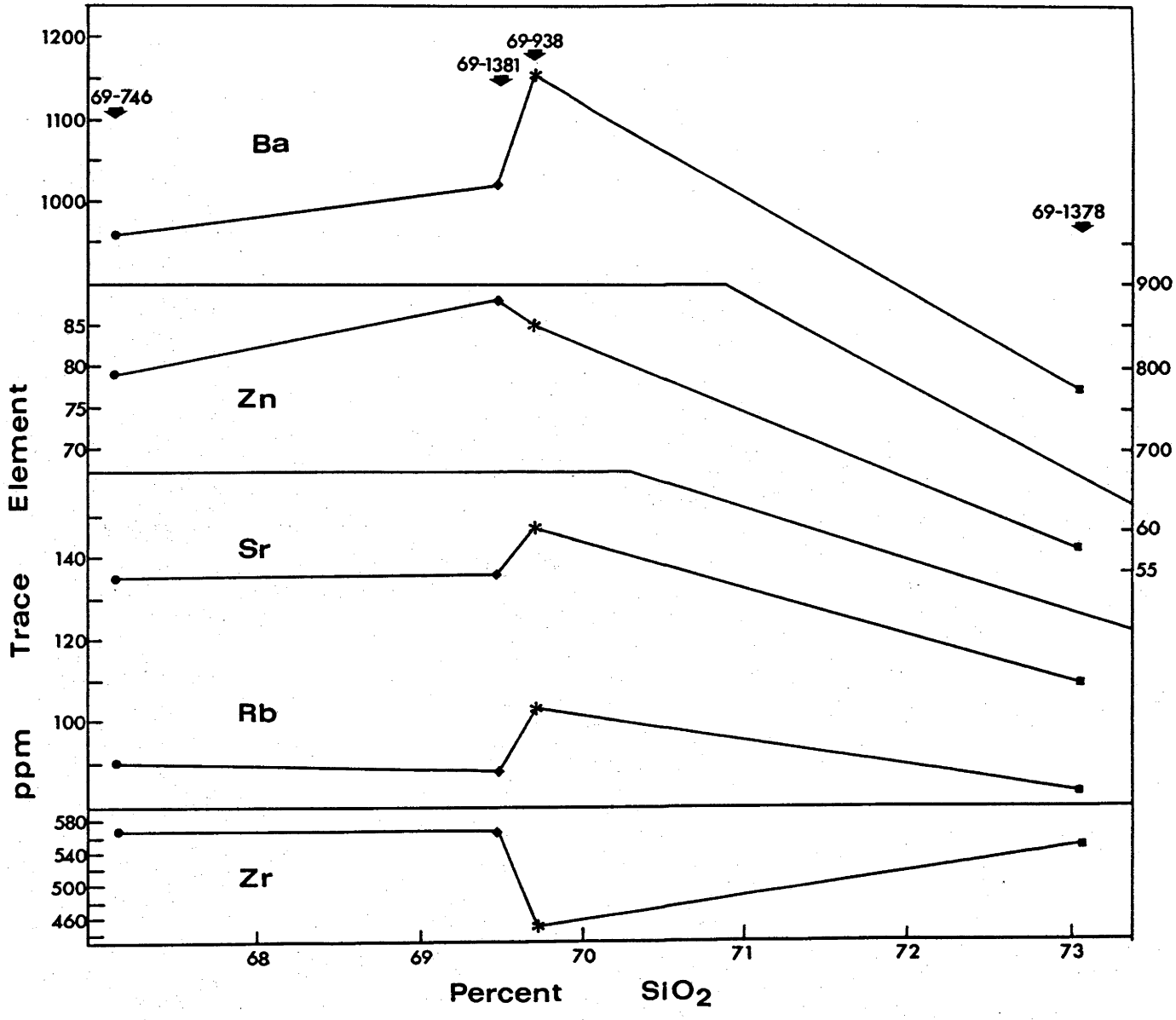

FIGURE 3.4 : ERRATIC VARIATION OF TRACE ELEMENTS IN THE GARNET-SYMPLECTITE CHARNOCKITES.

the close association with undoubtedly sedimentary graphitic calc-silicate rocks (appendix E) indicate that the garnet-symplectite charnockites are of sedimentary origin. Their very high Fe/Mg ratios suggest they are a sedimentary facies transitional to the iron formations further to the north (Whitten & Risley, 1968). It is tempting at first to suggest sedimentary derivation of the garnet-symplectite gneisses by erosion of the broadly similar charnockite pluton, however the vast differences in trace element geochemistry especially in the diagnostic zircon Zr/Nb indicate completely different provenance.

An outstanding characteristic of the garnet-symplectite charnockites is the moderate FeO (3.2 - 5.1%) and low MgO (0.18 - 0.33%) yielding the extremely high molar FeO/(FeO+MgO) ratios (0.89 to 0.91) responsible for the formation of garnet and garnet-quartz symplectites at lower pressures than required in other charnockites (chapter 6).

The major element composition of the garnet-symplectite charnockites is close to the average adamellite (column 2 of table 3.5) except that Al_2O_3 is $\sim$ 2% low, MgO is $\sim$ 1% low and total FeO is $\sim$ 2% high. Also, the trace element geochemistries are completely different: Ba, Zn, Zr and Hf are too high in the garnet-symplectite charnockites and Rb, Sr, Th, U, Sc, V, Cr, Co, Ni, Cu and Li are too low. Similar geochemical objections arise if a granodioritic composition is considered (tables 3.2 and 3.5). Geochemistry precludes the possibility of an adamellitic-granodioritic igneous origin.

The major element compositions of the charnockites are intermediate to the low-silica arkose and greywacke (columns 2 and 3 of table 3.5), except that total Fe is higher and Mg lower. Trace element data for arkoses were assumed similar to the average granite (the average granite major element chemistry is quite close to the arkose, except for lower Ca and hence lower Sr: table 3.5). Sr, V, Cr, Co, Ni and Cu can be very low in granites (and arkoses) (table 3.5) and the low Sr, V, Cr, Co, Ni and Cu in the charnockites

TABLE 3.5

COMPARISON OF GARNET-SYMPLECTITE CHARNOCKITE GEOCHEMISTRY WITH COMPILED AVERAGES

	Average of 4 Garnet-Symplectite Charnockites		Average Adamellite	Average low SiO_2 Arkose	Average Granite		Average Greywacke		Average of Greywacke and Granite
	(1)	S.D.		(2)	(3)	R/2	(4)	R/2	(5)
SiO_2	69.9	2.5	69.8	73.7	72.9	3.6	68.8	2.3	70.9
TiO_2	0.6	0.1	0.5	0.4	0.3	0.2	0.7	0.2	0.5
Al_2O_3	12.8	0.5	14.7	12.0	13.8	0.9	14.6	0.9	14.2
*total FeO	5.8	1.2	3.4	3.0	2.5	2.2.	4.9	0.5	3.7
MnO	0.1	0.03	0.1	0.3	0.1	—	0.2	0.05	0.2
MgO	0.3	0.06	1.3	0.3	0.7	1.2	2.4	0.6	1.6
CaO	2.6	0.5	2.3	2.1	1.1	0.7	3.1	0.5	2.1
Na_2O	2.8	0.2	3.3	2.7	3.1	1.0	3.2	0.4	3.2
K_2O	4.2	0.3	4.1	5.1	4.8	0.6	2.0	0.2	3.4
P_2O_5	0.2	0.04	0.3	—	0.2	—	0.2	0.05	0.2
Total	99.3		99.8	99.6	99.5		100.1		100.0
Rb	91	9	193		251	109	51	—	151
Ba	977	157	769		644	738	356	105	500
Sr	132	16	318		111	149	204	70	158
Ga	20	1.5	19		18	4	14	—	
Th	10.	3	18		23	10			
U	0.5	0.2	6		8	5			
Pb	26	2	25		28	7			
Zr	532	57	197		169	67	291	109	230
Nb	16	2	21		21	—			
La	58	7	42		38	20			
Ce	119	15	92		95	158			
Y	62	16	30		29	8			
Sc	9	3	11		6	6	8	—	7
V	3	2	49		28	29	94	27	61
Cr	<1	—	26		16	26	174	34	95
Co	<3	—	8		5	8	31	9	18
Ni	<1	—	12		8	13	56	23	32
Cu	4	2	16		10	13	34	3	22
Zn	78	14	40		39	—	54	8	47
Li	5	2	31		35	7	40	—	38
Cs	—	—	6		8	6			
Hf	10**		4		5	4			
***K/Rb	383				159		326		

*total iron as FeO
**average of 2
***K/Rb of average

Notes: (1) R/2 is one half the maximum range of averages used in grand average
(2) S.D. is standard deviation.

Data Compiled as follows:

granite: same sources as granodiorite in table (3.2); "adamellite": average of average granite and granodiorites; arkose: Pettijohn (1956); Greywacke: Pettijohn (1956), (1963); Poldervaart (1955), Taylor (1962), Rivalenti & Sighinolfi (1969).

could be partly explained by incorporation of granitic detritus. The high Ba could also be explained by granitic detritus rich in Ba (table 3.5). However the average granitic-arkose/greywacke composition (table 3.5, column 5) is still much too low in Zr. The high Zr could be explained by a zircon-rich sediment. Field relationships, major element and trace element compositions support a sedimentary origin and preclude a granitic-granodioritic batholithic origin. The best approximation to the garnet-symplectite charnockite composition is a granitic-arkose/greywacke sediment in which the granitic detritus was rich in Ba and Zr and relatively poor in Rb, Li, V, Cr, Co, Ni and Cu. The iron-rich character and unusual trace element geochemistry of the sediments is probably due to conditions similar to those resulting in deposition of iron formations further to the north.

The garnet-symplectite charnockites cover a wider field in normative Q-Ab-Or and Q-Ab-Or-An plots than the high-K garnet-free charnockites (figures 3.5, 3.6 and 3.7): the scatter indicates that the charnockites were not melts formed under uniform conditions, in direct contrast to the high-K garnet-free charnockites. The charnockites plot within the granite field close to the 0.5 - 1 kb Pe_{H_2O} minima (figure 3.6) and are only slightly removed from the Ab-Or-An liquidi and minima (figure 3.7) and Q-Ab-Or minimum melts predicted by An-contents (figure 3.5). The total Q+Ab+Or for the charnockites are very high (75 to 83½%) approaching that of the average granite (87%). Geochemical data indicate that the garnet-symplectite charnockites are not granitic-granodioritic melts. However, their compositions are extremely favourable for anatexis, and melting would commence readily if free water vapour were present. If appreciable water were present, either as vapour or combined in hydrous minerals (chapter 8), extensive melting would have occurred during metamorphism. Pegmatites are reasonably common associates, but are of minor volume compared with massive apparently unmelted garnet-symplectite charnockites, and water must have been considerably restricted. If "pure" water-bearing fluid existed before commencement of melting,

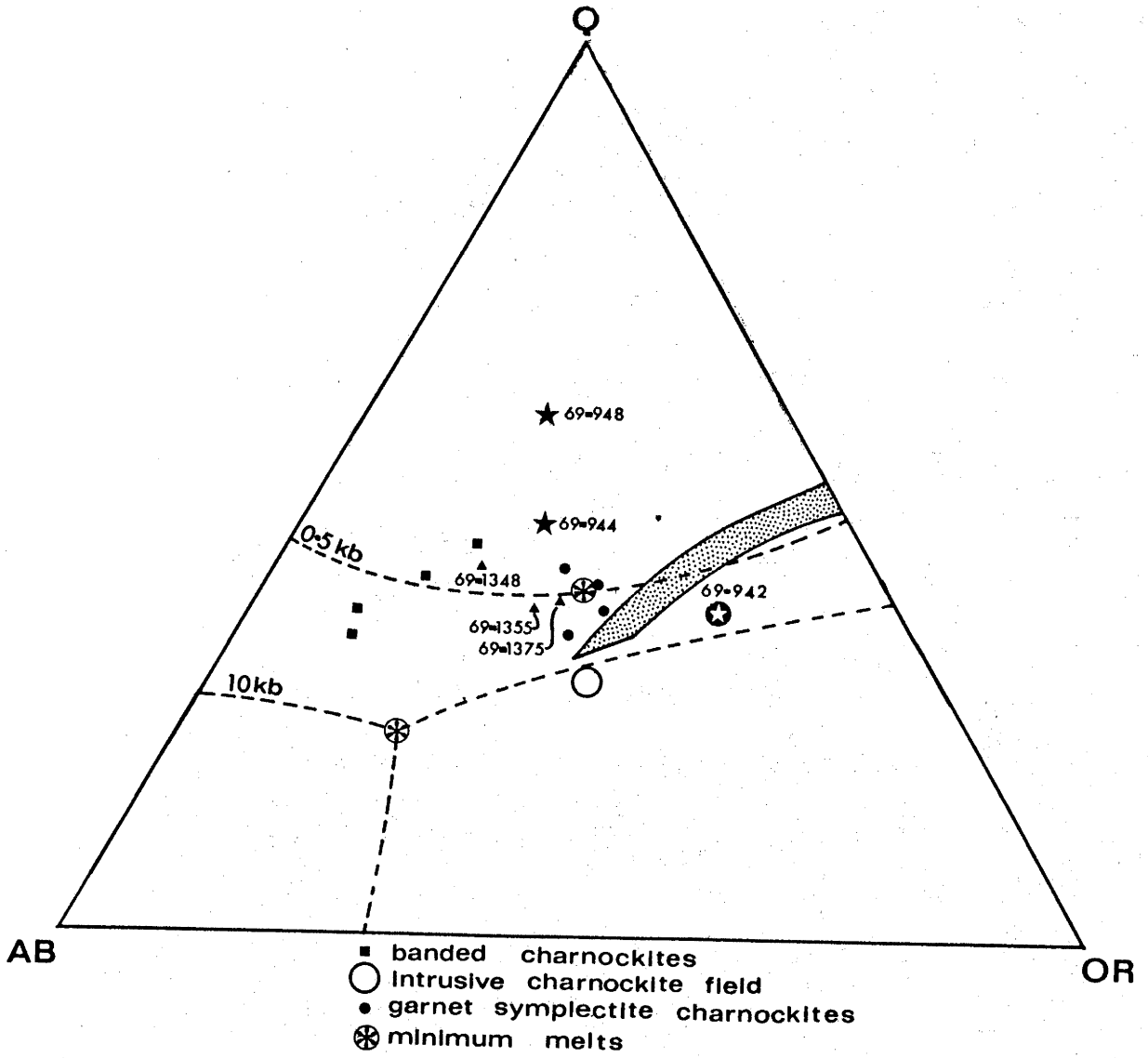

FIGURE 3.5 : NORMATIVE Q-AB-OR PLOT FOR THE ACID GNEISSES.

The stippled band represents the minimum melt compositions predicted by experimental data (Tuttle & Bowen, 1958; Luth et al., 1964; von Platen, 1965a&b; and James & Hamilton, 1969) for the garnet-symplectite charnockites, the banded charnockites, two garnet-gneisses (69-1348 and 69-1375) and the migmatite (69-1355), for Pe_{H_2O} ranging from ∿8 kb (at the lower end of the stippled band) to ∿1 kb (at the upper end of the stippled band). (The effect of An on minimum melt compositions was assumed to be similar for high and low Pe_{H_2O}, and the nett effect of An (8-20%), Ab/An (2-4) and Pe_{H_2O} was then estimated.) The cotectics and minimum melts (*) for 0.5 to 10 kb Pe_{H_2O} for the "granite" system are from Tuttle & Bowen (1958) and Luth et al., (1964). The open circles numbered 1, 2 and 3 are the average granite, adamellite and granodiorite from tables 3.2 and 3.5.

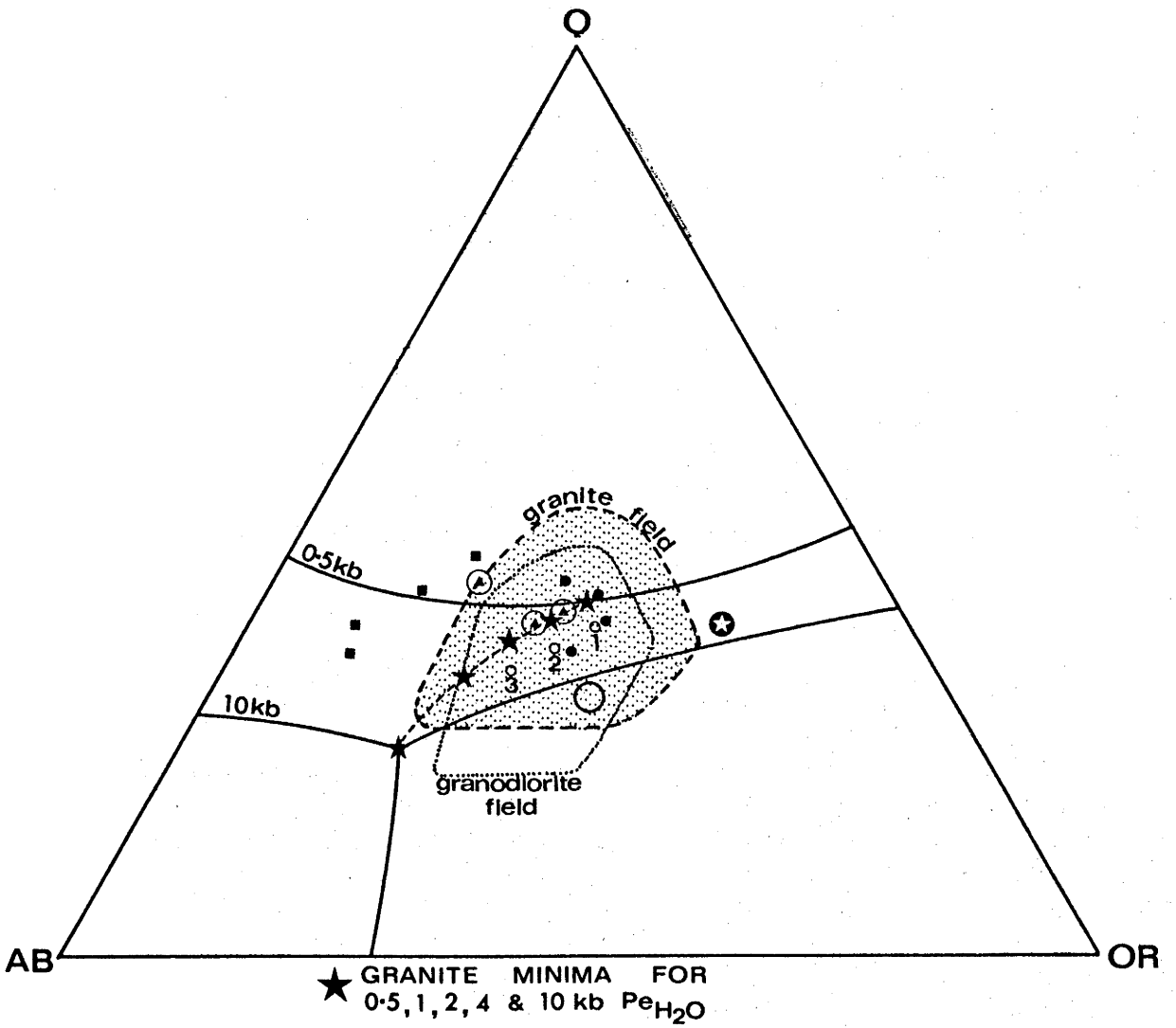

FIGURE 3.6 : NORMATIVE Q-AB-OR PLOT FOR THE ACID GNEISSES.

The fields of maximum concentration for granites (Q+Ab+Or > 80%) (stippled field) and for granodiorites (Q+Ab+Or+An > 80%) are from Winkler & von Platen (1961b) and James & Hamilton (1969). (The granodiorites contain up to 13% An.) All symbols used correspond to those in figure 3.5, except that the three triangles are encircled for clarity, and the stars in figure 3.6 represent granite minima.

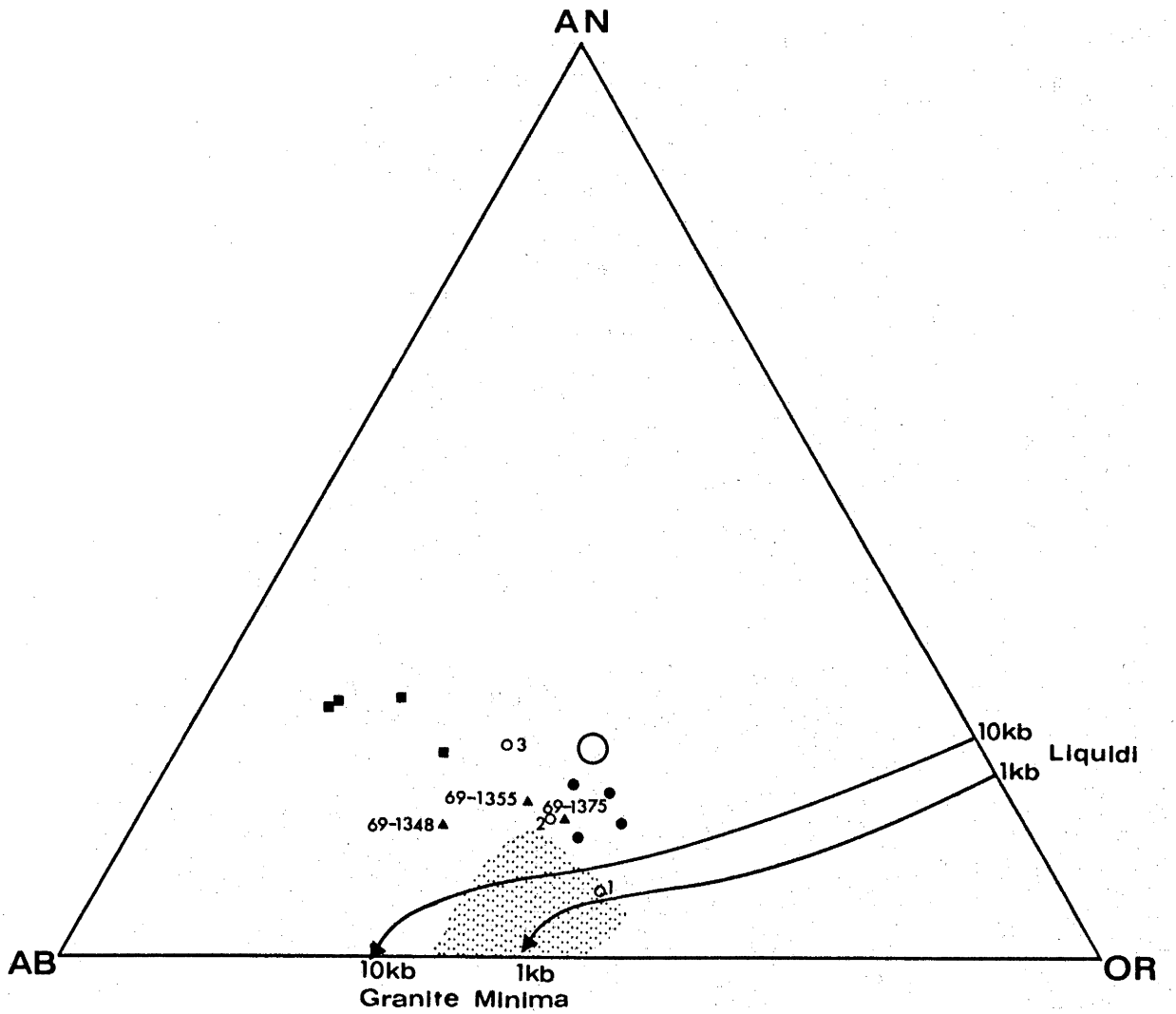

FIGURE 3.7 : NORMATIVE AB-OR-AN PLOT FOR THE ACID GNEISSES.

The 1 kb Pe_{H_2O} liquidus and minimum, and the field of granites are from James & Hamilton (1969). The 10 kb Pe_{H_2O} liquidus and minimum are estimated from the experimental data of Luth et al., (1964) assuming similar geometry to the 1 kb liquidus. All symbols used correspond to those in figures 3.5 and 3.6.

fluid-Pe_{H_2O} must have equalled total pressure (viz. 7-9 kb) but would have decreased rapidly to zero as the restricted water dissolved in the melt. (More detailed discussions of fluid composition and pressure will be included in chapters 6 and 8).

No accurate estimates were made of the volume of pegmatites, which was less than about 10%. If 15% water solubility in the melt is assumed, approximately 6½% water-saturated melt can form from an initial water content of 1%. The volume of pegmatites (assumed water-saturated) observed is in accordance with an initial water content of about 1%. Allowing for the melts to be up to 50% under-saturated with water and the volume of melt to approach 10% raises the estimate to 3% initial water prior to anatexis - the figure estimated by Burnham (1967) for likely water content of high grade metasediments prior to anatexis at pressures of 7-9 kb.

3.3 THE COMPOSITIONALLY BANDED CHARNOCKITES

(Samples analysed: 69-787, 69-951, 69-1363, 69-1367: appendix C).

3.3.1 Field Appearance

The compositionally banded charnockites are characterised in the field by alternating light and dark coloured metre to centimetre scale layers. The darker layers are similar to the other charnockite types except for finer-grained appearance. The charnockite handspecimens contain alternating light and dark grey to bluish-grey layers, or alternating light and dark greyish-green to green layers. Some handspecimens may contain only one type of compositional layer. One calc-silicate rock (69-777) was observed interlayered with the banded charnockites. Pegmatites are commonly associated with the charnockites.

3.3.2 Mineralogy

Quartz, plagioclase, orthoclase and lesser amounts of orthopyroxene, hornblende and biotite are the dominant

minerals in the banded charnockites (appendix A). The mafic minerals are much less abundant in the lighter-coloured bands. One of the charnockites (69-1367) contained minor garnet. No minerals from the charnockites were analysed.

3.3.3 Geochemistry

The low-melting components in the banded charnockites are sufficiently high to be granodioritic melts (total Q+Ab+Or range from 71 to 81% compared with 71% for the average granodiorite; and total Q+Ab+Or+Ab from 89 to 94% compared with 86% for the average granodiorite). However, the charnockites plot outside the Q-Ab-Or granitic-granodioritic melt field (figure 3.6) and significantly distant from the liquidi and minima in the Ab-Or-An diagram (figure 3.7). Low-melting component plots indicate that the banded charnockites are not grandioritic melts, and favour sedimentary origin.

The large variation in geochemistry (appendix C) and the banded nature of the charnockites also suggest a sedimentary origin. The compositionally banded charnockites are characterised by high Na, Na/K and K/Rb, low K, Rb and Zr, and are similar to the average greywacke (table 3.6). The charnockites are slightly richer in Si, Al, Ca, Na, Ba and Sr, and poorer in K, Rb, Fe, Mg and Zr than the average greywacke, but most are not significantly outside the range of greywacke compositions. V, Cr, Co and Ni are much lower than in the greywacke and probably reflect the same sedimentary environment which led to depletion of these elements in the garnet-symplectite charnockites. Li, Rb and Zr are lower than expected in greywackes and will be discussed in chapter 8.

3.4 THE GARNET-GNEISSES

(Samples analysed: 69-942, 69-944, 69-948, 69-1348, 69-1375: appendix C).

TABLE 3.6

COMPARISON OF COMPOSITIONALLY BANDED CHARNOCKITES AND GREYWACKE

	Average Charnockite	Greywacke Average	Greywacke ±R/2**
SiO_2	69.7	68.8	2.3
TiO_2	0.4	0.7	0.2
Al_2O_3	15.5	14.6	0.9
*total FeO	3.2	4.9	0.5
MnO	0.1	0.2	0.1
MgO	1.1	2.4	0.6
CaO	3.8	3.1	0.5
Na_2O	4.2	3.2	0.4
K_2O	1.8	2.0	0.2
P_2O_5	0.1	0.2	0.1
Total	99.9	100.1	
Rb	28	51	--
Ba	595	356	105
Sr	246	204	70
Zr	161	291	109
V	36	94	27
Cr	10	174	34
Co	9	31	9
Ni	5	36	23
Li	10	40	--
K/Rb	577	326	

*total Fe as FeO; ** R/2 is one half of the range of averages used for grand average; Greywacke is from table 3.5.

3.4.1 Field Appearance

The garnet-gneisses are characterised in the field by pink to pinkish-mauve garnet set in a light-coloured white to bluish-grey matrix of quartz and feldspars, (in contrast to the dark-coloured charnockite quartz and feldspars). Several of the garnet-gneisses are characterised in the field by complexly deformed and folded centimetre-scale compositional layering (69-942, 69-944, 69-948 and 69-1348). One of these (69-942) occurs intimately and conformably interbanded on a metre-scale with graphitic schist and graphitic calc-silicate rocks of undoubted sedimentary origin (appendix E). One massive garnet-gneiss (69-1375) has poorly defined gneissic foliation but no obvious compositional banding. Pegmatites and migmatites are common associates.

3.4.2 Mineralogy

The garnet-gneisses are dominantly composed of quartz, plagioclase, orthoclase, garnet and biotite (appendix A). Many of the gneisses contain sillimanite (e.g. 69-942, 69-944, 69-948). Orthoclase and biotite may be minor. The garnets from two garnet-gneisses (table 3.7) are dominantly almandine-pyrope with minor andradite, spessartine, grossular and uvarovite. The garnets are enriched in Sc, V, Cr, Co and Y due to the strong partitioning of these elements into residual garnet during anatectic fractionation (chapter 8). The biotite coexisting with one of the garnets is very rich in V, Cr, Co and Ni (table 3.8). The biotite probably crystallised at the expense of garnet after anatexis ceased, and V, Cr, Co and Ni originally in the garnet were strongly partitioned into the biotite. The very low Ni in the other garnet (69-948), but high Ni in the host gneiss, may be due to minor coexisting biotite or to the presence of sulphides. (Ni would be very strongly partitioned into the sulphide phase.)

TABLE 3.7

GARNETS FROM GARNET-GNEISSES

	69-944	69-948
SiO_2	38.98	38.64
TiO_2	0.04	0.05
Al_2O_3	22.38	22.28
Fe_2O_3	1.67	0.95
FeO	23.44	25.26
MnO	0.35	0.66
MgO	11.51	10.19
CaO	1.11	1.11
Na_2O	nd	nd
K_2O	0.03	0.04
Trace*	0.16	0.18
Total	99.67	99.36
Sc	72	95
V	250	260
Cr	600	510
Co	45	35
Ni	--	~8
Cu	6	8
Y	140	325
MOLE PERCENT OF END MEMBERS		
Pyrope	42.8	39.9
Almandine	51.2	55.5
Grossular	--	0.1
Spessartine	0.8	1.5
Andradite	2.8	2.8
Uvarovite	0.3	0.2
Khoharite	2.1	--

*Sc_2O_3, Y_2O_3, Cr_2O_3 and V_2O_5; Ba, Sr and La not detected by emission spectroscopy; nd means not determined; - means not detected; End members are in mole % (khoharite is Mg-Fe^{3+} garnet).

TABLE 3.8

BIOTITE FROM GARNET GNEISS (69-944)

SiO_2	37.56
TiO_2	5.16
Al_2O_3	16.20
Fe_2O_3	0.42
FeO	10.89
MnO	0.02
MgO	16.14
CaO	0.09
Na_2O	0.13
K_2O	9.24
H_2O+	2.89
H_2O-	0.55
F	0.81
Trace*	0.56
Total**	100.43

Rb	350
Ba	~ 1500
Sc	8
V	1070
Cr	1070
Co	76
Ni	220
Cu	8
Li	29
Cs	2.1
K/Rb	219

Structural Formula Based on 22 oxygens (anhydrous basis)

	Si	5.462
	AlIV	2.538
Y	AlVI	0.239
	Ti_{3+}	0.564
	Fe^{3+}	0.046
	Fe^{2+}	1.325
	Mn	0.003
	Mg	3.498
X	Ca	0.014
	Na	0.036
	K	1.714
	Sum X	1.764
	Sum Y	5.675

*includes Cr_2O_3, V_2O_5, NiO, BaO and Rb_2O

**Corrected for O=F

3.4.3 Geochemistry

3.4.3.1 Garnet-Gneisses Rich in Garnet (69-944 & 69-948)

The garnet-rich gneisses are enriched in Fe, Mn, Mg, V, Cr, Co, Ni and Y (table 8.13).

The gneisses plot significantly above the 0.5 kb cotectic and minimum (figure 3.5), due to quartz in excess of the minimum melt proportions. The total content of low melting components in one (69-948) (total Q+Ab+Or+An = 66%) is well below that expected in even granodiorites (86%). The total low-melting components in the other (69-944) are also significantly below the granodiorite values (total Q+Ab+Or+An of 75% cf. 86%). Both gneisses are considered to be depleted in low melting components by anatexis. Their geochemistry and fractionation will be considered in chapter 8.

3.4.3.2 Biotite-K-feldspar-sillimanite-garnet Gneiss (69-942)

The gneiss has distinctive geochemistry, with very high K, Rb, Pb, Th, U and Li (table 3.9). The major element chemistry corresponds closely to the average silt (table 3.9) except SiO_2 and Al_2O_3 are $\sim$ 1% higher, total FeO is $\sim$ 3% lower and MgO is $\sim$ 1½% lower. Th, U, Pb, Ba and Rb are higher than in the average silt, greywacke or shale (tables 3.5 and 3.9). Major and trace element geochemistries are within or only slightly outside the shale range (table 3.9), except that Fe, V, Ni, are considerably higher (but are much closer to the silt) and K is considerably lower (although corresponding closely with the silt). On this evidence, the gneiss could be a potassic shaly-silt. However, REE data (3.6 and figure 3.11) indicate a fractionated igneous origin. The strongly fractionated REE pattern with negative Eu anomaly precludes a wholly sedimentary origin, but does not necessitate a totally pegmatitic melt origin, and some sedimentary residuum could be present. The gneiss contains alternating schlieren of K-feldspar-quartz and biotite-sillimanite but very little plagioclase.

TABLE 3.9

COMPARISON OF 69-942 WITH AVERAGE SHALE AND SILT

		69-942	Average Glacial Silt	Average Shale	R/2
	SiO_2	67.66	66.4	64.5	2.7
	TiO_2	0.59	0.3	0.7	---
	Al_2O_3	17.77	16.6	16.7	0.5
*total	FeO	2.48	5.4	6.5	0.3
	MnO	0.02	---	0.1	---
	MgO	1.30	2.8	2.9	0.6
	CaO	0.38	0.9	3.0	0.7
	Na_2O	1.73	1.1	1.4	---
	K_2O	6.33	6.0	3.6	0.1
	P_2O_5	0.13	0.1	0.2	0.1
	Total	98.39	99.6	99.6	
	Rb	234	93	187	25
	Ba	873	455	695	115
	Sr	191	118	172	102
	Ga	24	16	21	3
	Th	38	---	12	---
	U	9.7	---	4	---
	Pb	47	18	26	8
	Zr	219	207	169	27
	Nb	23	---	11	---
	La	59	---	66	27
	Ce	116	---	68	9
	Y	35	---	40	12
	Sc	7	8	16	4
	V	55	66	125	5
	Cr	67	55	98	10
	Co	< 2.5	9	18	1
	Ni	12	22	61	9
	Cu	11	22	33	14
	Zn	43	---	95	---
	Li	40	28	66	41
	Cs	1.6	3	7	4
	Hf	3.5	---	3	---
**K/Rb		225	536	160	
Zr/Nb		9.5			

*total iron as FeO
**Ratios are those of the average

Data compiled as follows:

Silt: Pettijohn (1956), Kolbe & Taylor (1966a);

Shale: Pettijohn (1956), Mason (1966), Poldervaart (1955), Heier & Adams (1964), Banno & Chappell (1969), Kolbe & Taylor (1966a).

Directly adjacent is a rock (69-941) containing coarse quartz-K-feldspar migmatitic veins with biotite-rich selvedges. Localised injection of anatectic melt enriched in light REE, K, Rb, Ba, Th, U and Li may have occurred from the migmatitic rock into the biotite-K-feldspar-sillimanite-garnet-gneiss. Although the field association of the gneiss with graphitic schist and calc-silicates intimates a sedimentary origin, the geochemistry indicates an igneous origin.

The gneiss is very rich in Or (figure 3.5), has very low An (0.6%), high Ab/An (28.5) and high total Q+Ab+Or (83%). This can be explained as a minimum melt formed by anatexis of a relatively calcic rock. Experimental data (chapter 8 and figure 3.5) suggest a source rock with Ab/An $\sim$ 1.2, and a relatively high Pe_{H_2O} of 5-8 kb. However the experimental work indicates that the liquid should have an An content of about 12% rather than the 0.6% observed. The experimental anatexis data are not consistent with geological observation. A Pe_{H_2O} of 5-8 kb would result in 10-15% water in the melt, if water-saturated melt were generated. The present water content is $\sim 1\frac{1}{2}\%$, and the large loss of water during crystallisation of the melt could explain the relatively large normative corundum of 8% through loss of alkalis with expelled fluid.

3.4.3.3 Massive Garnet-Gneiss (69-1375)

The low-melting components of the massive garnet-gneiss are very close to those of the average granodiorite (total Q+Ab+Or = 74% cf. 71%; and total Q+Ab+Or+An = 84% cf. 86% for the average granodiorite). The gneiss plots within the granitic-granodioritic melt field between the 0.5 and 1 kb minima and close to the average adamellite (figure 3.6). The gneiss also plots close to the average adamellite and reasonably close to the Ab-Or-An minima and liquidi (figure 3.7). The low melting component data suggests that the gneiss is an acid plutonic melt.

The gneiss has a strongly fractionated REE pattern with a negative Eu anomaly (figure 3.11) indicating a fractionated

igneous origin. The geochemistry of the garnet-gneiss is similar to the average granodiorite and adamellite (table 3.10). The only elements significantly outside the granodiorite range are Th (considerably higher) and Li and U (considerably lower). The garnet-gneiss has a relatively massive appearance with gneissic foliation but no compositional banding, and probably represents a metamorphosed granodiorite older than the high-K charnockites.

3.4.3.4 Banded Garnet-Gneiss (69-1348)

The low-melting components of the banded garnet-gneiss are close to those of the average granodiorite (total Q+Ab+Or = 76% cf. 71%; and total Q+Ab+Or+An = 84% cf. 86%). The gneiss plots on the border of the Q-Ab-Or granite melt field and just outside the granodiorite melt field (figure 3.6). It is reasonably close to the Ab-Or-An liquidi and minima (figure 3.7). The data suggest that the gneiss could be either a plutonic acid melt or a sediment containing a high proportion of low-melting components. The banded garnet-gneiss has major and trace element geochemistry (table 3.10) very similar to and within the range of the average granodiorite and adamellite except Sr, Th, U and Li are lower and Cr higher than usually encountered. The garnet-gneiss has a sedimentary REE pattern (figure 3.12) with no obvious Eu anomaly (cf. the igneous high-K charnockites), favouring sedimentary origin. Geochemistry cannot prove either sedimentary or igneous origin, but the banded field appearance suggests it is a sediment.

3.5 QUARTZ-FELDSPAR-GARNET-ORTHOPYROXENE "MIGMATITE" (69-1355)

3.5.1 Field Appearance

The gneiss is characterised in the field by deformed migmatitic appearance. Irregular light-coloured quartzofeldspathic bands alternating with garnetiferous dark-green charnockitic bands are complexly folded together. The gneiss occurs near the contact of charnockite with apparently mobilised "garnet-pegmatite" (69-1356).

TABLE 3.10

COMPARISON OF THREE GNEISSES WITH AVERAGE GRANODIORITE AND ADAMELLITE

	69-1348	69-1355	69-1375	Average Granodiorite	Range ±R/2	Average Adamellite
SiO_2	70.7	69.0	68.5	66.7	1.6	69.8
TiO_2	0.4	0.6	0.7	0.7	0.4	0.5
Al_2O_3	14.2	13.9	14.7	15.6	0.7	14.7
*total FeO	3.9	4.9	4.6	4.3	0.5	3.4
MnO	0.05	0.1	0.1	0.1	---	0.1
MgO	2.3	1.7	2.0	1.9	0.3	1.3
CaO	1.7	2.6	2.0	3.4	0.8	2.3
Na_2O	3.5	3.2	2.9	3.4	0.6	3.3
K_2O	2.6	3.5	3.7	3.3	0.7	4.1
P_2O_5	0.05	0.3	0.1	0.3	0.1	0.3
Rb	66	71	95	134	83	193
Ba	567	747	734	893	525	769
Sr	71	181	134	525	384	318
Th	2.9	6.6	51	12	4	18
U	0.3	0.5	0.7	3	0.6	6
Pb	9	19	14	22	7	25
Zr	135	254	262	224	95	197
Nb	13	7.7	27	20	---	21
V	71	53	72	70	16	49
Cr	122	52	58	35	14	26
Co	15	10	15	11	4	8
Ni	33	19	18	16	7	12
Zn	56	68	59	60	---	40
Li	11	9	8	27	8	31

*total iron as FeO. Average adamellite, granodiorite and range (±R/2) from tables 3.2 and 3.5 .

3.5.2 Mineralogy

The migmatite consists dominantly of quartz, orthoclase and plagioclase with lesser amounts of garnet and orthopyroxene. Quartzo-feldspathic zones alternate with irregular garnet-orthopyroxene-rich schlieren. No minerals from the migmatite were analysed.

3.5.3 Geochemistry

The migmatite has low-melting component contents similar to the average granodiorite (total Q+Ab+Or = 75% cf. 71% and Q+Ab+Or+An = 85% cf. 86%). The migmatite plots within the granitic-granodioritic melt field near the average adamellite and 1 kb minimum (figure 3.6) and reasonably close to the minima and liquidi in the Ab-Or-An plot (figure 3.7). The data suggest that the migmatite could be an acid plutonic melt.

The migmatite has similar geochemistry to the massive garnet-gneiss (69-1375: table 3.10). Major and trace element geochemistries are within or not significantly outside the granodiorite range (table 3.10) except for Nb, Li, U and Cu which are low. The low Nb results in a considerably higher Zr/Nb (33) compared with the average granodiorite (11). The migmatite has a REE pattern within and subparallel to the sedimentary field (figure 3.12) although Y is slightly depleted relative to the light REE. This suggests a sedimentary origin.

3.6 REE GEOCHEMISTRY

REE are normalised to chondritic and shale abundances, and Y in "partial" patterns is plotted at the Ho position (appendix D). The large granite-granodiorite field (figure 3.8) contains REE patterns of widely differing degrees of fractionation (chondrite-normalised La/Yb (appendix D) range from 2 to 130). All analysed acid gneisses (figure 3.9) plot within or very nearly within the granite-granodiorite field, which clearly cannot be used for identification of parent rock types.

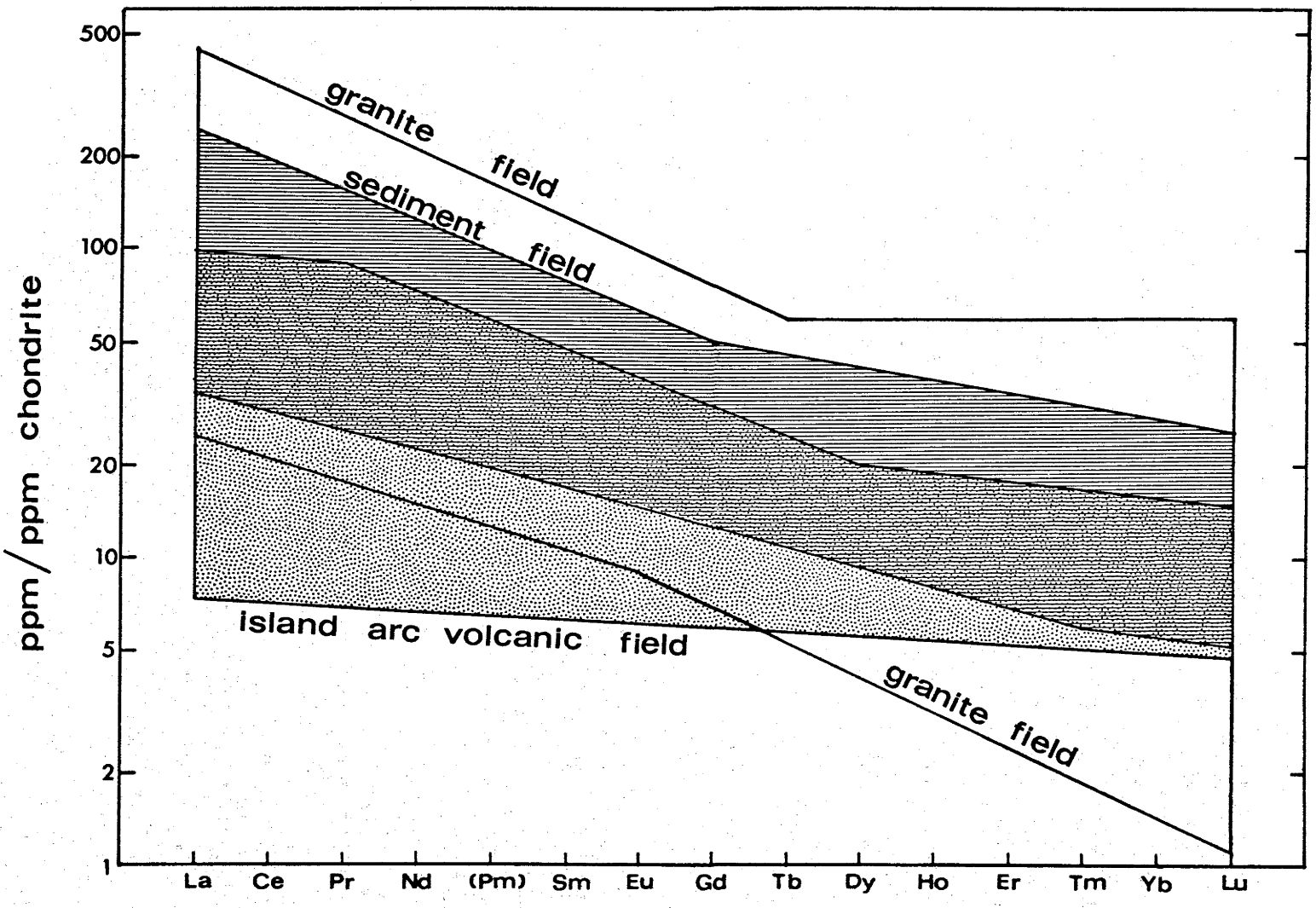

FIGURE 3.8 : COMPARISON OF THE RARE EARTH ELEMENT FIELDS FOR GRANITIC-GRANODIORITIC BATHOLITHS, ANDESITIC-DACITIC ISLAND ARC VOLCANIC ROCKS AND SEDIMENTS.

The granitic-granodioritic field was compiled from Haskin et al., (1966) and Buma et al., (1971). The island arc volcanic field was compiled from Taylor et al., (1969) and Jakeš & Gill (1970). The sedimentary field was compiled from Haskin et al., (1966, 1968).

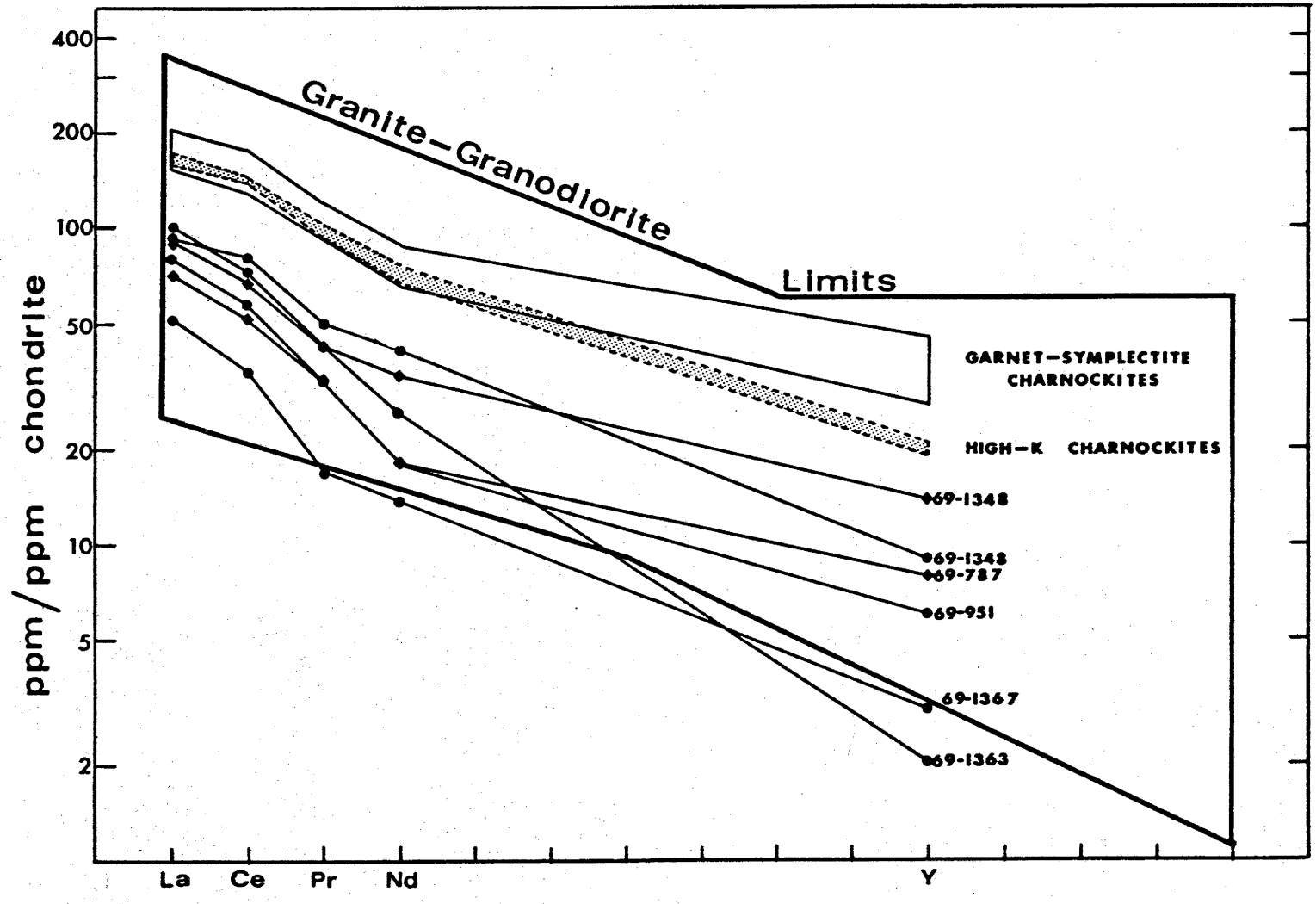

FIGURE 3.9 : COMPARISON OF THE GRANITIC-GRANODIORITIC RARE EARTH ELEMENT FIELD WITH PARTIAL RARE EARTH PATTERNS OF THE ACID GNEISSES.

The granitic-granodioritic rare earth field is from figure 3.8.

Two acid gneisses plot within the andesite-dacite island arc volcanic field (figure 3.10). The degree of REE fractionation in one of the gneisses (69-1348: chondrite-normalised La/Yb=7) is equivalent to the maximum fractionation in the island arc acid-intermediate volcanic rocks (chondrite-normalised La/Yb ranges from 3 to 7). The other gneiss (69-787: chondrite-normalised La/Yb = 11) is more fractionated than the island arc volcanic rocks. All the other acid gneisses plot above the island arc volcanic field and/or are more fractionated (chondrite-normalised La/Yb range from 6 to 28) (figures 3.9, 3.11, 3.12 and 3.13) than the island arc volcanic rocks. REE data indicate that the acid gneisses are not island arc volcanic rocks. An island arc volcanic origin for the acid gneisses is precluded by REE data, the dominantly potassic nature of the acid gneisses ($Na_2O/K_2O < 1$) and the relatively small quantities of associated continental tholeiitic basic rocks (cf. Jakeš & Gill, 1970).

The REE patterns of sediments are parallel to or subparallel to the North American composite shale, and are usually characterised by "normal" Eu abundances (Haskin *et al.*, 1966, and Wildeman & Haskin, 1972). However, slight Eu anomalies (shale-normalised Eu/Eu* from 0.7 to 1.2) are not uncommon in sediments (Wildeman & Haskin, 1972). A sedimentary REE pattern suggests but cannot prove a sedimentary origin, because intrusive granites and granodiorites commonly have "sedimentary" REE patterns. In fact, the REE patterns of the high-K intrusive charnockites are subparallel to the sedimentary field (figure 3.3) and have negative Eu anomalies (shale-normalised Eu/Eu* of 0.7-0.8) within the expected sedimentary range. However, the charnockites are undoubtedly of igneous origin (chapter 3).

Two garnet-gneisses (69-942 and 69-1375: figure 3.11) have strongly fractionated igneous REE patterns (chondrite-normalised La/Yb of 22 and 28 respectively) with very pronounced Eu anomalies (chondrite-normalised Eu/Eu* of 0.54 and 0.42 respectively). The gneisses are fractionated

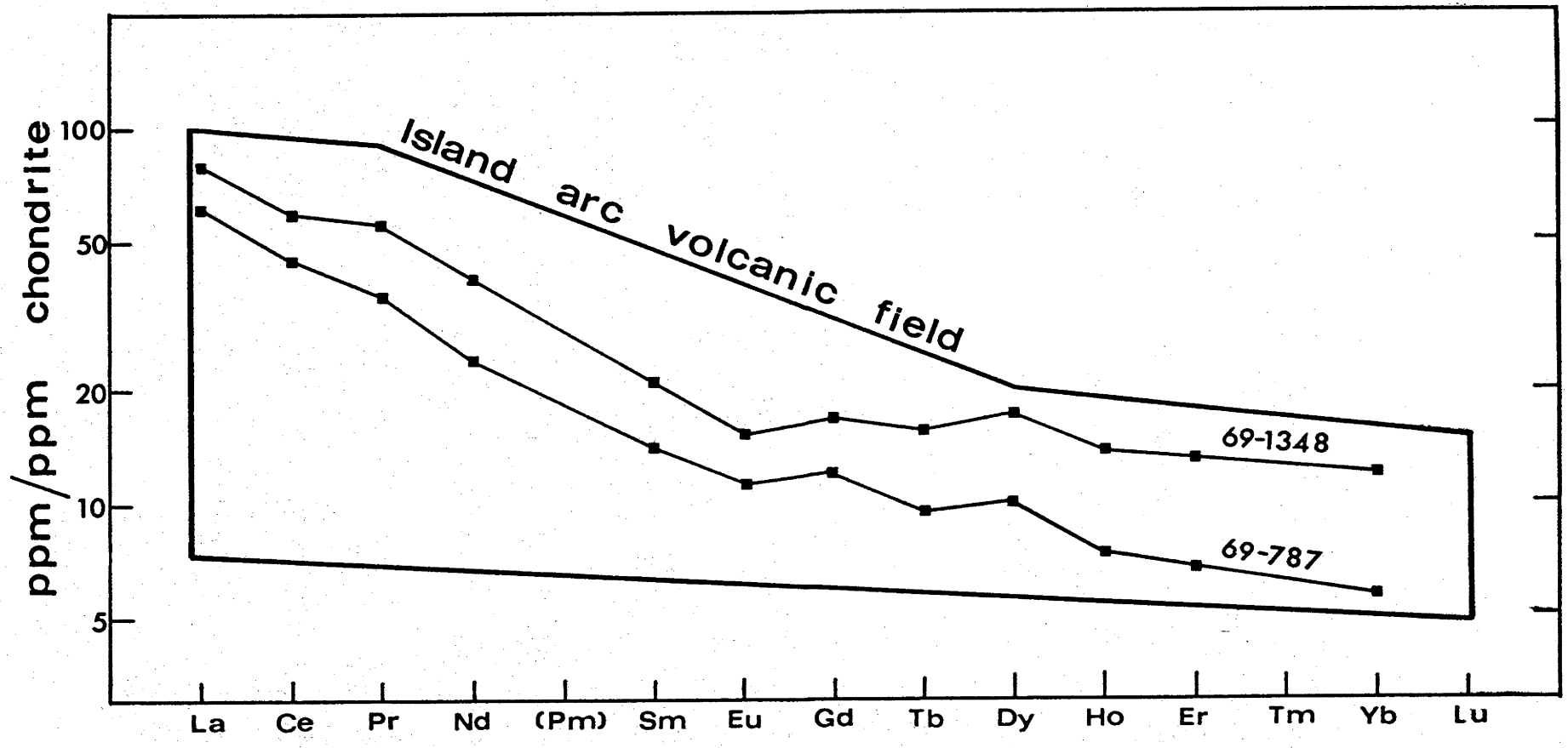

FIGURE 3.10 : RARE EARTH PATTERNS OF TWO ACID GNEISSES PLOTTING WITHIN THE ISLAND ARC VOLCANIC RARE EARTH ELEMENT FIELD.

The island arc volcanic rare earth element field is from figure 3.8.

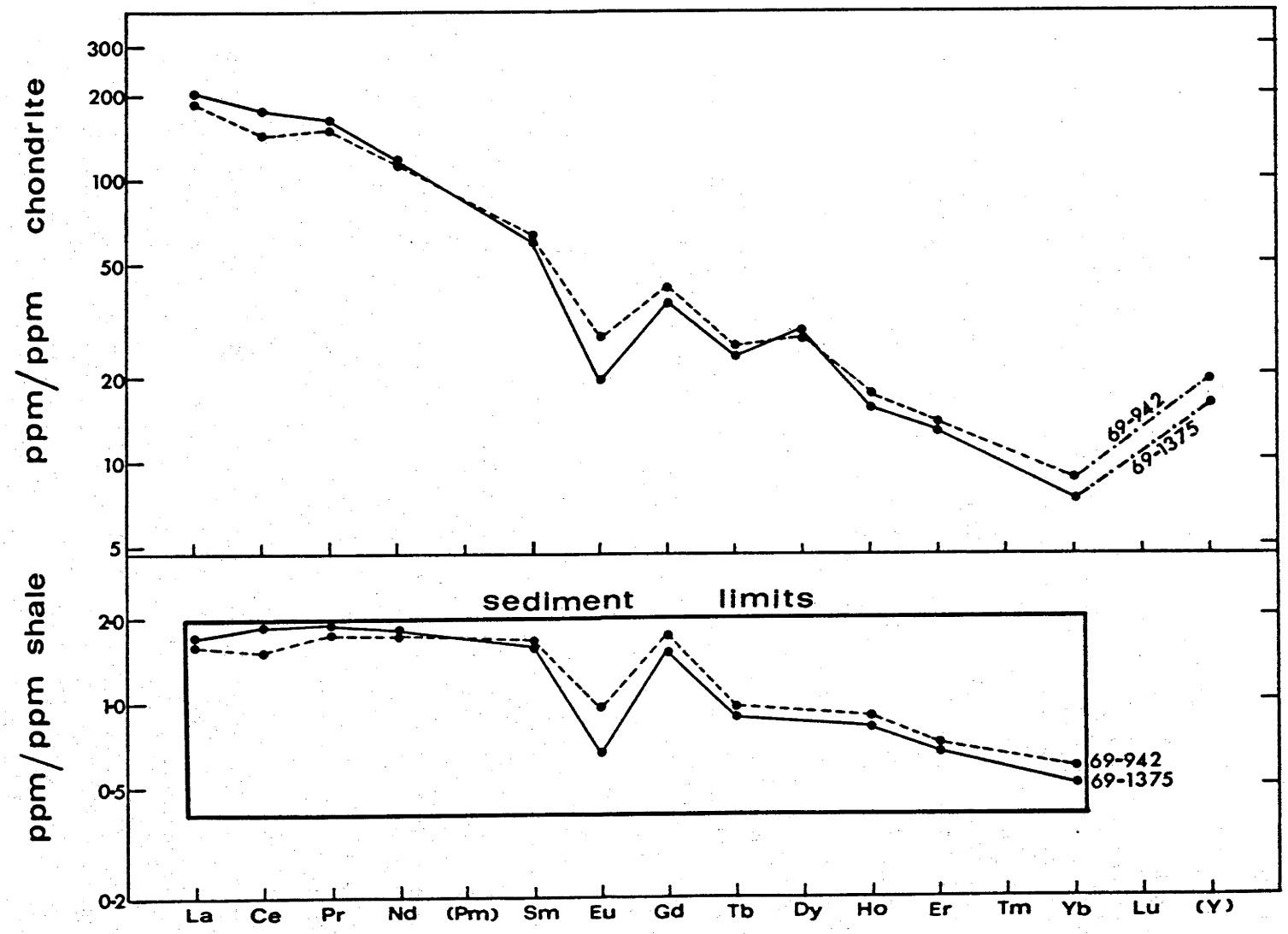

FIGURE 3.11 : IGNEOUS RARE EARTH PATTERNS OF TWO ACID GNEISSES STRONGLY FRACTIONATED RELATIVE TO THE SEDIMENTARY RARE EARTH ELEMENT FIELD.

The sedimentary rare earth element field is from figure 3.8. The rocks in the shale-normalised plot correspond to those in the chondrite-normalised plot.

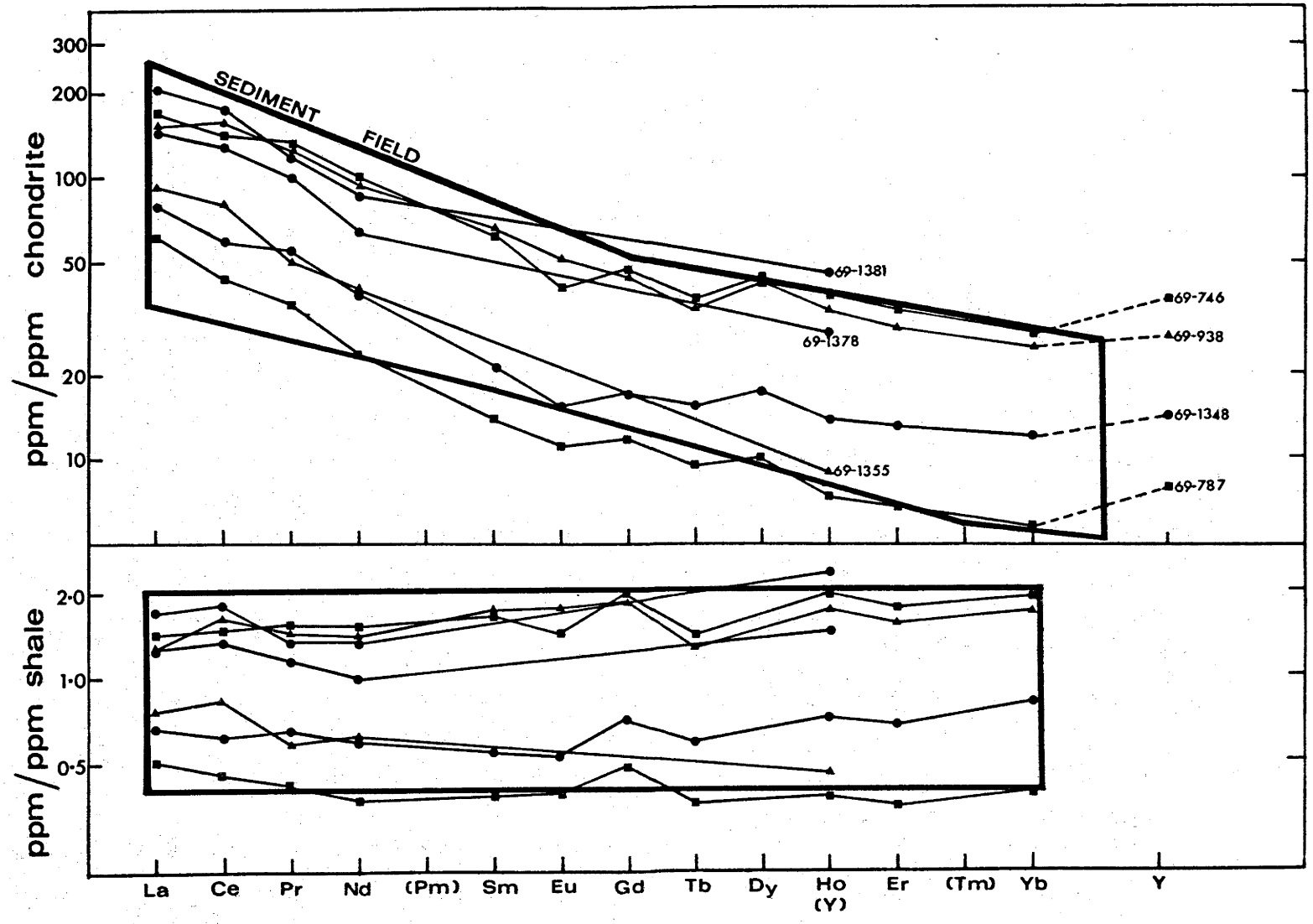

FIGURE 3.12 : RARE EARTH PATTERNS OF ACID GNEISSES SUBPARALLEL TO AND WITHIN THE SEDIMENTARY RARE EARTH ELEMENT FIELD.

The sedimentary rare earth element field is from figure 3.8. The rocks in the shale-normalised plot correspond to those in the chondrite-normalised plot.

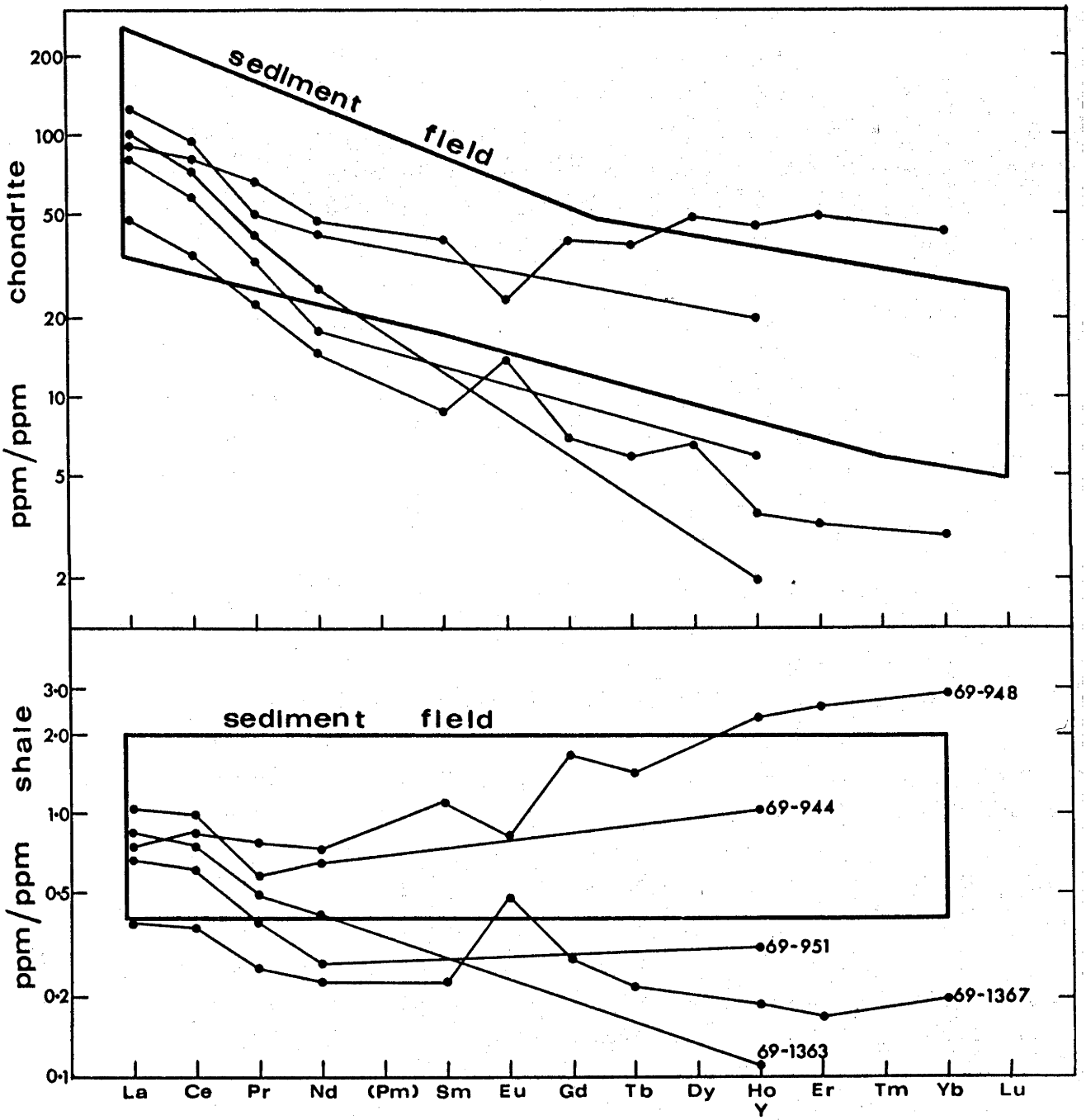

FIGURE 3.13 : RARE EARTH PATTERNS OF ACID GNEISSES FRACTIONATED RELATIVE TO THE SEDIMENTARY RARE EARTH ELEMENT FIELD.

The sedimentary rare earth element field is from figure 3.8. The rocks in the shale-normalised plot correspond to those in the chondrite-normalised plot.

relative to the sedimentary REE field and have Eu anomalies considerably larger than encountered in sediments. The REE patterns may have been generated by extended fractional crystallisation of feldspar or by anatectic fractionation involving feldspathic residuum.

Seven gneisses plot within or very nearly within the sedimentary REE field and are subparallel to the sedimentary abundances (figure 3.12). The sedimentary REE patterns suggest (but do not prove) a sedimentary origin for these gneisses which include the garnet-symplectite charnockites, a banded charnockite (69-787), a banded garnet-gneiss (69-1348) and the migmatite (69-1355). One of the garnet-symplectite charnockites has a distinct negative Eu anomaly (shale-normalised Eu/Eu* = 0.8).

The REE patterns of three banded charnockites (69-951, 69-1363 and 69-1367) are fractionated relative to the sedimentary field (figure 3.13). One of the gneisses (69-1367) is depleted relative to the sedimentary field in all REE except La, (Ce) and Eu, and has a pronounced positive Eu anomaly. Two garnet-gneisses (69-944 and 69-948) are enriched in heavy REE relative to sedimentary patterns (figure 3.13). All of these gneisses (figure 3.13) are considered to be metasediments and the deviation of their REE from "normal" sedimentary REE patterns must be explained by fractionation during metamorphism (chapter 8).

CHAPTER 4

CALC-SILICATE ROCKS

4.1 FIELD APPEARANCE

A wide band of graphitic calc-silicate rock (69-939) occurs adjacent to the garnet-symplectite charnockites (chapter 3). The graphitic calc-silicate occurs close to a graphite-carbonate rock (70-1202) and an extremely weathered forsterite marble (Tilley, 1921c). The rock contains alternating dark-green clinopyroxene-rich layers, pale-green quartz-rich layers and white quartzite layers. Graphite-rich bands occur parallel to the compositional layers. A narrow band of dark gneissic calc-silicate rock (69-777) is interbanded with some banded charnockites (chapter 3).

4.2 MINERALOGY

The graphitic calc-silicate rock contains clinopyroxene, quartz and graphite. The calc-silicate gneiss is dominantly composed of pale hornblende and clinopyroxene (table 4.1). The hornblende and clinopyroxene are Mg-rich and poor in Ti, Fe, Sc, V, Co and Ni reflecting the composition of the gneiss (table 4.2). The clinopyroxene is moderately aluminous, and all Al is present as Tschermak component.

4.3 GEOCHEMISTRY

The low Ti, Sc, V, Cr, Co, Ni and Cu in the calc-silicate rocks (table 4.2) are highly unlikely in basic volcanic sediments. The geochemistry of the calc-silicate rocks is consistent with derivation from impure dolomitic sediments. The graphitic calc-silicate rock (69-939: table 4.2) is relatively Si-rich and Al-poor. This can be explained by an original quartz-rich and clay-poor sediment. The carbonate-component of the sediment was close to pure dolomite (wt. % CaO/MgO≃1.5). Clay component in sediments commonly adsorbs large cations such as K^+, Rb^+ and Ba^{2+}. The low K, Rb, Ba and Ga in the rock are explained by low initial clay content. The calc-silicate gneiss (69-777: table 4.2) is less Si-rich and more Al-rich than the graphitic

TABLE 4.1

HORNBLENDE AND CLINOPYROXENE
FROM CALC-SILICATE (69-777)

	Hornblende	Clinopyroxene
SiO_2	42.62	51.68
TiO_2	0.27	0.17
Al_2O_3	14.72	3.70
Fe_2O_3	2.67	0.96
FeO	4.71	3.12
MnO	0.36	0.52
MgO	15.96	15.90
CaO	12.86	24.30
Na_2O	1.71	0.24
K_2O	1.66	0.05
H_2O+	1.18	nd
H_2O-	0.06	nd
F	0.55	nd
Trace	0.15*	0.01**
Total	99.25***	100.65

STRUCTURAL ANALYSES BASED ON:

	23 Oxygens (anhydrous basis)		6 Oxygens
Si	6.157		1.887
AlIV	1.843		0.113
Y: AlVI	0.663		0.047
Y: Ti	0.029		0.005
Y: Fe^{3+}	0.290		0.026
Y: Fe^{2+}	0.569		0.095
Y: Mn	0.044		0.016
Y: Mg	3.437		0.866
X: Ca	1.990		0.951
X: Na	0.479		0.017
X: K	0.306		0.002
Sum X	2.775		
Sum Y	5.032	Sum (X+Y)	2.025
Rb	26		--
Ba	850		40
Sr	250		90
Sc	4		--
V	20		--
Co	9		--
Ni	~5		--
La	140		--
Y	18		--
Li	11		nd
Cs	~0		nd
K/Rb	530		nd

*includes BaO, La_2O_3 and Y_2O_3; ** SrO; *** Corrected for O=F
Cr and Cu were not detected by emission spectroscope; - means not detected; nd means not determined.

TABLE 4.2

CALC-SILICATE GNEISSES

	69-777	69-939
SiO_2	48.64	60.49
TiO_2	0.15	0.02
Al_2O_3	9.39	0.27
Fe_2O_3	1.15	0.68
FeO	2.78	5.55
MnO	0.43	0.66
MgO	14.01	11.47
CaO	21.02	20.47
Na_2O	0.56	0.13
K_2O	0.73	0.11
P_2O_5	0.02	0.20
H_2O+	0.83	0.17
H_2O-	0.04	0.07
CO_2	0.59	0.46
Total	100.32	100.75
Molar $MgO/(MgO+FeO)$	0.900	0.786
Molar $Fe_2O_3/(Fe_2O_3+FeO)$	0.16	0.05
Rb	20	0.7
Ba	670	~8*
Sr	324	38
Ga	12	<1.3
Th	< 2.3	0.6**
U	< 1.7	0.8**
Pb	14	19
Zr	69	4
Nb	2	1.5
La	68	8
Ce	109	14
Pr	8	2
Nd	26	9
Y	7	5
Sc	n.d.*	n.d.*
V	7	6
Cr	< 1.1	≲ 0.7
Co	4	≲ 2.5
Ni	< 1.3	< 0.6
Cu	< 0.8	< 0.7
Zn	85	22
K/Rb	303	1302

* Emission spectroscope
** Gamma spetrometer

All other data XRF

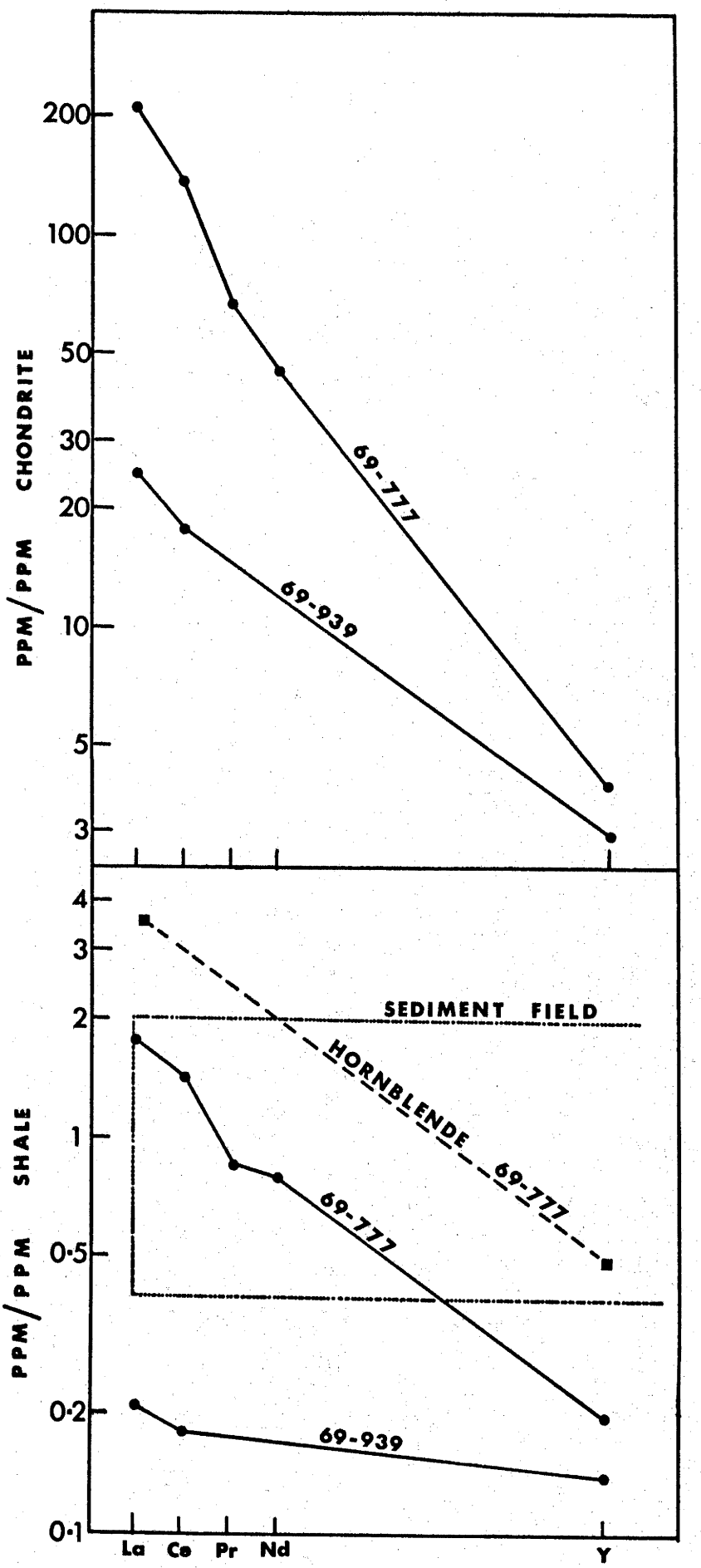

FIGURE 4.1 : RARE EARTH PATTERNS FOR THE CALC-SILICATE ROCKS
The sedimentary rare earth element field is from figure 3.8.

calc-silicate rock, and was derived from a sediment poorer in quartz and richer in clay. The higher clay content results in higher K, Rb, Ba and Ga. The carbonate component of the original sediment was more Ca-rich than pure dolomite (wt. % CaO/MgO≃1.8, cf. 1.5 for dolomite). The calc-silicate gneiss is richer in Sr, Zr, Nb, light REE and Zn than the graphitic calc-silicate rock. The REE pattern of the calc-silicate gneiss (69-777) is the most fractionated Eyre Peninsula gneiss pattern determined (figure 4.1). The gneiss is strongly fractionated relative to the sedimentary field. The REE are dominantly contained in the hornblende which closely parallels the whole-rock pattern. The highly fractionated REE pattern of the calc-silicate gneiss (69-777) is unusual since recent carbonate-sediments are always sub-parallel to the sedimentary field (Haskin et al., 1966). The graphitic calc-silicate rock has a much less fractionated REE pattern, and is only weakly fractionated relative to the sedimentary field. The rock is depleted in REE relative to the sedimentary abundances. The fractionation of REE in the calc-silicate rocks is discussed in chapter 8.

CHAPTER 5

CONTACT GNEISSES

5.1 FIELD APPEARANCE

The "reaction zone" or "contact" gneisses occur at the contacts of garnet-gneisses or charnockites and basic pyroxene granulites. The contact zones are characterised by a spectrum of garnetiferous acid to basic rocks, representing products of reaction between the basic inclusion and acid host gneiss. Obvious reaction at acid gneiss/basic granulite contacts is not ubiquitous. The width of all observed reaction zones, from garnet-free basic rock to garnet-free charnockite or "normal" pale garnet-gneiss, was less than about ½ metre, and usually less than about 10 cm. The wider reaction zones were migmatitic. Dark garnetiferous inclusions or "knots" of basic appearance occur in many garnet-gneisses. These probably represent "undigested" remnants of basic inclusions. Garnetiferous selvedges also occur at the contacts of some pegmatites.

5.2 MINERALOGY

The contact gneisses are characterised by the presence of garnet. The mineralogy of the gneisses changes systematically across the zones, from that of two-pyroxene basic granulite through varieties of contact gneiss into garnet-gneiss (appendix A). The idealised sequence of assemblages is:

(1) orthopyroxene + clinopyroxene + plagioclase ± quartz (basic granulite)
(2) orthopyroxene + plagioclase + quartz ± clinopyroxene
(3) orthopyroxene + garnet + plagioclase + quartz
(4) orthopyroxene + garnet + biotite + K-feldspar + plagioclase + quartz
(5) garnet + biotite + K-feldspar + plagioclase + quartz (garnet-gneiss)

TABLE 5.1

GARNETS FROM CONTACT GNEISSES

	69-950	69-1377
SiO_2	38.33	37.21
TiO_2	0.04	0.04
Al_2O_3	21.92	20.99
Fe_2O_3	1.82	2.38
FeO	26.11	27.29
MnO	0.72	2.84
MgO	8.45	2.07
CaO	2.19	7.28
Na_2O	nd	nd
K_2O	0.05	0.07
*Trace	0.08	0.10
Total	99.71	100.27
Sc	130	22
V	85	82
Co	41	25
Cu	23	17
Y	290	760
MOLE PERCENT OF END MEMBERS		
Pyrope	33.7	8.5
Almandine	58.4	63.2
Grossular	0.8	14.2
Spessartine	1.6	6.7
Andradite	5.5	7.4

*includes Sc_2O_3, Y_2O_3 and V_2O_5

trace elements not detected by emission spectroscope: Cr, Ni, Ba, Sr and La

nd means not determined.

TABLE 5.2

ORTHOPYROXENES FROM CONTACT GNEISSES

	69-741	69-950
SiO_2	50.62	50.05
TiO_2	0.16	0.11
Al_2O_3	1.76	5.03
Fe_2O_3	1.39	2.03
FeO	28.14	21.39
MnO	0.50	0.20
MgO	15.80	20.42
CaO	0.70	0.17
Na_2O	0.09	0.04
K_2O	0.04	0.02
H_2O+	nd	0.44
Trace*	0.12	0.04
Total	99.32	99.94

STRUCTURAL FORMULAE BASED ON 6 OXYGENS

Si	1.965	1.875
AlIV	0.035	0.125
AlVI	0.045	0.097
Ti	0.005	0.003
Fe^{3+}	0.041	0.057
Fe^{2+}	0.914	0.670
Mn	0.016	0.006
Mg	0.914	1.140
Ca	0.029	0.007
Na	0.007	0.003
K	0.002	0.001
Cr	0.001	0.000
Sum(X+Y)	1.974	1.984
Sc	89	54
V	380	230
Cr	290	--
Co	83	62
Ni	53	43
Cu	14	8
Ba	9	~4
Y	45	—

*V_2O_5, Sc_2O_3 and Cr_2O_3
nd means not determined
- means not detected
La and Sr not detected by emission spectroscope.

TABLE 5.3

CONTACT GNEISS BIOTITES AND HORNBLENDE

	Hornblende 69-1377	Biotites 69-741	Biotites 69-950
SiO_2	39.90	36.39	37.19
TiO_2	1.92	5.86	4.08
Al_2O_3	12.25	14.03	15.82
Fe_2O_3	4.18	0.01	0.64
FeO	18.39	18.75	12.26
MnO	0.32	0.07	0.02
MgO	6.11	10.74	16.41
CaO	11.08	0.40	0.15
Na_2O	1.73	0.11	0.10
K_2O	1.98	9.15	9.38
H_2O+	1.51	3.12	3.07
H_2O-	0.13	0.48	0.29
F	0.48	0.49	0.35
Trace	0.18*	0.64**	0.44**
Total***	99.96	100.03	100.05
STRUCTURAL FORMULAE BASED ON: (On an ANHYDROUS BASIS)	**23 OXYGENS**	**22 OXYGENS**	
Si	6.174	5.539	5.448
AlIV	1.826	2.461	2.552
Y AlVI	0.408	0.056	0.180
Y Ti	0.223	0.671	0.450
Y Fe^{3+}	0.487	0.001	0.071
Y Fe^{2+}	2.380	2.387	1.502
Y Mn	0.042	0.009	0.003
Y Mg	1.409	2.437	3.583
X Ca	1.837	0.065	0.024
X Na	0.519	0.033	0.029
X K	0.391	1.777	1.753
Sum X	2.747	1.875	1.806
Sum Y	4.949	5.561	5.789
Rb	20	~480	(~700)
Ba	64	(~2300)	~1750
Sr	~10	—	—
Sc	44	44	19
V	260	810	880
Cr	~ 9	1320	27
Co	51	72	81
Ni	600	180	170
Cu	5	5	4
La	100	—	—
Y	350	—	—
Li	4	32	(~80)
Cs	~0	2.3	4.5
K/Rb	822	158	(111)

*includes NiO, V_2O_5, Y_2O_3, La_2O_3; **includes NiO, Cr_2O_3, V_2O_5, BaO and Rb_2O; ***corrected for O=F; - means not detected by emission spectroscope; Rb, Ba and Li values in brackets suffered badly from self-absorption.

The series may be represented diagrammatically on an ACF plot (figure 5.1). The transition may be smooth or irregular, with development of agmatitic or migmatitic mixtures of the various mineral assemblages.

Garnets, orthopyroxenes, biotites and one hornblende from contact gneisses were analysed (tables 5.1, 5.2 and 5.3). One garnet (69-950) is dominantly almandine-pyrope and is similar to the garnets from the garnet-gneisses (chapter 3). The other garnet (69-1377) is dominantly almandine-grossular with smaller pyrope, spessartine and andradite contents. The orthopyroxenes from the contact gneisses are very Al-rich, especially for pyroxenes co-existing with garnet. One of the orthopyroxenes (69-950) is the most Al-rich pyroxene analysed in this study. The high Al correlates with the most intense pleochroism (appendix A). The hornblende and biotites from the contact gneisses are very Ti-rich. One biotite (69-950) is texturally a retrograde mineral and contains significantly higher Li, Rb and Cs and lower Ti than the other biotite (69-741), which is texturally a primary mineral.

5.3 GEOCHEMISTRY

5.3.1 Reaction Zone Series

The component members of three reaction zone series are plotted (figures 5.2, 5.3 and 5.4) and tabulated in order of increasing silica (tables 5.4 and 5.5, and appendix C). One sample (69-1349) contained quartz schlieren, and was corrected for the estimated quartz-excess. The major element variation is smooth and within the limits of acid and basic reactants for two series (figures 5.3 and 5.4). The variation in the third series (figure 5.4 and appendix C) is smooth for Ti, Al and Fe, and less regular or erratic for the other major elements. In this series the major element variation is not entirely within the limits of acid and basic reactants, and Al, Na and K exhibit pronounced concentration maxima in some of the reaction zone gneisses. The variation of trace elements across the reaction zones is generally irregular (tables 5.4 and 5.5, and appendix C).

TABLE 5.4

REACTION ZONE SERIES (1)

	Basic 69-1374	Reaction Zone 69-1373	Acid 69-1375
	ELEMENTS NOT SIGNIFICANTLY OUTSIDE ACID/BASIC LIMITS		
Ba	131	601	734
Sr	110	149	134
Ga	20	16	17
Zr	107	270	262
Nb	6	22	27
Sc	35	13	11
V	318	77	72
Cr	66	68	58
Co	34	14	15
Ni	62	28	18
Cu	61	30	26
Zn	96	51	59
	ELEMENTS SHOWING SIGNIFICANT MAXIMA OUTSIDE ACID/BASIC LIMITS		
Rb	10	132	95
Pb	9	26	14
Th	1.4	70	51
La	12	86	60
Ce	29	188	135
Pr	~5	21	13
Nd	~13	68	45
Y	21	42	29
K/Rb	382	227	327
Zr/Nb	17.8	12.3	9.7

TABLE 5.5

REACTION ZONE SERIES (2)

	Basic 69-1366	Reaction Zone 69-1368	Reaction Zone 69-1357	Acid 69-1367
ELEMENTS NOT SIGNIFICANTLY OUTSIDE ACID/BASIC LIMITS				
Rb	4.2	3.2	22	20
Sr	93	87	161	339
Ga	22	19	15	19
Nb	9.3	10	8.6	3.8
La	55	20	21	17
Ce	128	46	35	28
Pr	15	~4	~3	~2
Nd	50	21	12	< 9
Y	36	25	31	6
Sc	41	34	19	3
V	266	242	125	42
Cr	171	81	153	13
Co	27	30	29	10
Ni	57	57	62	9
Zn	128	130	76	38
Li	6	9	9	16
ELEMENTS SHOWING SIGNIFICANT MAXIMA OUTSIDE ACID/BASIC LIMITS				
Ba	91	80	748	420
Zr	83	71	208	100
Cu	~2	55	52	3
K/Rb	672	752	396	569
Zr/Nb	8.9	7.1	24	26

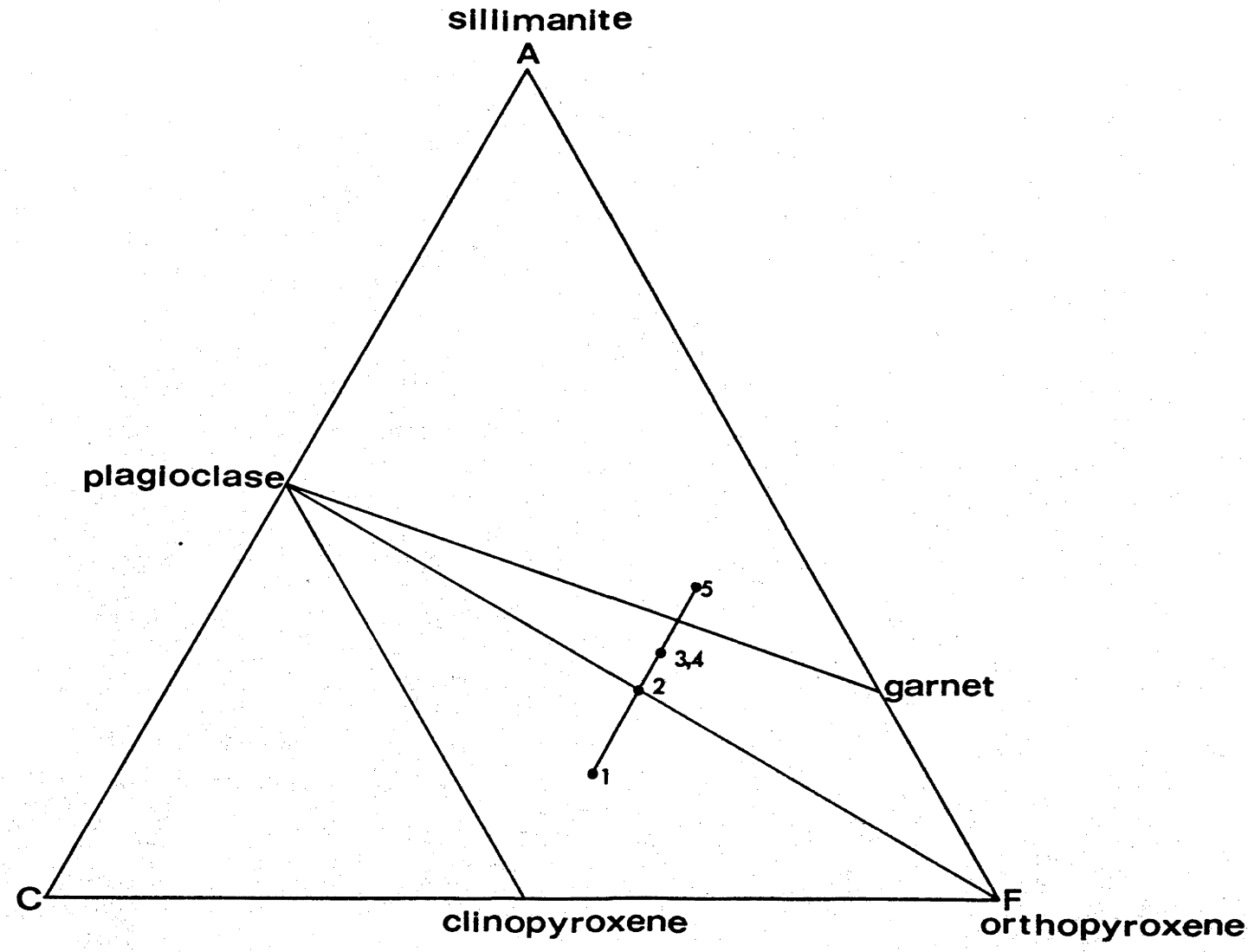

FIGURE 5.1 : DIAGRAMMATIC REPRESENTATION OF ASSEMBLAGES IN THE REACTION ZONE SERIES

(See text for explanation).

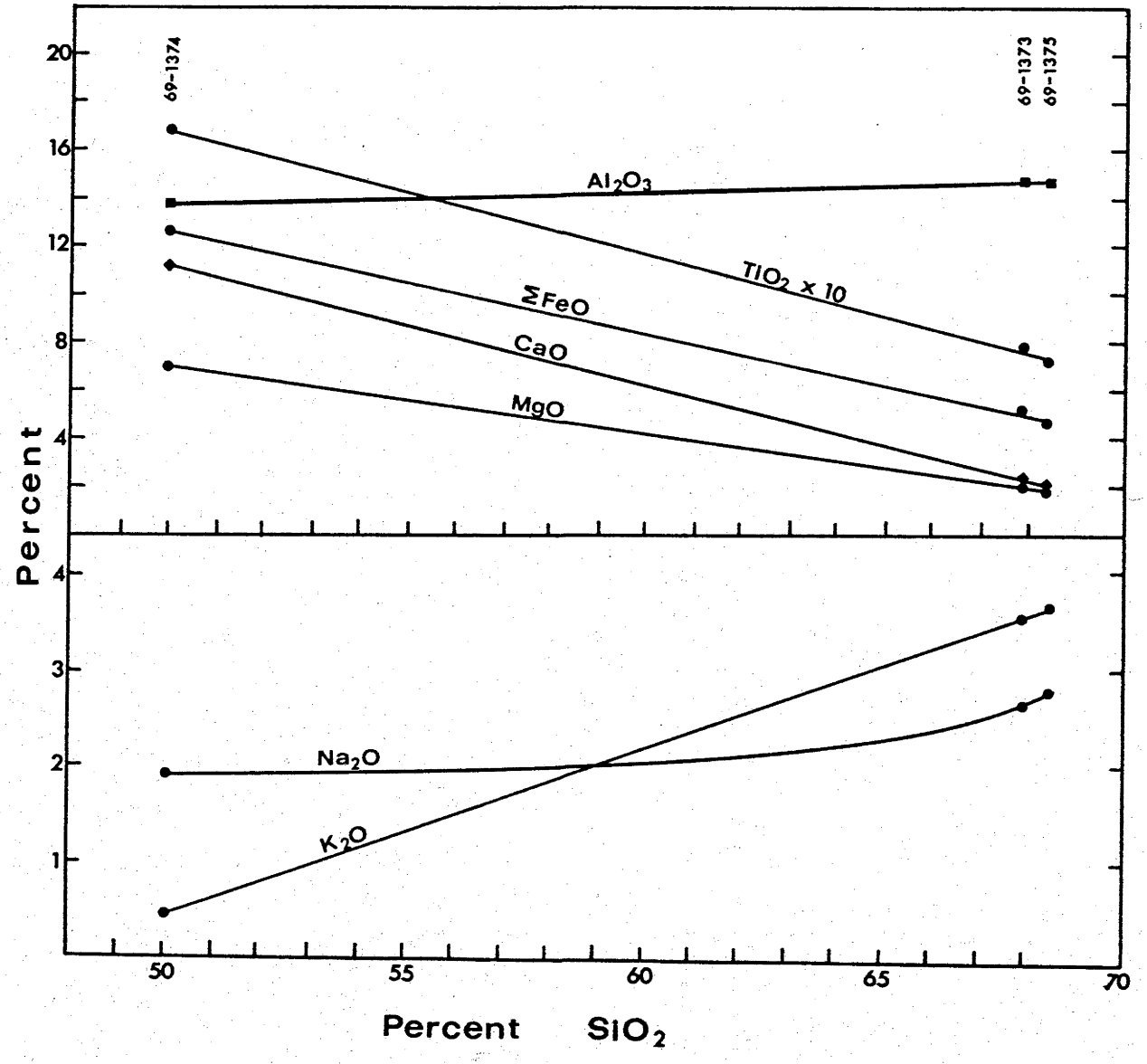

FIGURE 5.2 : MAJOR ELEMENT VARIATION IN REACTION ZONE (SERIES 1)

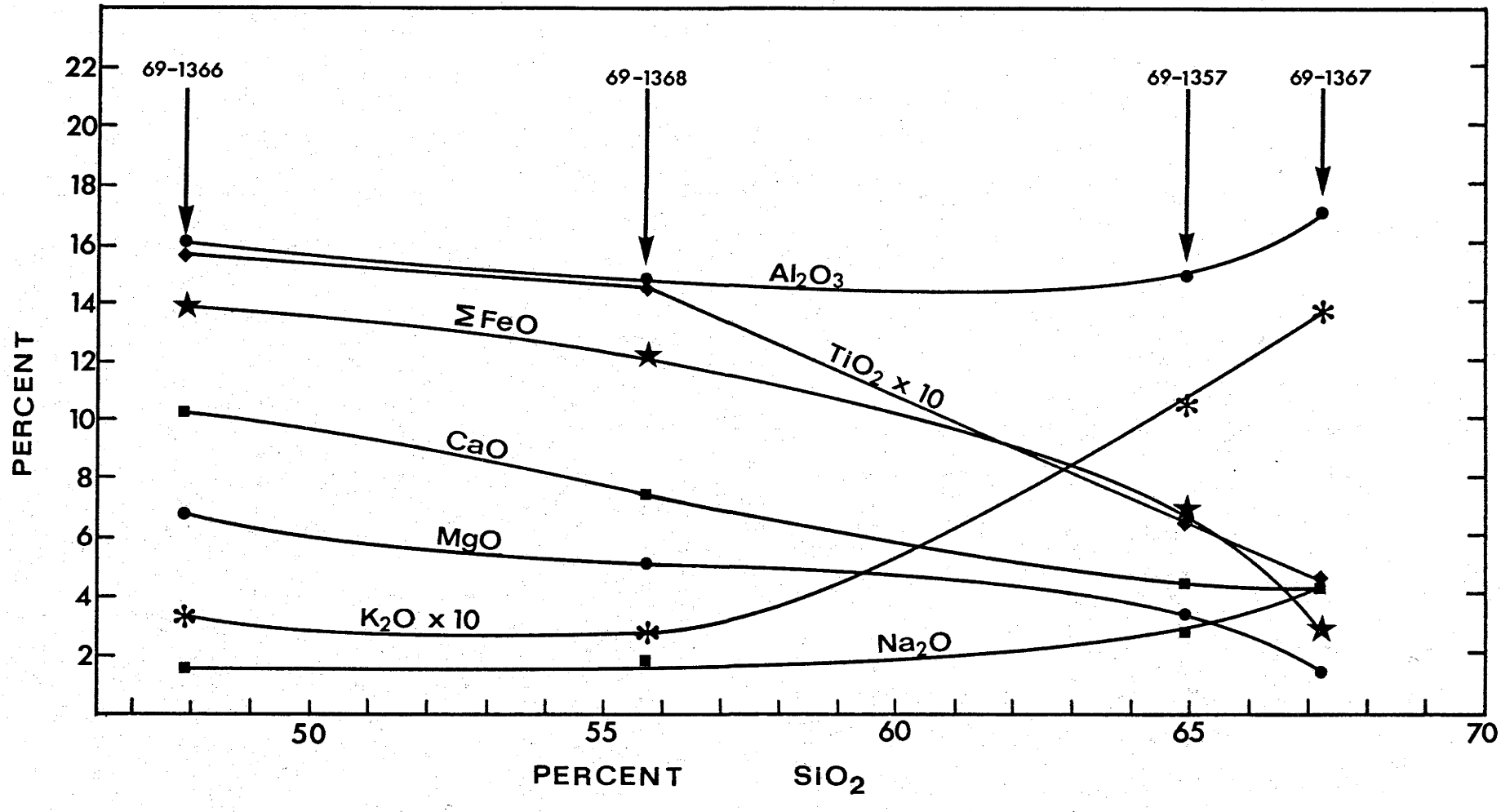

FIGURE 5.3 : MAJOR ELEMENT VARIATION IN REACTION ZONE (SERIES 2)

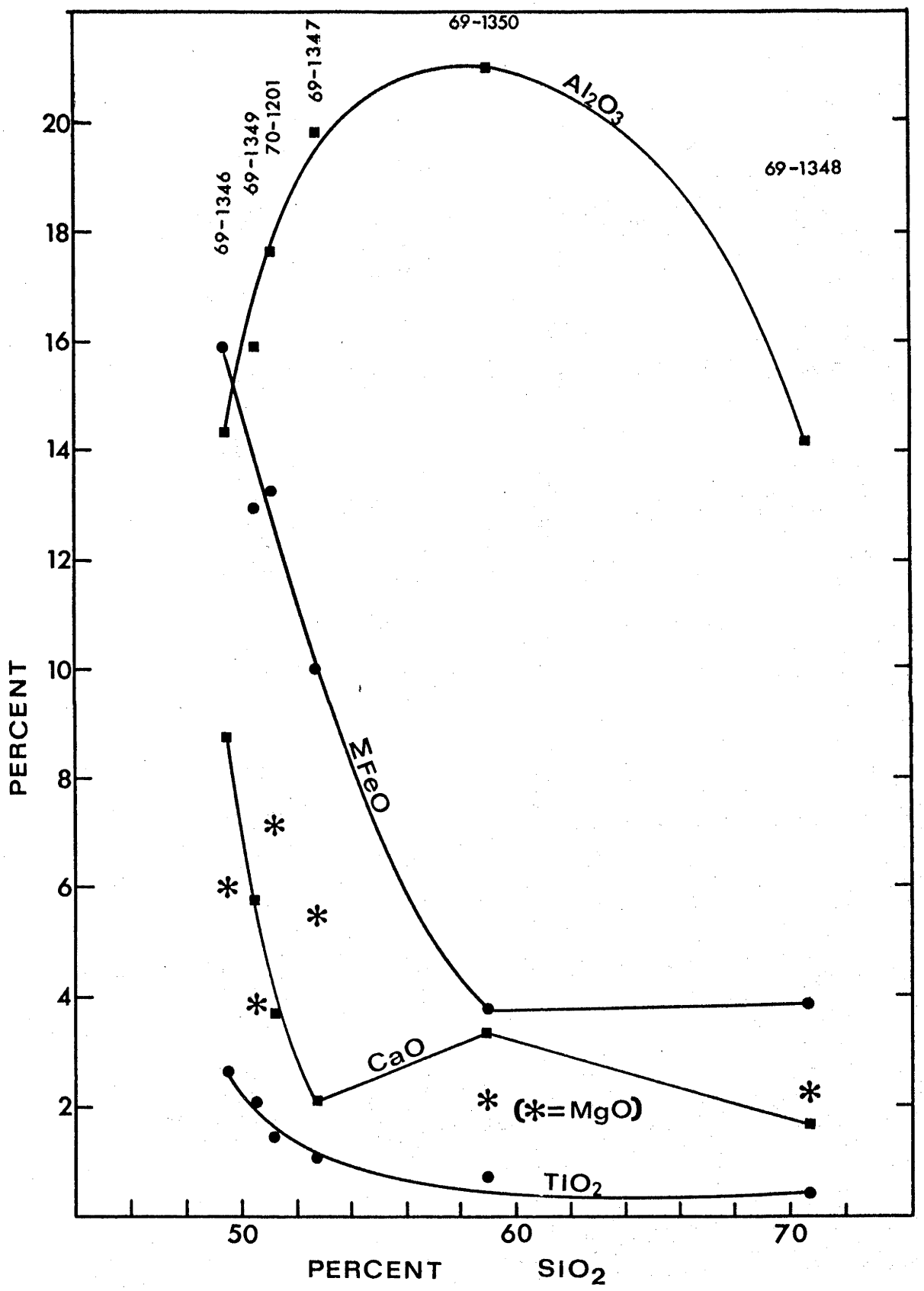

FIGURE 5.4 : MAJOR ELEMENT VARIATION IN REACTION ZONE (SERIES 3)

The concentrations of most trace elements in the reaction zones are within the limits or only slightly outside the limits defined by the acid and basic reactants, but many exhibit pronounced concentration maxima. Trace elements exhibiting pronounced concentration maxima in many reaction zones are Rb, Ba, Pb, Th, REE, Y, Zr and Cu. The Cu maximum correlates with an S maximum (reaction series 2: appendix C).

The correlation between geochemical and mineralogical variation was not obvious. The pronounced Al-maximum in reaction series (3) correlates with Na and Ca maxima and is due to higher plagioclase content. REE and Y maxima could not be correlated with modal garnet maxima, nor could Rb and Ba maxima be correlated with biotite maxima.

5.3.2 Individual Contact Gneisses

Two dark garnetiferous inclusions in acid gneisses (69-741 and 69-950) and two garnetiferous pegmatite selvedges (69-1361 and 69-1377) are characterised by peculiar major element compositions (appendix C) similar to many of the reaction zone gneisses. This suggests the rocks were formed in a similar manner to the reaction zone gneisses. Their geochemistry is discussed in chapter 8. The geochemistry of one contact gneiss (69-1356) is very similar to the garnet-gneisses (chapter 3) and was little modified by reaction with the basic rock.

5.4 DISCUSSION

The chemical potential gradients existing at the contacts between acid and basic rocks may be sufficient at elevated temperatures to cause diffusion of components across the contact. Such diffusion would cease when the chemical potential gradients were reduced below some critical diffusion threshold. The common formation of reaction zones and smooth major element gradients across many of the zones indicate that this has occurred. The extent of reaction is relatively small except where minor amounts of water were present and allowed generation of more extensive migmatitic

reaction zones. The limited extent of reaction in non-migmatitic contact zones indicates the extreme inefficiency of solid-solid diffusion even at high temperatures. The amount of reaction is significantly increased when minor melt is formed allowing the much more efficient transfer of components by solid-liquid diffusion. The critical importance of water is especially obvious when the relatively limited reaction zones are compared with extensively re-crystallised and reacted basic rocks adjacent to major pegmatite bodies.

The irregular major element variation across some reaction zones, and the commonly erratic trace element variation indicate that the reaction process is not simply controlled by chemical potential gradients, and is a more complex function of nucleation and crystallisation of new minerals in the reaction zones.

CHAPTER 6

THE GRANULITE METAMORPHISM

6.1 METAMORPHIC PARAMETERS AND DEFINITIONS

Important physical parameters are temperature (T), load or total pressure (P_{total}), equilibrium water pressure (Pe_{H_2O}) and oxygen fugacity (f_{O_2}). Other parameters include equilibrium carbon dioxide pressure (Pe_{CO_2}) and sulphur fugacity (f_{S_2}).

Pe_{H_2O} is here defined relative to fluid phase containing water as the only volatile component and in equilibrium with silicates at the same P_{total} and T (Holloway, 1972). Prior definitions used pure water for the reference states, but at elevated P_{total} and T aqueous fluids contain appreciable dissolved silicate (Burnham, 1967), and Pe_{H_2O} cannot equal that of pure water at the same P_{total} and T. Definition relative to aqueous fluid in equilibrium with silicates allows attainment of $Pe_{H_2O} = P_{total}$. Equilibrium pressure and fugacity are interchangeable at constant temperature. Rock porosities are assumed negligible at high metamorphic pressure and temperature and minute traces of fluid are sufficient for $Pe_{H_2O} = P_{total}$.

6.2 EVALUATION OF METAMORPHIC PARAMETERS

Metamorphic reactions are subdivided into solid-solid reactions involving no nett production or consumption of fluid, and reactions producing or consuming fluid phase. The first reaction type is independent of fluid composition, and pressure-dependency is restricted to P_{total}. The second reaction type is dependent on fluid composition and equilibrium pressure of the fluid-species consumed or produced. Examples of the first reaction type include the sillimanite-kyanite polymorphic transformation, reactions involved in the anhydrous basalt to eclogite transformation (Green & Ringwood, 1967a) and anhydrous garnet-cordierite equilibria (Hensen, 1971). Examples of the second reaction type include decomposition reactions of micas and amphiboles.

6.2.1 Oxygen Fugacity

Oxygen fugacity may be determined by analysis of coexisting minerals containing Fe^{2+} and Fe^{3+}. Compositions of coexisting magnetite-ulvöspinel and ilmenite-hematite solid solutions (Buddington & Lindsley, 1964), or coexisting biotite-magnetite-K-feldspar (Eugster & Wones, 1962, and Wones & Eugster, 1965) are dependent on f_{O_2} and T. Other examples are oxygen buffer assemblages such as magnetite-wüstite (MW), quartz-fayalite-magnetite (QFM), nickel-nickel oxide (NNO) and hematite-magnetite (HM).

Coexisting magnetite/ilmenite pairs at Eyre Peninsula have exsolved to form abundant lamellar and granular intergrowths. Some grains have recrystallised into subgrains, and sulphides have intergrown with and replaced the oxides in many samples. Hence, f_{O_2} cannot determined from the coexisting magnetite-ilmenite pairs.

Two biotites coexisting with magnetite and K-feldspar (69-741 and 69-944: tables 5.3 and 3.8) have extremely low Fe^{3+}, indicating f_{O_2} lower than expected on the QFM buffer (figure 6.1). Other analysed biotites coexist with magnetite but not K-feldspar. These include two biotites from intensely "retrogressed" rocks (69-788 and 69-794: table 7.7), and three biotites from rocks with relatively minor "retrogression" (69-785, 69-786 and 69-950: tables 7.7 and 5.3). The data of Wones & Eugster (1965: figure 6.1) cannot be used to determine the f_{O_2} active during crystallisation of these biotites, since they do not coexist with K-feldspar. However, application of the data allows determination of the maximum possible f_{O_2}. The extremely low Fe^{3+} in the biotites from rocks with minor "retrogression" indicate f_{O_2} at least as low as the QFM buffer (figure 6.1). The Fe^{3+} in the biotites from intensely retrogressed rocks are significantly higher and indicate a maximum f_{O_2} between the QFM and NNO buffer (figure 6.1). The higher oxidation state of the "retrograde" biotites is consistent with progressive oxidation observed during rehydration (chapter 7).

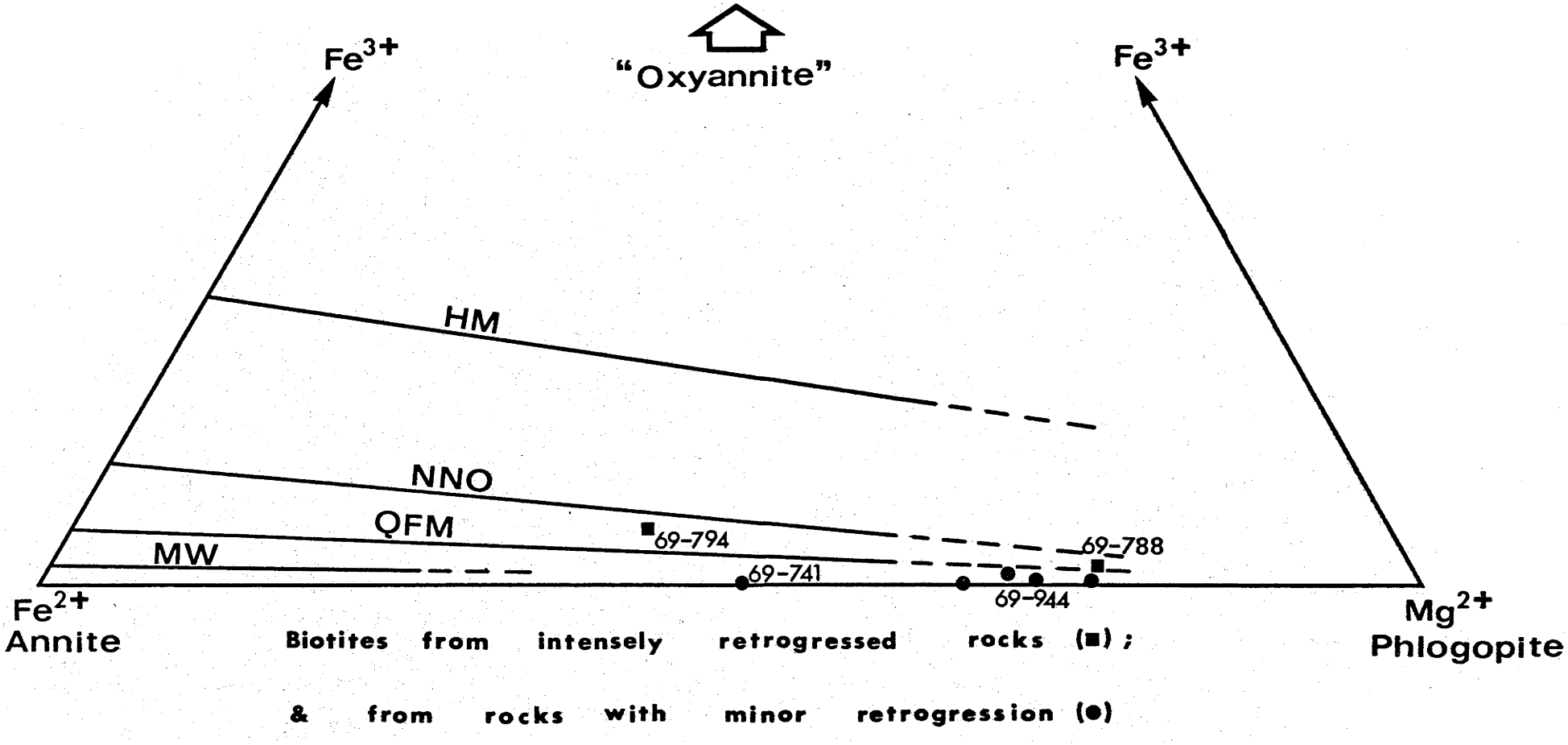

FIGURE 6.1 : EYRE PENINSULA BIOTITES AND ESTIMATED COMPOSITIONS OF BIOTITES COEXISTING WITH VARIOUS OXYGEN BUFFERS.

Biotite/oxygen buffer data from Wones & Eugster (1965).

Disseminated pyrrhotite is common in Eyre Peninsula acid and basic gneisses. The sulphides are moulded upon and replace oxide phases but appear to coexist stably with garnet and orthopyroxene. Crystallisation of sulphides requires high fS_2 and hence low f_{O_2}. Several samples (69-741, 69-944, 69-948, 69-1357 and 69-1368: appendix C) with relatively high S (0.15 - 0.23%) have low oxidation states (molar $Fe_2O_3/(Fe_2O_3+FeO)$ = 0.004 = 0.04).

Reduction of f_{O_2} during metamorphism at Eyre Peninsula would occur adjacent to graphite-bearing rocks:

$$C + O_2 = CO_2$$

$$C + 2H_2O = 2H_2 + CO_2$$

$$2H_2 + O_2 = 2H_2O$$

Excess hydrogen generated readily diffuses into neighbouring rocks resulting in decreased f_{O_2} (Miyashiro, 1964). The mobility of H_2 allows greater apparent mobility of O_2.

6.2.1.2 Summary

Miyashiro (1964) showed that the oxidation states of rocks are progressively reduced with increasing metamorphic grade. Therefore it is expected that granulite metamorphism takes place in a chemically reduced environment (Oliver, 1969, and Wilson, 1969).

Eyre Peninsula metamorphic rocks have low oxidation states (molar $Fe_2O_3/(Fe_2O_3+FeO)$ ratios range from 0.002 to 0.27, and average 0.10), supporting reducing conditions during metamorphism. The compositions of metamorphic biotites indicate that f_{O_2} was at least as low as the QFM buffer, and possibly increased to near the NNO buffer during "retrogressive" metamorphism. The presence of graphite and sulphides suggests f_{O_2} may have been even lower in restricted regions. f_{O_2} during metamorphism is considered to have been sufficiently low to cause minimal decrease in stability of Fe^{2+}-bearing minerals. f_{O_2} was also comparable to that in experiments utilised in later sections.

6.2.2 Basalt to Eclogite Transformation

Reactions transforming anhydrous basalt to eclogite were studied in detail by Green & Ringwood (1967a). The reactions are dependent on P_{total}, T and f_{O_2}. Experimental conditions were relatively reducing and applicable to high grade metamorphism. Eyre Peninsula basic pyroxene granulites are quartz tholeiites very similar to the experimental quartz tholeiite A composition of Green & Ringwood (1967a) (table 6.1). Quartz tholeiite A has higher Ti and Mg/Fe ratio.

Orthopyroxene coexists stably with plagioclase in Eyre Peninsula basic pyroxene granulites with molar MgO/(MgO+FeO) between 0.4 and 0.7. This limits P_{total} below and T above the band representing divariant reaction between orthopyroxene and plagioclase to yield garnet, clinopyroxene and quartz (figure 6.2).

6.2.3 Hornblende Stability

Complete decomposition of hornblende in Eyre Peninsula basic rocks occurred only in those containing free quartz. Several rocks were observed in which hornblende had completely decomposed only in the presence of quartz, and was stable in quartz-free zones. Hornblende characterised by sharp grain boundaries and polyhedral grains was never observed in contact with quartz (appendix A). The presence of quartz in the hornblende-free pyroxene granulites is not due to oxidation state (the molar $Fe_2O_3/(Fe_2O_3+FeO)$ of pyroxene granulites ranges from 0.03 to 0.19; and that of hornblende granulites, retrogressed granulites and amphibolites ranges from 0.03 to 0.20).

The maximum stability of hornblende in basaltic rocks and in the absence of quartz was not exceeded during metamorphism. This limits T below the maximum amphibole stabilities in figure 6.2.

6.2.4 Garnet-Cordierite Equilibria

Cordierite was not observed in the southern Eyre Peninsula garnet-gneisses by Tilley (1921a&b). Intensive

TABLE 6.1

COMPARISON OF PYROXENE GRANULITES AND EXPERIMENTAL COMPOSITIONS

		Quartz Tholeiite A	Average of 8 Eyre Peninsula Pyroxene Granulites
	SiO_2	49.9	49.7
	TiO_2	2.1	1.7
	Al_2O_3	13.9	14.1
total	FeO	12.2	14.2
	MnO	0.2	0.2
	MgO	8.5	6.8
	CaO	10.8	10.6
	Na_2O	1.8	1.8
	K_2O	0.1	0.3
	P_2O_5	0.2	0.3
Total		99.7	99.7

Quartz Tholeiite A from Green & Ringwood (1967).

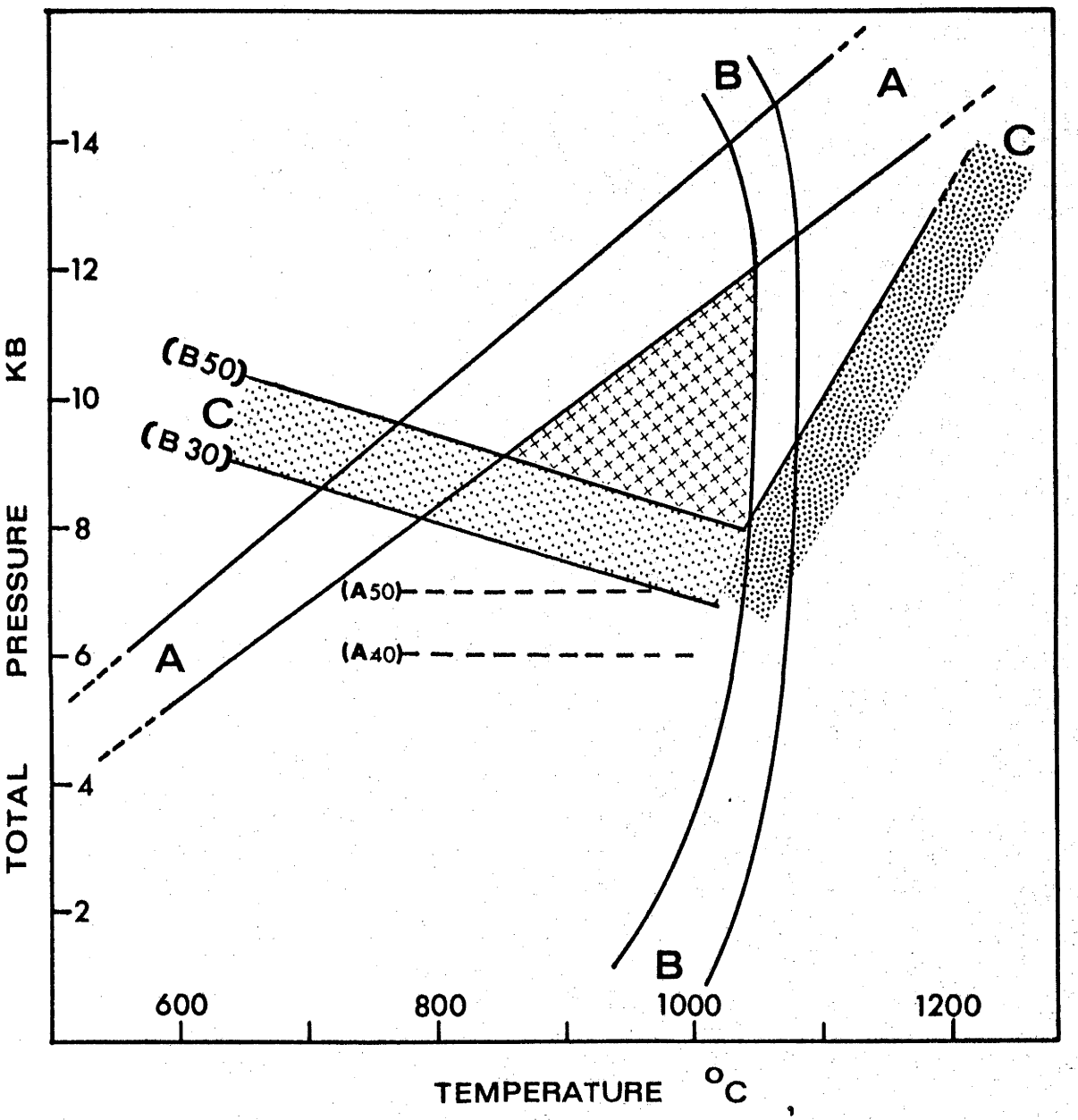

FIGURE 6.2 : P-T CONSTRAINTS ON CONDITIONS OF THE GRANULITE FACIES METAMORPHISM.

The field of metamorphic conditions is marked with crosses. The band A-A marks the first formation of garnet in anhydrous quartz tholeiite with molar MgO/(MgO+FeO) from 0.4 to 0.7 (Green & Ringwood 1967a). The band B-B marks the maximum stability of amphibole in basic rocks (Lambert & Wyllie, 1970; Bryhni et al., 1970; Irving, 1971; Holloway & Burnham, 1972; and Holloway, 1972). The band C-C represents the upper stability limit of cordierite (light stipple) and the stability field of sapphirine (heavy stipple) in the B30 to B50 experimental compositions. The dashed lines represent the upper stability limits of cordierite in A40 and A50 experimental compositions. (Cordierite and sapphirine data from Hensen, 1970 and Hensen & Green, 1971).

TABLE 6.2

COMPARISON OF GARNET GNEISSES WITH EXPERIMENTAL COMPOSITION

	(1)	(2)	(3)
SiO_2	68.2	52.8	52.8
Al_2O_3	15.5	22.8	24.9
total FeO	7.1	10.6	11.1
MgO	3.1	4.5	6.2
CaO	1.7	2.6	2.4
Na_2O	2.1	3.2	1.2
K_2O	2.3	3.5	1.4
Wt%MgO/FeO		0.43	0.56

(1) Average of two biotite-poor garnet-sillimanite-gneisses recalculated to 100% excluding TiO_2, MnO, P_2O_5 and loss

(2) Average (1) with SiO_2 adjusted to B50 value by subtraction of 31.7% SiO_2 as quartz.

(3) B50 composition from Hensen & Green,(1971).

petrographic and X-ray study of the garnet-gneisses from Eyre Peninsula confirmed the absence of cordierite. Sapphirine was not observed in the garnet-gneisses.

Various anhydrous equilibria involving garnet, cordierite, orthopyroxene, olivine, sapphirine, spinel, sillimanite and quartz were discussed and experimentally investigated by Hensen (1970, 1971) and Hensen & Green (1968, 1970, 1971). The equilibria are dependent on P_{total}, T and f_{O_2}. The experimental work was carried out at low f_{O_2}, comparable to those thought to prevail during the Eyre Peninsula metamorphism (6.2.1). All of the analysed garnet-gneisses contain quartz, feldspar, garnet and some contain orthopyroxene or minor sillimanite. The presence of biotite does not affect the anhydrous equilibria, but alters the relative proportions of anhydrous phases and may eliminate one of the phases (Hensen, 1971). Since the $Mg/(Mg+Fe^{2+})$ ratios of cordierite > orthopyroxene > garnet (Hensen, 1971) and biotite > orthopyroxene > garnet (chapter 7), cordierite is the phase most likely to be eliminated by the presence of biotite. Thirteen Eyre Peninsula garnet-gneisses are compared in figure 6.3 with the experimental compositions. The experimental stability data is applicable to only four which contain negligible biotite (< 1%). However the compositional variation is probably applicable to several other biotite-deficient garnet-gneisses in which cordierite was absent, but which were not analysed (69-941, 69-943, 69-949, 69-952: appendix A). One rock (69-942) plots in the C-series fields in both ACF and AFM diagrams and contains abundant sillimanite. The rock cannot be used with experimental data because it contains abundant biotite. Most of the rocks plot in the A-series fields in both AFM and ACF diagrams with molar MgO/(MgO+FeO) from 0.4 to 0.6. The two deficient in biotite have molar MgO/(MgO+FeO) between 0.4 and 0.5. The absence of cordierite in these rocks restricts P_{total} above the band for elimination of cordierite in A40-A50 compositions. Most of the garnet-gneisses have an An-content higher than the A-series compositions. This does not affect garnet-cordierite equilibria if the "An" component is present as plagioclase but if present as

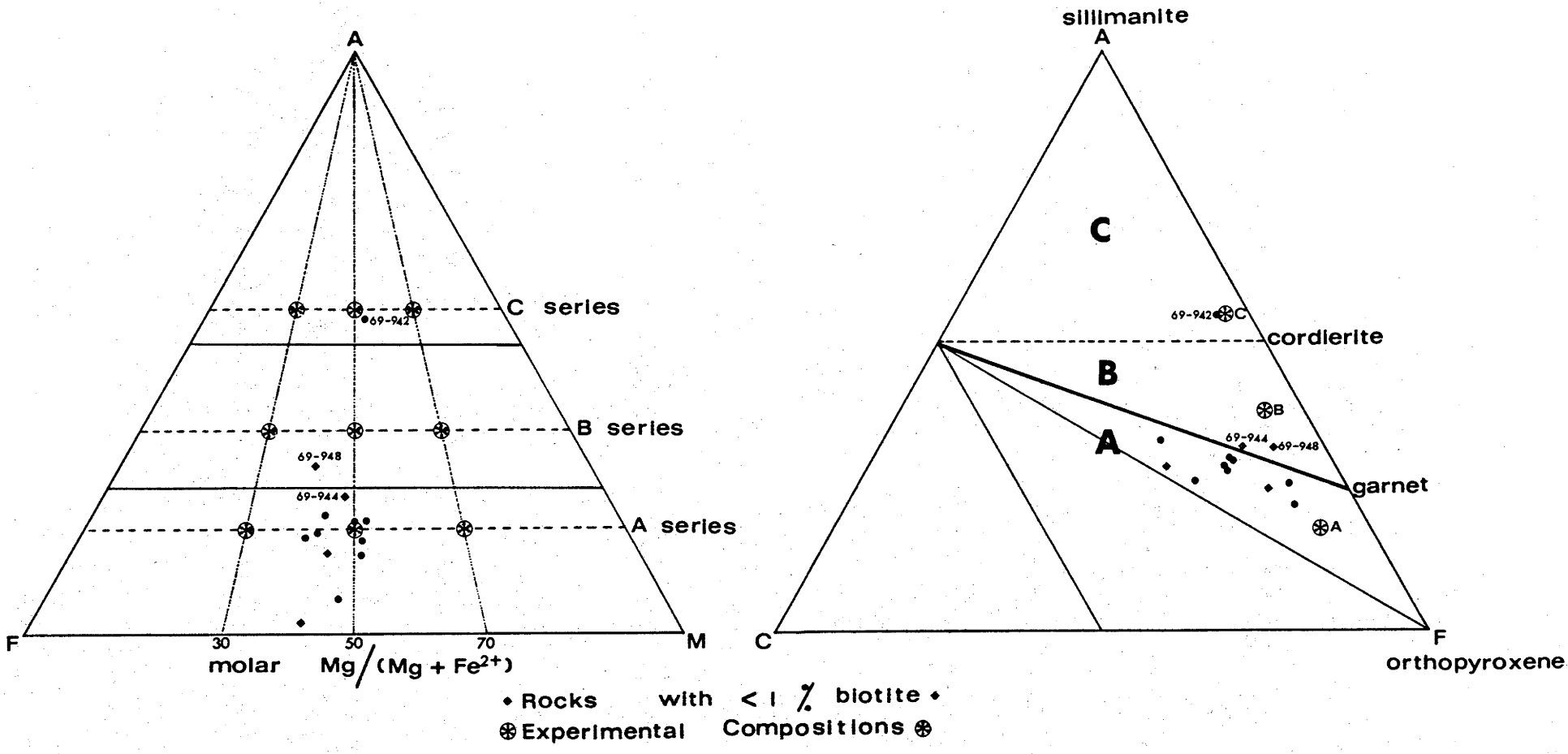

FIGURE 6.3 : COMPARISON OF GARNET-GNEISSES WITH EXPERIMENTAL COMPOSITIONS. (Experimental Compositions from Hensen (1970) and Hensen & Green (1971)).

grossular component in garnet, it stabilisies garnet to lower pressures (Hensen, 1970). Two rocks (69-944 and 69-948) plot in the B-series field in the ACF diagram. Both contain minor sillimanite and are clearly B-series compositions, although one plots slightly within the A-series field in the AFM diagram. The average of the two rocks is given in table 6.2. The rocks contain ∿32 and ∿37% normative quartz, considerably in excess of the amount present in the experimental compositions. Since the amount of quartz present does not affect garnet-cordierite equilibria, quartz has been subtracted and the average recalculated to the same SiO_2 as the B50 experimental composition. The recalculated garnet-gneiss average is similar to B50 composition except that Al, Fe, Mg and Mg/Fe are slighly lower and Na and K higher. The closenss of Ca is critical. Na and K are considerably higher than B50 but do not affect the stability of garnet and cordierite (Hensen, 1970). Hence the compositional differences between the garnet-gneisses and B50 composition have no significant effect on garnet-cordierite stability relationships and the two may be used as P_{total} and T indicators.

Absence of cordierite in the two garnet-gneisses corresponding to B-series compositions and with molar MgO/(MgO+FeO) ratios of 0.41 and 0.48 restricts P_{total} and T above the band in figure 6.2 representing elimination of cordierite in B30 to B50 compositions. The absence of sapphirine in the same rocks restricts T below that of the sapphirine stability field.

6.2.5 P-T Conditions of the Granulite Metamorphism

The combination of P_{total}-T restraints in 6.2.2, 6.2.3 and 6.2.4 restricts metamorphic conditions to the field bounded by 850°C at 9 kb and 1050°C at 8 to 12 kb. This field is marked with crosses in figure 6.2.

Stringent application of P_{total}-T restraints may not be valid for the garnet-cordierite relationship. These restraints should be more flexible, since relatively small amounts of biotite may eliminate the minor cordierite present

just below the "cordierite-out" boundaries. However cordierite was an abundant experimental phase for pressures more than ∿1 kb below the "cordierite-out" boundaries. Allowing ∿1 kb latitude expands the P_{total}-T field to the B30 "cordierite-out" boundary. This expands the lower portion of the metamorphic field to ∿800°C at 8 kb and to ∿1000°C at 7 kb. The field of metamorphism is represented in later diagrams as a triangle bounded by solid lines for the first field (marked with crosses in figure 6.2) and the more "cautious" extension marked by dashed lines.

6.3 ADDITIONAL MINERALOGICAL P_{total}-T CONSTRAINTS

6.3.1 Alumino-silicate Stability

The sillimanite-kyanite transformation is dependent solely on P_{total} and T. Compilation of recent data (figure 6.4) indicate that sillimanite must be the stable alumino-silicate phase in Eyre Peninsula metamorphic rocks. This is consistent with the observed mineralogy.

6.3.2 Muscovite Stability

Muscovite in quartz-bearing assemblages melts incongruently at high pressures. The decomposition is dependent on P_{total}, Pe_{H_2O} and T. Because muscovite decomposes by melting, reduction of Pe_{H_2O} may result in slightly increased stability, but not decreased stability (see 6.4). Hence the maximum stability of muscovite for $Pe_{H_2O} = P_{total}$ (figure 6.4) may be slightly less than the maximum possible stability. Muscovite is not stable in Eyre Peninsula acid gneisses limiting P_{total} below and T above the decomposition band in figure 6.4. This is consistent with indicated conditions of metamorphism.

6.3.3 The Eclogite Transformation

6.3.3.1 Basaltic Rocks

Mineralogical reactions in the transformation of anhydrous basalt to eclogite relevant to metamorphism at Eyre Peninsula include:

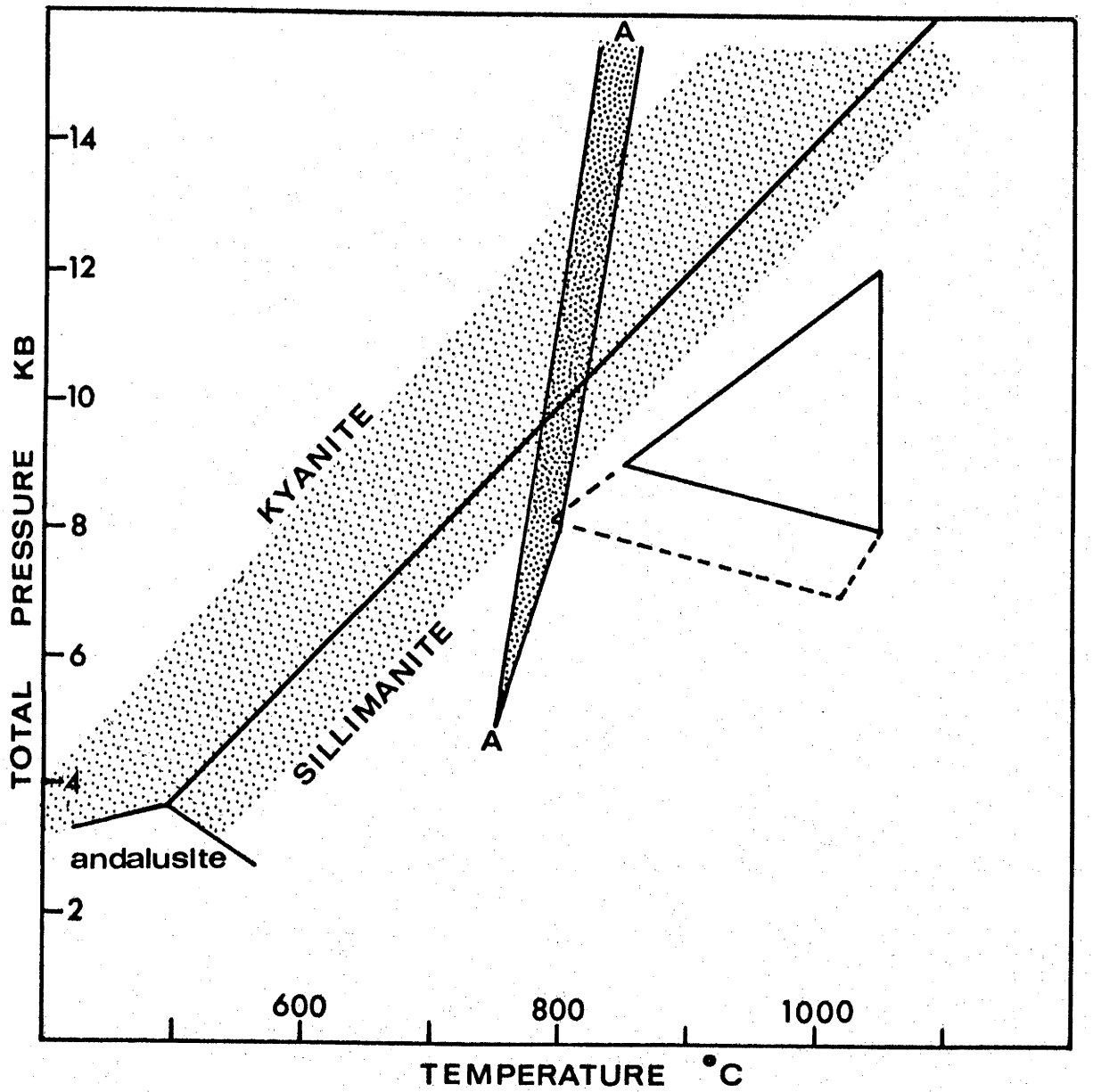

FIGURE 6.4 : P-T CONDITIONS OF THE GRANULITE FACIES METAMORPHISM (TRIANGULAR AREA) COMPARED WITH THE MAXIMUM STABILITY OF MUSCOVITE AND THE SILLIMANITE-KYANITE TRANSFORMATION.

The band A-A (heavy stipple) representing the maximum stability of muscovite in quartz-bearing rocks for $Pe_{H2O} = P_{total}$ is from Segnit & Kennedy (1961). The kyanite-sillimanite-andalusite transformations (solid lines) and the lightly stippled field representing the spread of most experimental determinations of the sillimanite-kyanite transformation are from Holdaway (1971)

olivine + anorthite = orthopyroxene + clinopyroxene + spinel (1)

orthopyroxene + clinopyroxene + spinel + anorthite = garnet (2)

olivine + anorthite = garnet (3)

orthopyroxene + anorthite = garnet + clinopyroxene + quartz (4)

6.3.3.1.1 Olivine-Spinel Relationships

Primary igneous olivine is unstable in contact with plagioclase in several metabasalts. One sample analysed (69-739) has picritic tholeiite composition with molar MgO/(MgO+FeO) ∿0.8 and ∿30% normative olivine. Olivine is either shielded from plagioclase by a rim of relict igneous pyroxene, or has reacted with plagioclase to produce a corona of orthopyroxene + clinopyroxene ± green spinel (the spinel may also occur as inclusions in the olivine). Reaction (1) was first observed at 1000°C and 7 kb by Green & Ringwood (1967a) in olivine tholeiite (molar MgO/(MgO+FeO) = 0.66 and 23% normative olivine). Olivine was eliminated and garnet first produced by reaction (2) at 9 kb and 1000°C. The corresponding reactions in the picritic tholeiite (69-739) would occur ∿1 kb higher because of the higher MgO/(MgO+FeO) and higher olivine content. The first instability of olivine + plagioclase, the elimination of olivine and formation of garnet are shown in figure 6.5A.

The instability of olivine (reaction 1) but preservation of abundant olivine and absence of garnet (reaction 2) are compatible with metamorphism in the lower portion of the stippled band in figure 6.5A. The portion of this field within the postulated metamorphic conditions is the hatched field in figure 6.5B & C.

6.3.3.1.2 Garnet-Olivine Relationships

Garnet occurs in one olivine tholeiitic metabasalt (69-1175) with molar MgO/(MgO+FeO) ∿0.5 and ∿10% normative

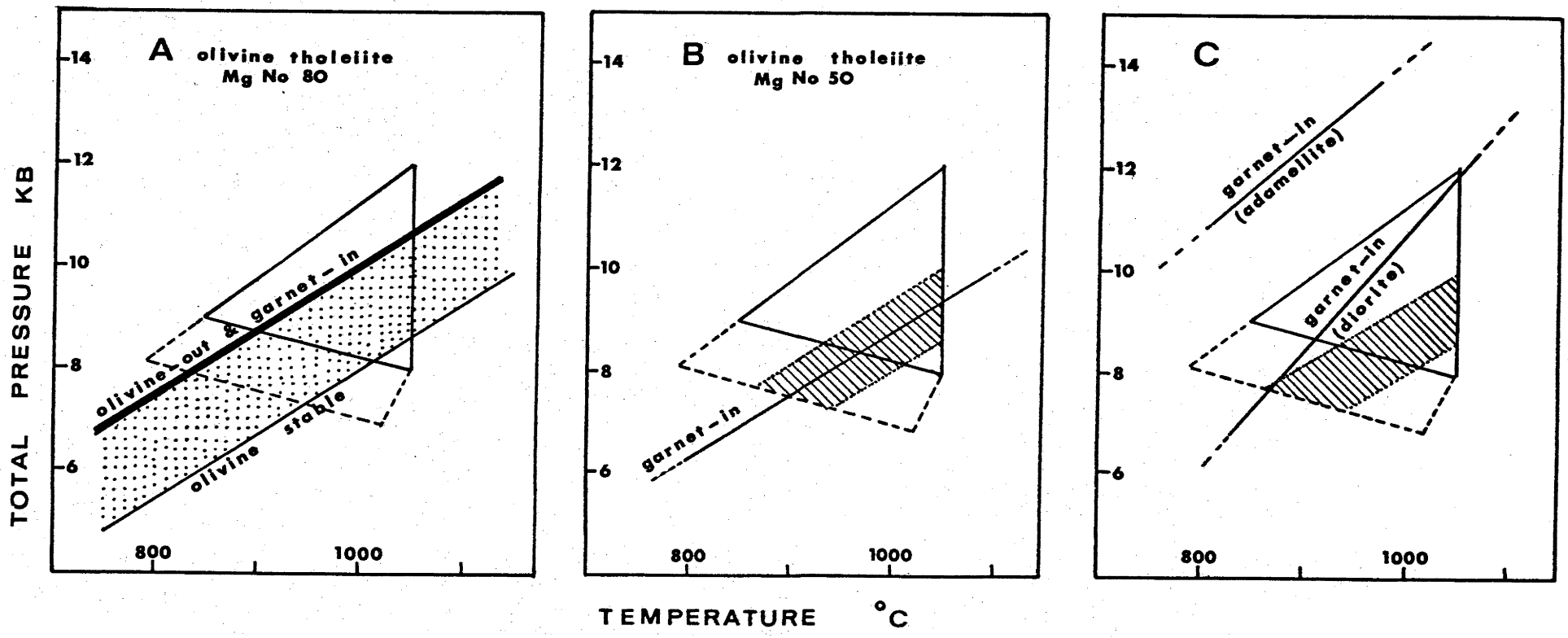

FIGURE 6.5 : COMPARISON OF THE P-T FIELD OF THE GRANULITE METAMORPHISM WITH VARIOUS HIGH PRESSURE REACTIONS.

A. The stippled band represents the reaction of olivine with plagioclase in olivine tholeiite with molar MgO/(MgO+FeO) ≈ 0.8. Olivine is eliminated, and garnet first appears at the top of the band (heavy solid line). (Extrapolated from data of Green & Ringwood, 1967a).

B. The "garnet-in"line marks the first appearance of garnet in olivine tholeiite with molar MgO/(MgO+FeO) ≈ 0.5 (Interpolated from data of Green & Ringwood 1967a). The hatched area represents the lower portion of the stippled field in A.

C. "Garnet-in" reactions for adamellite (Green & Lambert, 1965) and diorite (Green, 1970).

olivine. The garnet occurs as discrete grains and as discontinuous rims to polygranular aggregates of orthopyroxene, clinopyroxene, opaques, biotite±hornblende. Some of the aggregates enclose cores of relict igneous orthopyroxene. Tilley (1921a) has observed identical mineralogical relationships in samples from the same location, but records one rock with olivine cores in addition to igneous pyroxene cores. Hence, the formation of garnet may be attributable to reaction (3).

Green & Ringwood (1967a) observed the formation of garnet in olivine tholeiites at pressures as much as 3 kb lower than in quartz tholeiites with the same MgO/(MgO+FeO). The first formation of garnet in olivine tholeiite with molar MgO/(MgO+FeO) ∿0.5 (= 69-1175) is shown in figure 6.5B. The P_{total}-T conditions are compatible with postulated conditions of metamorphism and conditions for reaction of olivine (figure 6.5A).

The formation of pyroxenes+spinel by reaction (1) in the picritic tholeiite (69-739) but garnet by reaction (3) in the tholeiite (69-1175) is due to different Fe/Mg ratios. Iron-rich compositions (e.g. 69-1175) produce direct reaction of olivine+plagioclase to garnet, or more rapid elimination of intermediate spinel-bearing assemblages (Green & Ringwood, 1967a).

The formation of garnet in the tholeiite is not due to exsolution of a complex high pressure pyroxene (cf. Lovering & White, 1969) since relict igneous clinopyroxene and orthopyroxene show no evidence of exsolution.

6.3.3.2 Acid Rocks

Garnet-forming reactions in acid to intermediate rocks analogous to those in the basalt to eclogite transformation have been experimentally studied by Green & Lambert (1965) and Green (1970). Green (1970) attributed formation of garnet in the diorite to reactions between plagioclase and both orthopyroxene and clinopyroxene. The first appearance of garnet in adamellite and diorite with molar MgO/(MgO+FeO) ∿0.5 are shown in figure 6.5B.

Garnet occurs in Mg-poor granodioritic gneisses (molar MgO/(MgO+FeO) about 0.1) as garnet rims and garnet-quartz symplectitic intergrowths surrounding clinopyroxene, orthopyroxene, hornblende and opaques (magnetite-ilmenite). The symplectite is restricted to zones between these minerals and feldspars (both K-feldspar and plagioclase). The formation of symplectites is due to the reactions:

opaque + anorthite + quartz = garnet

orthopyroxene + anorthite = garnet + quartz

clinopyroxene + anorthite = garnet + quartz

The observation of the coronas or symplectites at K-feldspar contacts may be explained by reaction with anorthite-component in K-feldspar, or with plagioclase either eliminated by reaction or not visible in the plane of the thin section. Coronas surrounding hornblende may be explained by reaction of pyroxenes and plagioclase with water to form hornblende plus garnet-quartz coronas.

The Eyre Peninsula gneisses are closest to the adamellite composition of Green & Lambert (1965). Garnet-formation may have occurred in the Eyre Peninsula gneisses at ∿8 kb and 900°C compared with ∿12 kb and 900°C in the adamellite. The main difference between the two is in MgO/(MgO+FeO) ratios (0.1 and 0.5 respectively). If the pressure difference is due solely to Mg/Fe it represents a shift of ∿4 kb for change of 0.4 MgO/(MgO+FeO) units. The corresponding shift in basics observed by Green & Ringwood (1967a) was only ∿2 kb for 0.3 MgO/(MgO+FeO) units. The pressure of garnet formation in acid gneisses may be more dependent on MgO/(MgO+FeO) ratios. The formation of garnet in diorite at lower pressures than in the adamellite may be due to higher activity of anorthite and lower activity of quartz, both favouring garnet formation. Allowing for Mg/Fe effects, garnet formation may occur in the lower portion of the postulated field of metamorphism.

Griffin & Heier (1969) suggested formation of similar coronas in anorthosites and mangerites at ∿850°C and 9 kb.

6.4 STABILITY OF AMPHIBOLES AND MICAS

6.4.1 The Stability of Hydrous Minerals

Hydrous mineral stability curves become increasingly steeper and finally develop negative slopes with increasing pressure (Essene et al., 1970). Pargasite-hornblende curves become negative at pressures of 10-12 kb (figure 6.2). Hydrous minerals decompose by dehydration or incongruent melting. Hornblende, ferropargasite, tremolite-ferrotremolite, anthophyllite-gedrite and biotite dehydrate without melting. Muscovite, pargasite and phlogopite dehydrate at low pressures (<5 kb for muscovite and <3 kb for pargasite and phlogopite), but melt incongruently at high pressures. Hydrous minerals rarely occur as monomineralic rocks and are usually part of a mineral assemblage. Dehydration is then possible only at temperatures below the water-saturated solidus of the host rock.

At high P_{total} and T, free water combines with anhydrous components to produce stable hydrous minerals until the rock composition is saturated in amphibole and/or mica, or until infinitesimal free water remains. "Excess" water-bearing vapour can coexist with rocks undersaturated in "potential" stable hydrous mineral only if the vapour is "impure" so that Pe_{H_2O} in the vapour equals that in the mineral. Fluid phase in deep crustal rocks is negligible compared with water combined in hydrous minerals.

Rocks containing hydrous minerals melt at water-saturated solidi in the presence of "pure" aqueous fluid, at water-undersaturated solidi in the presence of "impure" aqueous fluid or at "vapour-absent" solidi. The "vapour-absent" solidus or beginning of melting curve (BoM) is defined by the locus of equal Pe_{H_2O} in hydrous mineral and first melt (Burnham, 1970; Fyfe, 1970; Brown & Fyfe, 1970; Green, 1971). The hydrous mineral melts fractionally as the temperature is raised above the BoM. Iron-rich end member melts selectively and residual hydrous mineral becomes more magnesian. The hydrous mineral must be completely eliminated before the stability of the Mg-rich end-member in equilibrium with water-undersaturated melt is exceeded. The band within which hydrous mineral coexists with

melt is a function of the relative stabilities of the mineral prior to melting and the most stable end member. The maximum stability of a hydrous mineral is marked by the BoM band regardless of whether melting commences at water-saturated, water-undersaturated or "vapour-absent" solidi.

6.4.2 The Stability of Amphiboles and Micas

The onset of granulite metamorphism is defined by the first appearance of orthopyroxene in basic rocks. The formation of orthopyroxene is commonly due to decomposition of amphibole, usually hornblende. Hence, factors influencing the decomposition of amphiboles are of critical importance in the study of granulite metamorphism. Formation of orthopyroxene from decomposition of biotite-phlogopite in acid rocks is complicated by melting and obscured by the common formation of secondary biotite-phlogopite. The following factors markedly affect amphibole and biotite-phlogopite stabilities.

(1) Fe^{2+}-Mg Substitution Fe^{2+} end members are less stable than Mg end members (Ernst, 1968; Wones & Eugster, 1965). For f_{O_2} on the QFM buffer, ferrotremolite and ferropargasite are ~400°C less stable than tremolite and pargasite respectively.

(2) Oxygen fugacity, f_{O_2} The stability of Fe^{2+}-bearing biotites and amphiboles is reduced by increased f_{O_2} (Ernst, 1968). Granulite metamorphism, however, is characterised by relatively low f_{O_2} and this effect is minimised.

(3) Fe^{3+} and Ti substitution Fe^{3+} and Ti substitution increase the stability of amphibole (Ernst, 1968; Holloway & Burnham, 1972). Ti substitution was suggested to increase the stability of biotite (Rutherford, 1969).

(4) F substitution for OH F substitution increases the low pressure dehydration stability of pargasite and phlogopite (Fedoseev *et al.*, 1970; Yoder & Eugster, 1954; Munoz & Eugster, 1969). However, if decomposition involves melting at higher pressures the stabilities should be reduced

because F has a much more enhanced effect of depression solidi than OH (Wyllie & Tuttle, 1961b).

(5) Silica Activity Amphibole decomposes more readily in the presence of quartz. Localised increase in a_{SiO_2} due to proximity of acid gneiss or melt may be sufficient to cause amphibole decomposition in basic gneisses.

(6) Equilibrium water pressure Decreasing Pe_{H_2O} decreases low pressure dehydration stability (Greenwood, 1961; Ernst, 1968; Bryhni et al., 1970) but may increase high pressure melting stability (Yoder & Kushiro, 1969; Holloway, 1972). Pe_{H_2O} may be decreased by dilution of aqueous fluid with melt-insoluble fluid (e.g. CO_2 below 15 kb: Hill & Boettcher, 1970), or by dissolution of water in melt.

Metamorphism of mixed acid and basic gneisses may melt the acid but not the basic gneisses. In consequence, hydrous minerals in acid gneiss must melt but those in basic gneisses will usually dehydrate. Amphiboles in high grade basic metamorphics range in composition from hornblende (in amphibolites) to edenitic or pargasitic hornblende (in granulites) (Binns, 1969). The last two compositions may melt at high pressures.

Hornblende in basic gneisses may decompose in response to decreased Pe_{H_2O} caused by melting in adjacent acid gneisses (Bryhni et al., 1970; Green & Mysen, 1972). Diffusion of water from the basic gneisses into the melt would be slow due to low permeability. However, hornblende may be completely decomposed and eclogite or pyroxene granulite stabilised due to reduced Pe_{H_2O}. The common association of desiccated basic gneisses and pegmatitic melted patches in adjacent acid gneisses (Green & Mysen, 1972) favours destabilisation of amphiboles by reduced Pe_{H_2O}. This infers that high grade edenitic or pargasitic hornblende dehydrate at high pressures.

6.4.3 The Stability of Hornblende at Eyre Peninsula

Pegmatitic melted acid gneiss is commonly observed adjacent to basic rock inclusions at Eyre Peninsula. The melting may have reduced Pe_{H_2O} and resulted in partial or complete decomposition of hornblende in the basic rocks. However, in most cases the basic rocks had been extensively rehydrated by water released during later crystallisation of the melt.

6.5 CONCLUSION

Mineralogical data indicate granulite metamorphic conditions at Eyre Peninsula of 800-950°C at 7-9 kb. Assuming a pressure gradient of 350 bars/km, this indicates formation at depths of 20-26 km. Geothermal gradients during metamorphism were relatively high (35-45C°/km). The terrain represents reasonably deep-crustal material which has undergone metamorphism in the medium pressure granulite field of Green & Ringwood (1967a).

The absence of abundant melting in acid gneisses is commonly used to restrict estimates of granulite facies temperatures to values near or below the water-saturated granite solidus. These estimates do not take into account the minor amounts of water present in high grade metamorphic rocks prior to anatexis. The restricted amount of water limits the volume of water-saturated melt generated. In consequence, temperatures 100-150C° higher than the water-saturated granite solidus may be attained before obvious volumes of melt are generated. The obvious volume of pegmatitic melts formed during metamorphism of the water-deficient Eyre Peninsula terrain suggests that temperatures ∿150C° above the water-saturated granite solidus (i.e. ∿800°C at 7-8 kb pressure) were attained during the metamorphism. This is consistent with the mineralogical temperature estimates.

CHAPTER 7

METAMORPHIC FACIES AND RETROGRESSION

7.1 THE METAMORPHIC FACIES CONCEPT

Metamorphic rocks have been subdivided into "facies of metamorphism" (Fyfe et al., 1958; Winkler, 1967; Turner, 1968). The definitions of metamorphic facies most commonly used are similar to the definition of Turner (1948):

> A metamorphic facies includes rocks of any chemical composition and hence of widely varying mineralogical composition, which have reached chemical equilibrium during metamorphism under a particular set of physical conditions.

Ideally, the mineralogical composition of a rock belonging to a specific metamorphic facies is determined uniquely by its chemical composition. Chemical equilibrium under the specific P-T conditions of metamorphism was included in the definitions of Eskola (1920/21), Tilley (1924), Turner (1948), Lambert (1965) and Winkler (1970). However, Eskola (1939), Fyfe et al., (1958), Turner & Verhoogen (1960) and Fyfe & Turner (1966) omitted P-T conditions and equilibrium from their definitions of metamorphic facies, and stated that metamorphic facies had to be used as purely descriptive terms applicable to "groups of mineral assemblages repeatedly associated with one another in space and time with a constant and predictable relationship between mineralogy and chemical composition." Fyfe et al., (1968), Turner & Verhoogen (1960) and Fyfe & Turner (1966) suggested that the mineral assemblages within a facies had attained approximate equilibrium within a definite range of temperature and pressure and that the repetition of facies is controlled by common recurrence of similar physical conditions of metamorphism. The range of physical conditions of metamorphism can generally be inferred from the stable mineral assemblages. Fyfe & Turner (1966) stressed that the boundaries between metamorphic facies are gradational, and are characterised by transitional mineral assemblages and/or the association of rocks from both metamorphic facies.

For any given set of external physical and chemical parameters (P_{total}, T, Pe_{H_2O}, Pe_{CO_2}, f_{O_2}, etc.) there is a constant and predictable relationship between the stable mineralogy and chemical composition of a metamorphic rock, provided that all compositional aspects (such as Fe/Mg and a_{SiO_2}) are taken into account. This constant and predictable relationship is due to chemical equilibration of the minerals in the rock under the specific conditions of the metamorphism, and is the basis of the metamorphic facies concept. The specific metamorphic facies are characterised by the nature of the relationship between their mineralogy and composition. The early usage of the metamorphic facies concept inferred that the mineralogy/composition relationship occurred within a specific P-T interval and consistently occurred in any terrain metamorphosed within this P-T interval. However, the mineralogy/composition relationship usually varies continuously with P_{total} and T, because many metamorphic reactions are "sliding reactions" involving complex solid-solutions whose compositions vary continuously. Variation of other parameters, such as Pe_{H_2O}, Pe_{CO_2} and f_{O_2}, independently of P_{total} and T, further complicates the predictability of the mineralogy/composition relationship. Metamorphic facies were subdivided into "subfacies" in an attempt to rationalise the more complex variation of mineralogy due to these factors. The subdivision of facies into subfacies was based on mineral reactions other than those defining facies (Turner & Verhoogen, 1960; de Waard, 1965, 1966; and Winkler, 1967). The subdivision has been criticised on thermodynamic grounds by Chesworth (1967) and Saxena (1969d), and on the grounds of impracticability by Turner (1968) and Fyfe & Turner (1966). It is now recognised that the subfacies scheme is inadequate to classify all metamorphic reactions, and abolition of subfacies has been proposed by Fyfe & Turner (1966), Turner (1968) and Winkler (1970). Winkler (1970) also proposed replacement of the present facies concept with a broader four-fold division into very low, low, medium and high metamorphic stages separated by "major isograds" marking the appearance and/or disappearance of specific minerals. Winkler (1970) also suggested that "isograds" within the metamorphic

stages could be used to mark other significant mineralogical changes. The term "isograd" was used by Winkler (1970) in the descriptive mineralogical sense with no P-T implications, since specific mineral reactions may be dependent on compositional variables such as Fe^{2+}/Mg, Pe_{H_2O} and f_{O_2} in addition to P_{total} and T.

The major difficulties facing the metamorphic facies concept include the widespread and incorrect assumption that a particular facies occurs within a unique P-T interval, and the complexity arising from earlier definitions which specified a unique correlation between mineralogy and composition, and led to the erection of the facies/subfacies scheme. It is suggested that the proposed abolition of subfacies be accepted, but that the present facies concept is too firmly entrenched in petrology to be replaced by an entirely new scheme as proposed by Winkler (1970). Use of metamorphic facies in the descriptive mineralogical sense is still viable, provided that application follows more flexible guidelines similar to those of Fyfe & Turner (1966), which allow for minor variation of mineralogy (in rocks of similar composition) within the broader framework of the facies. It must also be realised that adjacent facies usually overlap considerably, and that rocks belonging to different facies may crystallise within the same P-T interval. The P-T conditions of metamorphism may be deduced from the metamorphic facies present, or from combination of data provided by two or more mineralogical isograds (Winkler, 1970) and the chemical composition of the rocks.

7.2 PROGRESSIVE AND RETROGRESSIVE METAMORPHISM

The progression from low P-T to high P-T conditions within an individual rock mass is an increase in "metamorphic grade" or "progressive metamorphism", and the reverse is "retrogressive metamorphism" or "retrogression". More specifically, retrogression means the replacement of a high P-T mineral assemblage (commonly anhydrous) by a lower P-T assemblage (commonly hydrous). In general, the terms "progressive metamorphism" and "retrogressive metamorphism"

are consistently applied to specific mineralogical reactions, although the causes of the reactions may be quite different in individual cases. For example, the replacement of orthopyroxene, clinopyroxene and plagioclase by hornblende is always termed "retrogression", but may theoretically be caused by: a decrease in T at constant Pe_{H_2O} and P_{total}; an increase in Pe_{H_2O} at constant T; an increase in Pe_{H_2O} with increasing T; or a decrease in f_{O_2} at constant Pe_{H_2O}, P_{total} and T.

7.3 GRANULITE FACIES METAMORPHISM

Granulite facies rocks are formed at extreme temperatures of regional metamorphism and are characterised by anhydrous mineral assemblages or hydrous mineral assemblages in which amphiboles and/or biotite-phlogopite micas have partly decomposed to yield anhydrous orthopyroxene-bearing products. The most common minerals in granulite facies rocks are quartz, orthoclase, plagioclase, orthopyroxene, clinopyroxene, garnet, cordierite, kyanite and/or sillimanite, amphibole (usually edenitic or pargasitic hornblende) and biotite-phlogopite. Rocks containing amphibole and/or biotite-phlogopite must also contain orthopyroxene in order to be classified as granulite facies metamorphic rocks.

The first formation of granulite facies rocks with increasing metamorphic grade is most commonly defined in the literature by the first appearance of orthopyroxene (enstatite-ferrosilite) resulting from decomposition of amphiboles or biotite-phlogopite (usually in basic rocks: Buddington, 1963; Binns, 1964; and Lambert, 1965) during regional metamorphism. The temperature at which orthopyroxene is first formed during progressive metamorphism is a complex function of total pressure, fluid pressure, fluid composition, oxygen and silica activities and chemical composition (especially Fe/Mg). The temperatures at which orthopyroxene is first formed (the "orthopyroxene isograd") with increasing metamorphic grade at pressures of 4 to 10 kb may range from 550°-600°C (in iron-rich rocks in metamorphosed iron formations: Klein, 1966), to 750°-800°C

(in common basic rocks: Binns, 1964, 1969b), or even up to 1000°-1100°C (the maximum stability of Mg-rich amphibole: Bryhni et al., 1969; Essene et al., 1970; Holloway, 1972). This P-T field covers the entire amphibolite and granulite facies fields of Fyfe et al., (1958), Winkler (1967), and most of Turner's (1968). Orthopyroxene is formed in Fe-rich basic rocks at temperatures lower than in Mg-rich basic rocks; and hornblende in quartz-bearing basic rocks decomposes to form orthopyroxene at temperatures lower than hornblende in quartz-free basic rocks. In consequence, basic rocks with different Fe/Mg ratios or different silica contents may be assigned to different metamorphic facies, although they equilibrated at the same P-T conditions.

It is critical to realise that granulite facies mineral assemblages are formed over a very wide P-T interval within which amphibolite facies mineral assemblages may also be stable. The P_{total} and T conditions of granulite metamorphism may only be determined after the effects of rock composition, f_{O_2}, a_{SiO_2}, and Pe_{H_2O} have been taken into account. Determination of Pe_{H_2O} is commonly impossible, since unpredictable lowering of Pe_{H_2O} may be caused by anatexis in adjacent acid gneisses. $Pe_{H_2O} \simeq P_{total}$ may be assumed if adjacent gneisses show no signs of anatexis and are carbonate-free.

7.4 GRANULITE/AMPHIBOLITE FACIES RELATIONSHIPS

The transition from amphibolite facies to granulite facies metamorphic terrain may occur at major structural discontinuities (Collerson et al., 1972), or may be gradational, with development of granulite facies assemblages in an increasingly larger proportion of the rocks in the terrain with increasing metamorphic grade (Binns, 1964).

Granulite facies rocks (especially pyroxene granulites) rarely occur independently of amphibolite facies rocks (e.g. de Waard, 1967; Jakeš, 1969). Pyroxene granulite "subfacies", hornblende granulite "subfacies" and amphibolite facies rocks are almost invariably intimately associated.

This association appears to be characteristic of terrains containing granulite facies metamorphic rocks, and is almost always dismissed as the result of retrogressive metamorphism. It is inferred that many of the rocks that attained granulite facies were partly or wholly re-crystallised to amphibolite facies mineralogy during declining metamorphic temperatures.

7.5 GRANULITE/AMPHIBOLITE RELATIONSHIPS AT EYRE PENINSULA

7.5.1 Field Relationships

Granulites and charnockites are absent and only amphibolite facies rocks are present in the portion of the Eyre Peninsula terrain marked with crosses in figure 1.1. All other locations sampled contain closely associated basic pyroxene granulites, hornblende granulites, retrogressed granulites and amphibolites. The associated acid gneisses are garnet-gneisses, charnockites, and less commonly, granitic gneisses. Amphibolite facies rocks are absent only in the Fishery Bay region (figure 1.1), which contains closely associated basic pyroxene granulites and hornblende granulites. The acid gneisses are charnockites and garnet-gneisses.

Many basic amphibolites and retrogressed granulites have been intruded and disrupted by pegmatites. The field evidence suggests that these basic granulites were recrystallised to amphibolite mineralogy in response to the higher Pe_{H_2O} associated with the intrusion and crystallisation of the pegmatites.

7.5.2 Petrographic Relationships

The presence of metamorphic orthopyroxene in basic rocks is characteristic of granulite facies metamorphism. The primary granulite assemblages in the basic rocks are characterised by polyhedral mineral grains. The minerals are orthopyroxene, clinopyroxene and plagioclase in the pyroxene granulites, and hornblende, orthopyroxene, clinopyroxene and plagioclase in the hornblende granulites.

Retrogression of the basic granulites causes crystallisation of secondary hornblende and/or biotite at the expense of orthopyroxene, clinopyroxene and plagioclase. The retrograde hornblende and/or biotite are characterised by coarser grain size, and cut across the primary polyhedral aggregate of granulite minerals. The hornblende and/or biotite are moulded upon and intergrown with the primary pyroxenes, and the contacts between the two types of minerals are fuzzy and gradational. The use of the above textural criteria generally allows subdivision of the basic granulites into pyroxene granulites, hornblende granulites, retrogressed pyroxene granulites and retrogressed hornblende granulites. The primary granulite assemblage may not be discernable in some intensely retrogressed rocks, which are classified as retrogressed granulites. Basic rocks in which orthopyroxene is absent are classified as amphibolites.

Many of the acid rocks have well-developed gneissic foliation and were more readily deformed during the metamorphism than the basic rocks (which have weakly developed gneissic foliation or are massive). The ready deformation of the acid gneisses facilitates entry of water and formation of secondary hydrous assemblages. Designation of hydrous minerals as primary or secondary on the basis of textural evidence is impossible due to the deformed nature of the acid gneisses. On these grounds the acid gneisses are unsuitable as indicators of metamorphic grade, and their mineralogy is not considered in this section. The compact interlocking nature of the granulite minerals in the basic rocks commonly prevented or restricted entry of water, and many primary granulite assemblages are preserved. Water entered many basic granulites and caused crystallisation of secondary hydrous minerals, but in most cases these could be distinguished texturally from the primary minerals. The basic rocks are therefore considered as the best indicators of metamorphic grade.

7.6 RETROGRESSION AT EYRE PENINSULA

7.6.1 The Effects of Retrogression

Several retrogressed granulites and amphibolites were excluded from the basic rock average for K, Rb and Ba (chapter 2). These include a basic xenolith from a charnockite batholith and rocks adjacent to pegmatites or pegmatitic acid gneiss bands (69-790 and 69-782, 69-788, 69-794, 69-1352: appendix C). The rocks have higher K and proportionally even higher Rb and Ba than the other basic rocks. This feature is evident in the low K/Rb ratios of the rocks (117, 248, 200, 163 and 330 respectively cf. the average K/Rb ratio of 487 for the other basic rocks). The higher K, Rb and Ba appear to be the result of reaction with pegmatitic fluids during retrogression. Several other partly retrogressed granulites and amphiboles have low K/Rb ratios (69-1175, 69-1397, 69-748, 69-775, 69-785 and 69-786: 197, 246, 195, 261, 150 and 176 respectively). However, K, Rb and Ba are within the normal continental tholeiite range, and cannot be used as evidence for enrichment of these elements during retrogression.

7.6.2 A Retrogression Sequence

Five pyroxenites were collected in reasonably close proximity. One (69-756) is not associated with pegmatites and is a pyroxene granulite with extremely minor retrogression. The others (69-786, 68-785, 69-1352 and 69-788) are associated with pegmatitic acid gneiss bands, and exhibit successively greater degrees of retrogression or rehydration evident in increasing hornblende and biotite, and due to different degrees of reaction with pegmatitic fluids (left to right in table 7.1). K, Rb, Ba, Sr, total H_2O and Fe_2O_3 increase regularly with increasing degree of retrogression. The increases in K, Rb and Ba are mainly controlled by the crystallisation of retrograde biotite. The high K/Rb (524) and low K, Rb and Ba (0.06%, 0.95 ppm and 26 ppm) of the least retrogressed pyroxenite (69-756) is considered more respresentative of the pyroxenites prior to retrogression. The low K/Rb and high K, Rb and Ba are the results of retrogression. The

TABLE 7.1

RETROGRESSION SEQUENCE IN PYROXENITES

——————INCREASING RETROGRESSION ——————→

	69-756	69-786	69-785	69-1352	69-788
SiO_2	52.21	52.00	53.33	44.76	43.34
TiO_2	0.37	0.46	0.45	2.21	2.22
Al_2O_3	2.87	5.83	5.95	7.20	6.03
Fe_2O_3	0.30	1.31	1.59	3.78	5.19
FeO	9.33	13.69	13.39	12.70	11.87
*total FeO	9.60	14.87	14.82	16.11	16.54
MnO	0.21	0.28	0.27	0.25	0.24
MgO	20.20	15.79	17.62	16.76	16.30
CaO	12.97	6.32	3.85	7.84	8.02
Na_2O	0.38	1.20	1.16	0.97	0.55
K_2O	0.06	0.68	0.67	1.79	2.53
P_2O_5	0.07	0.15	0.11	0.11	0.29
total H_2O	0.31	0.78	0.88	0.83	1.81
Rb	0.95	32	37	45	105
Ba	26	178	175	221	737
Sr	75	80	85	96	132
Zr	38	69	84	124	147
Nb	< 0.8	5	5	30	36
Hf	1.0	--	--	--	2.8
Th	0.4	--	--	1.1	3
U	0.2	--	--	0.4	0.9
La	9	10	9	20	34
K/Rb	524	176	150	330	200

*total iron as FeO

smooth increase in Sr does not correlate with Na or Ca, and also appears to be due to the retrogression.

Ti, Zr, Nb, Hf, La and Th also increase smoothly with increasing retrogression. All of these elements are immobile during alteration and metamorphism of basic rocks (chapter 2), and the observed variation must be a primary feature. The parallel increase in Ti, Zr, Nb, La and Th is predicted by the significant positive correlation of these elements (table 2.2). U may be mobile during metamorphism of the basic rocks, and the increase in U may be due to the retrogression. Two intensely retrogressed samples (69-788 and 69-1352) have low Si and high Ti; while the converse is true of the less retrogressed samples (this is consistent with the significant negative correlation between Si and Ti for all Eyre Peninsula basic rocks). This could be explained in two ways: (1) the samples with high Ti and higher abundance of Ti-rich opaques which provided more efficient nuclei for growth of hornblende and biotite (nucleation of hornblende and biotite on opaques was commonly observed); (2) the samples with high Ti (and hence low Si) contained no quartz, and hornblende and biotite were more stable than in the samples with higher Si and modal quartz (appendices A and C).

No consistent correlation was observed between Ti-content and metamorphic grade or degree of retrogression, suggesting that the first explanation does not apply. However, all the pyroxene granulites are quartz-normative, whereas retrogressed granulites and amphibolites include both quartz-normative and olivine-normative samples (appendix C), suggesting the second explanation is correct.

7.6.3 Other Examples of Retrogression

Other basic rocks were retrogressed by reaction with pegmatites or pegmatitic acid gneiss (69-748, 69-753, 69-782, 69-794, 69-937 and 69-1501: table 7.2). K, Rb and Ba increase together, and K/Rb ratios decrease overall with increasing degree of reaction. K, Rb and Ba were markedly increased by the retrogression in two of the samples (69-782

TABLE 7.2

INTERACTION BETWEEN BASICS AND PEGMATITES OR HOST GNEISSES

BASICS ASSOCIATED WITH PEGMATITES

	K_2O%	Rb ppm	Ba ppm	K/Rb
69-753	0.85	11	33	641
69-1501	0.92	11	32	694
69-937	1.24	30	42	343
69-748	1.34	57	276	195
69-782	2.60	87	664	248
69-794	3.08	157	698	163

BASICS WITH NO ASSOCIATED PEGMATITES

		K_2O%	Rb ppm	Ba ppm	K/Rb
	69-1167	0.85	15	87	470
(host gneiss)	69-951	1.88	33	663	473
	69-1175	1.07	45	241	197
	69-775	1.13	36	100	261

BASIC XENOLITH AND HOST MAGMA

		K_2O%	Rb ppm	Ba ppm	K/Rb
	69-790	3.84	273	432	117
(host)	69-956	4.25	200	856	188

and 69-794). Another sample (69-748) has moderate K, Rb and Ba, possibly due to reaction. The other samples (69-753, 69-937 and 69-1501) have lower Rb and Ba, and slightly lower K. These samples are not obviously altered by reaction. All of these basic rocks were extensively rehydrated by pegmatites, but increased K, Rb and Ba were obvious in only a few.

One basic pyroxene granulite (69-1358) survived at a pegmatite contact with minor retrogression (less than ∿5% of hornblende + biotite). This suggests that some of the pegmatites were water-deficient. The pegmatites are much more commonly associated with intensely rehydrated granulites and amphibolites, indicating that most of the pegmatites contained appreciable water.

Three amphibolitic basic rocks (with moderate $K_2O \sim 1\%$) included in acid gneiss, but not associated with pegmatites, (69-1167, 69-1175 and 69-775: table 7.2) show no obvious evidence of increased Rb and Ba as a result of retrogression. The host acid gneiss of one sample (69-1167) contains low Rb and relatively low K and Ba. The limited reaction in this case may be partly due to a lower chemical potential gradient of K, Rb and Ba than would have occurred at a pegmatite contact.

K, Rb and Ba in a basic xenolithic schlieren (69-790) were greatly increased by reaction with host plutonic charnockite magma rich in these elements (69-757 and 69-956: table 7.2).

7.7 PRIMARY AND SECONDARY (RETROGRADE) MINERALOGY

7.7.1 Compositional Relationship between Primary and Secondary Mineralogy

The retrograde minerals are in textural disequilibrium with the primary granulite minerals. This suggests that the retrograde minerals are in chemical disequilibrium with the primary granulite minerals, and that the minerals may be compositionally zoned. Electron microprobe scans of the

primary pyroxenes (table 7.3) from the cores of coarser grains to rims adjacent to secondary biotite (69-786) and hornblende (69-788) show no significant compositional zoning. The small variation in compositions is irregular and largely within analytical precision. The absence of zoning in the pyroxenes suggests that the retrogression occurred at similar temperatures to the primary granulite metamorphism, or that the retrograde minerals crystallised at lower temperatures but did not re-equilibrate with the remaining primary granulite minerals. Analyses of retrograde hornblende (table 7.3) show minor compositional zoning.

The absence of pronounced compositional zoning in the minerals analysed by electron microprobe indicate that the minerals separated from the rocks are representative of individual grains. Exceptions to this are the slightly different compositions of the coarse relict igneous pyroxene prisms with exsolution lamellae (69-786 and 69-788: table 7.5). These occur in relatively minor proportions compared with the recrystallised metamorphic pyroxenes and were probably partially removed from the analysed separates due to their slightly lower Fe/Mg ratios (and hence lower magnetic susceptibility).

7.7.2 Pyroxene Compositions

Primary high P-T pyroxenes in rocks with restricted compositional range from the Lizard peridotite contain significantly higher Al than secondary pyroxenes which had recrystallised at lower P-T (Green, 1964). In addition to P-T dependence, the Al-content of orthopyroxenes and, to a lesser extent, clinopyroxenes are dependent on host-rock composition and mineralogy (Binns 1962, 1969a; Leelanandam, 1967; and White, 1969.) Orthopyroxene tends to have lower Al when coexisting with garnet. Pyroxenes coexisting with more sodic plagioclase tend to be more aluminous than those coexisting with calcic plagioclase. Al favours orthopyroxene in spinel-bearing assemblages but favours clinopyroxene in quartz-bearing assemblages. The Al-contents of all the Eyre Peninsula clinopyroxenes analysed are higher than those of the coexisting orthopyroxenes (tables 7.4 and 7.5). The

TABLE 7.3

COMPOSITIONAL VARIATION IN
METAMORPHIC PYROXENES AND HORNBLENDES

	GRANULITE WITH MINOR RETROGRESSION (69-786)				
	Orthopyroxenes			Clinopyroxenes	
SiO_2	52.60	52.38	52.34	51.82	52.40
TiO_2	--	--	--	0.15	--
Al_2O_3	0.89	0.82	0.75	1.77	1.80
total FeO	21.93	21.66	22.15	7.62	7.76
MnO	0.35	0.28	0.36	--	--
MgO	22.89	23.10	22.94	13.94	14.21
CaO	0.52	0.45	0.47	22.73	22.82
Na_2O	--	--	--	0.58	0.36
Cr_2O_3	--	--	--	0.35	0.44
Total	99.18	98.70	99.00	98.96	99.79

	RETROGRESSED GRANULITE (69-788)					
	Orthopyroxenes			Clinopyroxenes		
SiO_2	51.45	52.09	52.19	51.35	52.06	51.23
TiO_2	--	--	--	0.20	0.18	0.20
Al_2O_3	0.62	0.70	0.51	1.86	1.74	1.86
total FeO	23.18	23.88	23.60	8.36	8.68	8.33
MnO	0.43	0.44	0.46	--	--	0.15
MgO	21.63	21.62	21.83	13.78	14.13	13.69
CaO	0.63	0.48	0.37	22.91	22.74	22.79
Na_2O	--	--	--	0.29	0.24	0.29
Cr_2O_3	--	--	--	--	0.18	--
Total	97.94	99.20	98.96	98.74	99.95	98.66

	Hornblendes		
SiO_2	44.10	43.48	43.76
TiO_2	1.38	1.52	1.27
Al_2O_3	11.09	10.99	11.15
total FeO	11.59	11.43	11.13
MnO	--	--	--
MgO	14.57	14.18	14.62
CaO	12.35	12.06	12.19
Na_2O	1.90	1.89	1.79
K_2O	1.64	1.72	1.69
Cr_2O_3	0.14	0.16	0.19
Total	98.77	97.43	97.79

Analyses by non-dispersive electron microprobe. The pyroxenes were scanned from grain cores to rims adjacent to secondary biotite (69-786) and hornblende (69-788). (Scans from cores on left, to rims on right).

pyroxenes from two groups of basic rocks with similar Al-contents may be directly compared.

The first group contains three primary granulite assemblages (69-742, 69-743 and 69-1371) and one secondary amphibolite assemblage (69-794). Al_2O_3 in the granulite clinopyroxenes is moderately high (2.20-2.35%) but that in the amphibolite clinopyroxene is lower (1.56%). Octahedral Al of the amphibolite clinopyroxene (0.026) is within the range of granulite clinopyroxenes (0.017-0.034), but tetrahedral Al of the amphibolite clinopyroxene (0.045) is lower than the granulite clinopyroxenes (0.069-0.081). The lower tetrahedral Al suggests that the amphibolite crystallised at lower temperatures than the granulites. The difference is not explicable by entry of Al into hornblende in the amphibolite because the hornblende contains considerably less Al than the andesine-labradorite plagioclases in the granulites. The pyroxenes in the hornblende granulite have the highest Al. In this case, the higher Al is due to the pyroxenes' coexisting with an additional phase, hornblende, less aluminous than the plagioclase in the pyroxene granulites.

The second group contains three low-Al granulites with differing degrees of retrogression (69-786, 69-785 and 69-788 in order of increasing retrogression). The primary granulite assemblages are identical to those in the first group. The lower Al-contents of the rocks are reflected in less modal plagioclase (or less hornblende and biotite in retrogressed samples) and in lower Al-contents of the pyroxenes compared with those in the first group. The variation of Al and tetrahedral Al in the clinopyroxenes with increasing retrogression is not systematic, suggesting that no re-equilibration occurred between the primary granulite clinopyroxenes and the retrograde minerals. The Al-contents of the orthopyroxenes decrease slightly with increasing retrogression. This suggests that some re-equilibration may have occurred between the primary orthopyroxene and the retrograde minerals. However, the electron microprobe data (7.6.1 and table 7.3) suggest that no

Table 7.4

Clinopyroxene Analyses

	Pyroxene Granulites		Hornblende Granulite	Retrogressed Granulites			Amphibolite
	69-743	69-1371	69-742	69-785	69-786	69-788	69-794
SiO_2	51.23	51.32	51.65	52.73	52.11	51.93	50.62
TiO_2	0.24	0.26	0.29	0.23	0.08	0.28	0.29
Al_2O_3	2.20	2.32	2.35	1.66	1.79	1.85	1.56
Fe_2O_3	2.13	2.43	1.22	0.15	---	1.70	1.23
FeO	9.01	8.56	7.84	7.04	7.69*	7.14	15.24
MnO	0.35	0.30	0.22	0.17	---	0.23	0.41
MgO	12.87	12.33	14.18	15.56	14.08	14.11	8.76
CaO	22.02	21.75	22.15	22.49	22.78	21.84	21.44
Na_2O	0.41	0.44	0.43	0.46	0.47	0.34	0.43
K_2O	0.02	0.02	0.04	0.04	---	0.11	0.06
H_2O+	nd	nd	nd	nd	nd	0.39	nd
H_2O-	nd	nd	nd	nd	nd	0.07	nd
Trace**	0.10	0.11	0.17	0.44	0.44*	0.12	0.03
Total	100.58	99.84	100.54	100.97	99.44	100.11	100.07
			STRUCTURAL FORMULAE BASED ON 6 OXYGENS				
Si	1.919	1.931	1.919	1.940	1.957	1.941	1.955
AlIV	0.081	0.069	0.081	0.060	0.043	0.059	0.045
AlVI	0.017	0.034	0.022	0.012	0.036	0.022	0.026
Ti	0.007	0.007	0;008	0.006	0.002	0.008	0.008
Fe^{3+}	0.060	0.069	0.034	0.004	---	0.048	0.036
Fe^{2+}	0.282	0.269	0.244	0.217	0.242	0.223	0.492
Mn	0.011	0.010	0.007	0.005	---	0.007	0.013
Mg	0.719	0.691	0.785	0.853	0.788	0.786	0.504
Ca	0.884	0.878	0.882	0.887	0.917	0.875	0.887
Na	0.030	0.032	0.031	0.033	0.034	0.025	0.032
K	0.001	0.001	0.002	0.002	---	0.005	0.003
Cr	0.000	0.001	0.004	0.010	---	0.002	0.000
Sum(X+Y)	2.011	1.992	2.019	2.029	2.019	2.001	2.001
Sc	160	140	72	84	nd	44	45
V	250	275	300	230	nd	98	140
Cr	87	130	800	2260	nd	410	47
Co	53	62	55	51	nd	66	56
Ni	35	54	210	460	nd	350	---
Cu	6	12	7	6	nd	21	4
Sr	---	---	---	12	nd	---	---
Ba	---	---	~8	~4	nd	10	---
La	---	---	---	---	nd	---	---
Y	270	140	---	43	nd	40	47

*total Fe as FeO (allocation of Fe^{3+} to give best structural formula gave 1.97% Fe_2O_3 and 5.93% FeO); **includes Sc_2O_3, V_2O_5, Cr_2O_3, NiO and Y_2O_3 when individual values are above 0.01%; ***Cr_2O_3 only; major elements by XRF except 69-786 by non dispersive electron microprobe (69-786 is the average of the analyses in table 7.3); trace elements by emission spectroscope; nd = not determined; --- means not detected.

Table 7.5
Orthopyroxene Analyses

	Pyroxene Granulites		Hornblende Granulite	Retrogressed Granulites			Relict Igneous Pyroxenes	
	69-743	69-1371	69-742	69-785	69-786	69-788	69-786	69-788
SiO_2	51.19	51.13	51.61	52.78	51.98	51.91	50.77	52.08
TiO_2	0.09	0.09	0.09	0.09	0.10	—	—	—
Al_2O_3	1.29	1.34	1.45	0.98	1.13	0.61	1.96	1.14
Fe_2O_5	2.05	2.63	0.80	2.03	2.29	4.09	—	—
FeO	24.81	24.81	23.00	19.01	22.87	19.87	21.40*	22.35*
MnO	0.89	0.72	0.53	0.41	0.44	0.44	0.32	0.48
MgO	18.51	18.22	20.91	23.46	20.06	21.69	22.05	21.74
CaO	0.71	0.59	0.59	0.59	0.68	0.49	0.60	0.48
Na_2O	0.04	0.03	0.06	0.05	0.06	—	—	—
K_2O	0.03	0.09	0.06	0.06	0.04	—	—	—
H_2O+	nd	nd	nd	nd	nd	0.76	nd	nd
H_2O-	nd	nd	nd	nd	nd	0.08	nd	nd
Trace**	0.01	0.04	0.09	0.21	0.20	—	—	—
Total	99.62	99.69	99.19	99.67	99.85	99.94	97.09	98.27
			STRUCTURAL FORMULAE BASED ON 6 OXYGENS					
Si	1.956	1.954	1.954	1.957	1.961	1.955	1.938	1.975
AlIV	0.044	0.046	0.046	0.043	0.039	0.027	0.061	0.025
AlIV	0.014	0.015	0.019	0.000	0.011	0.000	0.027	0.026
Ti	0.003	0.003	0.003	0.003	0.003	—	—	—
Fe^{3+}	0.059	0.076	0.023	0.057	0.065	0.116	0.035	—
Fe^{2+}	0.793	0.793	0.728	0.590	0.722	0.626	0.649	0.709
Mn	0.029	0.023	0.017	0.013	0.014	0.014	0.010	0.015
Mg	1.054	1.038	1.180	1.297	1.128	1.217	1.255	1.229
Ca	0.029	0.024	0.024	0.023	0.028	0.020	0.025	0.020
Na	0.003	0.002	0.004	0.004	0.004	—	—	—
K	0.002	0.004	0.003	0.003	0.002	—	—	—
Cr	0.000	0.000	0.001	0.004	0.003	—	—	—
Sum(X+Y)	1.986	1.978	2.002	1.994	1.980	1.993	2.001	1.999
Sc	54	43	18	18	40	nd	nd	nd
V	53	70	66	58	120	nd	nd	nd
Cr	26	43	290	850	710	nd	nd	nd
Co	87	115	100	110	100	nd	nd	nd
Ni	34	72	250	590	450	nd	nd	nd
Cu	7	6	2	~3	11	nd	nd	nd
Ba	—	—	—	~7	—	nd	nd	nd

*Total Fe as FeO; **includes Sc_2O_3, V_2O_5, Cr_2O_3, CoO, NiO when individual oxides are greater than 0.01%; nd = not determined; — means not detected; major elements by XRF except 69-788, and igneous 69-786 and 69-788, which are by non-dispersive electron microprobe (69-788 is the average of the three analyses in table 7.3); trace elements by emission spectroscope; Sr, La and Y were not detected.

systematic re-equilibration occurred between the primary and secondary minerals, and the above observation is probably fortituous. Two orthopyroxenes ("relict igneous orthopyroxenes 69-786 and 69-788" in table 7.5 and figure 7.1) analysed by electron microprobe have slightly higher Al and slightly lower Fe/Mg than the majority of coexisting orthopyroxenes. The orthopyroxenes contain clinopyroxene exsolution lamellae, and are considered to be relict igneous pyroxenes. Although the pyroxenes adjusted to declining temperatures by exsolving the high-temperature igneous pyroxene solid-solution, the exsolution must have occurred at temperatures higher than those of the granulite metamorphism in order to explain the higher Al and lower Fe/Mg than in the completely recrystallised metamorphic orthopyroxenes.

Lovering & White (1969) estimated that the Delegate eclogites crystallised at 1000°-1200°C and 10-15kb. Clinopyroxenes in some of the Delegate eclogites (with Al_2O_3 from 12.5 to 15.2%) contain 0.172 to 0.249 atoms of Al^{IV} per 6 oxygens. Clinopyroxenes from three Eyre Peninsula granulites with Al_2O_3 similar to the Delegate eclogites (69-742, 69-743 and 69-1371: 12.9 to 15.4% Al_2O_3) have Al^{IV} (0.069 to 0.081 atoms per 6 oxygens: table 7.4) significantly lower than the Delegate clinopyroxenes. This indicates that the Eyre Peninsula clinopyroxenes crystallised at considerably lower temperatures. The Al in the eclogite clinopyroxenes may be lower due to their coexistence with garnet, and the temperature difference between the eclogites and granulites may be even larger than apparent from the Al^{IV}-contents of their respective clinopyroxenes. Chappell & White (1970) estimated that the Sittampundi "eclogite" (16.4% Al_2O_3) crystallised at ~850°C. The Al-content of the "eclogite" is slightly larger than that of the three Eyre Peninsula granulites, and should partly offset the reduction of Al in clinopyroxene in the "eclogite" due to the presence of garnet. Thus, the clinopyroxenes in the "eclogite" and the granulites should be directly comparable. Clinopyroxene from the "eclogite" contains 0.108 Al^{IV} atoms per 6 oxygens, compared with 0.069 to 0.081 Al^{IV} atoms per

6 oxygens in the granulite clinopyroxenes. This suggests that the granulites crystallised at slightly lower temperatures than the "eclogite". The granulites may have equilibrated at temperatures in the lower part of the range postulated in chapter 6 (viz. ∿800°C). The Al^{IV} in the remaining granulite clinopyroxenes are even lower (0.043 to 0.060: table 7.4) due to the lower Al of the host rocks (69-785, 69-786 and 69-788: 5.8 to 6.0% Al_2O_3).

White (1964, 1969) and Lovering & White (1969) indicated the importance of jadeite to Tschermak's component ratios (Jd/Ts) of clinopyroxenes to distinguish between granulite facies and eclogite facies. Clinopyroxenes from true eclogites had Jd/Ts > 4/5 and those from granulites had Jd/Ts < ½. This observation was consistent with increased octahedral Al (jadeitic Al) with increasing pressure and increased tetrahedral Al (Tschermakitic Al) with increasing temperature. (Pyroxene end-members are assigned in the order acmite, jadeite, Tschermak's component, hedenbergite and diopside; where acmite = Fe^{3+}, jadeite = Na^{+}-Fe^{3+}, and Tschermak's component = Al^{IV}: White, 1964; and Chappell & White, 1970). All the analysed clinopyroxenes except one (69-786) have zero jadeite component and Jd/Ts = 0, and are well within the granulite Jd/Ts limits. The exception (69-786) has Jd/Ts = 0.49 and is also within the granulite limits defined above. The low or zero jadeite components in the Eyre Peninsula clinopyroxenes is consistent with their crystallisation below the basalt-eclogite transformation band.

The decrease in the miscibility gap between coexisting orthopyroxene and clinopyroxene with increasing temperature of metamorphism was demonstrated by Binns (1962) and Davidson (1968, 1969). The miscibility gap between co-existing pyroxenes at Eyre Peninsula is comparable to that for the highest grades encountered by Binns and Davidson (figure 7.1). Binns estimated that the maximum temperatures attained were 750-850°C.

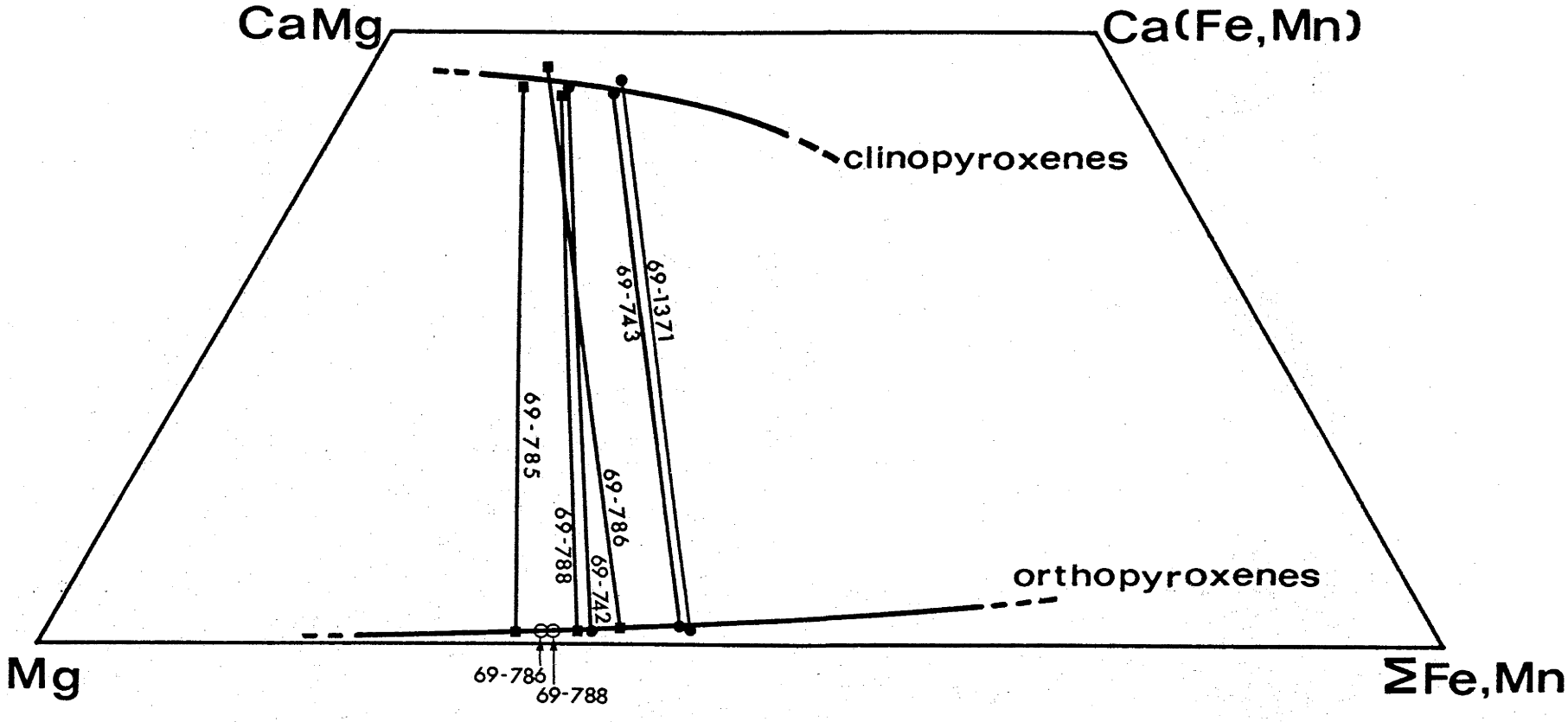

FIGURE 7.1 : COEXISTING EYRE PENINSULA PYROXENES & HIGH GRADE METAMORPHIC MISCIBILITY GAP OF DAVIDSON (1969).

7.7.3 Hornblende Compositions

Binns (1965, 1969a) showed that with increasing metamorphic grade, hornblende becomes richer in Ti, Al^{IV}, and edenite alkalis, and poorer in Al^{VI} (figures 7.2A & B). Jakeš (1969) noted that the reverse trend occurred with increasing degree of retrogression. Engel & Engel (1962) observed increased Ti, Cr, V, Sc and alkalis with increasing metamorphic grade, and decreased Fe/Mg, Mn, OH and F.

The compositions of Eyre Peninsula hornblendes from basic rocks are summarised in tables 5.3 and 7.6 and figure 7.2. The hornblendes from the hornblende granulite (69-742) and a granulite with minor retrogression (69-785) are relatively Mg-rich compared with the hornblendes from the amphibolites (69-782, 69-794 and 69-1377) and the intensely retrogressed granulite (69-788). This suggests that the primary granulite hornblende and the hornblende formed during early stages of retrogression (69-742 and 69-785) crystallised at higher temperatures than the hornblendes formed in later stages of retrogression. (Mg-rich hornblende has a higher thermal stability, is the last to decompose during progressive metamorphism, and also the first to form during retrogression.) The F-contents of these two hornblendes are the lowest of those analysed, supporting their crystallisation at higher temperatures (Engel & Engel, 1962). The similar Mn, Sc and V contents of the parent basic rocks (excluding 69-1377) allows direct comparison of these elements in the hornblendes. The "high grade" hornblendes (69-742 and 69-785) have the lowest Mn, highest V and among the highest Sc as predicted by Engel & Engel (1962). This supports a higher temperature origin. However, the Ti-content of one amphibolite hornblende (69-794) is greater than both of the "high grade" hornblendes, suggesting a higher temperature of crystallisation for the amphibolite hornblende. The high Ti in the latter, however, is partly due to the very high Ti in the host basic rock.)

Figure 7.2 shows the gradual increase in Ti, and increase in edenite alkalis with parallel decrease in Al^{VI} in

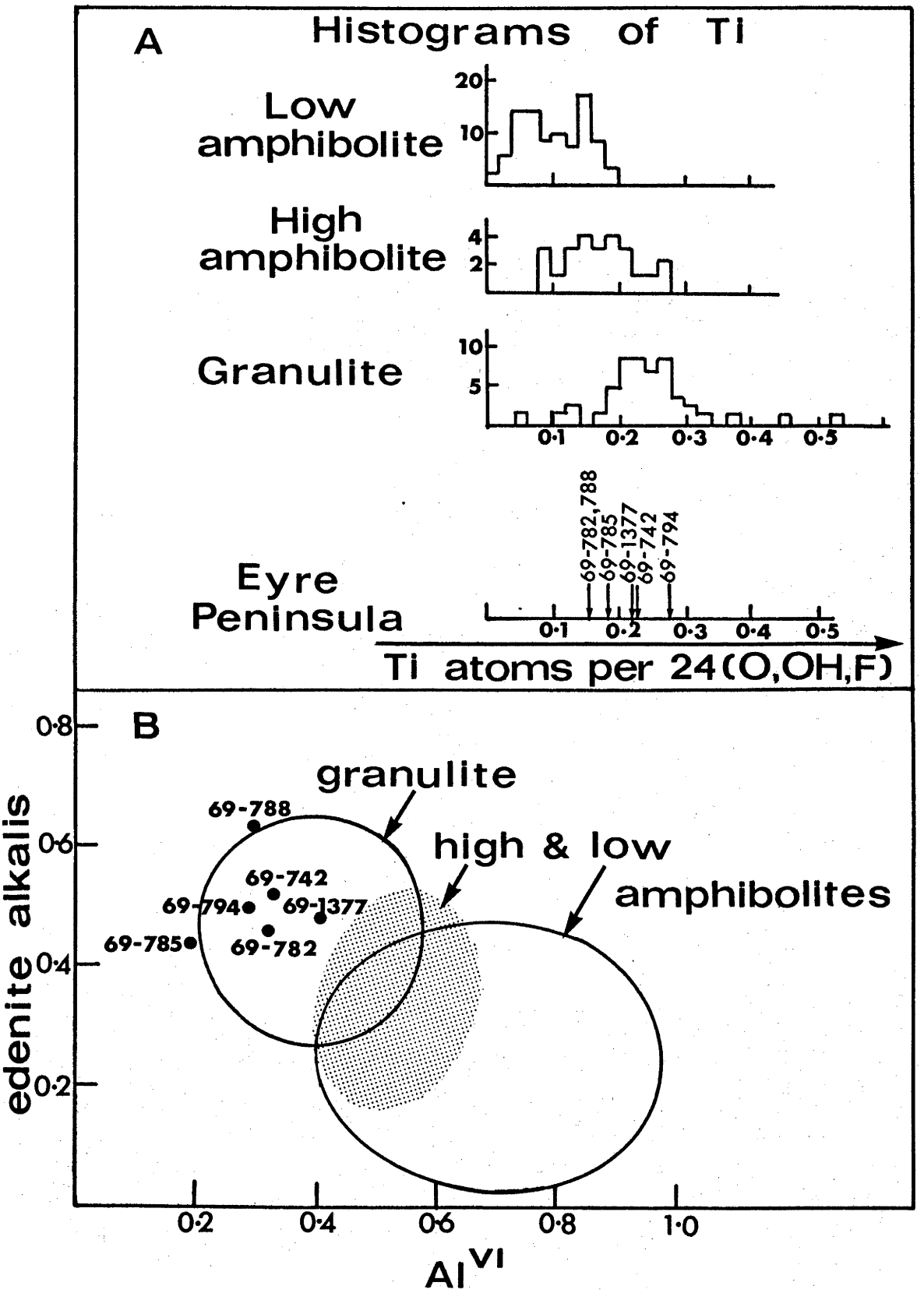

FIGURE 7.2 : EYRE PENINSULA HORNBLENDES AND METAMORPHIC HORNBLENDE FIELDS OF BINNS (1969).
(Edenite alkalis = Al^{IV}-Al^{VI}-Fe^{3+}-Ti)

TABLE 7.6

HORNBLENDE ANALYSES

	Hornblende Granulite	Amphibolites and Retrogressed Basic Granulites			
	69-742	69-782	69-785	69-788	69-794
SiO_2	43.57	40.96	46.67	43.78	40.59
TiO_2	2.01	1.33	1.69	1.39	2.44
Al_2O_3	11.15	11.02	9.12	11.08	11.32
Fe_2O_3	2.83	6.07	1.49	3.37	3.57
FeO	9.80	15.51	7.89	8.35	18.23
MnO	0.12	0.32	0.10	---	0.25
MgO	13.40	7.99	16.13	14.46	6.88
CaO*	12.04	11.58	11.97	12.20	11.33
Na_2O	1.49	1.49	1.40	1.86	1.77
K_2O	1.49	1.51	1.06	1.68	1.87
H_2O+	1.30	1.71	1.41	1.23	1.29
H_2O-	0.07	0.09	0.08	0.13	0.15
F	0.17	0.34	0.25	0.71	0.61
Trace**	0.42	0.07	0.80	0.33	0.10
Total***	99.79	99.85	99.95	99.97	100.14

STRUCTURAL FORMULAE BASED ON 23 OXYGENS(ANHYDROUS BASIS)

	69-742	69-782	69-785	69-788	69-794
Si	6.398	6.271	6.740	6.392	6.238
AlIV	1.602	1.729	1.360	1.608	1.762
Y (AlVI	0.328	0.260	0.192	0.299	0.289
Y (Ti	0.222	0.153	0.184	0.153	0.282
Y (Fe^{3+}	0.313	0.699	0.162	0.370	0.413
Y (Fe^{2+}	1.203	1.986	0.953	1.020	2.343
Y (Mn	0.015	0.042	0.012	---	0.033
Y (Mg	2.933	1.823	3.472	3.147	1.576
X (Ca	1.894	1.900	1.852	1.909	1.866
X (Na	0.424	0.442	0.392	0.527	0.527
X (K	0.279	0.295	0.195	0.313	0.367
Sum X	2.593	2.637	2.439	2.749	2.760
Sum Y	5.014	4.963	4.975	4.989	4.936
Rb	44	25	9	9	48
Ba	230	66	65	123	100
Sr	---	---	38	370	---
Sc	76	85	95	64	51
V	510	410	430	290	370
Cr	1700	50	4230	1100	130
Co	75	74	70	70	81
Ni	360	81	710	500	77
Cu	4	38	6	23	4
La	---	---	---	140	80
Y	55	90	97	97	99
Li	~4	43	~6	~2	7
Cs	~0	~0	~0	~0	~0
K/Rb	281	501	978	1550	323

*&*** as for table ; ** includes BaO, SrO, NiO, Cr_2O_3, V_2O_5 & Y_2O_3 when individual oxides are above 0.01%; major elements by XRF, except 69-788 by non-dispersive electron microprobe (69-788 is the average of the three analyses in table 7.3); trace elements by emission spectroscope; --- means not detected.

hornblendes with increasing metamorphic grade. The hornblendes from two retrogressed granulites (69-785 and 69-788) and one amphibolite (69-782) plot at moderate Ti and close to the middle of the high amphibolite facies range (figure 7.2A). The other hornblendes, from the hornblende granulite (69-742) and two amphibolites (69-794 and 69-1377), plot at higher Ti, and closer to the middle of the granulite facies range. All of the hornblendes plot at metamorphic grades above the high amphibolite facies field in the edenite alkalis - octahedral Al plot (figure 7.2B). The three amphibolite hornblendes (69-782, 69-794 and 69-1377) plot close to the hornblende granulite hornblende (69-742), and all four plot within the granulite facies field. The two retrogressed granulite hornblendes (69-785 and 69-788) plot at metamorphic grades higher than the previous four, and slightly above the granulite field.

The hornblendes from amphibolites and retrogressed granulites probably crystallised at lower temperatures or at similar temperatures and higher Pe_{H_2O} than the primary granulite hornblendes. The edenite alkalis-octahedral Al data suggest that several of the amphibolite hornblendes crystallised at similar temperatures to the granulite hornblende, and that some of the retrogressed hornblendes crystallised at higher temperatures. The Ti-contents of the hornblendes suggest that one amphibolite hornblende crystallised at higher temperatures than the granulite hornblende. The other amphibolite hornblendes and retrogressed granulite hornblendes crystallised at similar or lower temperatures than the granulite hornblende. The data are not consistent with either higher or lower temperature origins for the amphibolites, retrogressed granulites or the hornblende granulites. The overlap of the characteristics of the hornblendes from amphibolites, retrogressed granulites and hornblende granulites may indicate that all were crystallised at similar temperatures.

7.7.4 Biotite Compositions

The Al-contents of biotite are very dependent on host gneiss composition and use as an indicator of metamorphic grade is difficult (Binns, 1969a). However, the number of Ti atoms per 24(O,OH,F) in biotite increases from ∿0.3 for greenschist facies, to ∿0.4 for lower granulite facies to 0.5-0.55 for upper granulite facies (Binns, 1969a).

The compositions of Eyre Peninsula biotites from retrogressed basic rocks are given in table 7.7, and the other biotites from garnet-gneisses are given in tables 3.8 and 5.3. All the biotites from basic rocks are from amphibolites and retrogressed granulites and have Ti atoms per 22 oxygens ranging from 0.35 to 0.62, suggesting equilibration at conditions ranging from slightly below lower granulite facies to upper granulite facies. The biotite from the most retrogressed granulite (69-788) has the lowest Ti. This is consistent with retrogression at lower temperatures. The highest Ti occurs in a biotite from an amphibolite (69-794), and is partly due to the very high Ti of the parent rock, but also suggests high temperatures of equilibration. The biotites from garnet-gneisses include two in which there is little textural evidence for retrogression, (69-741 and 69-944) and one in which the biotite is replacing orthopyroxene (69-950). The first two have high Ti (0.67 to 0.56 Ti atoms per 22 oxygens) and the last has lower Ti (0.45). The Ti-contents of these biotites suggest relatively high temperatures of equilibration. The retrograde biotites were not consistently more Mg-rich than these in which there is no evidence for retrogression. The Ti-contents of the biotites suggest that some of the retrograde minerals crystallised at high T.

7.8 THE DISTRIBUTION OF ELEMENTS BETWEEN COEXISTING PHASES

7.8.1 Introductory Discussion

The distribution of components between phases coexisting at equilibrium may theoretically be used as a geothermometer. The theoretical aspects of major element distribution are

TABLE 7.7

BIOTITE ANALYSES

	RETROGRESSED BASIC GRANULITES			AMPHIBOLITE
	69-785	69-786	69-788	69-794
SiO_2	38.89	37.74	39.05	36.33
TiO_2	4.74	4.97	3.20	5.36
Al_2O_3	13.48	13.85	13.75	13.69
Fe_2O_3	0.31	0.01	1.09	2.64
FeO	10.02	13.55	9.88	20.02
MnO	0.05	0.04	0.05	0.11
MgO	17.99	15.28	18.52	8.76
CaO*	0.22	0.19	0.43	0.22
Na_2O	0.21	0.07	0.13	0.18
K_2O	9.66	9.61	9.73	9.14
H_2O+	2.59	3.79	2.40	3.07
H_2O-	0.44	0.35	0.27	0.48
F^-	0.78	nd	1.29	0.60
Trace**	1.10	1.28	0.57	0.38
Total***	100.10	100.73	99.82	100.73

STRUCTURAL FORMULAE BASED ON 22 OXYGENS (ANHYDROUS BASIS)

Si	5.669	5.610	5.684	5.549
AlIV	2.316	2.390	2.316	2.451
Y AlVI	0.000	0.037	0.043	0.013
Y Ti	0.519	0.556	0.350	0.616
Y Fe^{3+}	0.034	0.001	0.120	0.303
Y Fe^{2+}	1.221	1.684	1.202	2.557
Y Mn	0.007	0.005	0.006	0.014
Y Mg	3.908	3.386	4.017	1.994
X Ca	0.034	0.031	0.067	0.036
X Na	0.059	0.020	0.036	0.054
X K	1.796	1.822	1.807	1.781
X	1.889	1.873	1.910	1.871
Y	5.689	5.669	5.738	5.497

Rb	(~600)	~440	(~500)	(~800)
Ba	~2000	(~2500)	~2200	~2000
Sc	18	17	--	--
V	390	850	200	220
Cr	4030	4530	820	140
Co	110	110	100	130
Ni	1330	1070	780	170
Cu	--	--	26	1
Li	37	(~60)	43	(~400)
Cs	3.8	2.8	1.1	7.5
K/Rb	(134)	181	(161)	(95)

*CaO was corrected for minor apatite inclusions: $CaO = CaO - 1.3\ P_2O_5$; **includes Cr_2O_3, V_2O_5, NiO, BaO and Rb_2O where individual oxides are above 0.01%; ***corrected for O = F; nd = not determined; -- means not detected; Rb, Ba and Li values in brackets suffered badly from self absorption; 69-788 contained 120 ppm Sr probably present in apatite inclusions; major elements by XRF; trace elements by emission spectroscope.

adequately summarised by Mueller (1960) and Kretz (1961), and aspects of trace element distribution are discussed by McIntire (1963). Theoretically, the equilibrium molar $Fe^{2+}/(Mg+Fe^{2+})$ ratios of mineral phases involved in a reaction at a given pressure are uniquely determined by temperature, if all mineral phases participating in the equilibrium are present (Sen, 1970). If one or more phases are absent there are fixed relationships at constant temperature between the molar $Fe^{2+}/(Mg+Fe^{2+})$ or Fe^{2+}/Mg ratios of the minerals controlled by exchange equilibria. The latter case is most common in geological examples since reactions usually proceed until one or more phases are eliminated. In granulite metamorphism, hornblende decomposition usually proceeds until quartz is eliminated and reaction is then "frozen". The compositions of the remaining minerals may then adjust to changes in temperature by exchange equilibria.

Distribution of major elements between two coexisting phases may approach ideality when only one site in both phases will accept the element, or when multiple sites are equally attractive to all elements. Only one crystal lattice site is available for Fe^{2+} and Mg in garnet, cordierite and biotite, and three approximately equivalent sites are available in hornblende. However, complex substitution of Ti, Fe^{3+} and Al also occurs in the sites available for Fe^{2+} and Mg in biotite and hornblende. As a result, Fe^{2+}/Mg distribution between biotite or hornblende and other phases is non-ideal and dependent on other competing ions. Two sites with unequal attractive power for Fe^{2+} and Mg substitution are available in pyroxene (M_1 and M_2 sites). Fe^{2+} and Mg substitution (for Ca) in clinopyroxene M_2 sites is very much less than that in orthopyroxene M_2 sites, and the effect of the two unequal sites is minor in clinopyroxenes. However, the effect of the two unequal sites in orthopyroxene is marked.

7.8.2 Garnet/Clinopyroxene Distribution

Fe^{2+}/Mg distribution between garnet and clinopyroxene is very nearly ideal (Saxena, 1969b) and has been successfully

applied by Lovering and White (1969) to differentiate between eclogites from different P-T environments (glaucophane schists, amphibolite-granulites, kimberlites and inclusions in nephelinites). The usefulness of the ideal solid-solution is greatly enhanced by the large temperature dependence, and the resulting large spread of observed distribution coefficients.

7.8.3 Garnet/Cordierite Distribution

Fe^{2+}/Mg distribution between garnet and cordierite should be ideal, and if sufficiently temperature dependent, should be a valuable geothermometer. The experimental data of Hensen & Green (1970) and Hensen (1970) indicate that the temperature dependency of the distribution is sufficient, and the compositions of coexisting garnet and cordierite may be used as a geothermometer and a geobarometer.

7.8.4 Orthopyroxene/Clinopyroxene Distribution

Mueller (1960) concluded that distribution of Fe^{2+} and Mg between coexisting orthopyroxene and clinopyroxene was ideal for orthopyroxenes with mole fractions of Fe^{2+} from 0.2 to 0.6. However, non-ideal distribution of Fe^{2+}/Mg between orthopyroxene and clinopyroxene was observed by Binns (1962) and Davidson (1968, 1969) for mole fractions of Fe^{2+} in orthopyroxene >0.4.

Crystal field stabilisation energy for Fe^{2+} in orthopyroxene M_2 sites is much greater than that in clinopyroxene M_1 sites, which in turn is greater than in orthopyroxene M_1 sites (Davidson 1969; and Saxena & Ghose, 1971). Mg^{2+} is not stabilised by crystal field energy and competes very unsuccessfully with Fe^{2+} for orthopyroxene M_2 sites. As a result, orthopyroxene attraction for Fe^{2+} is much greater than that of clinopyroxene if the orthopyroxene M_2 site is not saturated with Fe^{2+}. The relative attractions of orthopyroxene and clinopyroxene for Fe^{2+} remain approximately constant with increasing Fe-content until orthopyroxene M_2 sites are "saturated" with Fe^{2+}. Then Fe^{2+} becomes progressively more attracted to clinopyroxene with increasing Fe. Hence, Fe^{2+}/Mg orthopyroxene/clinopyroxene distribution

coefficients for a given temperature remain approximately constant with increasing mole fraction of Fe^{2+} in orthopyroxene up to ∿0.4, and then decrease markedly (figure 7.3A). The Fe^{2+}/Mg orthopyroxene/clinopyroxene distribution coefficient will be abbreviated to K_D(opx/cpx); and equals the molar ratio of (Fe^{2+}/Mg) for orthopyroxene divided by that for clinopyroxene. Ray & Sen (1970) suggested that the decreased distribution coefficient was due to decreased Ca in clinopyroxene and hence availability of more M_2 sites to compete with orthopyroxene. Substitution of Fe^{2+} and Mg for Ca in the M_2 site of metamorphic clinopyroxene is relatively small for Mg-rich varieties but increases with increasing Fe-content (figure 7.1). Hence the effect of orthopyroxene M_2 sites becoming saturated with Fe^{2+} is enhanced by increasingly available clinopyroxene M_2 sites. The effect of Fe-content on distribution is shown in figure 7.3. K_D(opx/cpx) is approximately constant for mole fractions of Fe^{2+} in orthopyroxene up to ∿0.4, or molar Fe^{2+}/Mg up to ∿0.6, and then decreases progressively.

Atkins (1969) demonstrated that ∿10% change of K_D(opx/cpx) (1.5 to 1.35) could be produced by changes of ∿200°C temperatures or ∿6 kb pressure. Hence the effect of pressure on the distribution coefficient is negligible compared with that of temperature. The observed natural range of K_D(opx/cpx) is from 2.3 to 1.3 (Green, 1964; Leelanandam 1967 and Saxena 1969c). In general, metamorphic values are ∿1.8 for 600-800°C, igneous values are ∿1.4 for 1000-1200°C (for basaltic magmas) and 1.2-1.3 for ∿1200°C (for high temperature peridotite nodules: Green, 1964). The temperature-dependency of orthopyroxene/clinopyroxene distribution coefficients is much less than observed for garnet/clinopyroxene pairs and use as a geothermometer much more restricted. The relatively small variations observed in natural K_D(opx-cpx) may be partly due to substitution of Ti, Al, Fe^{3+} and other ions in the pyroxene structure. Geothermometric uses should be restricted to samples with comparable Ti, Al and Fe^{3+} and to orthopyroxenes with molar Fe^{2+} below 0.4. Attempts by Binns (1962) and Leelanandam (1967) to deduce metamorphic grade from empirical orthopyroxene/

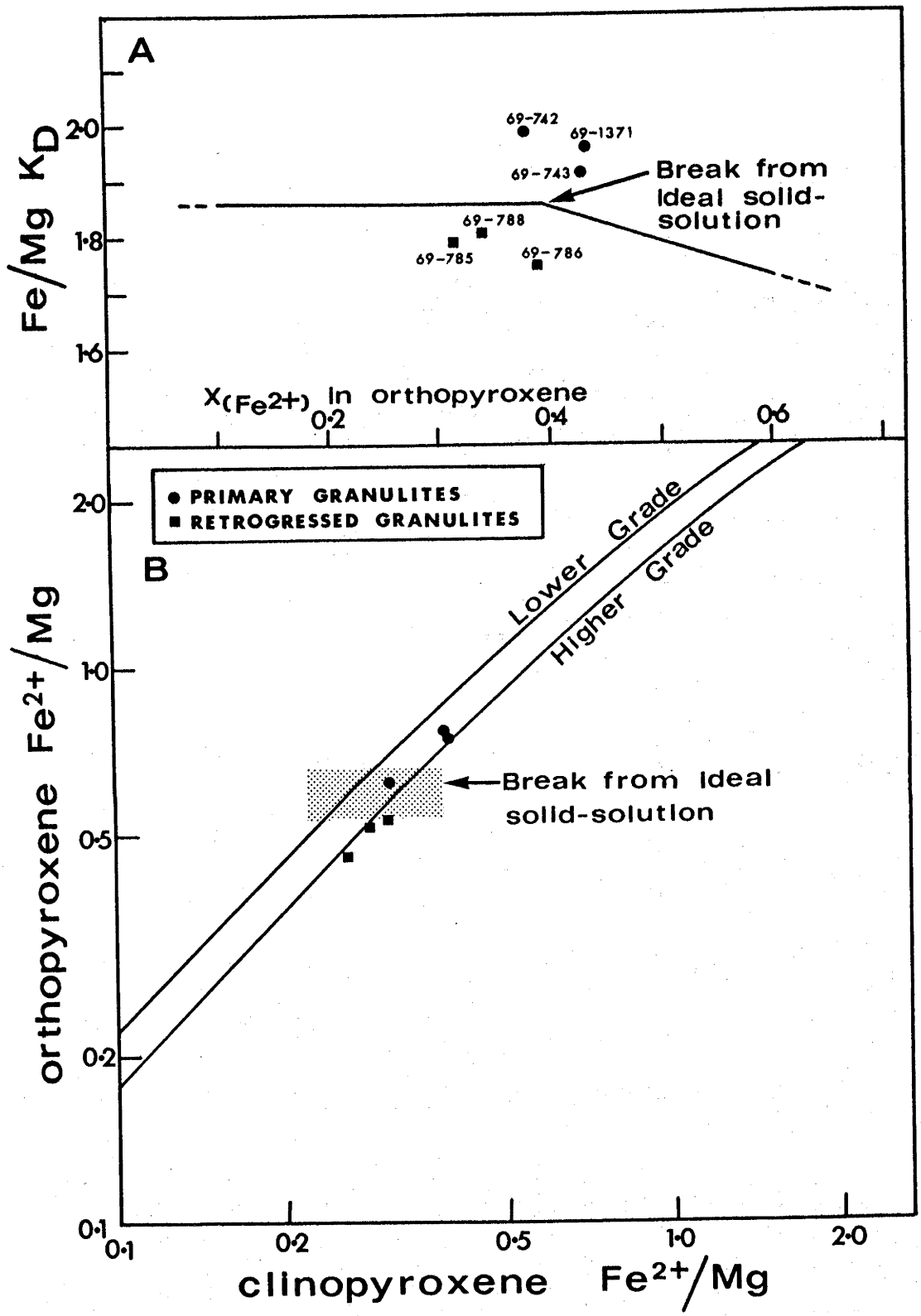

FIGURE 7.3 : Fe^{2+}/Mg^{2+} DISTRIBUTION BETWEEN COEXISTING EYRE PENINSULA ORTHOPYROXENES AND CLINOPYROXENES. The solid line in 7.3A shows the variation of distribution coefficients with increasing mole fraction of Fe^{2+} in orthopyroxene for the high grade metamorphisms of Binns (1962) and Davidson (1968,1969) . The higher and lower grade trends in 7.3B are from data of Binns (1962) and Davidson (1968,1969).

clinopyroxene distribution plots have no rigorous thermodynamic basis and must be treated with caution until more careful study has been made of the effects of components other than Fe^{2+} and Mg. Future studies of orthopyroxene/clinopyroxene Fe^{2+}/Mg distribution should also take into account M_1-M_2 distribution within orthopyroxene (Saxena & Ghose, 1971).

7.8.5 Garnet/Biotite Distribution

Saxena (1969a) demonstrated that distribution of Fe^{2+} and Mg between garnet and biotite was significantly influenced by compositional factors including Ti and Al in biotite, and Ca and Mn in garnet. Saxena deduced a "transformed" distribution coefficient based on temperature estimates by previous workers, but extremely cautious estimates of granulite metamorphic temperatures (600°C) were used and the temperature - transformed K_D plot is of limited value.

7.8.6 Hornblende/Pyroxene Distribution

Ray & Sen (1970) concluded that tetrahedral aluminium in hornblende had a very strong influence on Fe^{2+}/Mg distribution between hornblende and pyroxenes and that influences such as Al^{IV}, Al^{VI} and Ti caused departure from ideality even when multiple site problems were absent. They also showed that the effects of tetrahedral aluminium on Fe^{2+}/Mg distribution were comparable to, or larger than, the effects of temperature.

7.8.7 Biotite/Pyroxene Distribution

Saxena (1969c) concluded that Fe^{2+}/Mg distribution between biotite and pyroxenes were non-ideal probably due to the effects of Ti, Al and Fe^{3+}.

7.8.8 Summary

Distribution of Fe^{2+} and Mg between coexisting clinopyroxene and garnet is nearly ideal, and temperature dependence is sufficiently large for accurate use as a geothermometer. Distribution of Fe^{2+}/Mg between clinopyroxene

and orthopyroxene is non-ideal for mole fractions of Fe^{2+} in orthopyroxene greater than ∿0.4, but nearly ideal for less than ∿0.4. However, the temperature dependence of the distribution is relatively small and usefulness as a geothermometer restricted. Distribution of Fe^{2+} and Mg between hornblende or biotite and pyroxenes is strongly influenced by the complex sugstitution of Ti, Al, Fe^{3+} and other ions in the first two, and use as a geothermometer unsuitable.

Theoretically, distribution of trace elements between coexisting phases should be ideal because the solid solutions are very dilute. However, substitution of major element cations usually affects the distortion of crystal lattices and results in variable attraction of mineral phases for trace elements, especially for the transition metals. In consequence, the distribution of trace element will probably be non-ideal and dependent on the major element compositions of the coexisting phases.

7.9 DISTRIBUTION OF ELEMENTS BETWEEN COEXISTING EYRE PENINSULA MINERALS

The distribution of Fe^{2+}/Mg, Mn, Ti and trace elements between coexisting minerals from granulites and retrogressed granulites were studied for observable effects of retrogression; and to see if distribution within the granulites was ideal or if equilibrium had been attained. The distribution of elements between coexisting Eyre Peninsula minerals is summarised in figure 7.3 and table 7.8. The analytical precision for Fe, Mg, Mn and Ti is sufficiently high to examine the primary granulite minerals for approach to equilibrium and to examine the effects of retrogression on the distribution of these elements. The lower analytical precision for Cu, Co, Sc, Cr, V and Ni results in less certain conclusions regarding approach to equilibrium and effects of retrogression. Conclusions regarding trace element distribution are also limited by the paucity of previous detailed work.

Major and trace elements generally exhibited definite preferences for certain mineral phases. Approximately equal

TABLE 7.8

DISTRIBUTION COEFFICIENTS

(A) Fe^{2+}/Mg Distribution Coefficients

Sample	Status	opx/cpx	opx/hnb	cpx/hnb	opx/biot	cpx/biot	hnb/biot
69-742	granulite	1.99	1.50	0.76	--	--	--
69-743	granulite	1.91	--	--	--	--	--
69-1371	granulite	1.96	--	--	--	--	--
69-785	retrogressed granulite	1.79	1.66	0.93	1.45	0.81	0.88
69-786	retrogressed granulite	1.75*	--	--	1.28	0.62	--
69-788	retrogressed granulite	1.81	1.59	0.88	1.72	0.95	1.08
69-794	amphibolite	--	--	0.66	--	0.76	1.16
69-741	granulite	--	--	--	1.02	--	--
69-950	granulite	--	--	--	1.40	--	--
69-777	calc-silicate	--	--	0.67	--	--	--

(Fe^{2+}/Mg distribution coefficients are given by $K_D(A/B) = (Fe^{2+}/Mg)_A \div (Fe^{2+}/Mg)_B$; opx = orthopyroxene; cpx = clinopyroxene; hnb = hornblende; biot = biotite; *electron microprobe data assuming all Fe as FeO).

(B) Distribution Coefficients for Trace Elements, Mn and Ti

Mineral Pair	Sample	Ti	Mn	Cu	Co	Sc	Cr	V	Ni
clinopyroxene/ orthopyroxene	69-742	3.2	0.42	3.5	0.55	4.0	2.8	4.6	0.84
	69-743	2.7	0.39	0.86	0.61	3.0	3.3	4.7	1.0
	69-785	2.6	0.42	2.0	0.46	4.7	2.7	4.0	0.78
	69-1371	2.9	0.42	2.0	0.54	3.3	3.0	3.9	0.75
hornblende/ orthopyroxene	69-742	22	0.23	2.0	0.75	4.2	5.9	7.7	1.4
	69-785	19	0.24	2.0	0.64	5.3	5.0	7.4	1.2
hornblende/ clinopyroxene	69-742	6.9	0.55	0.57	1.4	1.1	2.1	1.7	1.7
	69-785	7.4	0.59	1.0	1.4	1.1	1.9	1.9	1.5
	69-788	5.0	--	1.1	1.1	1.5	2.7	3.0	1.4
	69-794	8.4	0.61	1.0	1.5	1.1	2.8	2.6	--
biotite/ clinopyroxene	69-785	21	0.29	0	2.2	0.21	1.8	1.7	2.9
	69-788	11	0.22	1.2	1.5	0	2.0	2.0	2.2
	69-794	19	0.27	0.25	2.3	0	3.0	1.6	--
biotite/ orthopyroxene	69-741	37	0.14	0.36	0.87	0.49	4.6	2.1	3.4
	69-950	37	0.10	0.50	1.3	0.35	--	3.8	4.0
	69-785	53	0.12	0	1.0	1.0	4.7	6.7	2.3
	69-786	50	0.09	0	1.1	0.43	6.4	7.1	2.4
biotite/ hornblende	69-785	2.8	0.50	0	1.6	0.19	0.95	0.91	1.9
	69-788	2.3	--	1.1	1.4	0	0.75	0.69	1.6
	69-794	2.2	0.44	0.25	1.6	0	1.1	0.60	2.2
garnet/biotite	69-944	0.008	18	0.75	0.59	9.0	0.56	0.23	0
	69-950	0.010	36	5.8	0.51	6.8	0	0.10	0

(The distribution coefficients are given by ppm in phase A/ppm in phase B).

partitioning of elements between coexisting minerals was observed in only a few examples. The order of partitioning of major and trace elements observed in the Eyre Peninsula minerals is as follows:

$\underline{Fe^{2+}/Mg}$: (a) orthopyroxene > biotite ≃ hornblende > clinopyroxene

(b) garnet > orthopyroxene > biotite

Sc: hornblende > clinopyroxene > biotite ≃ orthopyroxene

Ti: biotite > hornblende > clinopyroxene > orthopyroxene

V: hornblende ≃ biotite > clinopyroxene > orthopyroxene

Cr: hornblende ≃ biotite > clinopyroxene > orthopyroxene

Mn: orthopyroxene > clinopyroxene > hornblende > biotite

Co: biotite ≃ orthopyroxene > hornblende > clinopyroxene

Ni: biotite > hornblende > orthopyroxene > clinopyroxene

Cu: hornblende ≃ clinopyroxene > orthopyroxene > biotite

Distribution coefficients for Fe^{2+}/Mg between coexisting orthopyroxene and clinopyroxene (table 7.8) range from 1.75 to 1.99 for mole fractions of Fe^{2+} in orthopyroxene from 0.31 to 0.43. The effects of Fe-content on distribution coefficients should be negligible in this range (see also figure 7.3A). The values for three primary granulites (69-742, 69-743 and 69-1371) are reasonably close (1.99, 1.91 and 1.96), and indicate close approach to equilibrium. The three granulites plot close to the higher grade trend (69-743) and between the higher and lower grade trends (69-742 and 69-1371) in the orthopyroxene/clinopyroxene plot (figure 7.3B). Binns (1962) estimated temperatures of 750°-850°C at 6-10 kb for the granulite facies metamorphism at Broken Hill. The higher and lower grade trends are for minerals metamorphosed in the highest and lowest grade portions respectively of the granulite facies metamorphism. This suggests temperatures of equilibration of 750°-800°C for the Eyre Peninsula granulites. The three retrogressed granulites (69-785,

69-786 and 69-788) have similar distribution coefficients for Fe^{2+}/Mg between orthopyroxene and clinopyroxene (1.79, 1.75 and 1.81), suggesting that the retrogression occurred at similar conditions in all three. The three plot at metamorphic grades close to, and slightly higher than, the high grade trend in figure 7.3B. This suggests that the retrogression occurred at temperatures higher than the primary granulite metamorphism, or that the retrogressed distribution coefficients are the result of disequilibrium. The electron microprobe data (7.6.1) indicate that limited re-equilibration occurred between primary and secondary minerals However, the low distribution coefficients in two of the retrogressed granulites (69-786 and 69-788) may be due to the effects of oxidation during retrogression. The distribution coefficient for the first sample was calculated from electron microprobe data assuming that all Fe occurred as FeO. In general, the clinopyroxenes contain higher Fe^{3+} than the coexisting orthopyroxenes and, if this is assumed, the value of the distribution coefficient would be increased. The second sample, an intensely oxidised and retrogressed granulite, contains orthopyroxene, with Fe^{3+} considerably higher than in the other orthopyroxenes. If the high Fe^{3+} is assumed to be due to the retrogression, allocation of a more realistic amount of Fe^{3+} would increase the distribution coefficient by about 10% to a value close to those of the primary granulites. The low distribution coefficient for the remaining retrogressed granulite (69-785) cannot be explained by oxidation during retrogression. (The Fe^{3+} in the orthopyroxene is not lower than usual; and the Fe^{3+} in the clinopyroxene is <u>lower</u> than in the other clinopyroxenes. Allocation of higher Fe^{3+} in the clinopyroxene would <u>decrease</u> the distribution coefficient.)

The distribution of Fe^{2+}/Mg between coexisting pyroxenes and hornblendes can be compared for one primary granulite (69-742), one primary calc-silicate (69-777), three retrogressed granulites (69-785, 69-786 and 69-788) and one amphibolite (69-794) (see table 7.8). The variation of the orthopyroxene/hornblende distribution coefficient with increasing degree of retrogression is erratic, and the

coefficient for the most retrogressed sample (69-788) lies between those of the primary granulite and a less retrogressed sample (69-785). Comparison of the clinopyroxene/hornblende distribution coefficients for the primary granulite (69-742) and two retrogressed granulites (69-785 and 69-788) suggests that this distribution coefficient may increase with increasing retrogression, but the coefficients for the calc-silicate and the amphibolite are lower than that of the primary granulite. The erratic variation of the pyroxene/hornblende distribution coefficients may be due to non-ideality and the effects of Ti and Al substitution in the hornblende, in addition to possible differences in conditions of crystallisation of the hornblendes.

The distribution coefficient of Fe^{2+}/Mg between coexisting pyroxenes and biotite increases with increasing degree of retrogression (viz. from 69-786 to 69-785 to 69-788) for the three retrogressed granulites. The amphibolite has a clinopyroxene/hornblende distribution coefficient within the range for the retrogressed granulites. Bhattacharyya (1970) proposed a preliminary geothermometric scheme involving the distribution of Fe^{2+}/Mg between coexisting orthopyroxene and biotite. Application of the scheme to the Eyre Peninsula orthopyroxene/biotite pairs (table 7.8) indicates temperatures of equilibration as follows: 460°C (69-741); 370°C (69-786); 340°C (69-950); 330°C (69-785); and 280°C (69-788). The scheme agrees with the order of increasing retrogression predicted by textural evidence for the three retrogressed granulites (viz. 69-786, 69-785 and 69-788). The highest temperature of equilibration predicted by the scheme is for one of the remaining granulites (69-741), and is consistent with the minimal textural evidence of retrogression observed in this rock. The biotite in the other granulite (69-950) crystallised in response to minor retrogression, and the temperature of equilibration predicted by the scheme is close to that in other granulites with minor retrogression (69-786 and 69-785). The relative temperatures obtained from the orthopyroxene/biotite geothermometer are consistent with the texturally predicted relationships, assuming that

retrogression occurs during decreasing temperatures of metamorphism. However, the absolute values of temperatures obtained are much lower than the primary granulite metamorphic temperatures, and "biotite retrogression" may have occurred at much lower temperatures than "hornblende retrogression", or the geothermometer requires more precise calibration. A similar conclusion is reached from the Ti-contents of the biotites. The Ti-contents of the biotites and the equilibration temperatures predicted by the geothermometer decrease together. However, the Ti-contents of the biotites are consistent with crystallisation in upper amphibolite to upper granulite facies metamorphism (7.6.4), and the low temperatures predicted by the geothermometer appear anomalous.

The distribution of Fe^{2+}/Mg between coexisting hornblende and biotite is erratic, and cannot be correlated with the degree of retrogression.

The close agreement between the distribution coefficients (table 7.8) of Mn between coexisting clinopyroxene-orthopyroxene, hornblende-orthopyroxene and hornblende-clinopyroxene pairs in three primary granulites (69-742, 69-743 and 69-1371), one slightly retrogressed granulite (69-785) and one amphibolite (69-794), suggests that the temperatures of equilibration and/or crystallisation of retrograde hornblende were similar in all five rocks and that the distribution of Mn approached ideality. The corresponding distribution coefficients for Ti support this view, with the exception of the hornblende/clinopyroxene coefficient for the amphibolite (69-794), which is higher than those for the granulite (69-742) and the slightly retrogressed granulite (69-785). The distribution coefficients for Ti are reasonably uniform, but not as uniform as those for Mn. This suggests that distribution of Ti also approached ideality, but not as closely as did the distribution of Mn. The corresponding distribution coefficients for Mn and Ti for the intensely retrogressed granulite (69-788) are significantly different, and suggest crystallisation at considerably different temperatures. The

distribution coefficients of Mn and Ti between coexisting biotite and pyroxenes (table 7.8) suggest that the retrograde biotite in two retrogressed granulites (69-785 and 69-786) and one amphibolite (69-794) crystallised at similar temperatures, and that the retrograde biotite in another retrogressed granulite (69-788) crystallised at different temperatures. The distribution of Cu, Co, Sc, Cr, V and Ni between coexisting biotite-pyroxene and biotite-hornblende pairs is usually erratic, and does not correlate with textural evidence, or with the evidence of Fe^{2+}/Mg distribution. However, the distribution of Cu, Co, Sc, Cr, V and Ni between coexisting clinopyroxene-orthopyroxene, hornblende-orthopyroxene and hornblende-clinopyroxene pairs is reasonably regular, and suggests reasonably close approach to equilibrium, when the precision of emission spectrographic determination of these elements, and the non-ideality of hornblende/pyroxene distribution are also considered.

In all examples where the distribution of elements between coexisting phases is regular, it can be assumed that the minerals were in chemical equilibrium, and that the distribution approached ideality. This applies to the distribution of Fe^{2+}/Mg, Mn and (to a lesser extent) Ti between orthopyroxene and clinopyroxene; and to the distribution of Mn and (to a lesser extent) Ti between coexisting hornblende and pyroxene in hornblende granulites and granulites with minor retrogression. In most other examples, however, the distribution of elements between coexisting phases was irregular or erratic and it was impossible to ascertain whether the irregularity was due to non-ideality, or disequilibrium, or both.

7.10 CONCLUSION

Application of the mineral facies concept to granulite facies metamorphism results in a very large P-T field within which granulite facies rocks are stable. The granulite facies rocks commonly coexist with amphibolite facies rocks in this P-T field. The temperature and pressure conditions of the metamorphism can only be determined if the effects of

rock composition, fluid composition and pressure, oxygen fugacity and silica activity can be ascertained.

Although not conclusive, much of the mineralogical data suggest that the P-T conditions of equilibration for several amphibolites and for retrogression of some of the granulites, were similar to those for equilibration of the primary pyroxene and hornblende granulites. This is consistent with the more flexible concept that granulite and amphibolite facies metamorphic rocks may crystallise at the same P_{total} and T, and may reflect variation in rock compositions or localised variation of Pe_{H_2O}. The data also suggest that some amphibolites and at least one retrogressed granulite may have crystallised at slightly lower temperatures than the primary granulites. Textural evidence and some of the mineralogical data suggest that retrograde hornblende crystallised at higher temperatures than retrograde biotite.

CHAPTER 8

ANATEXIS AND CRUSTAL FRACTIONATION

8.1 CRUSTAL FRACTIONATION

8.1.1 Introduction

Continental crust comprised of Archaean rocks is now characterised by low average heat flow and concentration of radioactive elements in a thin surface layer (Hyndman et al., 1968). Archaean basic-ultrabasic belts have even lower heat flow. Hyndman et al., (1968) calculated the vertical distribution of radioactive elements in the upper 10 km of dominantly granitic Archaean crust, and extrapolated the results to deep crustal estimates (figure 8.1). The marked vertical zonation of Th, U and K (table 8.1) was attributed to anatectic depletion of these elements in deep crust during high grade metamorphism. Granitic-granodioritic intrusions enriched at radioactive elements were emplaced in high crustal levels, and resulted in concentration maxima. Subsequent erosion may expose the maxima at the surface or remove them entirely. The latter resulted in the crustal zonation predicted by calculations and postulated by Heier (1965) and Lambert (1967).

8.1.2 Fractionation of the Radioactive Elements Th and U

The depletion of Th and U in high grade metamorphic rocks is summarised in table 8.1. It must be stressed that all results tabulated are averages, and many individual samples do not reflect the overall trend. The differences between the amphibolite facies monzonite and the granulite facies charnockite may be magmatic rather than metamorphic.

Lambert & Heier (1968) suggested that U was leached by aqueous fluids produced during medium grade metamorphic reactions prior to anatexis. This increased Th/U ratios. Anatexis at higher metamorphic grades depleted Th relative to U and decreased Th/U ratios. The mobility of U is markedly increased by higher oxidation state. Thus, the Th/U ratios and depletion of U in high grade metamorphic rocks depend on

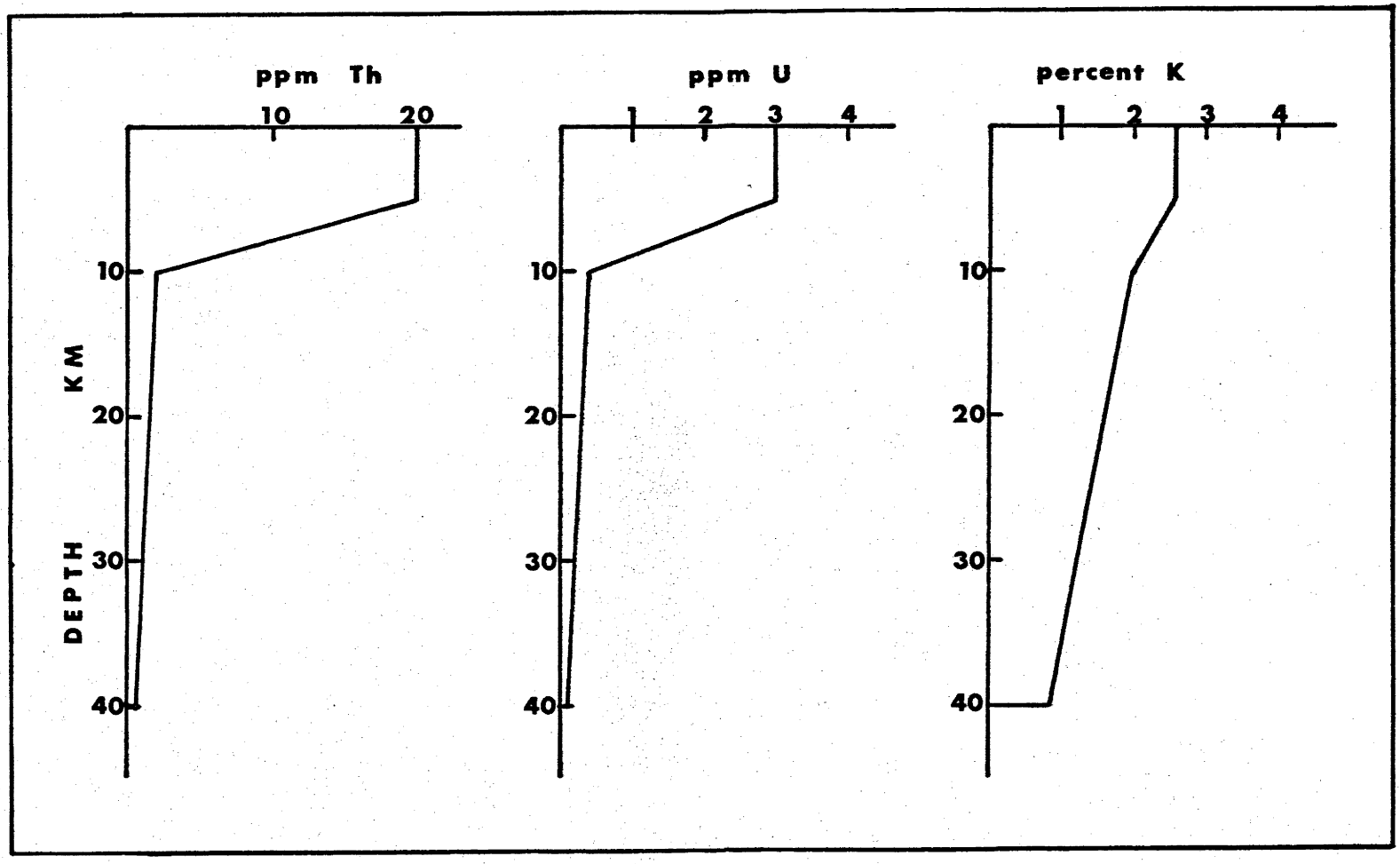

FIGURE 8.1 : VERTICAL ZONATION OF Th, U and K IN CONTINENTAL CRUST COMPRISED OF GRANITIC ARCHAEAN ROCKS (Hyndman et al., 1968)

TABLE 8.1

FRACTIONATION OF Th AND U

(A) AVERAGE SHIELD ABUNDANCES WITH CRUSTAL DEPTH

Depth	Th	U	K
0-16 km	4.0	1.0	1.6
16-37 km	1.5	0.4	0.6

(B) AVERAGE ABUNDANCES WITH INCREASING METAMORPHIC GRADE

	Low Amphibolite	High Amphibolite	Low Pressure Granulite	Medium Pressure Granulite	High Pressure Granulite
Th	26	9.4	4.1	---	0.9
U	3.5	1.2	0.9	---	0.4
Th/U	7.4	7.8	4.5	---	2.3
Th	14	9	---	5	---
U	2.2	1.1	---	0.5	---
Th/U	12	5	---	8	---

(C) VARIATION WITHIN AN INTRUSION

	Monzonite (Amphibolite)	Charnockite (Granulite)
Th	8.5	2.5
U	1.4	0.7
Th/U	6.1	3.6

Data from: Heier (1965), Heier & Adams (1965) Heier & Thoresen (1970), Smithson & Heier (1971).

the history of oxidation, dehydration and anatexis. The use of Th/U ratios as indicators of crustal fractionation is further complicated by the range of parent ratios.

Th is not always depleted during high grade metamorphism. Disturbances of the lead isotopes in the Th and U decay series (Gray, 1971) indicated that an average depletion of 6 ppm U, but no common profound loss of Th had occurred during high pressure granulite metamorphism ($\sim$ 900°C at 10 kb). Similar U depletion factors (9 to 40) would be more than sufficient to account for observed U and Th/U fractionation observed elsewhere. The absence of Th fractionation may be due to the water-deficient nature of the area studied by Gray (1971), and the near-absence of anatexis.

8.1.3 Fractionation of Elements Other Than Th and U

Fractionation of various elements including K and U was suggested by comparison of granulites and nearby amphibolites or upper crustal rocks. Fractionation processes were attributed to dehydration reactions and anatexis during attainment of granulite metamorphism. Depletion of Si, K, Rb, Pb, Cs, Li, Th and U, and enrichment of Fe, Mg, Mn, Ca, Ba, Sr, Zr, Nb and Y in medium to high pressure granulites were postulated by Lambert (1967), Lambert & Heier (1967, 1968), Sighinolfi (1969, 1970, 1971), Sheraton (1970) and Heier & Thoresen (1970). The fractionation resulted in increased K/Rb, K/Cs, Rb/Cs and Ba/Rb ratios and an intermediate lower crustal composition. These relationships are summarised in tables 8.2 and 8.3. The variation of Ba in the Australian Shield rocks, and the variation of Sr and Zr are irregular.

Upper crustal enrichment in K, Rb, Si, Ba and light REE, presumably with complementary lower crustal depletion, was suggested to explain volcanism of the Andean type (Jakes & White, 1971). This differs from other postulated deep crustal fractionation in that Ba should be depleted.

TABLE 8.2

POSTULATED EFFECTS OF CRUSTAL FRACTIONATION IN ACID TO SUBACID GNEISSES

	Average Low Amphibolite	Average High Amphibolite	Average Medium Pressure Granulite
%K	3.1	3.2	2.5
Rb	155	81	56
Ba	605	619	1162
Sr	338	183	572
Pb	24	11	15
Zr	128	360	144
K/Rb	297	539	629

	Average Amphibolite	Average Medium Pressure Granulite
%K	3.6	3.4
Li	90	16
Rb	163	76
Cs	1.2	0.25
K/Rb	225	489
$K/Csx10^{-3}$	46	227
Rb/Cs	197	551
%K	2.7	1.5
Rb	119	40
K/Rb	231	505

Data from: Heier & Thoresen (1970), Sighinolfi (1969, 1970, 1971) and Heier & Brunfelt (1970).

TABLE 8.3

AUSTRALIAN SHIELD ACID-SUBACID
GNEISS AVERAGES

	Amphibolites	Low Pressure Granulites	High Pressure Granulites
K_2O	4.0	3.8	4.0
Rb	184	190	155
Ba	1005	797	968
Sr	176	133	199
Pb	35	36	29
Zr	283	334	156
K/Rb	226	210	324

Data from: Lambert (1967) (Rocks with $SiO_2 > 65\%$) High pressure granulites from Musgrave and Fraser Ranges; Low pressure granulites from Cape Naturaliste, Kimberly block and Northampton; amphibolites from the SW shield and the above locations.

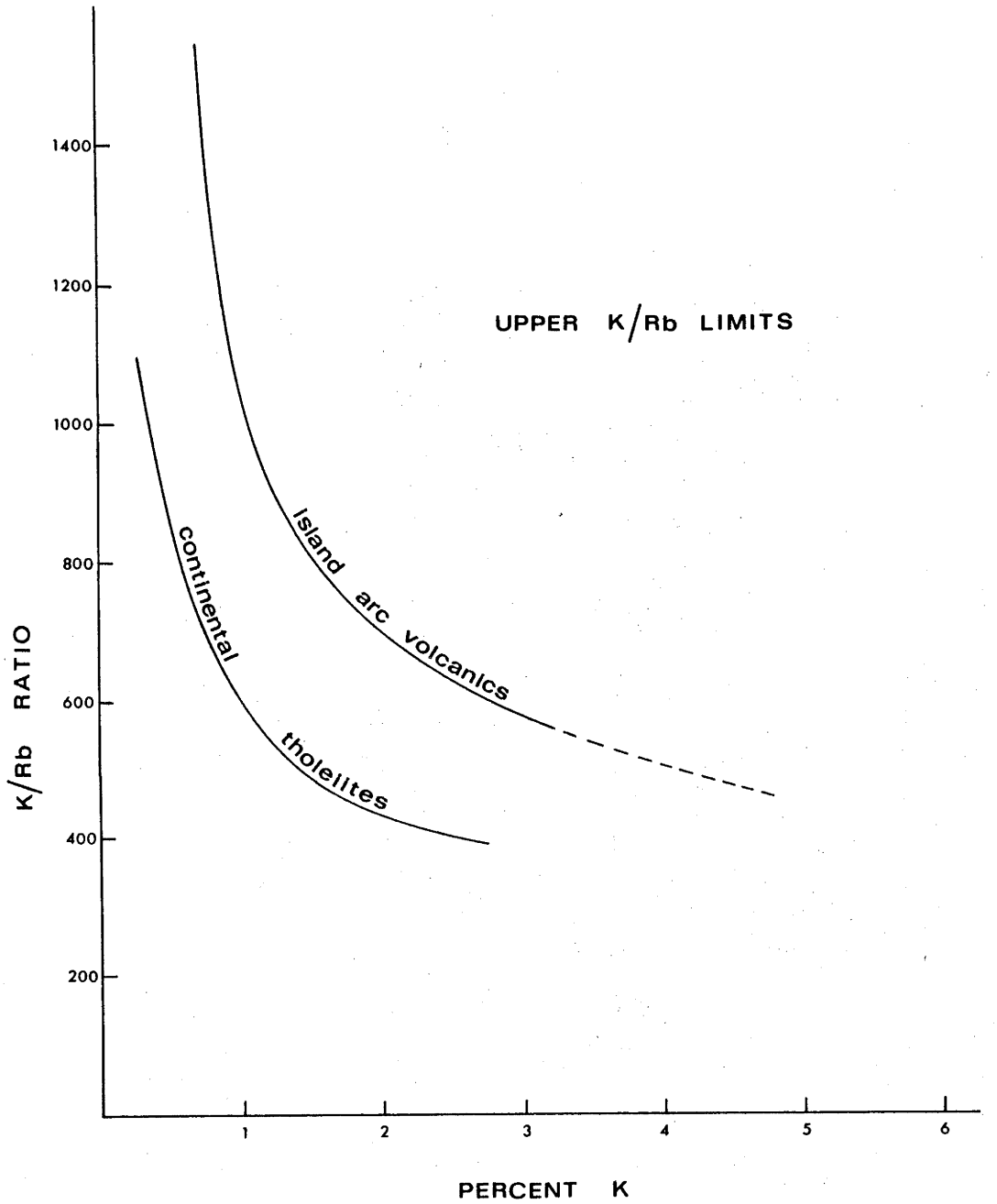

FIGURE 8.2 : UPPER K/Rb LIMITS FOR ISLAND ARC VOLCANIC ROCKS AND CONTINENTAL THOLEIITES

Island arc data were compiled from: Taylor & White (1966; Ewart et al., (1968); Taylor (1969); Taylor et al., (1969); Gill (1970); Jakeš & White (1970, 1971); Lowder & Carmichael (1970); and White et al., (1971). Continental tholeiite data were compiled from: Cox & Hornung (1966); Cox et al., (1967); Compston et al., (1968); Rivalenti & Sighinolfi (1970); and Weigand & Ragland (1970).

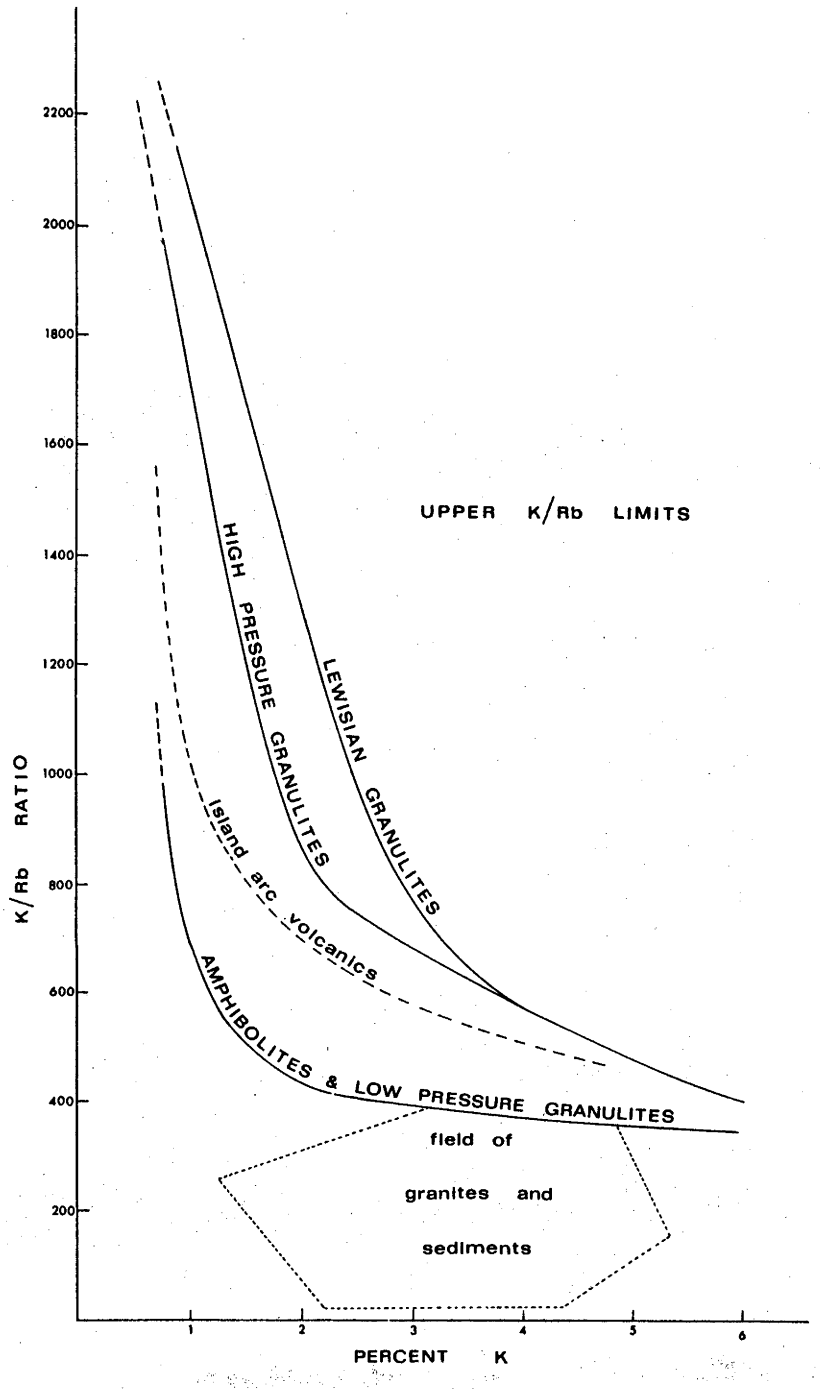

FIGURE 8.3 : UPPER K/Rb LIMITS FOR LEWISIAN GRANULITES, HIGH PRESSURE GRANULITES, ISLAND ARC VOLCANIC ROCKS, AMPHIBOLITES AND LOW PRESSURE GRANULITES, AND K/Rb FIELD OF SEDIMENTS AND GRANITIC-GRANODIORITIC BATHOLITHS.

High pressure granulite limits include medium to high pressure granulites from: Australia (Musgrave & Fraser Ranges: Lambert, 1967), Norway (Lofoten-Vesteraalen: Heier et al., 1969, Heier & Compston, 1969, Green et al., 1969), Scotland (Lewisian Gneisses : Sheraton, 1970), Brazil and Italy (Bahia and Valle Strona respectively : Sighinolfi, 1969, 1970, 1971). The amphibolite and low pressure granulite limits include all the amphibolites from the medium-high pressure granulite sources, and rocks from low pressure granulite terrains as follows: Australia (Kimberley Block, Cape Naturaliste and the South-West Shield: Lambert, 1967), North America (Adirondacks : Whitney, 1969). The granite/sediment field was compiled from the sediment data of Pettijohn (1956, 1963), Banno & Chappell (1969), Rivalenti & Sighinolfi (1969) and the granite-granodiorite data of Butler et al., (1962), Kolbe & Taylor, (1966a&b), White (1966), White et al., (1967), Taylor et al., (1968) and de Albuquerque (1971).

Green et al., (1972) tentatively concluded that no REE fractionation had occurred during progressive metamorphism from amphibolite to granulite facies. However, REE had been fractionated by a two-stage melting mechanism during the granulite metamorphism. The first stage of melting left residua with high K/Rb and small positive Eu anomalies. The second stage of melting resulted in high K/Rb "mangeritic" melts with small but significant positive Eu anomalies, and anorthositic residua with extremely high K/Rb ratios and very large positive Eu anomalies. The anorthosites were considerably depleted in all REE other than Eu.

"Retrogression" may cause the reverse effects to progressive metamorphic fractionation (table 8.4). "Retrogression" of Eyre Peninsula basic rocks is accompanied by increased K, Rb and Ba (Chapter 7). However, Heier & Thoresen (1970) and Green et al., (1972) considered that the effects of retrogression were "statistically not significant" compared with those of progressive metamorphism.

8.1.4 K/Rb Fractionation

High grade metamorphic depletion of Rb relative to K resulting in increased K/Rb ratios has been demonstrated, but most workers used average K/Rb ratios and made no allowance for the dependence of K/Rb on K. The dependence of K/Rb ratios on K was noted by Reynolds et al., (1969), Sheraton (1970) and Gray (1971) (see also figure 8.2 and 8.3). The upper K/Rb limit increases with decreasing % K especially below $\sim$ 2% K. Average K/Rb ratios are meaningful only if samples have restricted ranges of K, or are from ranges in which the dependence of K/Rb on K is negligible. Metamorphic K/Rb fractionation may be demonstrated by averaging K/Rb ratios for samples above $\sim$ 2% K. (K/Rb averages for samples below $\sim$ 2% K are less meaningful because it is impossible to distinguish fractionation effects from those due to the large dependence of K/Rb on K.) Under these conditions K/Rb fractionation may be meaningfully demonstrated by comparison of average metamorphic K/Rb ratios with those of postulated parent material. The parent compositions prior

TABLE 8.4

EFFECTS OF "RETROGRESSION"

	Average Granulite	Average Retrogressed Granulite
K_2O	1.0	1.9
Rb	16	41
Ba	994	1175
Sr	1198	1207
Pb	14	22
K/Rb	1076	371
K_2O	5.0	6.0
Rb	50	72
K/Rb	825	687
Th	0.6	1.2
U	0.3	0.7

Data from: Heier & Thoresen (1970)and Moorlock et al., (1971).

to metamorphism may be island arc volcanic material with high K/Rb, or sedimentary and granitic-granodioritic batholithic material with low K/Rb.

Progressive metamorphism from amphibolite facies to low pressure granulite facies increased average K/Rb in quartzofeldspathic gneisses (K greater than about 1.5%): the average K/Rb increased from 231 to 307 with standard deviations of 42 and 45 respectively (Whitney, 1969). The magnitude of the K/Rb increase due to low pressure granulite metamorphism is considerably smaller than that due to medium to high pressure granulite metamorphism (tables 8.2 and 8.3, c.f. Whitney, 1969). This is also supported by the absence of significant differences between the fields of low pressure granulites, amphibolites, granites, granodiorites and sediments, which were combined in one field in figure 8.3. The low pressure granulite field is approximately that obtained by combining the tholeiitic basalt field and granitic/sedimentary field, and represents the most likely range of K/Rb ratios expected in parent material (other than island arc volcanic rocks). The low pressure granulite/amphibolite field has considerably lower K/Rb limits than the island arc volcanic field indicating that the low pressure granulite terrains studied did not contain island arc volcanic parent material. The high pressure granulite fields extend to considerably higher K/Rb than the low pressure granulite or island arc volcanic fields. The higher K/Rb ratios are undoubtedly the result of crustal fractionation. It is unlikely that all the high pressure terrains examined contained island arc parent material, and crustal fractionation is wholly responsible for the large increase in the upper K/Rb limit from the amphibolite and low pressure granulite limit to the high pressure granulite limit. If some of the high pressure areas studied contain arc volcanic parent the necessary increase in K/Rb is smaller. Sheraton (1970) suggested that the Lewisian high pressure granulites resulted from metamorphic enhancement of initially high island arc volcanic K/Rb ratios. The necessary increase in K/Rb in this case is not as large and the Lewisian K/Rb limits are marked separately.

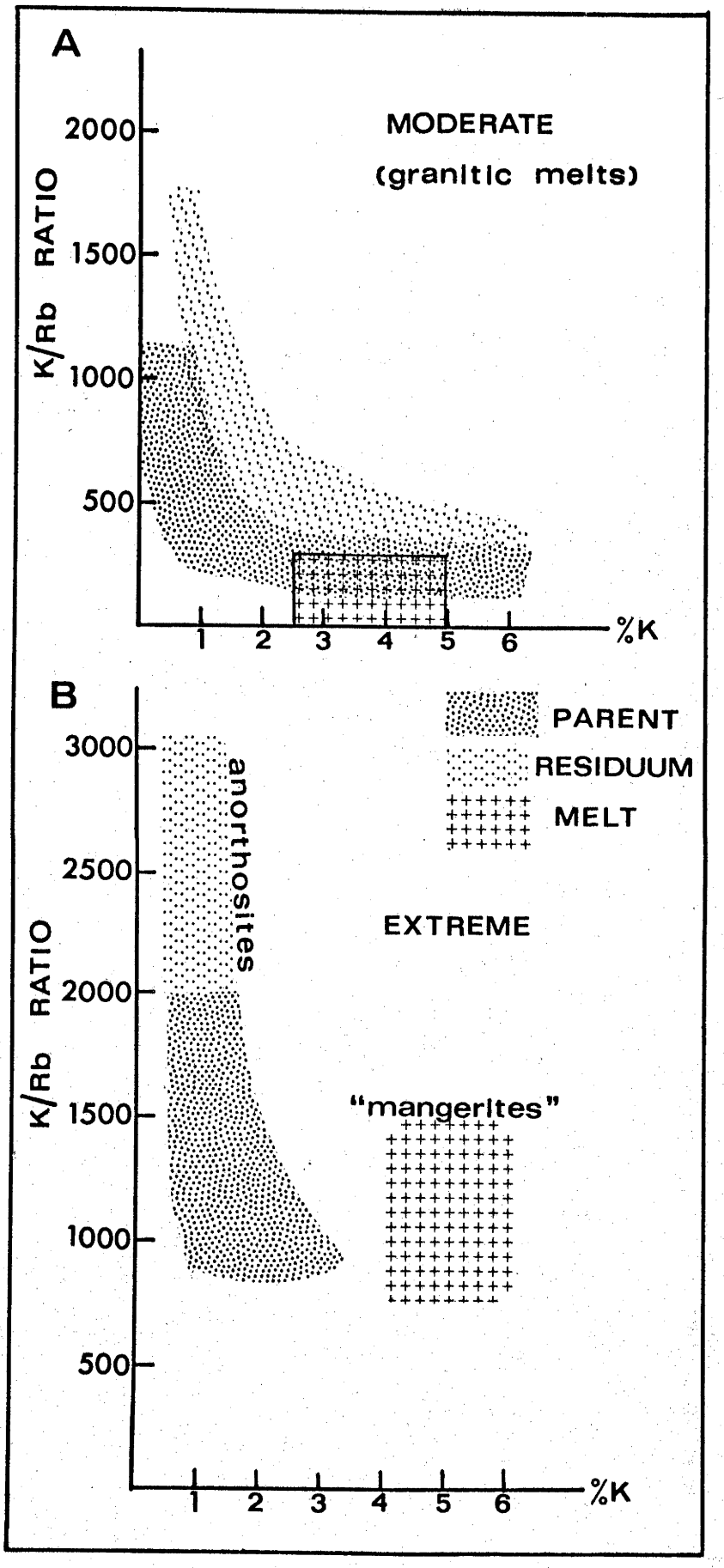

FIGURE 8.4 : COMPARISON OF MECHANISMS FOR MODERATE AND EXTREME K/Rb FRACTIONATION OF THE CRUST.

K/Rb fractionation is the direct consequence of removal of granitic to granodioritic melts with low K/Rb. This results in decreased K and increased K/Rb (figure 8.4A). Green et al., (1972) postulated formation of "mangeritic" melts with high K/Rb (500-1400) and anorthositic residua with extremely high K/Rb (>2000) from two-stage melting of granulite gneisses (with K/Rb of 200-500). Gneisses close to the anorthosite also had extremely high K/Rb (>2000). A mechanism for this fractionation is suggested in figure 8.4B. The generation of high K/Rb melts results from the very high K/Rb parent. Moorlock et al., (1971) observed the even more extreme generation of anorthositic melts from pyroxene granulites.

8.1.5 Mechanism of Fractionation

Fractionation is attributed to upward diffusion of elements with aqueous fluids produced by dehydration reactions and to removal of anatectic melts. Dehydration fractionation is suggested as the mechanism for the early depletion of U and Cs, and to a lesser extent, Rb. Explanation of the more extreme fractionation of K, Rb, Ba, Sr, Zr, Th and other elements is possible only by anatexis.

8.2 ANATEXIS

8.2.1 Experimental Anatexis

8.2.1.1 The System Q-Ab-Or-An-H_2O

The system Q-Ab-Or-An was studied at 1 kb Pe_{H_2O} by James & Hamilton (1969) using synthetic compositions, and at 2 kb Pe_{H_2O} by von Platen (1965a,b) using a natural obsidian composition. Allowing for the differences in Pe_{H_2O}, the remarkably close agreement of the two studies suggest that components other than Q, Ab, Or and An (in particular, ferrosilite and enstatite components) do not significantly affect melting behaviour. This is also supported by the close agreement between the compositions of melts predicted by the system Q-Ab-Or-An and those observed during experimental anatexis of greywackes and shales (Winkler, 1957; Wyllie &

Tuttle, 1961a; Winkler & von Platen, 1958, 1960, 1961a, 1961b; von Platen, 1965a).

For any given P_{total} and fluid composition the minimum temperature for anatexis of quartzo-feldspathic rocks is that of the minimum melt composition in the system SiO_2-$NaAlSi_3O_8$-$KAlSi_3O_8$ (Q-Ab-Or). Increasing Pe_{H_2O} decreases the temperature at which anatexis commences and results in progressively more Ab-rich minimum melts (table 8.5). Most metamorphic rocks are not adequately represented by the system Q-Ab-Or, due to the presence of $CaAl_2Si_2O_8$ (An) component. Increasing An-content increases the temperature at which anatexis commences and results in more Q-Or-rich and Ab-poor minimum melts (table 8.5). The effect of increasing An-content is the opposite to that of increasing Pe_{H_2O}. The term "minimum melt" is used here to denote melts first formed during anatexis of specific rock compositions.

Anatexis of quartz-K-feldspar-plagioclase assemblages generates minimum melts on the ternary cotectic in the system Q-Ab-Or-An-H_2O (Winkler, 1967 and James & Hamilton, 1969). Increasing An-content of the parent rock causes migration of the minimum melt up the cotectic away from the Q-Ab-Or minimum, resulting in progressively more Q-Or-rich melts with slightly higher An-content. The composition of the melt also moves up the cotectic with increasing temperature and melt-volume. Quartz and K-feldspar contribute substantially to early melts, especially those formed from An-rich parent rocks. In consequence, quartz or K-feldspar is commonly the first phase consumed during anatexis. If K-feldspar is completely consumed, the melt leaves the ternary cotectic and migrates across the quartz-plagioclase binary cotectic surface becoming more Ab-rich. The temperature increases necessary to reach this stage of melting in common sedimentary or acid igneous rocks are relatively small (less than $\sim$100°C). If quartz is completely consumed first, considerably higher temperature increases are required to continue melting. Complete disappearance of plagioclase at an early stage is less common, and results in continued melting on the quartz-K-feldspar cotectic

TABLE 8.5

TEMPERATURES AND NORMATIVE COMPOSITIONS OF MINIMUM MELTS

(1) THE SYSTEM Q-Ab-Or

Pe_{H_2O} kb	T°C	Minimum Melt Q	Ab	Or
0.5	770	39	30	31
1.0	725	37	34	29
2.0	685	35	40	25
4.0	655	31	46	23
5.0	650	27	50	23
10.0	625	23	56	21

(2) THE SYSTEM Q-Ab-Or-An AT 2 kb Pe_{H_2O}

Original Rock %An	Ab/An	T°C	Minimum Melt Q	Ab	Or
0	∞	660	29	38	33
4	7.8	665	34	35	31
6	5.2	680	38	30	32
8	3.8	690	39	23	38
15	1.8	700	40	15	45

(3) THE SYSTEM Q-Ab-Or-An at 1 kb Pe_{H_2O}

%An in Melt	T°C	"Ternary Cotectic Melt*" Q	Ab	Or
3	730	38	31	28
5	745	40	21	34
7,5	780	43.5	10	39

*The"ternary cotectic melt"is the maximum temperature melt coexisting with quartz, K-feldspar and plagioclase.

Data from: Tuttle & Bowen (1958), Luth et al. (1964), von Platen (1965a,b), Winkler (1967); James & Hamilton (1969).

surface with relatively small increases in temperature. The compositions of melts generated from anatexis of quartz-K-feldspar-plagioclase rocks migrate up the ternary cotectic with increasing temperature until one phase is completely consumed. Melting continues with relatively small temperature increment only if this phase is one of the feldspars. If the first phase to disappear is quartz, the larger temperature increments necessary to melt K-feldspar-plagioclase rocks precludes further significant melting. The expected variation of melt compositions projected onto the Q-Ab-Or face of the Q-Ab-Or-An tetrahedron are shown in figure 8.5. The "final stages of anatexis" are reached when excessively large temperature increments are necessary for continued melting. The final stage of anatexis for $Pe_{H_2O} = P_{total}$ is reached within 100-150C° of the beginning of melting.

Melts generated from rocks rich in K-feldspar remain rich in Or-component, whereas those from rocks rich in plagioclase are Or-rich at first, then become richer in Ab-component. This pattern is clearly seen in the experimental work of Winkler & von Platen (1958-1961). Initial melts were potassic in all cases. Late stage melts remained potassic only for the Or-rich shales, but became progressively more Ab-rich (and An-rich) for the Or-poor greywackes. Final melts generated from the greywackes were granitic, granodioritic or tonalitic.

8.2.1.2 Hydrous Minerals

Anatexis of rocks containing potassic hydrous minerals (muscovite or biotite) but no K-feldspar produced melts essentially identical in composition to those in rocks containing K-feldspar (von Platen, 1965b; Brown & Fyfe, 1970). Or-component was supplied by decomposition of the hydrous mineral during early stages of melting. Anatexis of hornblende-bearing assemblages produced granodioritic melts (Brown & Fyfe, 1970), since much less Or-component is supplied to the melt by decomposition of the hydrous mineral.

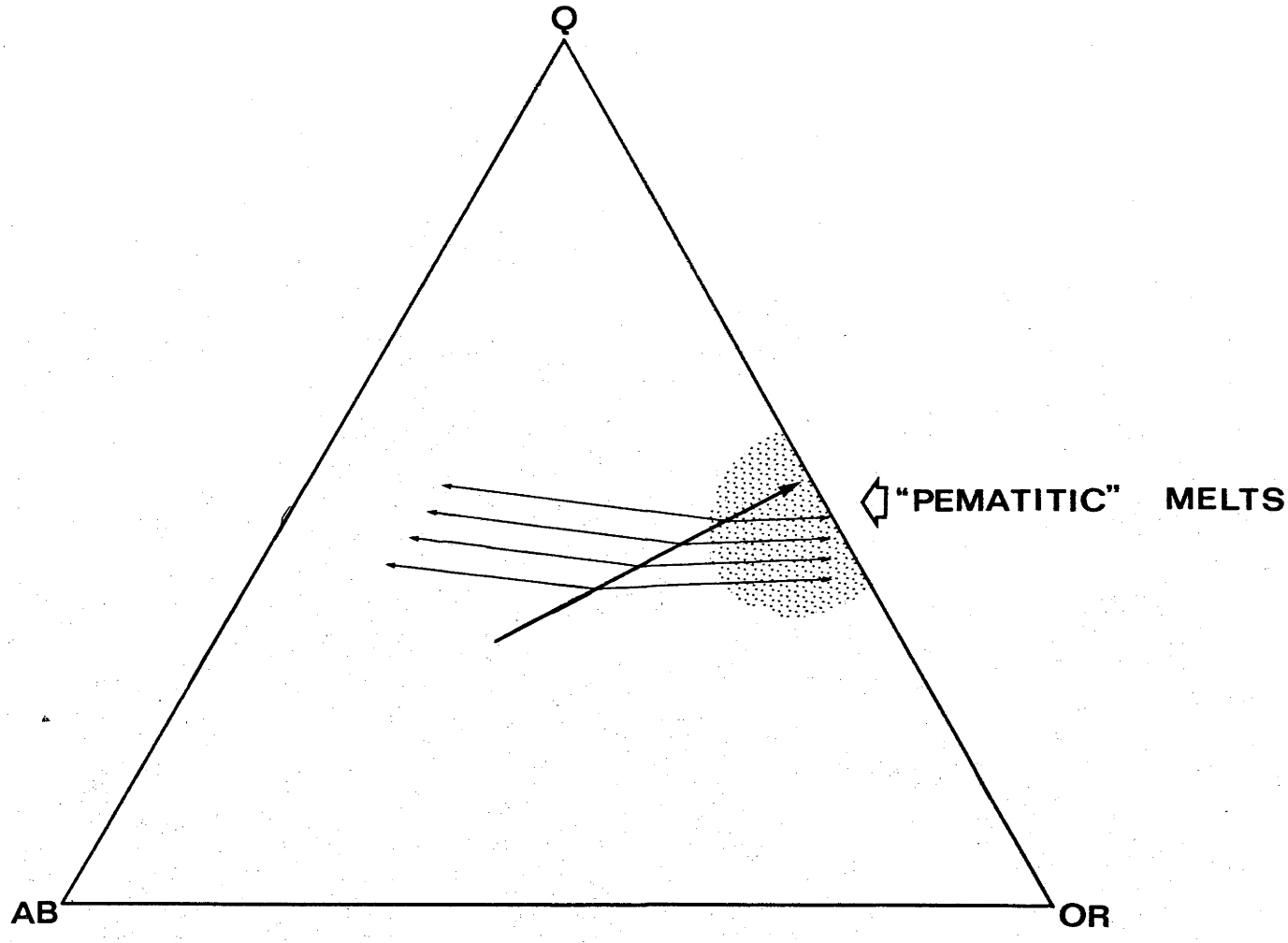

FIGURE 8.5 : DIAGRAMMATIC VARIATION OF MELT COMPOSITIONS FORMED DURING ANATEXIS.

The heavy arrow-headed line shows the variation of melt compositions along the ternary cotectic with increasing temperature. The light arrow-headed lines represent some possible paths for variation of melt compositions with increasing temperature across the Q-Ab binary cotectic surface (arrows pointing to the left) after Or is completely consumed, and across the Q-Or binary cotectic surface (arrows pointing to the right) after Ab is completely consumed.

8.2.1.3 Fluid Composition

The composition of fluid phase may greatly affect melting behaviour (Wyllie & Tuttle, 1959, 1961b, 1964; Burnham, 1967). Water is the most common fluid phase. Water dissolves in silicate melt and efficiently depresses solidus and liquidus temperatures. At high pressures and temperatures appreciable silicate dissolves in aqueous fluid. Accordingly unit activity of water is here defined relative to that of fluid containing water as the only volatile component in equilibrium with silicate at the same P_{total} and T (Holloway, 1972). The small reduction of Pe_{H_2O} due to dissolved silicate is then taken into account and the condition $Pe_{H_2O} = P_{total}$ is attainable. Fluorine (as F or HF) depresses solidus temperatures even more efficiently than water. F is efficiently "fixed" in crystalline phases (Burnham, 1967) and the low F contents of intrusive igneous rocks indicate low F contents in the original magmas. The appreciable F-content of many metamorphic minerals is far greater than present in the fluid phase during crystallisation of the minerals (Munoz & Eugster, 1969). F appears to be minor in most natural fluids. Most fluid components other than H_2O or F are insoluble in silicate melts within the crust and result in elevation of melting temperatures. The most common of such fluid components is CO_2, which is insoluble in silicate melts at pressures less than 15 kb (Hill & Boettcher, 1970). CO_2 causes elevation of melting temperatures by diluting the aqueous phase and reducing Pe_{H_2O}.

8.2.2 Compositions of Natural Anatectic Melts

Anatexis during high grade metamorphism results in formation of migmatites and veined gneisses. More extensive anatexis may generate melts capable of coalescing to form "pools" of granitic to granodioritic magma. If the volume of such melts is sufficient, and the melts are sufficiently water-undersaturated, the magma may intrude overlying crust to form high-level batholiths. The concentration maxima of "granitic" (Q+Ab+Or>80%) and "granodioritic" melts (Q+Ab+Or+An>80%) (figure 3.6) indicate

that the granodiorites have slightly lower Q. The highly potassic early melts predicted from experimental studies are not found as major batholiths, but do occur in migmatites (von Platen, 1965b; White, 1966). This indicates that conditions are not suitable for intrusion of these melts.

It has been realised relatively recently that granitic-granodioritic magmas are water-undersaturated (Burnham, 1967; Brown & Fyfe, 1970; Fyfe, 1970; Harris et al. 1970; Brown, 1971). This conclusion was based on the low initial water contents of the rocks melted, and restrictions placed on intrusion of water-saturated melts by liquidus geometry (figure 8.6). Intrusion of water-saturated granodiorite melt (figure 8.6A) along a path A-B would result in immediate commencement of crystallisation. Fluid would boil off and crystallisation would proceed rapidly with intrusion. The magma must be completely crystalline by B, but intrusion would cease before B due to decreased mobility. A water-undersaturated granodiorite melt intruding along a path C-D-E would reach D before crystallisation commenced. Crystallisation must be complete by E, but intrusion would cease before the melt reached E. The water-undersaturated melt would be capable of intruding $\sim$8 km ($\sim 3\frac{1}{2}$kb) further than the water-saturated melt. The water-saturated granite solidus has an inflexion at 4 kb due to muscovite stabilisation (figure 8.6B). Intrusion of water-saturated granite may be possible along a path such as F-G-H, however the cooling rate is critical. Water-undersaturated melts (4%, 2%, 0% water) intrude nearly to the surface before crystallisation (unlabelled dashed paths in figure 8.6B). The early potassic "pegmatitic" melts should also have a "muscovite-in" inflexion and their failure to intrude is probably due to small melt volumes rather than liquidus geometry.

8.2.3 Anatexis During Metamorphism

Water in metamorphic rocks prior to anatexis occurs mainly in hydrous minerals. Burnham (1967) estimated pore

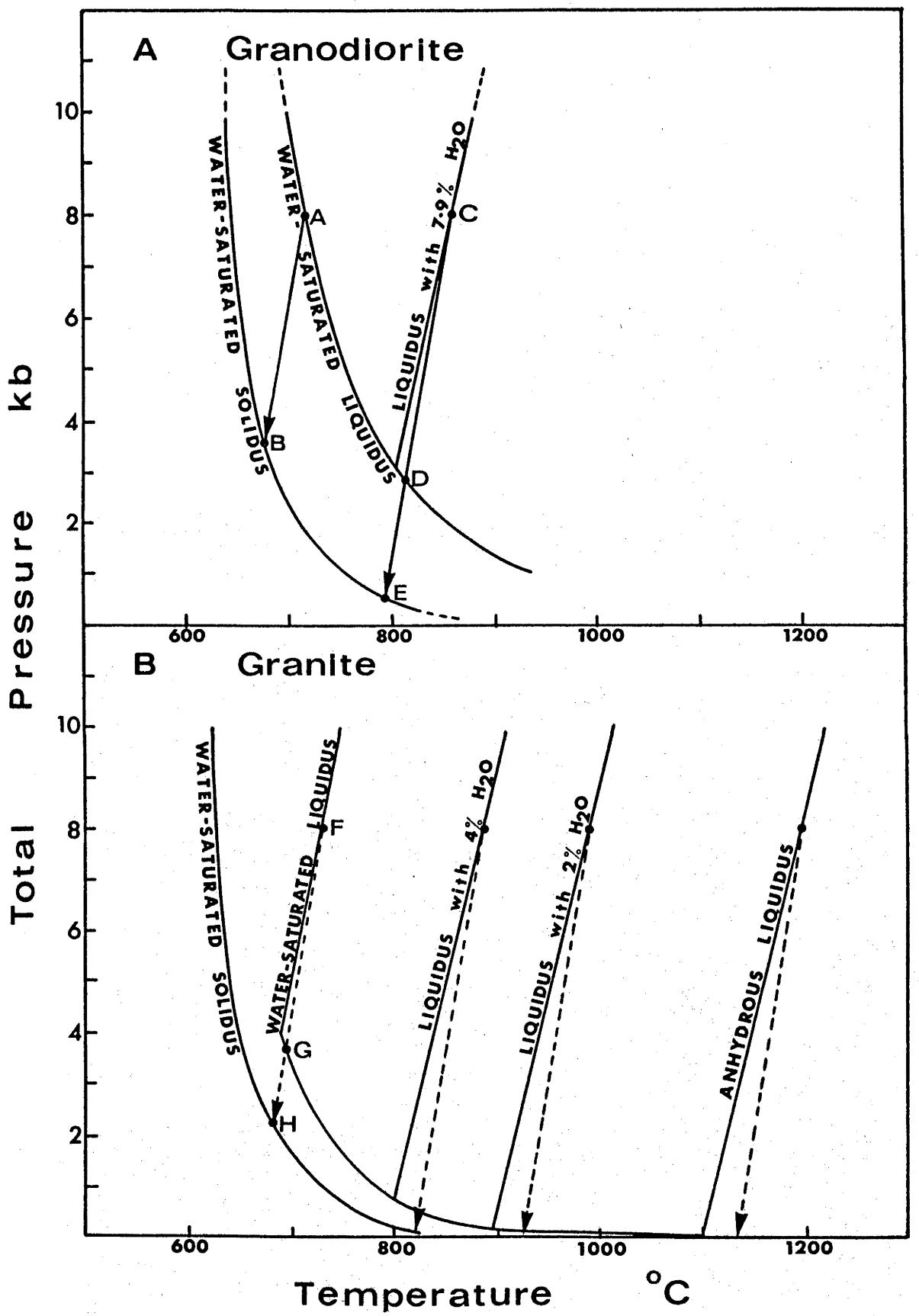

FIGURE 8.6 : GEOMETRY OF SOLIDI AND WATER-SATURATED & WATER-UNDERSATURATED LIQUIDI FOR GRANODIORITE AND GRANITE.

The diagrams are from Burnham (1967) and Harris et al., (1970). The solid and dashed arrow-headed lines (A-B, C-D-E, F-G-H and others) represent hypothetical P-T paths for intrusion and crystallisation of the melts (see text for detailed explanation).

fluid contents in metamorphic rocks of less than 1% at pressures of 7-8 kb, and maximum total water contents of 4% for metasediments. The pore fluid may contain "pure" water, or water mixed with other volatiles. Water and carbon dioxide are by far the most common metamorphic pore fluids. A reasonable estimate of pore fluid contained in metamorphic rocks at ∿8 kb prior to anatexis is ½%. Assuming the fluid is "pure" water, anatexis first occurs at the water-saturated solidus ($Pe_{H_2O} = P_{total}$) and forms about4% of water-saturated melt before the fluid is completely dissolved. With continued melting, the melt becomes water-undersaturated and Pe_{H_2O} is progressively reduced. Pore fluid containing CO_2 cannot dissolve entirely in the melt. At equilibrium, Pe_{H_2O} in the fluid must equal that in the melt, and some water must remain in the fluid at all stages of melting. Melting commences at a water-undersaturated solidus of similar configuration to the undersaturated liquidi in figure 8.6. The melt becomes more undersaturated in water as melting continues, and the amount of water in the fluid phase is considerably reduced.

Rocks containing hydrous minerals may melt at a vapour-absent solidus or BoM (6.4.1). The hydrous mineral defining the BoM may melt in a relatively small temperature interval above the BoM. If melting commences at water-saturated or water-undersaturated solidi, the hydrous mineral becomes unstable and melts in the same temperature interval (now a "metastable BoM"). If the rock contains additional hydrous phases, these melt at metastable BoM bands at progressively higher temperatures and greater degree of water-undersaturation. Melt may leave the site of anatexis and intrude overlying gneisses if melt-volume and water-undersaturation conditions are suitable. Renewal of anatexis is likely if all hydrous mineral has not melted, and commences at new vapour-absent solidi defined by the remaining hydrous mineral.

Rocks may be subjected to anatexis more than once during metamorphism. The first cycle of melting dissolves the fluid-phase and melts the least stable hydrous mineral

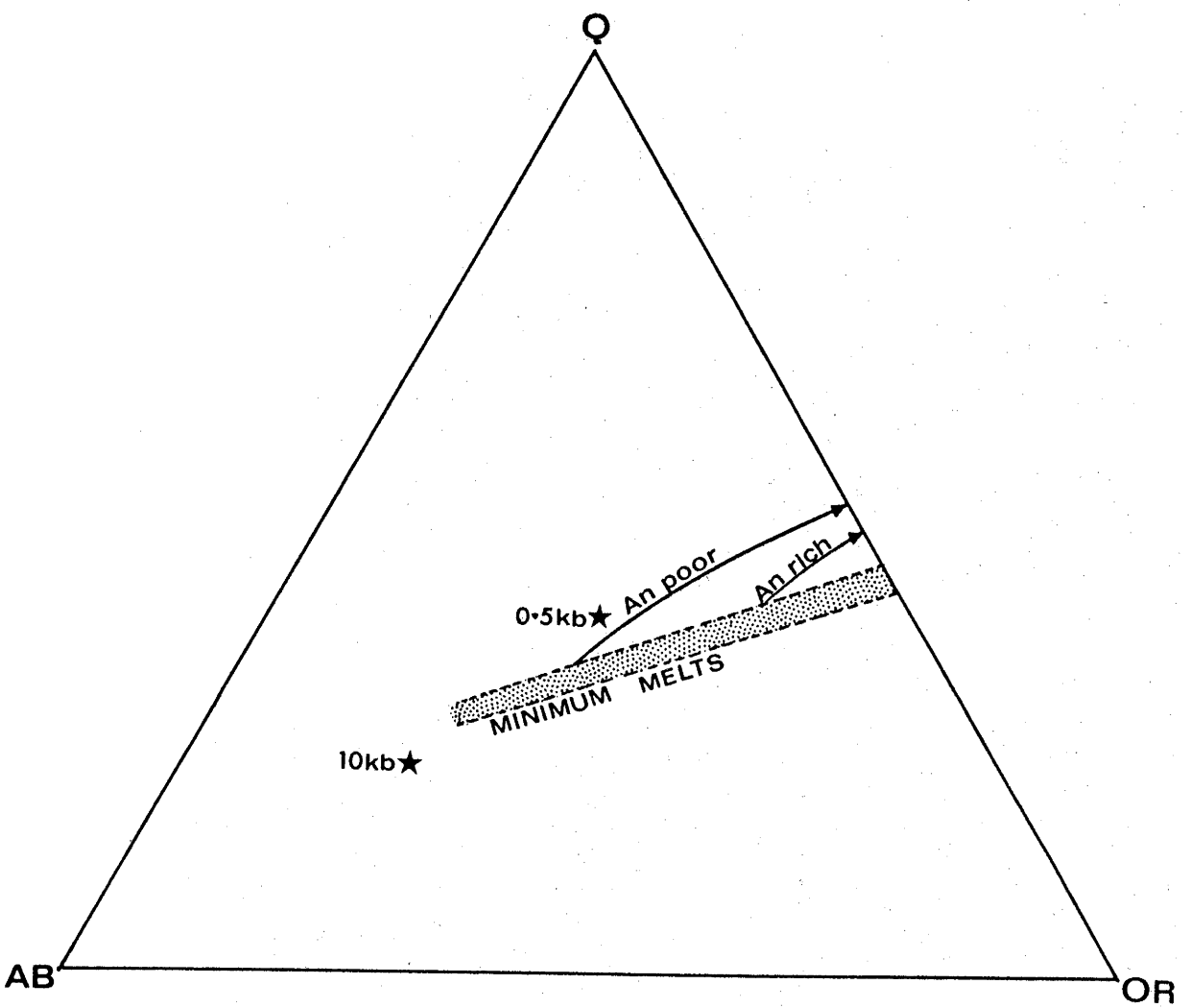

FIGURE 8.7 : DIAGRAMMATIC VARIATION OF MELT COMPOSITIONS FORMED DURING EARLY STAGES OF ANATEXIS.

The stippled band represents approximate minimum melt compositions for 8 kb Pe_{H_2O} and for parent rocks with An-contents ranging from zero (at left) to about 10% and greater (at right). The arrowed lines indicate the expected variation of melt compositions with increasing temperature for An-poor and An-rich rocks after formation of the minimum melts.

(muscovite or biotite) before intrusion. The second cycle of melting usually occurs only in the presence of residual hydrous mineral such as Mg-rich biotite or hornblende. The second cycle of melting eliminates remaining hydrous minerals. Additional cycles of melting can only occur at extreme temperatures. The melting process active during anatexis is equilibrium partial fusion. Fractional fusion makes a minor contribution to the process if more than one cycle of melting occurs.

8.2.4 Anatexis at Eyre Peninsula

The first anatectic melts from the Eyre Peninsula acid gneisses are formed at $Pe_{H_2O} = P_{total}$ (viz. ∿7-8 kb.) and have compositions within the band A-B in figure 8.7. With increased melting, the melt compositions migrate up the ternary cotectic and towards lower Pe_{H_2O} compositions. The compositions of early melts from An-rich and An-poor rocks are shown diagrammatically in figure 8.7. The early melts are more granitic and later melts are more "pegmatitic".

Coarse feldspar pegmatites and hornblende pegmatites at Eyre Peninsula are commonly associated with intense rehydration and disruption of basic bands. This evidence strongly favours water-rich melts, and coupled with the low initial water-contents of the rocks restricts the volume of anatectic melts formed.

8.3 A FRACTIONATION MODEL

8.3.1 The Fractionation Model

Residuum compositions were computed using the fractionation equations of Shaw (1970). Equilibrium partial melting and fractional partial melting by 5% batches were considered.

Initial mineralogies were modelled on a variety of Eyre Peninsula gneisses (table 8.6). Mineralogies used were mainly anhydrous (A1 to A6), assuming elimination of hydrous minerals in early melt fractions. However, a few compositionally equivalent hydrous mineralogies were considered (H1 to H3).

TABLE 8.6

INITIAL MODES USED IN COMPUTED FRACTIONATION

Percent :	Qz	Pl	Or	Op	Ga	Hb	Bi	Ap	Zr
A1	33	17	40	--	10	--	--	--	--
A2	28	32	27	--	12	--	--	0.3	0.04
A3	21	43	27	8	--	--	--	0.6	0.04
A4	21	43	27	8	--	--	--	--	--
A5	30	36	25	7	1	--	--	0.4	0.08
A6	30	38	19	--	12	--	--	0.1	0.02
H1	25	37	22	--	5	--	10	0.3	0.03
H2	28	32	24	--	10	--	5	0.3	0.04
H3	21	41	25	5	--	3.5	3.5	0.6	0.04

A-prefixes are anhydrous. H-prefixes contain hydrous minerals. Composi- were modelled on samples as follows: (A1) 69-942; (A2, H1 & H2) 69-1375; (A3, A4 & H3) High-K intrusive charnockites; (A5) Garnet symplectite charnockites; (A6) 69-1348.

Qz = quartz; Pl = plagioclase (Ab+An); Or = K-feldspar;
Op = orthopyroxene; Ga = garnet; Hb = hornblende; Bi = biotite;
Ap = apatite; Zr = zircon.

Minimum melts formed from Eyre Peninsula gneisses range from granitic to potassic "pegmatitic" compositions (figures 3.6 & 8.7). The granitic melts form at higher Pe_{H_2O} and become progressively more "pegmatitic" with increased melting and decreased Pe_{H_2O}, until K-feldspar and potassic hydrous minerals are consumed. The latter stage of anatexis was not attained at Eyre Peninsula since nearly all the acid gneisses contain K-feldspar. Hence the anatectic melts have granitic to pegmatitic compositions. Although the proportions and compositions of minerals contributing to the melt vary continuously during anatexis, constant melting mode was assumed. Two idealised melt compositions were used in computed fractionation: (1) "granite" (40% quartz, 32% plagioclase and 28% K-feldspar); and (2) "pegmatite" (41% quartz, 11% plagioclase and 48% K-feldspar). For melting of hydrous assemblages it was arbitrarily assumed that 20% of the melt was generated by decomposition of hydrous minerals. The remaining 80% of melt was composed of pegmatite or granite. Quartz, feldspars, biotite and hornblende were assumed to melt, and garnet, orthopyroxene, zircon and apatite assumed to remain in the residuum.

Apatite and zircon are common constituents of intrusive granites and must be dissolved to some extent during anatexis. Melting of zircon is favoured by high Pe_{H_2O} (Marshall, 1969) and by sodic melts (Dietrich, 1968). Early anatectic melts are water-rich but sodium-poor, and dissolution of zircon is only partly favoured. Limited dissolution of zircon and apatite is supported by the moderate Zr (219 ppm) and P_2O_5 (0.13%) of one pegmatite (69-942). Intense enrichment of Zr at one pegmatite contact (69-1377) indicates efficient zircon dissolution by this pegmatitic melt. The Eyre Peninsula gneisses contain zircon and apatite, and field evidence suggests that most of the gneisses have been partly melted and anatectic melts removed. This indicates that zircon and apatite are residual phases. The degree to which zircon and apatite dissolve in anatectic melts is uncertain, and the minerals were not used as components of the melting mode. The effects of residual apatite and zircon were examined by

TABLE 8.7

RANGE OF LIQUID/CRYSTAL DISTRIBUTION COEFFICIENTS AND VALUES USED

Element	Plagioclase	K-Feldspar	Biotite	Hornblende
Rb	17(2-50)	1.5	0.3(0.3-1.1)	100(70-125)
Ba	5(0.3-20)	0.3(0.2-0.3)	0.16(0.1-0.2)	20(18-50)
Sr	0.7(0.03-0.8)	0.3(0.2-0.3)	8.3(1.5-13)	15(10-45)
Cs	50(1.3-50)	10*	0.5	50*
La	8(2-7)	20	25*	1.5*
Ce	10(3-50)	23	25(3-25)	1(0.5-2)
Nd	12(4-50)	40	22(3-25)	0.5(0.2-1)
Sm	14(5-50)	56	17(3-17)	0.3(0.1-0.6)
Eu	5(0.2-17)	0.88	6.7(2-7)	0.3(0.2-07)
Gd	20(4-50)	100	12.5(3-13)	0.25(0.5)
Tb	22(5-30)	135	11*(3.8)	0.2*
Dy	23	165	10(5-10)	0.2(0.1-0.4)
Ho	25*	180*	8*	0.2*
Er	28(3-100)	165	6.3(5-7)	0.2(0.1-0.4)
Yb	33(3-100)	85	5.6(2-6)	0.2(0.1-0.5)

Element	Orthopyroxene	Garnet	Zircon	Apatite
Rb	500(300-2000)	118	10^4*	10^4*
Ba	350(300-400)	59	10^4*	0.04*
Sr	50(22-120)	66	10^4*	0.5*
Cs	10^4*	10^4*	10^4*	10^4*
La	8*	3.0*	0.18*	0.038*
Ce	7(4-13)	2.9	0.20(0.14-0.4)	0.029(0.02-0.06)
Nd	6(3-9)	1.9	0.22(0.15-0.5)	0.020(0.01-0.04)
Sm	5.5(3-8)	0.37	0.27(0.15-0.4)	0.017(0.01-0.04)
Eu	5(4-9)	0.67	0.33(0.2-0.9)	0.029(0.02-0.05)
Gd	4(4-6)	0.095	0.10*	0.018*
Tb	3.2*	0.051	0.05*	0.019*
Dy	2.5(1.8-3.8)	0.035	0.022(0.019-0.026)	0.020(0.015-0.04)
Ho	2.1*	0.029*	0,015*	0.025
Er	1.7(1.4-2.3)	0.023	0.0077(0.007-0.008)	0.029(0.02-0.05)
Yb	1.2(1.0-1.4)	0.025	0.0038(0.003-0.004)	0.04(0.03-0.08)

*Estimated or interpolated; Where no range is given in brackets, only one value was obtained from the literature.

Data from: (1) zircon & apatite: Nagasawa(1970); (2) remainder: Dudas et al., (1971); Higuchi & Nagasawa (1969); Schnetzler & Philpotts (1970); Philpotts & Schnetzler (1970); Griffin & Murthy (1969); Korringa & Noble (1971); Nagasawa & Philpotts (1971).

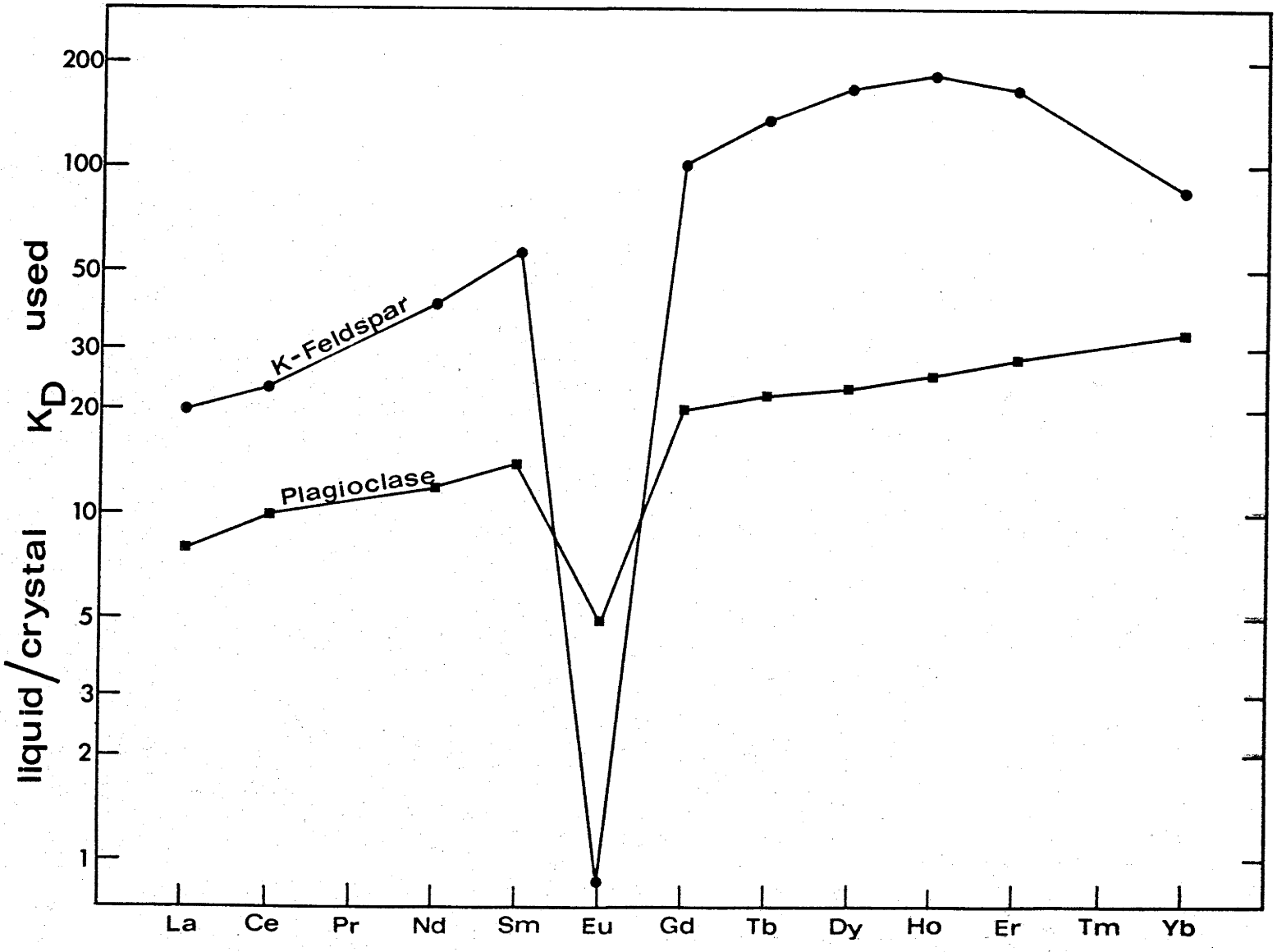

FIGURE 8.8 : COMPARISON OF RARE EARTH ELEMENT LIQUID-CRYSTAL DISTRIBUTION COEFFICIENTS FOR PLAGIOCLASE AND K-FELDSPAR.

The values plotted are those used in the fractionation model (table 8.7).

assuming the minerals remained in the residuum and by using (zircon+apatite)-bearing and (zircon+apatite)-free initial mineralogies.

Nagasawa & Schnetzler (1971) noted that crystal/liquid distribution coefficients for mafic minerals were considerably higher in acid rocks than those in basic rocks, but that coefficients for feldspars in acid and basic rocks were comparable. Hence, mafic mineral distribution coefficients for acid to intermediate rocks were used. Feldspar distribution coefficients were selected for acid through to basic rocks. The range of liquid/crystal distribution coefficients together with the selected values used in computed fractionation are shown in table 8.7. The selected distribution coefficients are reasonable values more commonly observed for acid melts. Distribution coefficients used for K-feldspar and plagioclase are compared in figure 8.8.

8.3.2 The Results of Computed Fractionation

8.3.2.1 Rubidium

Rb is strongly depleted by equilibrium anatexis producing granitic melts (figure 8.9). Biotite is the only residual phase enriched in Rb relative to the melt, but its abundance is insufficient to result in residuum enrichment. However, the rate of Rb depletion is considerably decreased by the presence of residual biotite. Rb is partitioned much more strongly into K-feldspar than plagioclase. Hence depletion of Rb is slower in rocks rich in K-feldspar. Conversely anatexis producing "pegmatitic" melt richer in K-feldspar results in more rapid depletion of Rb.

8.3.2.2 Cesium

Cs is extremely depleted by anatexis producing granitic melts (figure 8.10). Biotite is the only phase enriched in Cs relative to the melt, but is present in insufficient proportions to cause Cs enrichment. However, residual biotite decreases the rate of Cs depletion. Cs fractionation

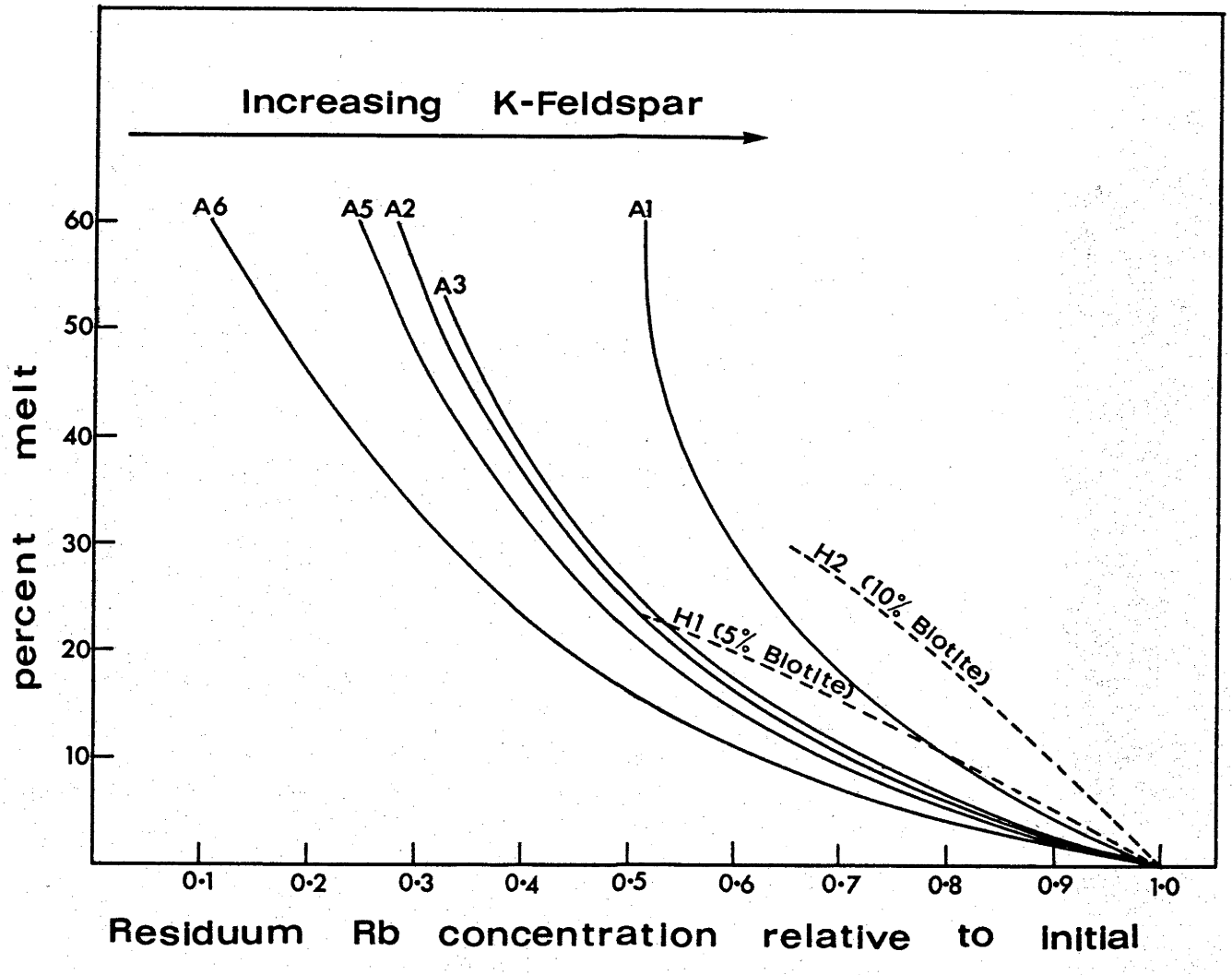

FIGURE 8.9 : RELATIVE CONCENTRATION OF Rb IN RESIDUUM DURING ANATEXIS.

Rb concentrations were computed by the fractionation model assuming equilibrium melting and production of granitic melts. The solid lines are for anhydrous parent mineralogies. The dashed lines are for hydrous parent mineralogies and show the effect of residual biotite. (H1 and H2 are approximately equivalent compositions to A2 but have 10% and 5% biotite in their initial mineralogies).

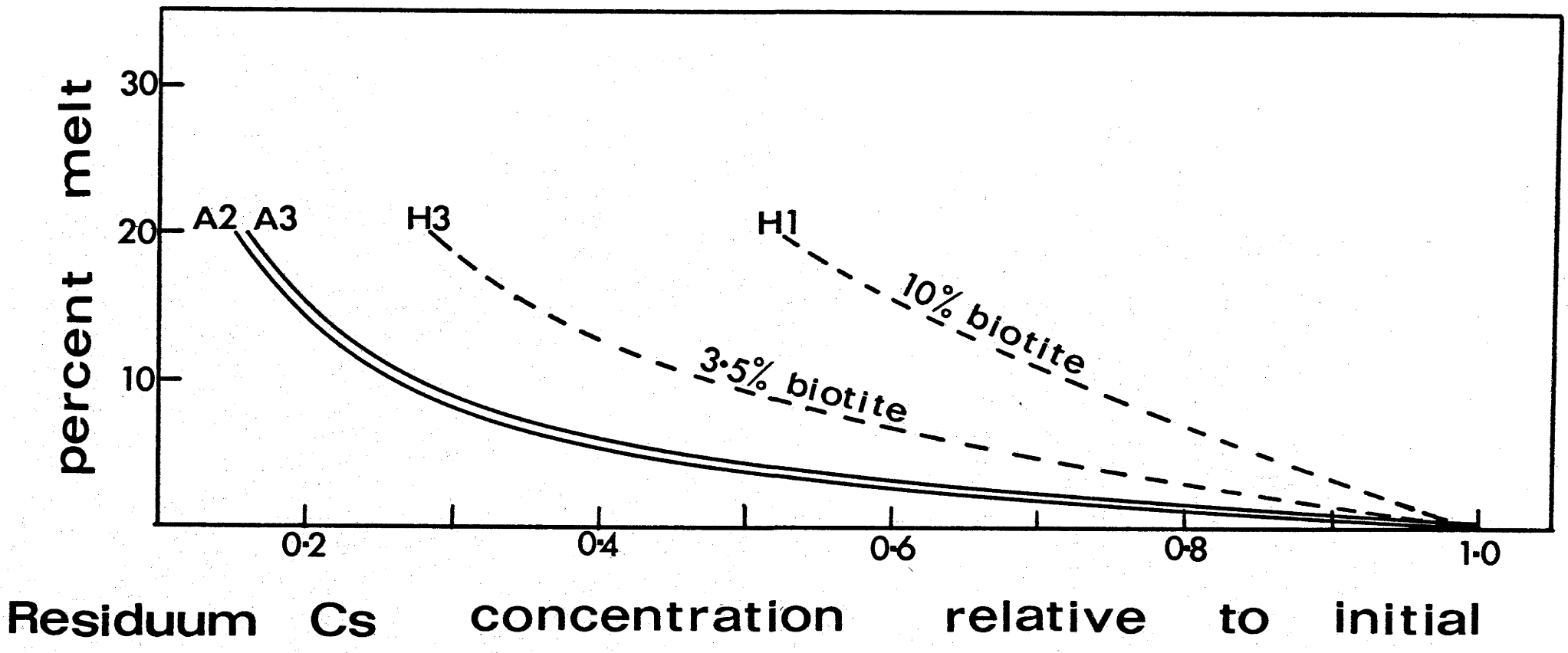

FIGURE 8.10 : RELATIVE CONCENTRATION OF Cs IN RESIDUUM DURING ANATEXIS.

(Explanation as for figure 8.9).

(H1 and H3 are approximately equivalent in compositions to A2 and A3 respectively but have 10% biotite, and 3.5% biotite and 3.5% hornblende respectively).

is essentially unaffected by production of "pegmatitic" instead of granitic melts.

8.3.2.3 Barium

Ba may be moderately enriched or moderately depleted during anatectic production of granitic melts (figure 8.11A). K-feldspar and biotite are enriched in Ba relative to the melt. Hence Ba enrichment is enhanced in K-feldspar-rich rocks and decreases with decreasing K-feldspar. Partitioning of Ba into biotite is only slightly stronger than into K-feldspar, and biotite in the residuum mildly increases retention of Ba (table 8.8). Production of pegmatitic melts eliminates K-feldspar more efficiently and usually results in depletion of Ba (figure 8.11B).

8.3.2.4 Strontium

Sr is usually enriched during anatectic fractionation producing granitic melts (figure 8.12A). Sr is depleted only by extensive melting of K-feldspar-poor rocks. Sr is mildly enriched in residual feldspars relative to melt, and slightly more enriched in K-feldspar than plagioclase. Hence Sr enrichment is more pronounced in K-feldspar-rich rocks. Fractionation involving "pegmatitic" melts decreases Sr enrichment, or causes mild Sr depletion in cases of extended melting (figure 8.12B).

8.3.2.5 Rare Earth Elements

Fractionation of REE during production of granitic melts is shown in figures 8.13 and 8.14. Differences between REE fractionation for granitic and "pegmatitic" melts are negligible, except that larger positive Eu anomalies are generated when granitic melt is removed, due to the residuum being richer in K-feldspar (figure 8.8). The REE are plotted relative to initial concentrations, and the patterns can be assumed equivalent to shale-normalised REE plots if initial sedimentary abundances are postulated.

REE are enriched in residuum garnet, zircon, apatite and hornblende, and Eu may be slightly enriched in feldspar

TABLE 8.8

EFFECT OF BIOTITE ON

RELATIVE Ba CONCENTRATION IN RESIDUA

Sample	A2	H1	H2
% Biotite	0%	5%	10%
% Melt	Concentration of Barium		
5	1.002	1.009	1.017
10	1.004	1.015	1.032
15	1.007	1.016	1.046
20	1.010	1.011	1.058

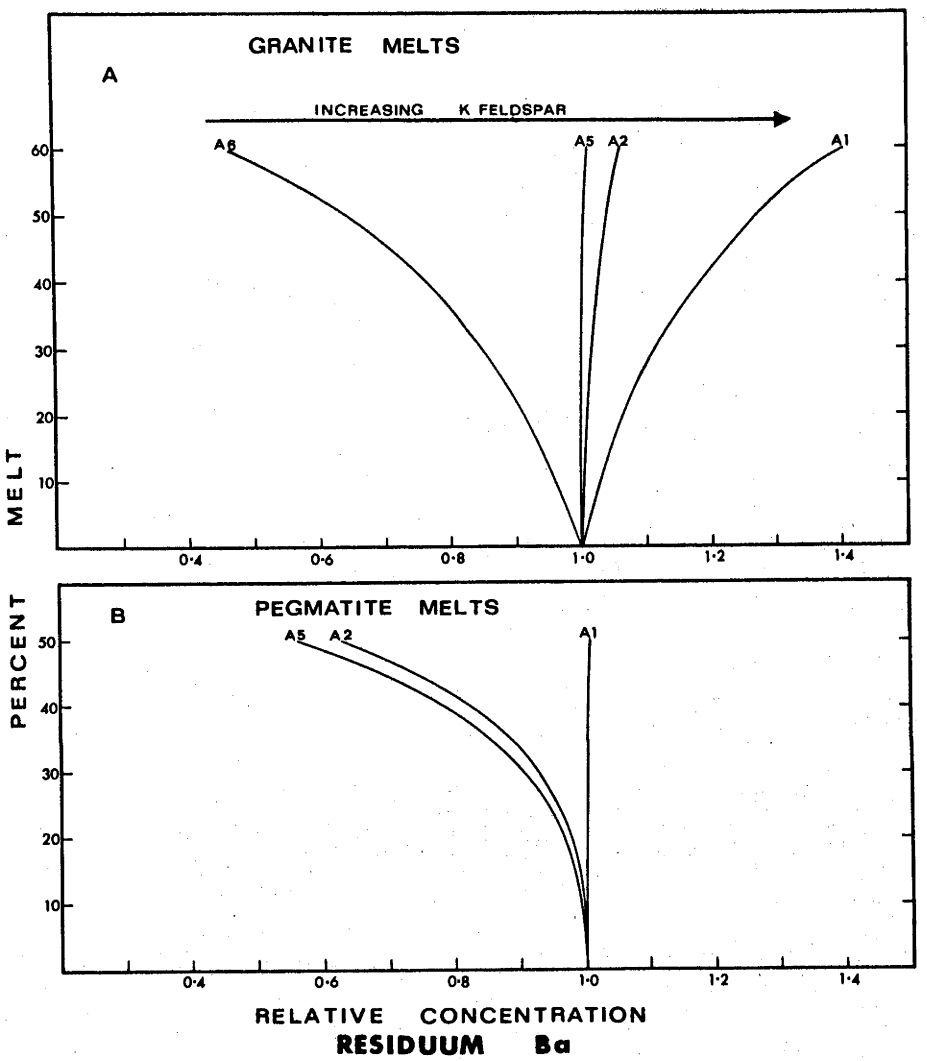

FIGURE 8.11 : RELATIVE CONCENTRATION OF Ba IN RESIDUUM DURING ANATEXIS.

Ba concentrations were computed by the fractionation model assuming equilibrium anatexis producing granitic melts (A) and pegmatitic melts (B).

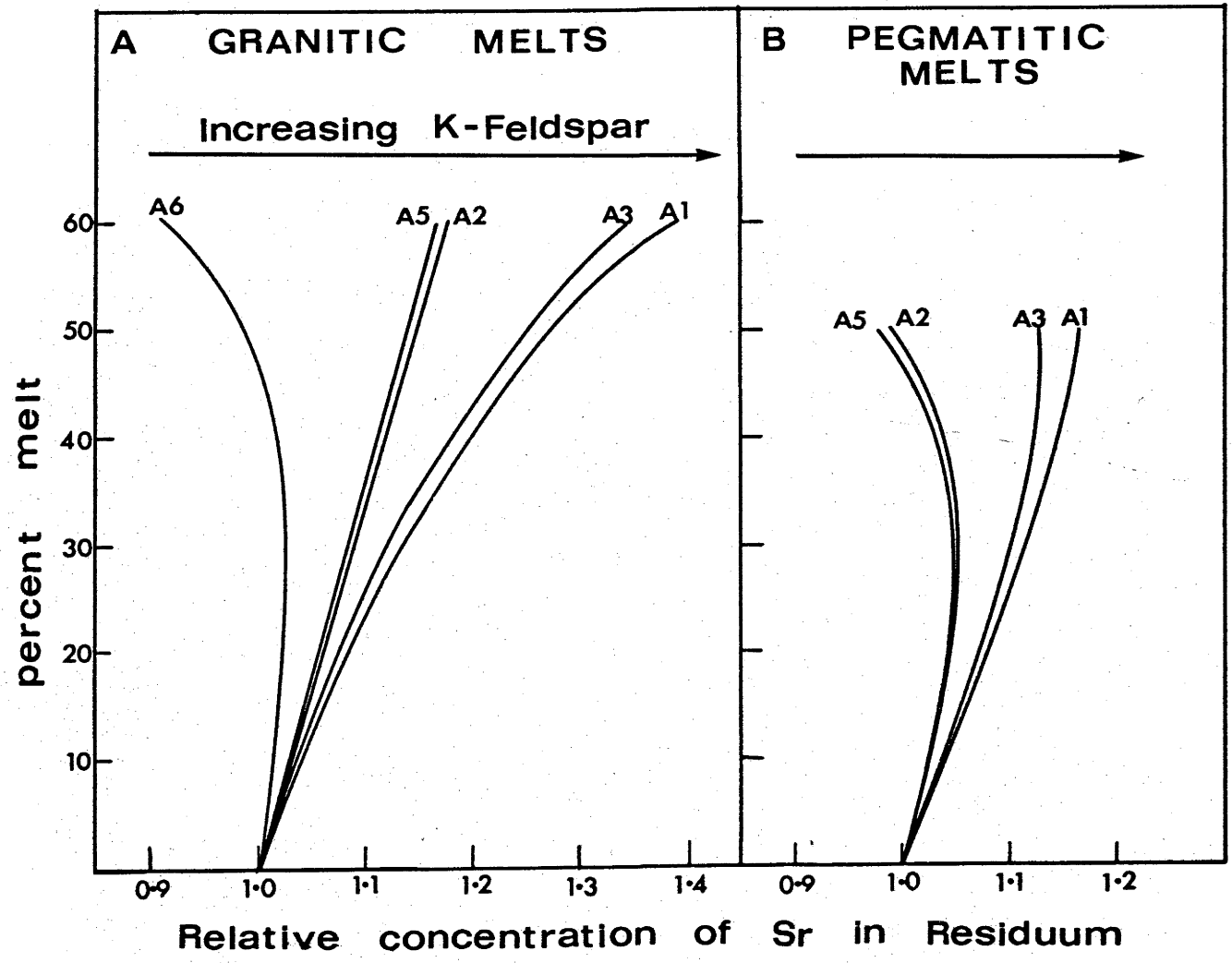

FIGURE 8.12 : RELATIVE CONCENTRATION OF Sr IN RESIDUUM DURING ANATEXIS.
(Explanation as for figure 8.11).

(table 8.7). Allowing for modal abundance, the effect of hornblende is negligible. Heavy REE are strongly enriched in garnet and zircon. However, relatively small amounts of garnet (∿0.5% or more) are sufficient to enrich heavy REE significantly in excess of the enrichment due to zircon, which is present in very minor proportions (0.02-0.08%, based on the assumption that all Zr is present in zircon). Apatite is strongly enriched in REE and is present in greater abundance than zircon (0.3-0.6%, assuming all P_2O_5 occurs in apatite). Apatite residuum has a comparable effect on heavy REE to ∿0.5% garnet. Hence ∿1% garnet or more dominates heavy REE fractionation even in the presence of zircon and apatite. REE fractionation of garnet-gneisses is shown in figure 8.13. An initial garnet content of 1% results in moderate depletion of light REE and mild enrichment of heavy REE. Initial garnet contents of 10% and 12% cause strong heavy REE enrichment but comparable light REE depletion.

Feldspars, biotite and orthopyroxene are depleted in REE relative to the melt, with the exception of Eu which may be mildly enriched. Eu is partitioned into feldspars much more strongly than adjacent REE (figure 8.8). Fractionation of residua involving only phases depleted in REE results in overall depletion of REE with generation of marked positive Eu anomalies (figure 8.14). The positive Eu anomaly is almost entirely prevented and the overall REE depletion arrested if accessory apatite and zircon are included as residual phases. The effects of accessory zircon and apatite on REE fractionation are masked by relatively minor amounts of garnet. However, apatite and zircon have drastic effects on fractionation of REE by feldspars, greatly reducing REE depletion and suppressing formation of positive Eu anomalies.

8.3.3 Variation of Distribution Coefficients and Melting Process

The effects of variation of liquid/crystal distribution coefficients (K_D) of a major phase are shown in figure 8.15. Variation if K_D above unity has negligible effect compared

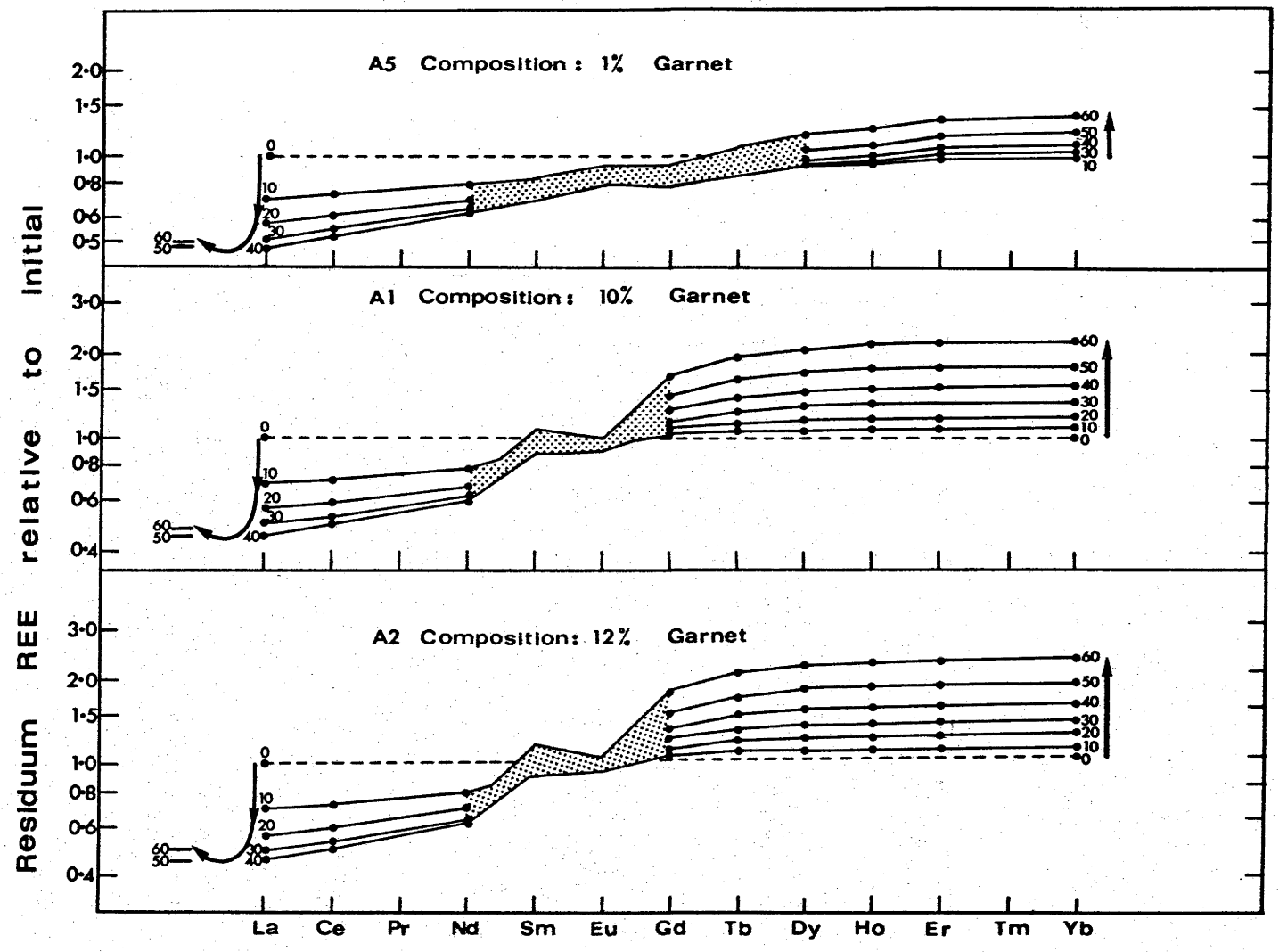

FIGURE 8.13 : ANATECTIC FRACTIONATION OF RARE EARTH PATTERNS INVOLVING GARNET-BEARING RESIDUA.

REE concentrations were calculated by the fractionation model assuming equilibrium anatexis producing granitic melt. The REE are plotted relative to initial concentrations and are equivalent to shale-normalised REE patterns if initial sedimentary abundances are postulated. Complex cross-over of the various REE patterns occurs in the stippled portions. The small numbers at each end are the percentages of melt removed. The arrows show the direction of fraction with increasing melting.

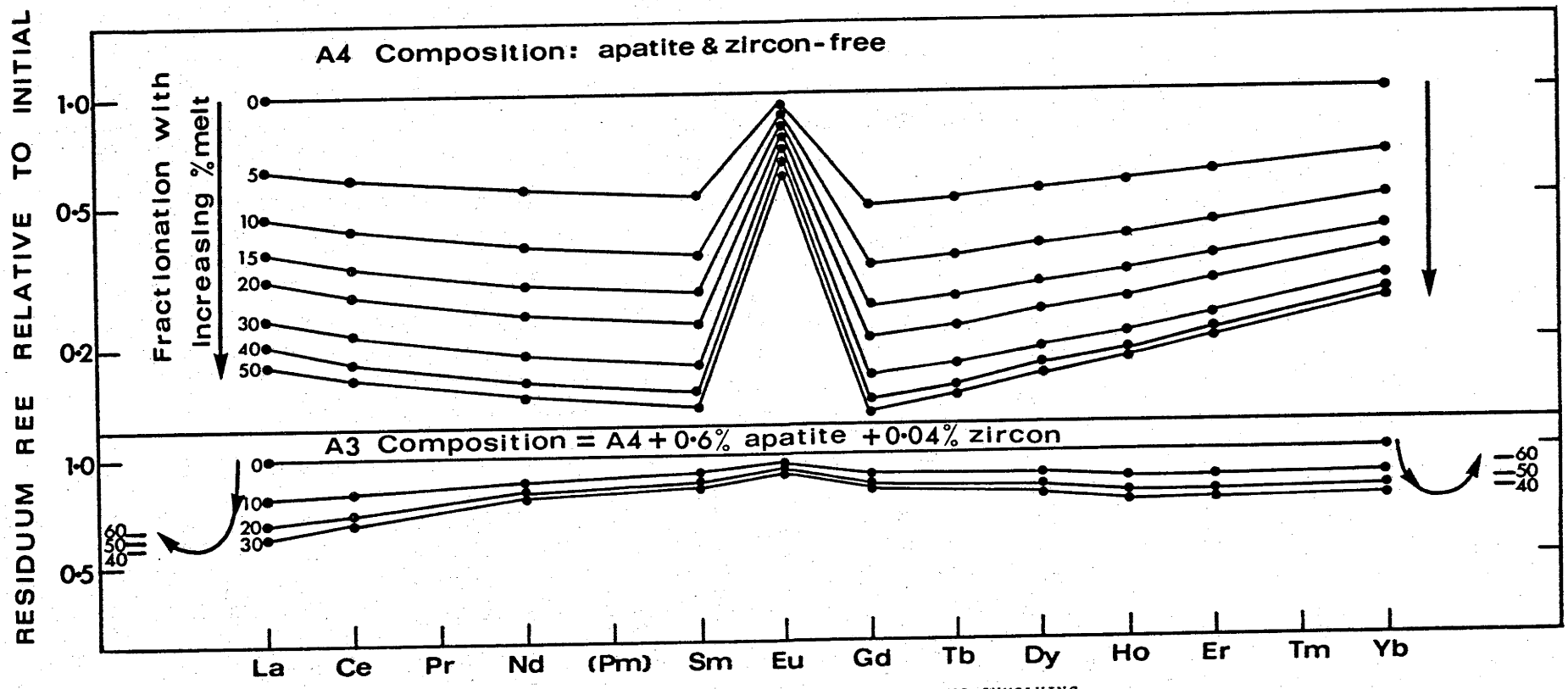

FIGURE 8.14 : ANATECTIC FRACTIONATION OF RARE EARTH PATTERNS INVOLVING QUARTZO-FELDSPATHIC RESIDUA WITH AND WITHOUT ACCESSORY APATITE AND ZIRCON.

(Explanation as for figure 8.13).

Depletion of REE in the apatite + zircon-bearing residua ceases at ∿ 30% melting for Nd to Yb and at ∿ 40% melting for La to Nd : further melting then causes mild enrichment of REE.

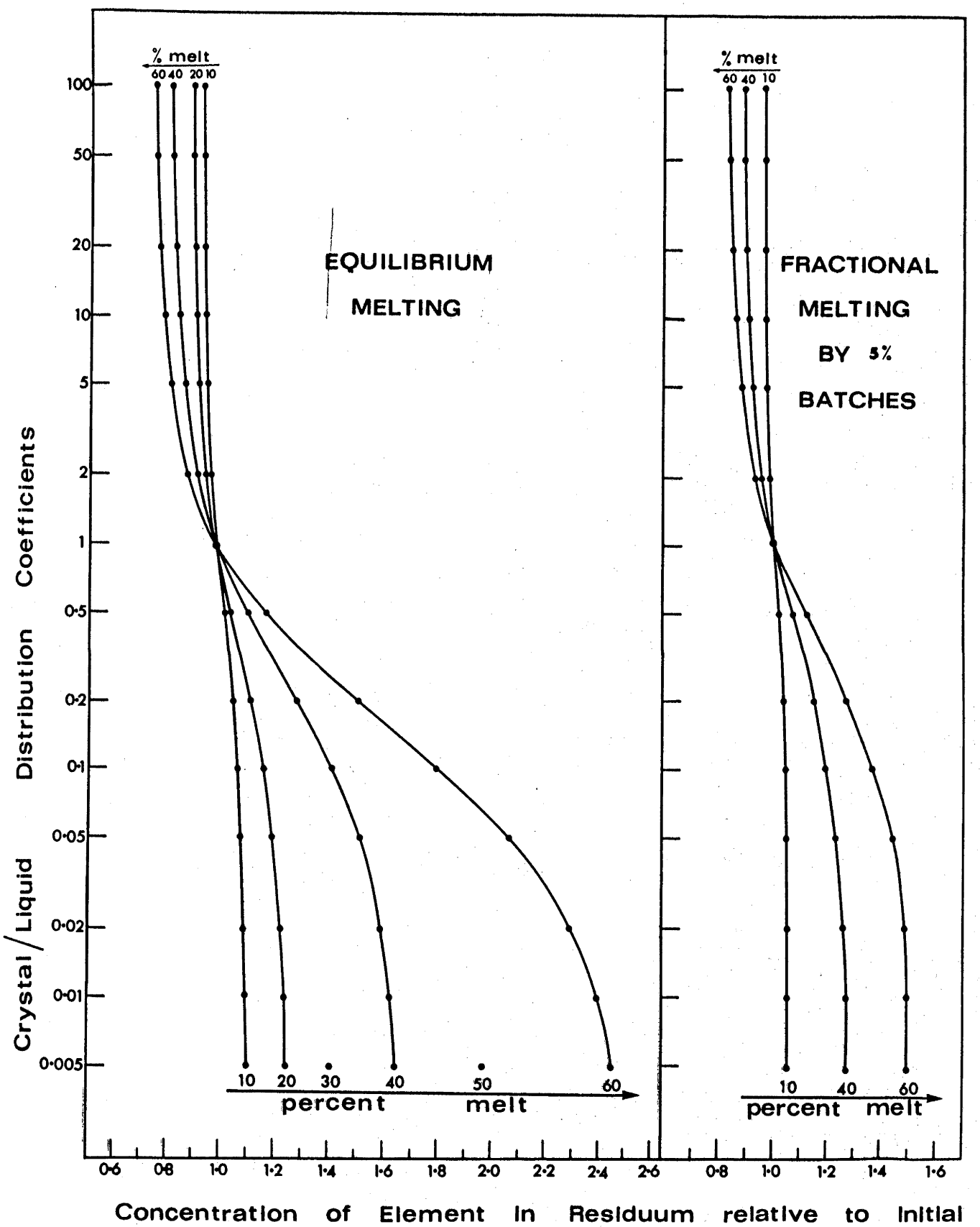

FIGURE 8.15 : EFFECT OF VARIATION OF LIQUID-CRYSTAL DISTRIBUTION COEFFICIENT OF A MAJOR PHASE ON THE CONCENTRATION OF AN ELEMENT IN THE RESIDUUM.

Modal melting was assumed for both equilibrium melting and fractional melting. The distribution coefficient varied was that of a major phase (33% initial abundance) which contributed to the melt. Distribution coefficients for all other phases were assumed to be unity.

with variation of K_D below unity. Increasing K_D from 1 to 100 results in minor decrease in the concentration of an element in residua. Decreasing K_D from 1 to 0.05 results in large increases in residuum concentration especially for equilibrium melting. However, further decrease of K_D (0.05-0.005) causes smaller increases in residuum concentration.

The range of K_D for plagioclase and K-feldspar is within the "insensitive" range (1-200) for Rb and REE other than Eu (table 8.7) and cannot significantly alter the fractionation effects predicted by the model. If the K_D of Eu for feldspars decreased significantly below 1, the size of predicted positive Eu anomalies would be increased. The K_D ranges of Sr for plagioclase and K-feldspar, and of Ba for plagioclase include values within the critically sensitive range (0.05-1). Variation of the K_D of Sr for feldspars will alter the degree of enrichment of Sr in computed fractionation and may cause depletion. Decreasing the K_D of Ba for plagioclase below unity will result in greater Ba enrichment and decrease the dependence of fractionation on melting mode and initial K-feldspar contents. Garnet is a major component in some gneisses but only one set of liquid/crystal distribution coefficients was available. The K_D values for Sm, Eu, Gd and Tb for the garnet are in the critically sensitive range and K_D decreases may cause significant increase in enrichment of these elements during computed fractionation. All other phases are present in considerably smaller proportions and the effects of K_D variation are minor.

Equilibrium partial melting is the main process active during anatexis, although fractional fusion makes a small contribution (8.2.3). The possible effects of minor fractional melting are shown in figure 8.15. For $K_D>1$ the effects of fractional and equilibrium fusion are very close, but for $K_D>1$ equilibrium melting results in greater enrichment of an element in residua. The possible contribution of fractional melting may result in slightly decreased residuum concentrations of elements with $K_D>1$.

8.4 CRUSTAL FRACTIONATION AT EYRE PENINSULA

Anatectic fractionation affects only low-melting acid to sub-acid gneisses in terrains containing acid to basic rocks. The temperatures generated during metamorphism at Eyre Peninsula were sufficient to cause anatexis of the acid gneisses. The basic rocks are refractory and were affected only by dehydration fractionation.

8.4.1 Dehydration Fractionation

Basic pyroxene granulites have been most affected by dehydration fractionation, and are depleted in K, Rb, Ba and Sr relative to the other basic rocks in which hornblende remained stable. The higher average K/Rb of the pyroxene granulites may be partly due to the dependence of K/Rb on %K. The rehydrated basic rocks are enriched in K, Rb and Ba and have lower K/Rb than the other two groups. The effects of rehydration or "retrogression" are the reverse of dehydration fractionation (progressive metamorphism), and are more enhanced (table 8.9).

8.4.2 Anatectic Fractionation

Meaningful estimates of bulk crustal fractionation must be based on reasonably accurate determination of the contribution of individual samples to the composition of the whole terrain. Averages of suites of samples selected at random may result in misleading average compositions of metamorphic terrains. The metamorphic terrain at southern Eyre Peninsula is composed dominantly of acid to sub-acid gneisses with minor contribution from basic gneiss inclusions. The average composition of the terrain is approximately that of the average acid to sub-acid gneiss. Two such averages based on samples collected at random (table 8.10) are markedly different. The average of samples collected for this thesis is "depleted" in K, Rb, Pb, Th and U and has a higher K/Rb than that of Lambert (1967). On the basis of the latter sampling, Lambert & Heier (1968) concluded that minor crustal fractionation had occurred in the "low pressure granulite" Eyre Peninsula terrain. This

TABLE 8.9

EYRE PENINSULA BASIC ROCKS

	Average Basic Pyroxene Granulite		Average Basic Rock with K<1.5% (excluding Pyroxene Granulites)		Average Retrogressed Basic Rock with K>1.5%	
	Average	S.D.	Average	S.D.	Average	S.D.
$\%K_2O$	0.26	0.11	0.79	0.31	2.77	0.76
Rb	5.0	3.4	23	16	133	88
Ba	60	37	134	80	550	219
Sr	78	31	128	40	122	46
K/Rb	514	218	415	335	212	82

S.D. is standard deviation

TABLE 8.10

COMPARISON OF TWO EYRE PENINSULA

ACID AND SUB-ACID GNEISS AVERAGES

	Lambert (1967) (10 samples)	This Thesis (18 samples)
K_2O	4.1	3.5
Rb	167	98
Ba	730	780
Sr	148	174
Pb	33	22
Th	30	13
U	2.2	1.5
Zr	184	298
K/Rb	272	395

(All gneisses have $SiO_2 > 65\%$)

thesis, however, indicates metamorphism in the medium pressure granulite field (Green & Ringwood, 1967a), and demonstrates that many of the gneisses are considerably more fractionated than shown by previous studies. The restricted number of samples collected, coupled with the absence of estimated contributions of individual samples to the whole terrain, make conclusive proof of bulk crustal fractionation impossible. However, fractionation of individual samples can be demonstrated.

The Eyre Peninsula gneisses plot within the low pressure granulite K/Rb field (figure 8.16) with the exception of three gneisses (69-994, 69-948 and 69-1367) which plot between the low and high pressure granulite limits. Some K/Rb ratios above the low pressure granulite limits are expected, due to fractionation under conditions transitional to low and high pressure granulite metamorphism.

Anatexis has extensively affected acid gneisses at Eyre Peninsula. Unfoliated coarse feldspar pegmatites and granitic pegmatites are abundant. In consequence, the acid gneisses must be modified by anatectic fractionation. However, the low water-contents of the metamorphic rocks restrict the volume of anatectic melt which can form, and limits the amount of major element modification. Hence, the major element compositions may be used to place constraints on parent trace element geochemistry, and fractionation can be suggested in many cases. The nature of trace element fractionation is also indicated by the composition of pegmatites.

8.4.3 The Composition of Pegmatites

The elements depleted in residuum gneisses are enriched in the anatectic pegmatitic melts removed. Pegmatite feldspars (table 8.11) are enriched in K, Rb, Ba, Pb and Sr. The feldspars have moderately low K/Rb ratios. The one analysed pegmatite (table 8.11) is enriched in K, Rb, Li, Th, U, Pb, light REE, mildly enriched in Ba and Cs, and has a low K/Rb. Two pegmatite selvedges are also included in table 8.11. The first (69-1361) is moderately enriched in

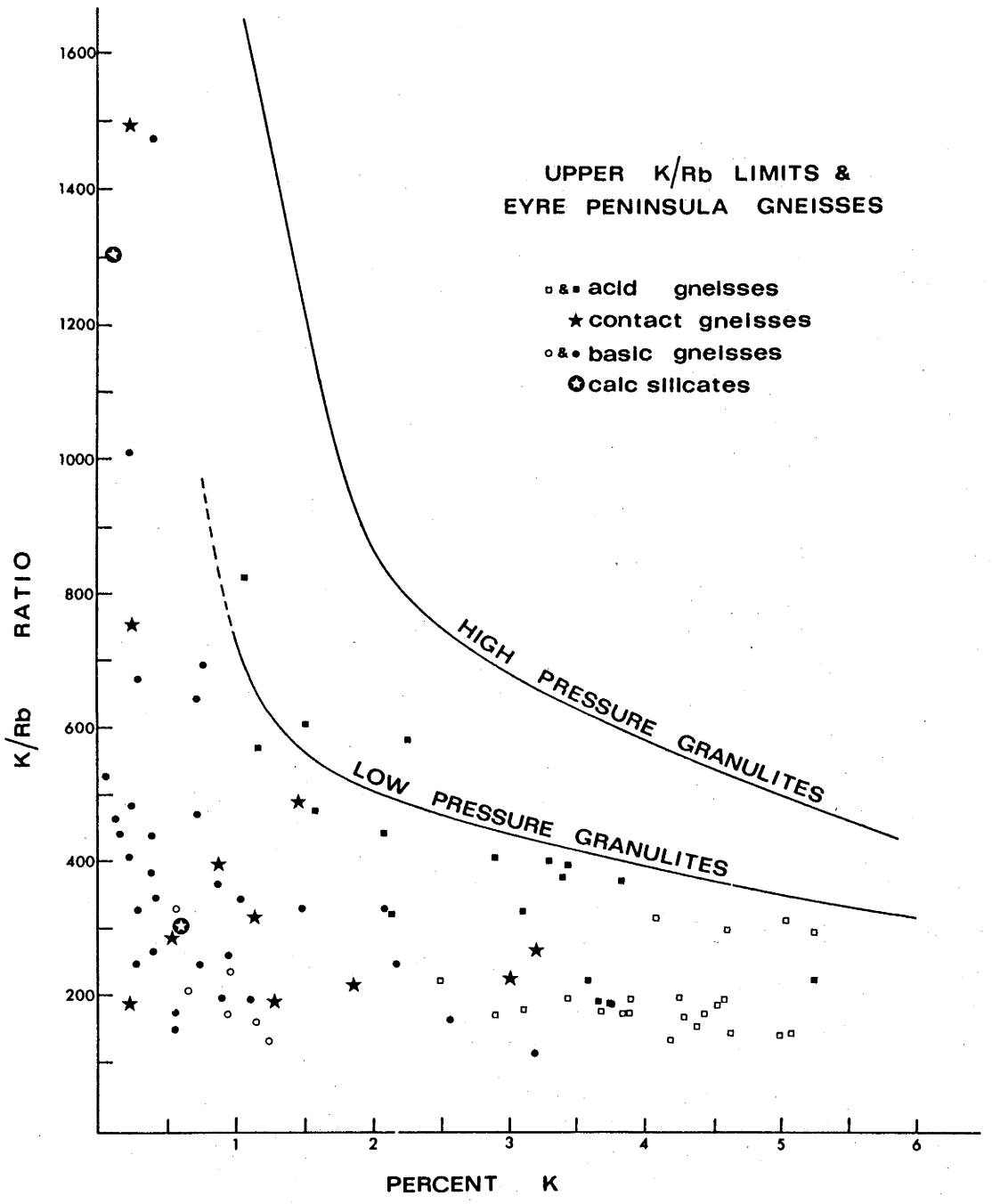

FIGURE 8.16 : COMPARISON OF EYRE PENINSULA GNEISSES WITH UPPER K/Rb LIMITS FOR HIGH PRESSURE AND LOW PRESSURE GRANULITES.

(Open symbols are from Lambert, 1967, and solid symbols are from this thesis).

TABLE 8.11

PEGMATITES AND PEGMATITE SELVEDGES

	Pegmatite K-Feldspars		Pegmatite	Pegmatite Selvedges	
	70-1212	70-1213	69-942	69-1361	69-1377
$\%K_2O$	12.14	12.91	6.33	1.52	1.05
Rb	502	328	234	65	24
Ba	1464	3740	873	446	76
Sr	412	601	191	193	172
Th	~0	~ 0	38	7	41
U	~0	~ 0	10	<2	3.4
Pb	160	74	47	37	28
Zr	--	--	219	204	1015
Nb	--	--	23	7.4	27
La	22	13	59	56	121
Ce	23	17	116	93	264
Y	1	2	35	34	146
Li	--	--	40	--	--
Cs	--	--	1.6	--	--
K/Rb	201	327	225	194	363

La, Ce and Pb, and has a low K/Rb. The second selvedge (69-1377) is strongly enriched in Th, U, Pb, Zr, Nb, light REE and Y. Neither pegmatite selvedge is strongly enriched in K, Rb, Ba or Sr. Basic rocks adjacent to pegmatites are commonly enriched K, Rb, Ba and Sr and K/Rb ratios decreased (chapter 7). Available geochemical data indicate that the Eyre Peninsula anatectic pegmatites are always enriched in K, Rb and Ba and commonly enriched in Th, U, Pb, Cs, Li, light REE and Sr. Some pegmatites are enriched in Zr, Nb and Y. The pegmatites have moderately low K/Rb ratios (200-300). Removal of pegmatitic melts depletes residuum gneisses in K, Li, Rb, Cs, Ba, Pb, Sr, light REE, Th and U, and in some cases Zr, Nb and Y. The residuum K/Rb ratios increase. Depletion of Sr in residua is inconsistent with the proposed fractionation model.

8.4.4 The Compositions of Residuum Gneisses

The residuum gneisses include all the acid gneisses (chapter 3) excluding the high-K intrusive charnockites and the pegmatite (69-942). The compositions of the residuum gneisses represent parent rock compositions modified to varying extents by removal of granitic to "pegmatitic" anatectic melts. The volume of anatectic melts removed is restricted by the limited water present in the parent metamorphic rocks. (An initial water-content of ∿2% allows generation of ∿15% of water-saturated melt, or ∿30% of melt assuming 50% water-undersaturation. In most cases about 30% melt or less would be removed.) Removal of potassium-rich pegmatitic-granitic melt would deplete most residual gneisses in K and enrich them in Ca. The melts are also rich in Si, Al and Na, but the residual gneisses may be either enriched or depleted in these elements, depending on their initial compositions. The major element composition of most of the gneisses is probably reasonably close to the parent rock compositions except that K may be depleted and Ca enriched. Three of the gneisses are close to adamellite-granodiorite composition, and the others are granitic to granodioritic arkose/greywacke compositions.

8.4.4.1 The Garnet-Symplectite Charnockites

The major element compositions of the garnet-symplectite charnockites correspond closely to an adamellitic arkose (chapter 3). However, Rb, Sr, Li and U in the charnockites are lower and Ba higher than the adamellitic arkose. A granitic arkose-greywacke composition has Rb and Sr closer to the charnockites, but Rb, Sr and Li in the charnockites are lower, and K and Ba are higher. The high Ba in the charnockites is explicable by a granodioritic parent composition, but Ca and Sr in the charnockites are too low and K too high. The low Li and U in the garnet-symplectite charnockites cannot be explained by a granitic, adamellitic or granodioritic arkose-greywacke parent composition, and is probably due to metamorphic fractionation. REE plots for the garnet-symplectite charnockites are subparallel to the sedimentary patterns (figure 3.12), although very slightly enriched in heavy REE relative to the light REE (shale-normalised Yb/La ∿1.3). A similar heavy REE enrichment was produced in the computed fractionation model by about 10% melting of the A5 composition which is modelled on the garnet-symplectite charnockites (figure 8.13). The 10% melting also depleted Rb (by ∿30%), and enriched Ba (<1%) and Sr (∿2%). Retention of Sr in residuum plagioclase and K-feldspar suggests that the low Sr in the charnockites is a primary feature. (Sr can be depleted in the model only by extreme degrees of anatexis.) Granitic rocks low in Sr tend to have low Ba. Hence the low Sr + high Ba in the charnockites may reflect the composition of the parent rocks. Restriction of melting in the garnet-symplectite charnockites to ∿10% is consistent with a relatively low initial water content of ∿1%. The composition of the garnet-symplectite charnockites is best explained by a granitic to adamellitic arkose/greywacke parent mildly depleted by anatectic fractionation in K, Rb and light REE, strongly depleted in Li and U, and mildly enriched in Ca and heavy REE. The relatively high average K/Rb (383) is probably due to the anatectic fractionation. The relatively low average Th (10 ppm) may be due to anatectic depletion.

8.4.4.2 The Compositionally Banded Charnockites

The compositionally banded charnockites are similar to the average greywacke (table 3.6). The charnockites have slightly lower K, lower Rb, Li and Zr and higher Ba and K/Rb than the greywacke. If a greywacke parent composition is assumed these differences must be explained. (Some features of the banded charnockites are shown in table 8.12.) The very low Li, Cs and U cannot be explained by arkosic or greywacke compositions and must be due to metamorphic fractionation. The low Th in two samples (69-787 and 69-1367) must be similarly explained. The undisturbed compositional banding and sedimentary REE pattern (figure 3.12) of one of the charnockites (69-787) suggest that the rock was not significantly melted during the metamorphism, since anatectic fractionation of quartzo-feldspathic rocks fractionates REE and generates positive Eu anomalies. The low K, Rb, Pb and Th, and high K/Rb of the charnockite are probably original geochemical features. The REE of another charnockite (69-1367) are depleted relative to sediments and have a pronounced positive Eu anomaly (figure 3.13). Similar REE patterns and comparable Eu anomalies (shale-normalised $Eu/Eu^* \sim 1.9$) were produced by ~5% melting in computed fractionation of apatite-free and zircon-free quartzo-feldspathic gneisses (figure 8.17). (69-1367 has a low P_2O_5 of 0.05% and a low Zr of 100 ppm, and the effects of apatite and zircon should be negligible). If an initial shale abundance of unity is assumed, 15-20% melting is required to deplete the residuum to the abundances (0.2 to 0.4 times shale) observed in the charnockite. However, 15-20% melting generates much larger Eu anomalies than observed, and the parent REE abundance would have to be lower or the estimated Eu distribution coefficients larger. The charnockite is poor in K-feldspar, and anatectic fractionation results in Ba depletion. Anatectic fractionation can also explain the low K, Rb, Cs, Th, U and Li, and high Sr and K/Rb in the charnockite (table 8.12). The fractionation of the REE patterns of the other two charnockites (69-951 and 69-1363) relative to the sedimentary field (figure 3.13) is explicable by anatectic fractionation similar to that discussed for the previous

TABLE 8.12

COMPARISON OF COMPOSITIONALLY BANDED CHARNOCKITES AND AVERAGE GREYWACKE

	69-787	69-951	69-1363	69-1367	Average Greywacke
$\%K_2O$	1.3	1.9	2.5	1.4	2.0
Rb	13	33	47	20	51
Ba	603	663	692	420	356
Sr	286	186	173	339	204
Zr	188	155	199	100	291
Pb	10	11	17	17	--
Th	0.6	--	11	0.2	--
U	0.3	--	0.3	0.2	--
Cs	0.1	--	--	0.2	--
Li	5	5	15	16	40
K/Rb	824	473	442	569	326

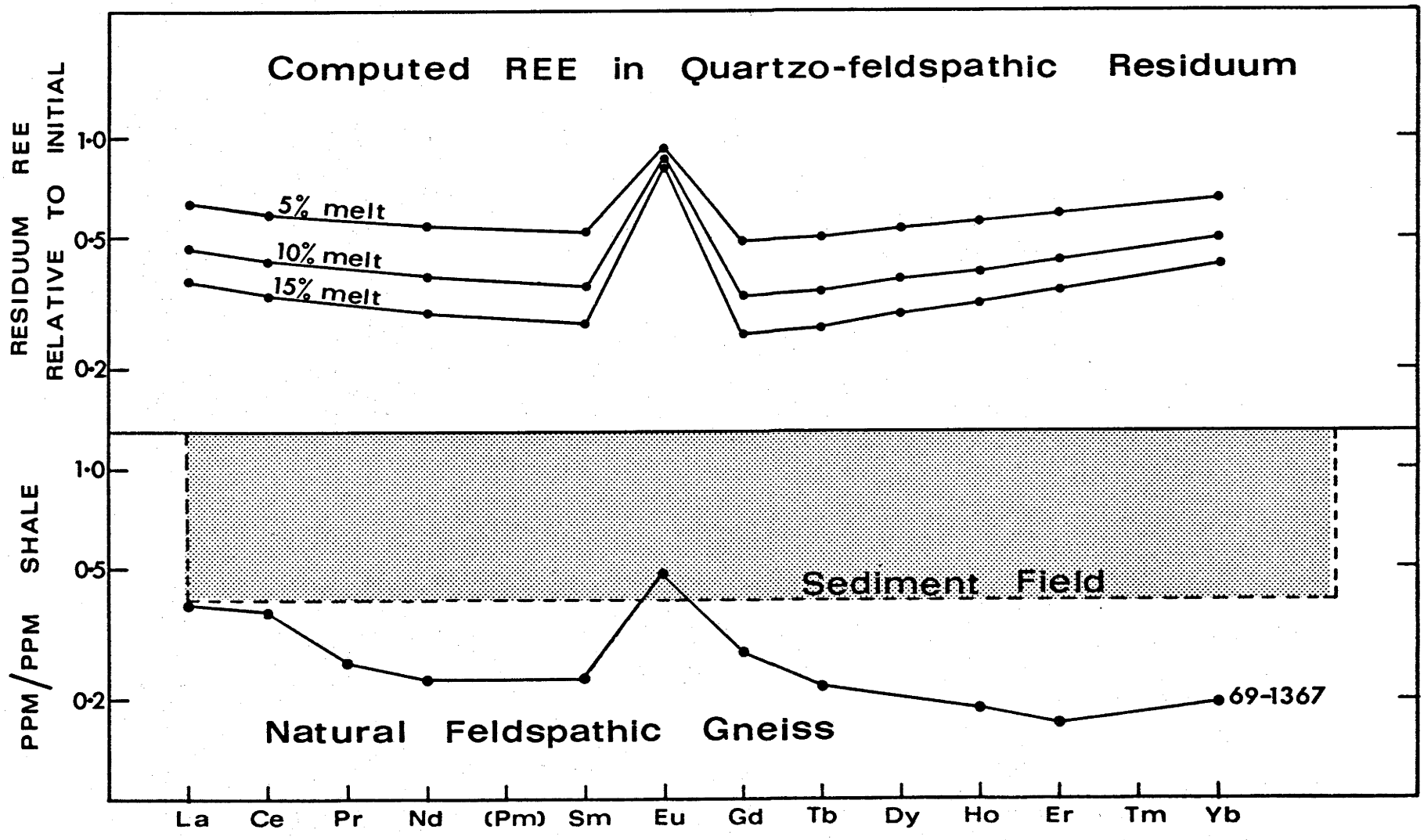

FIGURE 8.17 : COMPARISON OF COMPUTED RARE EARTH PATTERNS WITH THE PATTERN OF ONE ACID GNEISS.

The computed patterns are from figure 8.14.

charnockite (69-1367). The low K, Rb, Ba, Li and U, and high K/Rb may also be partly due to anatectic fractionation.

8.4.4.3 The Garnet-Gneisses

The massive garnet-gneiss (69-1375) has a strongly fractionated igneous REE pattern with a pronounced negative Eu anomaly (figure 3.11). The major element composition of the gneiss is very close to the average granodiorite and adamellite (table 3.10). Li and U are considerably lower than the granodiorite range and must have been depleted by metamorphic fractionation. Rb and Pb are both low in the granodiorite range and may have been depleted also. Sr is very low for a granodiorite. The low Sr may also be due to metamorphic fractionation, but cannot be explained by the fractionation model. The high Th cannot be explained by metamorphic fractionation and may be inherited from the parent granodiorite.

The major element composition of the migmatite (69-1355) is similar to the average adamellite and granodiorite (table 3.10). The REE pattern of the migmatite is sub-parallel to the sedimentary patterns, although slightly enriched in light REE (figure 3.12). Although the rock is migmatitic, no obvious enrichment in pegmatitic elements has occurred, and Rb, Th, U (Pb and Zr) are not enriched. If a granodioritic or adamellitic parent is assumed the very low U and Li must be explained by metamorphic depletion. Low Rb and Th, and high K/Rb (407) may also be explained by metamorphic depletion. Low Sr may be due to metamorphic fractionation.

The major element composition of the banded garnet-gneiss is similar to the average adamellite except for lower K in the gneiss (table 3.10). The gneiss has a sedimentary REE pattern with minor heavy REE enrichment (figure 3.12). The very low Th and U must be explained by metamorphic fractionation. Low K, Rb, Sr, Pb, Cs (0.6 ppm) and Zr may also be explicable by metamorphic fractionation. If an arkosic sedimentary parent is assumed, explanation of the low Zr is difficult other than by dissolution of zircon in

melt. However, the absence of significant garnet-controlled REE fractionation limits melting to ∿5%.

The garnet-rich garnet-gneisses (69-948 and 69-944) both contain quartz in excess of low melting compositions (3.4.3.1). The excess quartz is considered due to anatectic depletion of low melting components leaving residua enriched in quartz and garnet. The considerable enrichment of Fe, Mg, Mn, Sc, V, Cr, Co, Ni and heavy REE in both gneisses is the result of strong partitioning of these elements into residual ferromagnesian phases during anatectic fractionation (table 8.13). Heavy REE enrichment in one of the garnet-gneisses (69-948) is almost identical to that postulated by the fractionation model (figure 8.18). About 50% anatexis of a gneiss initially containing ∿12% garnet results in nearly identical REE patterns to the garnet-gneiss and very similar heavy REE enrichment (shale-normalised Yb/La ∿ 4). The resulting residuum of ∿24% garnet is also very similar to the garnet-gneiss. If the REE fractionation model is directly applicable, the assumed parent sedimentary REE pattern of the garnet-gneiss is required to be about 1½ times shale abundance. Y in the other garnet-gneiss (69-944) is enriched relative to Pr and Nd, but La and Ce are of comparable abundance to Y (figure 3.13). The enrichment of Y is probably due to metamorphic fractionation similar to that for the first garnet-gneiss and enrichment of La and Ce relative to Pr and Nd possibly due to parent REE pattern fractionated relative to sedimentary abundance. Anatectic fractionation of the first garnet-gneiss (69-948) depleted K, Na, Rb, Ba, Th, U, Li and Cs, and increased the K/Rb. The low P and Sr, and high Zr may also be due to metamorphic fractionation. The very low Zr/Hf ratio (24) may be the result of extended anatectic fractionation under conditions of low f_{O_2} (cf. Taylor, 1972, and Taylor et al., 1972). Anatectic fractionation depleted Rb, Pb, Th, U and Li in the second garnet-gneiss (69-944), and increased the K/Rb.

Anatexis and reaction are common at the contacts of basic inclusions with host acid gneiss (chapter 5). Garnet rich "reaction zone knots" are formed when the original basic inclusions are almost entirely "digested" by this

TABLE 8.13

COMPOSITIONS OF GARNET GNEISSES

	Garnet-rich Residua		Garnet-rich "Reaction" Residua	
	69-944	69-948	69-741	69-950
FeO*	6.0	8.1	11.1	20.1
MnO	0.1	0.2	0.2	0.3
MgO	2.9	3.2	5.0	8.1
K_2O	2.7	1.8	0.6	0.3
Rb	39	25	18	11
Ba	912	464	201	42
Sr	208	115	94	44
Pb	13	15	9	7
Th	5	3	< 2	< 2
U	< 2	0.5	< 2	< 2
Zr	223	436	113	117
La	41	34	14	12
Ce	75	66	28	22
Pr	6	6	3	3
Nd	24	16	17	8
Y	36	65	25	65
Sc	22	27	26	45
V	96	105	210	360
Cr	153	168	148	6
Co	27	23	--	47
Ni	70	115	72	47
Li	6	5	--	--
Cs	--	0.2	--	--
K/Rb	583	604	286	189

*Total Fe as FeO

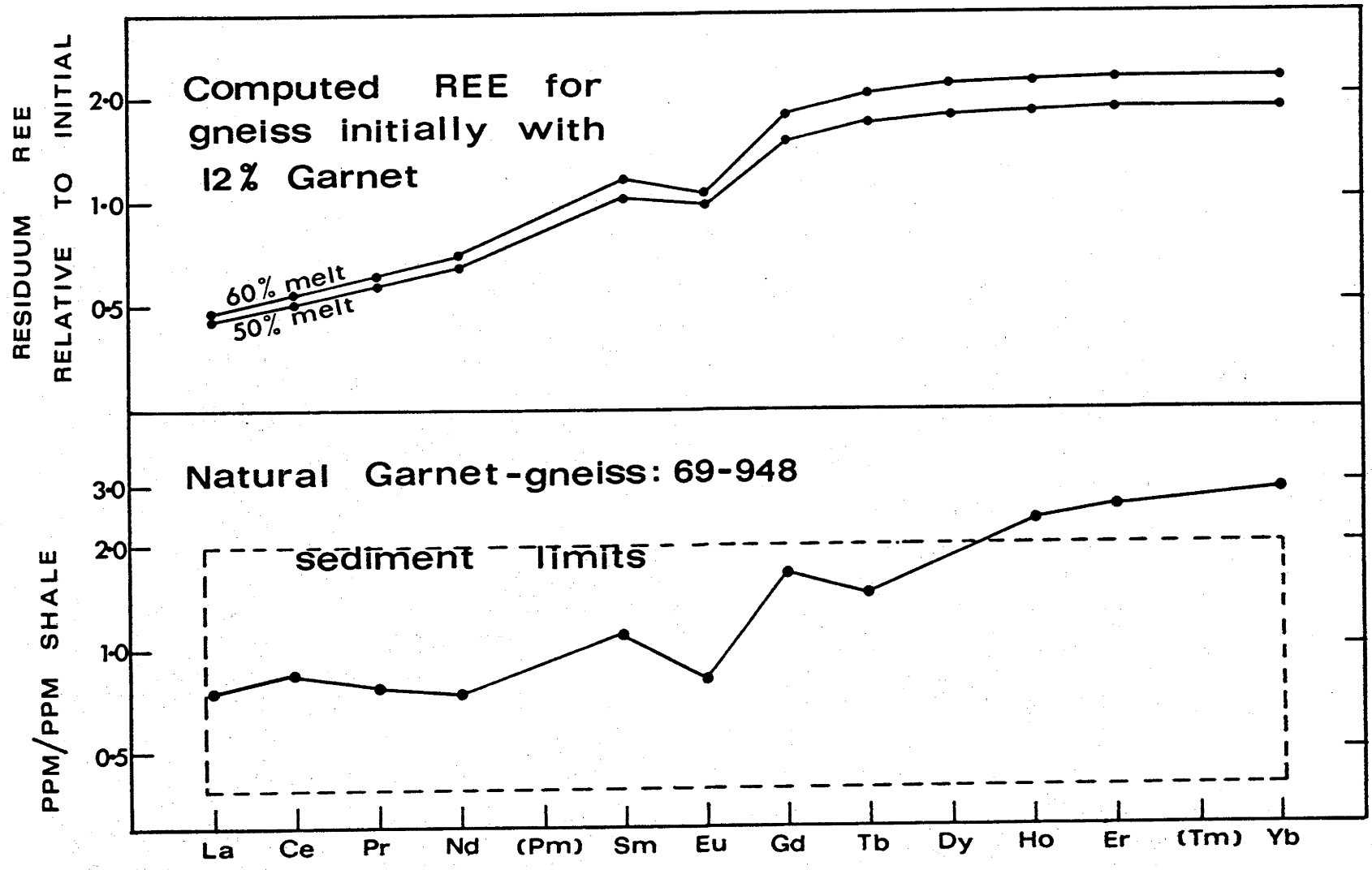

FIGURE 8.18 : COMPARISON OF COMPUTED RARE EARTH PATTERNS WITH THE PATTERN OF ONE GARNET-GNEISS.

The computed patterns are from figure 8.13.

reaction. Two such garnet-rich "reaction zone knots" (69-741 and 69-950: table 8.13) are enriched in Fe, Mg, Mn, Sc, V, Co, Ni, Cu and Y, and one (69-741) is enriched in Cr as well. Both gneisses are depleted in K, Rb, Ba, Sr, Th, U, Pb and Zr. The fractionation is the result of partitioning of elements between melt and residuum during reaction between acid melt and basic inclusion.

8.4.5 REE Fractionation during Decarbonation of Calc-Silicate Gneisses

One calc-silicate gneiss (69-777) has the most fractionated REE pattern of all Eyre Peninsula gneisses analysed (figure 4.1). The other calc-silicate rock (69-939) is mildly fractionated, and depleted relative to the sedimentary field (figure 4.1). The gneisses are considered to be metamorphosed dolomitic sediments, presumably with parent sedimentary REE patterns. Subsequent metamorphism caused decarbonation and formation of hornblende-clinopyroxene (69-777) and clinopyroxene-quartz (69-939) assemblages. REE including heavy REE are soluble in CO_2-rich and F-rich fluids (Haskin et al., 1966). It is postulated that REE were leached by CO_2-rich fluids during decarbonation of the gneisses. (The hornblende in one of the gneisses contains 0.6% F indicating that some F was also present in the metamorphic fluid.) Light REE were preferentially retained in hornblende (figure 4.1) in the first gneiss (69-777) and resulted in a REE pattern highly enriched in light and depleted in heavy REE. Clinopyroxene in the second gneiss (69-939) did not selectively retain either heavy or light REE, and all REE were depleted relative to sediments without marked fractionation.

8.4.6 Discussion

Li, Cs and U are depleted in most of the residuum acid gneisses and K, Rb, Ba, Pb and Th are depleted in many. The relatively high K/Rb ratios of many of the gneisses suggest depletion of Rb relative to K. REE in several quartzo-feldspathic metasediments are fractionated relative to sedimentary abundances. Fe, Mg, Mn, Sc, V, Cr, Co, Ni,

heavy REE and Y are enriched and REE patterns fractionated relative to sedimentary abundances in several garnet-gneisses. The depletion of K, Rb, Ba, Cs and the fractionation of REE (and Y) are explained by the proposed fractionation model. Enrichment of Fe, Mg, Mn, Sc, V, Cr, Co and Ni are also explained by the strong partitioning of these elements into residual ferromagnesian phases during anatexis. The depletion of K, Th and U in many of the gneisses is consistent with lower crustal abundances predicted by heat-flow data. Depletion of residua in Sr is suggested by the low Sr in most gneisses and the moderate Sr in the pegmatites. The fractionation model predicts that Sr is usually enriched in residua, and is depleted only in extensively melted K-feldspar-poor gneisses. Liquid/crystal distribution coefficients for Sr larger than those used in the fractionation model may cause depletion of Sr in residuum gneisses during anatexis, and explain the low Sr observed.

CHAPTER 9

CONCLUSIONS

The Eyre Peninsula metamorphic terrain is composed dominantly of metasediments intruded by at least one granodiorite batholith prior to, or early in, the granulite facies metamorphism, and intruded by charnockite batholiths during the metamorphism. The presence of the metamorphosed granodiorite suggests that the terrain may have been metamorphosed prior to the granulite metamorphism. One of the charnockite batholiths contains several fractionated components. The metasediments are comprised of a varied banded sequence of arkosic to greywacke compositions, with minor amounts of limestones, dolomites and impure sandy to clayey dolomites. Continental tholeiite dykes were intruded prior to, during and late in the granulite facies metamorphism. The dykes are dominantly composed of "normal" tholeiitic basalts with smaller amounts of "pyroxenites" or picritic basalts. The latter can be explained as crystal-enriched accumulates containing orthopyroxene ± clinopyroxene (formed by fractionation of olivine tholeiite at ~13.5 kb) or olivine+orthopyroxene (formed by fractionation of olivine tholeiite at 9-12 kb).

The metamorphism resulted in formation of amphibolite and granulite facies mineral assemblages, including pyroxene granulites, hornblende granulites, retrogressed granulites and amphibolites. Mineralogical P_{total}-T constraints (obtained from the stability of hornblende in the absence of quartz, the stability of orthopyroxene in the presence of plagioclase, and the stability of pyrope-almandine garnet but absence of cordierite and sapphirine) limit the field of metamorphism to 800°-950°C at 7-9 kb. These P-T conditions are consistent with the stability of sillimanite rather than kyanite, the instability of muscovite, and the instability of olivine in the presence of plagioclase. The temperatures are adequate to cause moderate degrees of anatexis in the water-deficient acid gneisses.

Anatectic fractionation of the acid gneisses is suggested by the abundant evidence of pegmatites and migmatites. Experimental data predict that granitic to "pegmatitic" (quartz-K-feldspar-rich) melts would be formed in early stages of anatexis of the acid gneisses. This is consistent with the abundance of quartz-K-feldspar pegmatites. Removal of granitic to pegmatitic melts would result in depletion of K in most of the residuum gneisses. Many of the acid gneisses are depleted in K, Rb, Cs, Sr, Th, U and Li, and have high K/Rb ratios. Several gneisses are depleted in Ba and Pb, and some garnet-gneisses are enriched in Fe, Mg, Mn, Sc, V, Cr, Co, Ni, heavy REE and Y. Many of the gneisses have REE patterns fractionated relative to sedimentary REE abundances. Most of these features can be explained by anatectic fractionation during high grade metamorphism.

A crustal fractionation model (involving removal of granitic and "pegmatitic" anatectic melts) predicts depletion of K, Rb and Cs, and enrichment of Sr in the residuum. Ba may be enriched or depleted, depending on the composition of anatectic melt removed and the mineralogy of the parent gneiss. The model also predicts fractionation of REE. Garnet-gneisses are enriched in heavy REE. Garnet-free quartzo-feldspathic gneisses are depleted in REE, but light REE and Eu are less depleted than heavy REE (and Y), resulting in fractionated patterns depleted relative to the sedimentary field and with pronounced positive Eu anomalies. The presence of zircon and/or apatite efficiently suppresses REE fractionation in quartzo-feldspathic gneisses. The fractionation model explains many of the geochemical features observed in the acid gneisses. Geochemical and field evidence strongly supports a sedimentary origin for many of the acid gneisses and the calc-silicate gneisses. This indicates that their REE patterns were initially those of sediments, and all the patterns fractionated relative to sedimentary abundances must be the result of anatectic REE fractionation. The fractionation of the REE patterns in the calc-silicate gneisses is attributed to leaching of REE by

CO_2-rich fluids produced during decarbonation of the original dolomitic sediments. The model is consistent with the observed depletion of K, Rb and Cs, and the fractionated REE patterns in many of the acid gneisses. The possible enrichment or depletion of Ba in some of the gneisses may also be explained by the model. The low Sr observed in the gneisses cannot be explained by the model, and may be a reflection of the initial geochemistry. The enrichment of K, Rb, Cs, Ba and light REE in anatectic pegmatites is also consistent with the model. The enrichment of some pegmatites and pegmatite selvedges in Li, Pb, Th and U is consistent with the depletion of these elements in many of the acid gneisses. Fe, Mg, Mn, Sc, V, Cr, Co and Ni were not included in the fractionation model. These elements are strongly partitioned into residual ferromagnesian phases during anatexis, resulting in their enrichment in gneisses initially containing appreciable mafic minerals.

Dehydration fractionation of the basic pyroxene granulites resulted in depletion of K, Rb and Ba, and higher K/Rb ratios than in the other basic rocks. Retrogression of several granulites (involving reaction with pegmatitic fluids) caused the reverse of the dehydration fractionation, and several intensely retrogressed samples are enriched in K, Rb and Ba relative to the other basic rocks excluding the pyroxene granulites. The average effect of the granulite/amphibolite facies metamorphism upon the compositions of the basic rocks included minor depletion of Si and Sr, limited redistribution of K, Rb, Ba, Li, Ca, Na and U, and no demonstrable effect on Ti, Al, Fe, Mn, Mg, P, Ga, Th, Pb, Zr, Nb, REE, Y, Sc, V, Co, Ni(?), Cr(?) and Zn(?). Cu was depleted and extensively redistributed.

The extent of reaction zones (at the contacts of acid and basic rocks) free of obvious melting suggests that diffusion during metamorphism in the absence of melt or fluid was restricted to less than about 10 cm. More extensive reaction (up to about 0.5 metres) was observed at migmatitic contacts, and very extensive reaction occurred at the

contacts of basic rocks and pegmatites. The evidence indicates that the range of diffusion during granulite metamorphism is negligible, except in the presence of anatectic melt.

Granulite facies, amphibolite facies and retrogressed granulite facies basic rocks with similar compositions are closely associated at Eyre Peninsula. The pyroxene granulites consistently contain quartz, the hornblende granulites are quartz-free, and the amphibolites and retrogressed granulites include both quartz-bearing and quartz-free rocks. (Apart from this, there is no consistent correlation between metamorphic facies and composition.) Pyroxene granulite and hornblende granulite subfacies commonly coexist in the one handspecimen due to localised differences in silica activity caused by quartz veining. The available mineralogical data suggest that many of the granulite facies, amphibolite facies and retrogressed granulite facies rocks crystallised at similar temperatures, but at different silica activities and/or different equilibrium water pressures. This is consistent with the common association of retrogressed granulites or amphibolites with pegmatites. Some evidence favours the crystallisation of some amphibolites and retrogressed granulites at temperatures lower than those for the primary granulites.

Application of the metamorphic facies concept in the descriptive mineralogical sense to granulite facies has no restricted P-T significance. Amphibolite and granulite facies mineralogies may coexist over a very wide P-T field, mainly due to differences in rock compositions and equilibrium water pressure. Retrogression of granulite facies to amphibolite facies may also occur within this P-T interval for the same reasons. (In this respect, granulite "facies" is very similar to eclogite "facies" in that the characteristic mineral assemblages may be formed within a very wide range of P-T conditions.) There can be no definite amphibolite/granulite facies boundary, even if this is defined in terms of a specific rock composition, because localised variations in equilibrium water pressure and oxygen

fugacity are still not predictable. The metamorphic facies concept can still be used in the descriptive mineralogical sense, but P-T significance must not be inferred directly from the mineralogy unless chemical composition and variables such as equilibrium water pressure, oxygen fugacity and silica activity are taken into account.

ACKNOWLEDGEMENTS

I am indebted to my supervisors, Dr S.R. Taylor and Prof. A.J.R. White, for their assistance with analytical techniques, mineral separation and sample preparation, and for many interesting and valuable discussions influencing this thesis. I would particularly like to thank Prof. A.J.R. White for suggesting the topic, and for his enthusiasm and continued interest in the project after leaving the A.N.U. to accept the Chair of Geology at La Trobe University, Melbourne. I would like to thank Dr S.R. Taylor for his sense of humour, which helped me to retain my sanity during the extremely difficult final stages of thesis writing.

I benefited from many useful discussions with Drs B.W. Chappell and D.H. Green. Dr B.W. Chappell also assisted considerably with X-ray fluorescence spectrography and by critically reading portions of the manuscript. My thesis has also benefited from discussions with Dick England (B.M.R.) and Drs B.J. Hensen, J.B. Gill, D.W. Haynes and S.E. Kesson (A.N.U.). Many of the ideas regarding the stability of hydrous minerals and anatexis evolved from discussion with Sue Kesson and Dr D.H. Green in the years following a lecture series on related topics given by Dr C.W. Burnham at the A.N.U.

I am especially grateful to Maureen Kaye and Jack Wasik for their patience and invaluable assistance with X-ray fluorescence spectrography, emission spectrography and chemical techniques. I would also like to thank Nick Ware for assistance with computing and the electron microprobe, Drs J.B. Gill and I. McDougall for help with the gamma-ray spectrometer, Jack Pennington for assistance with X-ray diffraction and preparation of samples for X-ray fluorescence spectrography, Elmer Kiss for helping with ferrous iron and fluorine determinations for minerals, and Richard Rudowski for assistance with mineral separation. Patricia Muir helped with mass spectrometer technique. Sno Pederson and Arthur Powell assisted by preparing thin-sections, and Morrie Cowan helped with rock crushing.

Finally, I would like to thank my wife, Joan, for her patience during the writing of this thesis, and for her invaluable assistance with the typing of the first draft and all of the painstaking text tables.

This project was completed during tenure of a Commonwealth Post-graduate Scholarship at the A.N.U., while on study leave from the N.S.W. Geological Survey.

REFERENCES

Adams, J.A.S. & Gasparini, P., 1970: Gamma-ray Spectrometry of Rocks. Elsevier.

Ahrens, L.H. & Taylor, S.R., 1961: Spectrochemical Analysis. Addison-Wesley.

Aoki, K., 1967: Petrography and petrochemistry of latest Pliocene olivine-tholeiites of Taos Area, northern New Mexico, U.S.A. Contr. Mineral. Petrol. 14, 190-203.

Atkins, F.B., 1969: Pyroxenes of the Bushveld Intrusion, South Africa. J. Petrology 10, 222-249.

Banno, S. & Chappell, B.W., 1969: X-ray fluorescent analysis of Rb, Sr, Y, Pb and Th in Japanese Palaeozoic slates. Geochem. J. 3, 127-134.

Bhattacharyya, C., 1970: Pyroxenes and biotites from charnockitic rocks. Mineral. Mag. 37, 682-692.

Binns, R.A., 1962: Metamorphic pyroxenes from the Broken Hill District, N.S.W. Mineral. Mag. 33, 320-338.

Binns, R.A., 1964: Zones of progressive regional metamorphism in The Willyama Complex, Broken Hill district, N.S.W. J. geol. Soc. Aust. 11, 283-330.

Binns, R.A., 1965: Mineralogy of basic metamorphic rocks from The Willyama Complex, Broken Hill, N.S.W. Part I : Hornblendes. Mineral. Mag. 35, 306-326.

Binns, R.A., 1969a: Ferromagnesian minerals in high-grade metamorphic rocks. Spec. Publs. geol. Soc. Aust. 2, 323-332.

Binns, R.A., 1969b: Hydrothermal investigations of the amphibolite-granulite facies boundary. Spec. Publs. geol. Soc. Aust. 2, 341-344.

Brown, G.C. & Fyfe, W.S., 1970: The production of granite melts during ultrametamorphism. Contr. Mineral. Petrol. 28, 310-318.

Brown, G.M., 1971: Granitic liquids : Their generation and intrusion. Geol. Mag. 108, 343-345.

Bryhni, I., Green, D.H., Heier, K.S. & Fyfe, W.S., 1970: On the occurrence of eclogite in Western Norway. Contr. Mineral. Petrol. 26, 12-19.

Buddington, A.F., 1963: Isograds and the role of water in metamorphic facies of orthogneiss in the Northwest Adirondacks Area, N.Y. Bull. geol. Soc. Amer. 74, 1155-1182.

Buddington, A.F. & Lindsley, D.H., 1964: Iron-titanium oxide minerals and synthetic equivalents. J. Petrology 5, 310-357.

Buma, G., Frey, F.A. & Wones, D.R., 1971: New England granites : trace element evidence regarding their origin and differentiation. Contr. Mineral. Petrol. 31, 300-320.

Burnham, C.W., 1967: Hydrothermal fluids at the magmatic stage. In Geochemistry of Hydrothermal Ore Deposits. (Ed., Barnes, H.L.) Holt, Rinehart & Winston.

Burnham, C.W., 1970: Unpublished thermodynamics lecture series. Geology Department, Australian National University.

Butler, J.R., Bowden, P. & Smith, A.Z., 1962: K/Rb ratios in the evolution of the Younger Granites of Northern Nigeria. Geochim. Cosmochim. Acta 26, 89-100.

Cann, J.R., 1970: Rb, Sr, Y, Zr and Nb in some ocean-floor basaltic rocks. Earth. Planet. Sci. Lett. 10, 7-11.

Chappell, B.W., 1971: Unpublished correction programme for X-ray fluorescence peak and background spectral interference. Geology Department, Australian National University.

Chappell, B.W., Compston, W., Arriens, P.A. & Vernon, M.J., 1969: Rb and Sr determinations by X-ray fluorescence spectrometry and isotope dilution below the part per million level. Geochim. Cosmochim. Acta. 33, 1002-1006.

Chappell, B.W. & White, A.J.R., 1970: Further data on an "eclogite" from the Sittampundi Complex, India. Mineral. Mag. 37, 555-560.

Chesworth, W., 1967. The Biotite-Cordierite-Almandine subfacies of the Hornblende-Granulite Facies - a discussion. Canad. Miner. 9, 263-268.

Clark, D.B., 1970: Tertiary basalts of Baffin Bay : possible primary magma from the mantle. Contr. Mineral. Petrol. 25, 203-224.

Clark, S.P., Peterman, Z.E. & Heier, K.S., 1966: Abundances of uranium, thorium and potassium. In "Handbook of Physical Constants" (Ed., Clark, S.P.). Mem. geol. Surv. Am. 97, 521-541.

Collerson, K.D., Oliver, R.L. & Rutland, R.W.R., 1972: An example of structural and metamorphic relationships in The Musgrave Orogenic Belt, Central Australia. J. geol. Soc. Aust. 18, 379-393.

Compston, W. & Arriens, P.A., 1968: The Precambrian geochronology of Australia. Canad. J. Earth. Sci. 5, 561-583.

Compston, W., McDougall, I. & Heier, K.S., 1968: Geochemical comparison of the Mesozoic basaltic rocks of Antarctica, South Africa, South America and Tasmania. Geochim. Cosmochim. Acta. 32, 129-149.

Condie, K.C. & Lo, H.H., 1971: Trace element geochemistry of The Louis Lake Batholith of early Precambrian age, Wyoming. Geochim. Cosmochim. Acta. 35, 1099-1119.

Cox, K.G. & Hornung, A., 1966: The petrology of the Karroo Basalts of Basutoland. Am. Miner. 51, 1414-1432.

Cox, K.G., Macdonald, R. & Hornung, G., 1967: Geochemical and petrographic provinces in the Karroo Basalts of Southern Africa. Am. Miner. 52, 1451-1474.

Davidson, L.R., 1968: Fe^{2+}-Mg distribution in metamorphic pyroxenes. Contr. Mineral. Petrol. 19, 239-259.

Davidson, L.R., 1969: Fe^{2+}-Mg^{2+} distribution in coexisting metamorphic pyroxenes. Spec. Publs. geol. Soc. Aust. 2, 333-339.

de Albuquerque, C.A.R., 1971: Petrochemistry of granitic rocks from Northern Portugal. Bull. geol. Soc. Am. 82, 2783-2798.

Deer, W.A., Howie, R.A. & Zussman, J., 1966: In Introduction to Rock-Forming Minerals. Longmans Green & Co.

de Waard, D., 1965: A proposed subdivision of the granulite facies. Am. J. Sci. 263, 455-461.

de Waard, D., 1966: The biotite-cordierite-almandite subfacies of the hornblende-granulite facies. Canad. Miner. 8, 481-492.

de Waard, D., 1967: "The occurrence of garnet in the granulite facies terrain of The Adirondacks Highlands, and elsewhere, an amplification and reply". J. Petrology 8, 210-232.

Dietrich, R.V., 1969: Behaviour of Zirconium in certain artificial magmas under diverse P-T conditions. Lithos 1, 20-29.

Dudas, M.J., Schmitt, R.A. & Harward, M.E., 1971: Trace element partitioning between volcanic plagioclase and dacitic pyroclastic matrix. Earth. planet. Sci. Lett. 11, 440-446.

Engel, A.E.J. & Engel, C.G., 1962: Hornblendes formed during progressive metamorphism of amphibolites, Northwest Adirondacks, N.Y. Bull. geol. Soc. Aust. 73, 1499-1514.

Ernst, W.G., 1968: Amphiboles. Springer-Verlag.

Eskola, P., 1920/21: The mineral facies of rocks. Norsk. Geol. Tiddskr. 6, 143-194.

Eskola, P., 1939: In "Die Enstehung der Gesteine" (T.F.W. Barths, C.W. Correns & P. Eskola), 263-339. Springer-Verlag.

Essene, E.J., Hensen, B.J. & Green, D.H., 1970: Experimental study of amphibolite and ecologite stability. Phys. Earth. planet. Interiors 3, 378-384.

Eugster, H.P. & Wones, D.R., 1962. The stability relations of the ferruginous biotite, annite. J. Petrology 3, 81-125.

Fedoseev, A.D., Grigor 'eva, L.F., Chigareva, O.G. & Romanov, D.P., 1970: Synthetic fibrous fluor-amphiboles and their properties. Am. Miner. 55, 854-863.

Frey, F.A., Haskin, M.A., Poetz, J.A. & Haskin, L.A., 1968: Rare earth abundances in some basic rocks. J. geophys. Res. 73, 6085-6098.

Fyfe, W.S., 1970: Some thoughts on granitic magmas. In "Mechanism of Igneous Intrusion". (Ed. Newall, G. & Rast, N.). Gallery Press.

Fyfe, W.S. & Turner, F.J., 1966: Reappraisal of the Metamorphic Facies Concept. Contr. Mineral. Petrol. 12, 354-364.

Fyfe, W.S., Turner, F.J. & Verhoogen, J., 1958: Metamorphic reactions and metamorphic facies. Mem. geol. Soc. Am. 73.

Gill, J.B., 1970: Geochemistry of Viti Levu, Fiji, and its evolution as an island arc. Contr. Mineral. Petrol. 27, 179-203.

Gill, J.B., 1972: The geochemistry of Viti Levu, Fiji. Unpublished Ph.D. Thesis. Australian National University.

Glaessner, M.F. & Parkin, L.W., 1957. The geology of South Australia. IV. Eyre Peninsula. J. geol. Soc. Aust. 5, 61-70.

Glikson, A.R., 1971: Primitive Archaean element distribution patterns: chemical evidence and geotectonic significance. Earth. planet. Sci. Lett. 12, 309-320.

Gray, C.M., 1971: Strontium isotopic studies on granulites. Unpublished Ph.D. thesis. Australian National University.

Green, D.H., 1964: Petrogenesis of the high temperature peridotite intrusion of the Lizard area, Cornwall. J. Petrology. 5, 134-188.

Green, D.H., 1971: Compositions of basaltic magmas as indicators of conditions of origin: application to oceanic volcanism. Phil. Trans. Roy. Soc. Lond. A. 268, 707-725.

Green, D.H. & Lambert, I.B., 1965: Experimental crystallisation of anhydrous granite at high pressures and temperatures. J. geophys. Res. 70, 5259-5268.

Green, D.H. & Mysen, B.O., 1972: Genetic relationship between eclogite and hornblende + plagioclase pegmatite in Western Norway. Lithos 5, 147-161.

Green, D.H. & Ringwood, A.E., 1967a: An experimental investigation of the gabbro to eclogite transformation and its petrological applications. Geochim. Cosmochim. Acta 31, 767-833.

Green, D.H. & Ringwood, A.E., 1967b: The genesis of basalt magmas. Contr. Mineral. Petrol. 15, 103-190.

Green, T.H., 1970: High pressure experimental studies on the mineralogical constitution of the lower crust. Phys. Earth. planet. Interiors 3, 441-450.

Green, T.H., Brunfelt, A.O. & Heier, K.S., 1969: Rare earth element distribution in anorthosites and associated high grade metamorphic rocks, Lofoten-Vesteraalen, Norway. Earth. planet. Sci. Lett. 7, 93-98.

Green, T.H., Brunfelt, A.O. & Heier, K.S., 1972: Rare-earth element distribution and K/Rb ratios in granulites, mangerites and anorthosites, Lofoten-Vesteraalen, Norway. Geochim. Cosmochim. Acta. 36, 241-257.

Greenwood, H.J., 1961: The system $NaAlSi_2O_6$-H_2O-Argon: Total pressure and water pressure in metamorphism. J. geophys. Res. 66, 3923-3946.

Griffin, W.L. & Heier, K.S., 1969: Paragenesis of garnet in granulite facies rocks, Lofoten-Vesteraalen. Contr. Mineral. Petrol. 23, 89-116.

Griffin, W.L. & Murthy, V.R., 1969: Distribution of K, Rb, Sr and Ba in some minerals relevant to basalt genesis. Geochim. Cosmochim. Acta. 33, 1389-1414.

Harris, P.G., Kennedy, W.Q. & Scarfe, C.M., 1970: Volcanism versus plutonism: The effect of chemical composition. In "Mechanism of Igneous Intrusion". (Ed. Newall, G. & Rast, N.). Gallery Press.

Hart, S.R., 1969: K, Rb, Cs contents and K/Rb, K/Cs ratios of fresh and altered submarine basalts. Earth. planet. Sci. Lett. 6, 295-303.

Hart, S.R., Brooks, C., Krogh, T.E., Davis, G.L. & Nava, D., 1970: Ancient and modern volcanic rocks: a trace element model. Earth planet. Sci. Lett. 10, 17-28.

Hart, S.R. & Nalwalk, A.J., 1970: K, Rb, Cs & Sr relationships in submarine basalts from the Puerto Rico trench. Geochim. Cosmochim. Acta 34, 145-155.

Haskin, L.A., Frey, F.A., Schmitt, R.A. & Smith, R.H., 1966: Meteoric, solar and terrestrial rare earth distributions. In "Physics and Chemistry of the Earth". Vol. 7. (Ed. Ahrens, L.H., Press, F. & Runcorn, S.K.). Permagon Press.

Haskin, L.A., Haskin, M.A., Frey, F.A. & Wildeman, T.R., 1968: Relative and absolute rare earth abundances. In "Origin and Distribution of the Elements". (Ed. Ahrens, L.H.). Permagon Press.

Haynes, D.W., 1972: Geochemistry of altered basalts and associated copper deposits. Unpublished Ph.D. Thesis. Australian National University.

Heier, K.S., 1965: Radioactive elements in continental crust. Nature 208, 479-480.

Heier, K.S. & Adams, J.A.S., 1964: Geochemistry of the alkali metals. In "Physics and Chemistry of the Earth". Vol. 5. (Ed. Ahrens, L.H., Press, F. & Runcorn, S.K.). Permagon Press.

Heier, K.S. & Adams, J.A.S., 1965: Concentration of radioactive elements in deep crustal material. Geochim. Cosmochim. Acta 29, 53-61.

Heier, K.S. & Brunfelt, A.O., 1970: Concentration of Cs in high grade metamorphic rocks. Earth planet. Sci. Lett. 9, 416-20.

Heier, K.S. & Compston, W., 1969: Interpretation of Rb-Sr age patterns in high grade metamorphic rocks, North Norway. Norsk. Geol. Tidsskr 49, 257-283.

Heier, K.S., Compston, W. & McDougall, I., 1965: Th and U concentrations and the isotopic composition of strontium in the differentiated Tasmanian Dolerites. Geochim. Cosmochim. Acta 29, 643-659.

Heier, K.S. & Rogers, J.J.W., 1963: Radiometric determination of thorium, uranium and potassium in basalts in two magmatic differentiation series. Geochim. Cosmochim. Acta 27, 137-154.

Heier, K.S. & Thoresen, K., 1970: Geochemistry of high grade metamorphic rocks, Lofoten Vesteraalen, North Norway. Geochim. Cosmochim. Acta 35, 89-99.

Hensen, B.J., 1970: Experimental study of the stability of cordierite and garnet. Unpublished Ph.D. Thesis. Australian National University.

Hensen, B.J., 1971: Theoretical phase relations involving cordierite and garnet in the system MgO-FeO-Al_2O_3-SiO_2. Contr. Mineral. Petrol. 33, 191-214.

Hensen, B.J. & Green, D.H., 1968: Experimental data on the stability of garnet and cordierite in high grade metamorphic rocks. Spec. Publs. geol. Soc. Aust., 2, 345-347.

Hensen, B.J. & Green, D.H., 1970: Experimental data on coexisting cordierite and garnet under high grade metamorphic conditions. Phys. Earth planet. Interiors 3, 431-440.

Hensen, B.J. & Green, D.H., 1971. Experimental study of the stability of cordierite and garnet in pelitic compositions at high pressures and temperatures. Contr. Mineral. Petrol. 33, 309-333.

Hermann, A.G. & Wedepohl, K.H., 1970: Untersuchungen an spilitischen Gesteinen der variskischen Geosyncline in Nordwestdeutschland. Contr. Mineral. Petrol. 29, 255-274.

Higuchi, H. & Nagasawa, H., 1969: Partition of trace elements between rock-forming minerals and host volcanic rocks. Earth. planet. Sci. Lett. 7, 281-287.

Hill, R.E.T. & Boettcher, A.L., 1970: Water in the earth's mantle: melting curves of basalt-water and basalt-water-carbon dioxide. Science 167, 980-982.

Holdaway, M.J., 1971: Stability of andalusite and the aluminium silicate phase diagram. Am. J. Sci. 271, 97-131.

Holloway, J.R., 1972: The system pargasite-H_2O-CO_2: a model for the melting of a hydrous phase with mixed-volatile fluid. I. Experimental results to 8 kb. Submitted to Geochim. Cosmochim. Acta.

Holloway, J.R. & Burnham, C.W., 1972: Melting relationships of basalt with equilibrium water pressure less than total pressure. J. Petrology 13, 1-29.

Hubbard, N.J., 1969: A chemical comparison of ocean-ridge, Hawaiian tholeiitic and Hawaiian alkalic basalts. Earth planet. Sci. Lett. 5, 346-352.

Hyndman, R.D., Lambert, I.B., Heier, K.S., Jaeger, J.C. & Ringwood, A.E., 1968: Heat-flow and surface radioactivity measurements in the Precambrian shield of Western Australia. Phys. Earth. planet. Interiors 1, 129-135.

Irvine, T.N. & Baragar, W.R.A., 1971: A guide to the classification of common volcanic rocks. Canad. J. Earth. Sci. 8, 523-548.

Irving, A.J., 1971: Geochemistry and high pressure experimental studies of xenoliths, megacrysts and basalts from Southeastern Australia. Unpublished Ph.D. Thesis. Australian National University.

Jakeš, P., 1969: Retrogressive changes in granulite facies rocks - an example from the Bohemian massif. Spec. Publs. geol. Soc. Aust. 2, 367-374.

Jakeš, P. & Gill, J.B., 1970: Rare earth elements and the island arc tholeiite series. Earth. planet. Sci. Lett. 9, 17-28.

Jakeš, P. & White, A.J.R., 1970. K/Rb ratios of rocks from island arcs. Geochim. Cosmochim. Acta. 34, 849-856.

Jakeš, P. & White, A.J.R., 1971: The composition of island arcs and continental growth. Earth. planet. Sci.Lett. 12, 224-230.

James, R.S. & Hamilton, D.L., 1969: Phase relationships in the system $NaAlSi_3O_8$-$KAlSi_3O_8$-$CaAl_2Si_2O_8$-SiO_2 at 1 kilobar water pressure. Contr. Mineral. Petrol. 21, 111-141.

Johns, R.K., 1961: The geology and mineral resources of southern Eyre Peninsula. Bull. South. Aust. Geol. Surv. 37.

Klein, C., 1966: Mineralogy and petrology of the metamorphosed Wabush Iron Formation, SW Labrador. J. Petrology. 7, 246-305.

Kolbe, P. & Taylor, S.R., 1966a: Geochemical investigation of the granitic rocks of the Snowy Mountains area, N.S.W. J. geol. Soc. Aust. 13, 1-25.

Kolbe, P. & Taylor, S.R., 1966b: Major and trace element relationships in granodiorites and granites from Australia and South Africa. Contr. Mineral. Petrol. 12, 202-222.

Korringa, M.K. & Noble, D.C., 1971: Distribution of Sr and Ba between natural feldspar and igneous melt. Earth. planet. Sci. Lett. 11, 147-151.

Kretz, R., 1961: Some applications of thermodynamics to coexisting minerals of variable compositions. Examples: orthopyroxene-clinpyroxene and orthopyroxene-garnet. J. Geol. 69, 361-387.

Lambert, I.B., 1967: Investigations of high grade regional metamorphic and associated rocks. Unpublished Ph.D. Thesis. Australian National University.

Lambert, I.B.& Heier, K.S., 1967: The vertical distribution of thorium, uranium and potassium in the continental crust. Geochim. Cosmochim. Acta 31, 377-390.

Lambert, I.B. & Heier, K.S., 1968: Geochemical investigations of deep-seated rocks in the Australian shield. Lithos 1, 30-53.

Lambert, I.B. & Wyllie, P.J., 1970: Melting in the deep crust and upper mantle and the nature of the low velocity zone. Phys. Earth. planet. Interiors 3, 316-322.

Lambert, R. St. J., 1965: The metamorphic facies concept. Mineral. Mag. 34, 283-291.

Leelanandam, C., 1967: Chemical study of pyroxenes from charnockitic rocks of Kondapalli, India, with special emphasis on distribution of elements in coexisting pyroxenes. Mineral. Mag. 36, 153-179.

Lovering, J.F. & White, A.J.R., 1969: Granulitic and ecologitic inclusions from basic pipes at Delegate, Australia. Contr. Mineral. Petrol. 21, 9-52.

Lowder, G.G. & Carmichael, I.S.E., 1970: The volcanoes and caldera of Talasea, New Britain: Geology and Petrology. Bull. Geol. Soc. Am. 81, 17-38.

Luth, W.C., Jahns, R.H. & Tuttle, O.F., 1964: The granite system at pressures of 4 to 10 kb. J. geophys. Res. 69, 759-773.

McCall, G.J.H. & Leisham, J., 1971: Eugeosynclinal peridotites and the nature of serpentinisation. Spec. Publs. geol. Soc. Aust. 3, 281-299.

Macdonald, G.A. & Katsura, T., 1964: The chemical composition of Hawaiian lavas. J. Petrology 5, 82-133.

McIntire, W.L., 1963: Trace element partition coefficients - a review of theory and applications to geology. Geochim. Cosmochim. Acta. 27, 1209-1264.

Marshall, B., 1968: Zirconium behaviour during extreme metamorphism. Spec. Publs. geol. Soc. Aust. 2, 349-351.

Mason, B., 1966: Principles of Geochemistry. Third Edition. Wiley & Sons.

Matthews, D.H., 1971: Altered basalts from Swallow Bank, an abyssal hill in the N.E. Atlantic, and from a nearby seamount. Phil. Trans. Roy. Soc. Lond. A268, 551-572.

Miyashiro, A., 1964: Oxidation and reduction in the earth's crust, with special reference to the role of graphite. Geochim. Cosmochim. Acta. 28, 717-729.

Moorlock, B.S.P., Tarney, J., & Wright, A.E., 1971: K/Rb ratios of intrusive anorthosite veins from Angmassalik, East Greenland. Earth. plan. Sci. Lett. 14, 39-46.

Mueller, R.F., 1960: Compositional characteristics and equilibrium relationships in mineral assemblages of a metamorphic iron formation. Am. J. Sci. 258, 449-497.

Munoz, J.L. & Eugster, H.P., 1969: Experimental control of fluorine reactions in hydrothermal systems. Am. Miner. 54, 943-959.

Nagasawa, H., 1970: Rare earth concentrations in zircons and apatites, and their host dacites and granites. Earth. planet. Sci. Lett. 9, 359-364.

Nagasawa, H. & Schnetzler, C.C., 1971: Partitioning of rare earth alkali and alkaline earth elements between phenocrysts and acidic igneous magma. Geochim. Cosmochim. Acta. 35, 953-968.

Norrish, K. & Chappell, B.W., 1967. X-ray fluorescence spectrography. In "Physical Methods in Determinative Mineralogy." (Ed. Zussman, J.). Academic Press.

Norrish, K. & Hutton, J.T., 1969: An accurate X-ray spectrographic method for analysis of a wide range of geological samples. Geochim. Cosmochim. Acta 33, 431-453.

Oliver, R.L., 1969: Some observations on the distribution and nature of granulite facies terrains. Spec. Publs. geol. Soc. Aust. 2, 259-268.

Osawa, G. & Goles, G.G., 1970: Trace element abundances in the Colombia River Basalts. In "Proc. Second Columbia River Basalt Symp." (Ed., Gilmour, E.H.). Eastern Washington State College Press.

Pearce, J.A. & Cann, J.R., 1971: Ophiolite origin investigated by discriminant analysis using Ti, Zr and Y. Earth. planet. Sci. Lett. 12, 339-349.

Pettijohn, F.J., 1956: "Sedimentary Rocks". Second edition. Harper & Bros., N.Y.

Pettijohn, F.J., 1963: Chemical composition of Sandstones. Prof. Paper U.S. geol. Surv. 440-S.

Philpotts, J.A. & Schnetzler, C.C., 1969: Submarine basalts: some K, Rb, Sr, Ba, rare-earth, H_2O and CO_2 data bearing on their alteration, modification by plagioclase and possible source material. Earth. planet. Sci. Lett. 7, 293-299.

Philpotts, J.A. & Schnetzler, C.C., 1970: Phenocryst-matrix partition coefficients for K, Rb, Sr and Ba with applications to anorthosite and basalt genesis. Geochim. Cosmochim. Acta. 34, 307-322.

Poldervaart, A., 1955: Chemistry of the Earth's Crust. Spec. Pap. geol. Soc. Am. 62, 119-154.

Ragland, P.C., Brunfelt, A.O. & Weigand, P.W., 1970: Rare earth abundances in Mesozoic dolerite dykes from Eastern United States. In "Activation Analysis in Geochemistry and Cosmochemistry". Proc. Nato Adv. Study Inst. Norway, 1970.

Rankama, K., 1963: Progress in isotope geology, 217-221. Wiley & Sons.

Ray, S. & Sen, S.K., 1970: Partitioning of major exchangeable cations among orthopyroxene, calcic pyroxene and hornblende in basic granulites near Madras. Neues Jb. Miner. Abh. 114, 61-88.

Reynolds, R.C., Whitney, P.R. & Isachsen, Y.W., 1969: K/Rb ratios in anorthositic and associated charnockitic rocks of the Adirondacks and their petrogenetic implications. In "Origin of Anorthosites and related rocks. NYS Museum and Science Service Memoir 18.

Rivalenti, G. & Sighinolfi, G.P., 1969: Geochemical study of Greywackes. Contr. Mineral. Petrol. 23, 173-188.

Rivalenti, G. & Sighinolfi, G.P., 1970: Geochemical and differentiation phenomena in basic dykes of the Frederikshåb district, S.W. Greenland. Atti. Soc. Tosc. Sci. Nat. Mem. Serie A. 77, 358-380.

Rutherford, M.J., 1969: An experimental determination of iron biotite-alkali feldspar equilibria. J. Petrol. 10, 381-408.

Saxena, S.K., 1969a: Silicate solid-solutions and geothermometry: Distribution of Fe and Mg between coexisting garnet and biotite. Contr. Mineral. Petrol. 22, 259-267.

Saxena, S.K., 1969b: Silicate solid solutions and geothermometry: Statistical study of chemical data on garnets and clinopyroxenes. Contr. Mineral. Petrol. 23, 140-156.

Saxena, S.K., 1969c: Distribution of elements in coexisting minerals and the problem of chemical disequilibrium in metamorphosed basic rocks. Contr. Mineral. Petrol. 20, 177-197.

Saxena, S.K., 1969d: Analysis of equilibria involving garnet in rocks of granulite facies. Am. J. Sci. 267, 523-527.

Saxena, S.K. & Ghose, S., 1971. Mg^{2+}-Fe^{2+} order-disorder and the thermodynamics of orthopyroxene crystalline solution. Am. Miner 56, 532-559.

Schilling, J.G. & Winchester, J.W., 1969: Rare earth contribution to the origin of Hawaiian lavas. Contr. Mineral. Petrol. 23, 27-37.

Schnetzler, C.C. & Philpotts, J.A., 1970: Partition coefficients of rare earth elements between igneous matrix material and rock-forming mineral phenocrysts - II. Geochim. Cosmochim. Acta. 34, 331-340.

Schwarcz, H.P., 1969: Carbon: in K.H. Wedepohl ed. In "Handbook of Geochemistry" Vol. II - 2. 6-B-9 & 6-B-13. Springer-Verlag.

Segnit, R.E. & Kennedy, W.Q., 1961: Reactions and melting relations in the system muscovite-quartz at high pressures. Am. J. Sci. 259, 280-287.

Sen, S.K., 1970: Magnesium-iron compositional variance in hornblende and pyroxene granulites. Contr. Mineral. Petrol. 29, 76-88.

Shaw, D.M., 1970: Trace element fractionation during anatexis. Geochim. Cosmochim. Acta. 34, 237-243.

Sheraton, J.W., 1970: The origin of the Lewisian Gneisses of N.W. Scotland, with particular reference to the Drumbeg area, Sutherland. Earth. planet. Sci. Lett. 8, 301-310.

Sighinolfi, G.P., 1969: K/Rb in high grade metamorphism: a confirmation of the hypothesis of continual crustal evolution. Contr. Mineral. Petrol. 21, 346-356.

Sighinolfi, G.P., 1970: Investigations into the deep crustal levels of continental crust: petrography and chemistry of the granulite facies of Bahia, Brazil. Atti. Soc. Tosc. Sc. Nat. Mem. Serie A 77, 327-341.

Sighinolfi, G.P., 1971: Investigations into deep crustal levels: fractionating effects and geochemical trends related to high grade metamorphism. Geochim. Cosmochim. Acta. 35, 1005-1021.

Smith, R.E., 1968: Redistribution of major elements during alteration of basic volcanics. J. Petrology 9, 191-219.

Smithson, S.B. & Heier, K.S., 1971: U and Th distribution between normal and charnockitic facies of a deep granitic intrusion. Earth. planet. Sci. Lett. 12, 325-326.

Taylor, S.R., 1962: The chemical compositions of Australites. Geochim. Cosmochim. Acta. 26, 685-722.

Taylor, S.R., 1965: Geochemical analysis by spark source mass spectrography. Geochim. Cosmochim. Acta. 29, 1243-1261.

Taylor, S.R., 1969: Trace element chemistry of andesites and associated calc-alkaline rocks. Proc. Andesite Confer. Oregon Dept. Geol. Min. Resources Bull. 65, 43-63.

Taylor, S.R., 1971: Geochemical application of spark source mass spectrography - II. Photoplate data processing. Geochim. Cosmochim. Acta. 35, 1187-1196.

Taylor, S.R., 1972: Variation in zirconium/hafnium ratios in lunar rocks. (In preparation).

Taylor, S.R., Capp, A.C., Graham, A.L., & Blake, D.H., 1969: Trace elements in andesites II: Saipan, Bougainville and Fiji. Contr. Mineral. Petrol. 23, 1-26.

Taylor, S.R., Ewart, A. & Capp, A.C., 1968: Leucogranites and rhyolites: trace element evidence for fractional crystallisation and partial melting. Lithos 1, 179-186.

Taylor, S.R., Johnson, P.H., Martin, R., Bennett, D., Allen, J. & Nance, W., 1970: Preliminary chemical analyses of Apollo 11 Lunar samples. Proc. Apollo 11 Lunar science Conference 2, 1627-1635.

Taylor, S.R., Kaye, M., Muir, P., Nance, W., Rudowski, & Ware,N.G., 1972: Compositions of the lunar uplands: Chemistry of Apollo 14 samples from Fra Mauro. Proc. 3rd Lunar Sci. Conf. Vol. 2 (in press).

Taylor, S.R. & White, A.J.R., 1966: Trace element abundances in andesites. Bull. Volcanologique Tome XXIX, 177-194.

Tilley, C.E., 1921a: The granite-gneisses of southern Eyre Peninsula (South Australia) and their associated amphibolites. Q.J. geol. Soc. Lond. 306, 75-134.

Tilley, C.E., 1921b: The Precambrian paragneisses of southern Eyre Peninsula, South Australia. Geol. Mag. 58, 251-259 & 305-312.

Tilley, C.E., 1921c: The graphite rocks of Sleaford Bay, South Australia. Econ. Geol. 16, 184-198.

Tilley, C.E., 1924. The facies classification of metamorphic rocks. Geol. Mag. 61, 167-171.

Turekian, K.H. & Wedepohl, W.H., 1961: Distribution of elements in some major units of the earth's crust. Bull. geol. Soc. Am. 72, 175-192.

Turner, F.J., 1948: Evolution of the metamorphic rocks. Mem. geol. Soc. Am. 30, 45-107.

Turner, F.J., 1968: Metamorphic Petrology: Mineralogical and Field Aspects. McGraw-Hill.

Turner, F.J. & Verhoogen, J., 1960: Igneous and Metamorphic petrology. Second Edition. McGraw-Hill.

Tuttle, O.F. & Bowen, N.L., 1958: The origin of granite in the light of experimental studies. Mem. geol. Soc. Am. 74.

Vallance, T.G., 1965: On the chemistry of pillow lavas and the origin of spilites. Mineral. Mag. 34, 471-481.

Vallance, T.G., 1967: Mafic rock alteration and isochemical development of some cordierite - anthophyllite rocks. J. Petrology. 8, 84-96.

von Platen, H., 1965a: Kristallisation granitischer Schmelzen. Contr. Mineral. Petrol. 11, 334-381.

von Platen, H., 1965b: Experimental anatexis and genesis of migmatites. In "Controls of Metamorphism". (Ed., Pitcher, W.S. & Flinn, G.W.). Oliver & Boyd.

Waters, A.C., 1961: Stratigraphic and lithologic variations in the Columbia River Basalts. Am. J. Sci. 259, 583-611.

Wedepohl, K.H. (editor), 1970: Yttrium and the Lanthanides: In "Handbook of Geochemistry" Vol. II - 2 , 39, 57 - 71 - E. Springer-Verlag.

Weigand, P.W. & Ragland, P.C., 1970: Geochemistry of Mesozoic dolerite dykes from eastern North America. Contr. Mineral Petrol. 29, 195-214.

White, A.J.R., 1964: Clinopyroxenes from eclogites and basic granulites. Am. Miner. 49, 883-888.

White, A.J.R., 1966: Genesis of migmatites from the Palmer Granite region of South Australia. Chem. Geol. 1, 165-200.

White, A.J.R., 1969: Some mineral characteristics of high temperature - high pressure granulite facies assemblages. Spec. Publs. geol. Soc. Aust. 2, 353-359.

White, A.J.R., 1971: H.J. Behr et al., Granulites - Results of a discussion. Neues. Jb. Miner. Mh. 3, 116-118.

White, A.J.R., Compston, W. & Kleeman, A.W., 1967: The Palmer Granite: a study of a granite in a regional metamorphic environment. J. Petrology. 8, 29-50.

White, A.J.R., Jakeš, P. & Christie, D.M., 1971: Composition of greenstones and the hypothesis of sea-floor spreading in the Archaean. Spec. Publs. geol. Soc. Aust. 3, 47-56.

Whitney, P.R., 1969: Variations of the K/Rb ratios in migmatitic paragneisses of the Northwest Adirondacks Geochim. Cosmochim. Acta. 33, 1203-1211.

Whittaker, E.J.W. & Muntus, R., 1970: Ionic radii for use in geochemistry. Geochim. Cosmochim. Acta. 34, 945-956.

Whitten, G.F. & Risley, B.G., 1968: A ground magnetic and gravity survey of the Warramboo Aeromagnetic Anomaly, Central Eyre Peninsula. South Aust. Dept. Mines Rept. Invest. 32.

Wildeman, T.R. & Haskin, L.A., 1972: Rare Earths in Precambrian Sediments. Geochim. Cosmochim. Acta. (in press).

Wilson, A.F., 1969: Granulite terrains and their tectonic setting and relationship to associated metamorphic rocks in Australia. Spec. Publs. geol. Soc. Aust. 2, 243-258.

Winkler, H.G.F., 1957: Experimentelle Gesteinemetamorphose I : Hydrothermale Metamorphose karbonatfreier Tone. Geochim. Cosmochim. Acta. 13, 42-69.

Winkler, H.G.F., 1967: Petrogenesis of Metamorphic Rocks. Springer-Verlag.

Winkler, H.G.F., 1970: Abolition of metamorphic facies, introduction of four divisions of metamorphic stage, and a classification based on isograds in common rocks. Neues Jb. Miner. Mh. Jahrgang 1970. 189-248.

Winkler, H.G.F. & von Platen, H., 1958: Experimentelle Gesteinemetamorphose II: Bildung von anatektischen granitischen Schmelzen bei der Metamorphose von NaCl-führenden kalkfreien Tonen. Geochim. Cosmochim. Acta 15, 91-112.

Winkler, H.G.F. & von Platen, H., 1960: Experimentelle Gesteinemetamorphose III : Anatektische Ultra-metamorphose kalkhaltiger Tone. Geochim. Cosmochim. Acta. 18, 294-316.

Winkler, H.G.F. & von Platen, H., 1961a: Experimentelle Gesteinemetamorphose IV : Bildung anatektischer Schmelzen aus metamorphisierten Grauwacken. Geochim. Cosmochim. Acta. 24, 48-69.

Winkler, H.G.F. & von Platen, H., 1961b: Experimentelle Gesteinemetamorphose V: Experimentelle anatektische Schmelzen und ihre petrogenetische Bedeutung. Geochim. Cosmochim. Acta. 24, 250-259.

Wones, D.R. & Eugster, H.P., 1965: The stability of biotite experiment, theory and application. Am. Miner. 50, 1228-1272.

Wyllie, P.J. & Tuttle, O.F., 1959: Effect of CO_2 on melting of granite and feldspars. Am. J. Sci. 257, 648-655.

Wyllie, P.J. & Tuttle, O.F., 1961a: Hydrothermal melting of shales. Geol. Mag. 98, 56-66.

Wyllie, P.J. & Tuttle, O.F., 1961b: Experimental investigation of silicate systems containing two volatile components. Part II: The effects of NH_3 and HF in addition to H_2O on melting temperatures of albite and granite. Am. J. Sci. 259, 128-143.

Wyllie, P.J. & Tuttle, O.F., 1964: Experimental investigation of silicate systems containing two volatile components. Part III: The effects of SO_3, P_2O_5, HCl and Li_2O in addition to water, on melting temperatures of albite and granite. Am. J. Sci. 262, 930-939.

Yoder, H.S. & Eugster, H.P., 1954: Phlogopite synthesis and stability range. Geochim. Cosmochim. Acta. 6, 157-185.

Yoder, H.S. & Kushiro, I., 1969: Melting of a hydrous phase: phlogopite. Am. J. Sci. Schairer Vol. 267-A, 558-582.

Zielinski, R.A. & Frey, F.A., 1970: Gough Island: evolution of a fractional crystallisation model. Contr. Mineral. Petrol. 29, 242-254.

APPENDIX A

PETROLOGICAL DESCRIPTION

A.1 PETROLOGICAL DEFINITIONS

"Charnockite" is used to describe an acid quartz-feldspar-orthopyroxene rock characterised by a dark greenish-blue, greyish-blue or grey appearance despite its acid composition. The feldspars are perthitic or anti-perthitic. Garnet, clinopyroxene, hornblende or biotite may be present.

"Pegmatite" is used to describe an unfoliated acid rock transecting the regional gneissic foliation, and generally with coarser grain size and lighter colour than the host gneiss. The pegmatites contain quartz-K-feldspar ± plagioclase ± biotite ± hornblende and are characterised by extremely coarse to medium grain sizes.

"Polyhedral-subequigranular" is used to describe the metamorphic texture in which the grains are of approximately equal size and have developed polyhedral shapes (i.e. are bounded by near-planar faces). (The term "granulitic" was originally used as a synonym, but textural use of "granulite" or "granulitic" is confusing and should be discontinued.)

"Primary Assemblage" is used to denote the earliest recognisable metamorphic mineral assemblage in a rock, and is characterised in basic rocks by polyhedral-subequi-granular texture. Primary assemblages are characterised by clean, sharp grain boundaries with no textural evidence of replacement or reaction between minerals. Recognition of primary assemblages in acid rocks is commonly impossible.

"Secondary Assemblage" is used to denote mineral assemblages replacing primary mineral assemblages. The secondary minerals are generally coarser and ragged, and transect primary polyhedral-subequigranular textures. The secondary minerals are moulded upon and irregularly

intergrown with primary minerals and commonly exhibit "fuzzy" or gradational contacts with primary minerals. Secondary assemblages are also referred to as "retrogressive", "retrograde" or "rehydrated" assemblages.

"Relict Igneous" or "Primary Igneous" is used to describe minerals which have crystallised from melts and adjusted to falling temperature by exsolution of opaques or pyroxene solid-solutions, without metamorphic recrystallisation of the original mineral. The bulk composition of exsolution products and host mineral is that of the primary igneous crystal. The preservation of delicate igneous zoning and hourglass structures is used as evidence for the absence of metamorphic recrystallisation. The relict igneous minerals are generally surrounded by rims of metamorphic recrystallisation products.

A.2 MINERALOGY

A.2.1 Plagioclase

The plagioclase in the mafic and ultramafic rocks ranges from andesine to labradorite (An_{30} to An_{60}). Normal and oscillatory zoning occurs in plagioclase in many of the basic rocks. The plagioclase in the acid rocks generally ranges from sodic andesine to calcic andesine (An_{30} to An_{40}). Some sodic oligoclases occur in late-stage granitic and pegmatitic veins. Antiperthitic plagioclase is common in the acid gneisses but is not observed in the mafic and ultramafic rocks.

A.2.2 Potash Feldspar

The potash feldspar (K-feldspar) is microcline in granitic gneisses, granitic veins, pegmatitic veins and coarse feldspar pegmatites, but is orthoclase in garnet-gneisses and charnockitic gneisses. K-feldspar is almost invariably perthitic. The perthitic intergrowth ranges from fine lamellar and lensoidal intergrowths to coarser patchy exsolution.

A.2.3 Orthopyroxene

Relict igneous orthopyroxene occurs in many metabasalts and several "pyroxenites". The orthopyroxene commonly occurs as euhedral prismatic or lath-shaped phenocrysts. The orthopyroxene is weakly pleochroic or colourless, and typically contains few opaque inclusions or lamellae. Clinopyroxene exsolution lamellae in the orthopyroxene are commonly minor or absent. Some zoned orthopyroxenes have clouded cores and clear rims.

The metamorphic orthopyroxenes analysed are ferro-hypersthenes. The orthopyroxenes range from colourless, through weakly pleochroic (X = pale pink, Y = Z = very pale green or colourless), to intensely pleochroic (X = deep pink, Y = pale yellow, Z = pale green). The palest ortho-pyroxenes are those first formed during metamorphic recrystallisation of primary igneous olivine or pyroxenes. Orthopyroxenes in basic granulites and charnockites are moderately to strongly pleochroic. The most intensely pleochroic orthopyroxenes occur in garnet-orthopyroxene reaction zones (chapter 5). Orthopyroxenes in the charnockitic gneisses and rehydrated basic granulites are commonly iron-stained and altered. Orthopyroxenes in the garnet-symplectite charnockites commonly contain opaque Schiller lamellae and clinopyroxene lamellae.

A.2.4 Clinopyroxene

Relict igneous clinopyroxene occurs in most of the meta-basalts and several "pyroxenites". The colourless clinopyroxene occurs as stumpy prismatic crystals containing abundant opaque lamellae and opaque inclusions. The clinopyroxenes are commonly twinned. Oscillatory zoning and hourglass structures are preserved in many of the clinopyroxenes, by zoning and regular orientation of opaque inclusions. Clinopyroxene commonly occurs intergrown with orthopyroxene.

Metamorphic clinopyroxene is usually colourless but may be pleochroic in pale greens. The most pleochroic

clinopyroxenes occur in the garnet-symplectite charnockites (X = pale green, Y = pale yellow or colourless, Z = olive-green).

A.2.5 Hornblende

The hornblendes in hornblende granulites, rehydrated granulites, amphibolites occurring near granulites, and the charnockitic gneisses are predominantly "brown" varieties (X = pale yellow or pale yellow-brown, Y = dark brown, Z = very dark brown or dark brown-green). "Green" hornblende (X = pale yellow or yellow, Y = yellow-brown or dark brown, Z = olive-green or green-brown) occurs in some amphibolites associated with granulites. The hornblende varieties occurring in granitic gneisses, pegmatitic and granitic veins and in amphibolites not associated with granulites are either "green" or "blue-green" (X = pale yellow, Y = brown-green, Z = deep blue-green). Some hornblendes have "brown" cores with "green" rims or "green" cores with "blue-green" rims.

A.2.6 Biotite

The biotites are deeply coloured and intensely pleochroic (X = pale brown to very pale yellow, Y = Z = very dark brown to very deep red-brown).

A.2.7 Olivine

Primary igneous olivine occurs in several metabasalts. The olivine is dusted with opaques and has 2V $\sim$ 90° indicating about Fo_{85} composition.

A.2.8 Opaque Minerals

Magnetite, titanomagnetite and ilmenite are the most common opaques. Pyrrhotite occurs disseminated throughout many acid and basic rocks, and commonly occurs intergrown with and replacing the opaque oxide phases. Minor pyrite and chalcopyrite occur in some rocks, and subordinate pendtlandite was observed in one Ni-rich pyroxenite.

TABLE A.1 - FIELD RELATIONSHIPS

69-739	concordant metadolerite (in 740)
69-740	massive charnockite (host to 739, 1168, 1311, 1312)
69-741	reaction zone (in 952)
69-742	basic pod
69-743	basic (in 949)
69-744	discordant metadolerite (in 757)
69-745	basic (in 1170)
69-746	ga-charnockite (host to 753)
69-747	basic (in 781)
69-748	basic (near 782)
69-749	metadolerite in augen gneiss
69-750	massive charnockite (host to 751)
69-751	discordant metadolerite (in 750)
69-752	medium hornblende pegmatite (in 938)
69-753	basic intruded by hornblende pegmatite
69-754	amphibolite (contact phase of 1172, 1399)
69-755	basic in garnet gneiss
69-756	pyroxenite (in 948)
69-757	massive charnockite (host to 790)
69-775	amphibolite (in 934)
69-776	reaction zone
69-777	calc-silicate in 787, near 1367)
69-778	basic (in 943)
69-779	basic infolded with banded gneiss
69-780	garnet-gneiss (host to 785, 786, 788)
69-781	ga-charnockite (host to 747)
69-782	basic from banded acid/basic with pegmatites
69-783	hybrid (?) mafic (adjacent 793, 789)
69-784	ga-charnockite (adjacent 936)
69-785	pyroxenite interbanded with acid gneiss and pegmatites (in 780)
69-786	(as 69-785)
69-787	banded charnockite (host to 777)
69-788	(as 69-785)
69-789	massive charnockite (host to 793)
69-790	xenolithic schlieren (in 757)
69-791	basic (in 1170)
69-792	basic pod (in 944)
69-793	basic schlieren (in 789)
69-794	shredded amphibolite adjacent hornblende pegmatite
69-933	acid)
69-934	acid) (host to 775)
69-935	acid)
69-936	ga-charnockite (host to 794)
69-937	amphibolite near hornblende-pegmatite (in 936)
69-938	ga-charnockite (host to 752)
69-939	banded calc-silicate
69-940	calc-silicate (near 70-1202)
69-941	migmatitic garnet-gneiss (adjacent 70-1202)
69-942	garnet-gneiss (adjacent 70-1202)
69-943	banded garnet-gneiss (host to 778, 779)
69-944	garnet-gneiss (host to 792)
69-945	hybrid (?) mafic between 748 and 1188
69-946	granitic gneiss
69-947	granitic gneiss
69-948	banded garnet-gneiss (host to 756)
69-949	banded garnet-gneiss (host to 743)
69-950	reaction zone (in 949)
69-951	banded charnockite (host to 1167)
69-952	garnet-gneiss (host to 741)
69-953	massive charnockite with hornblendic schlieren
69-954	massive charnockite
69-955	massive charnockite
69-956	massive charnockite (host to 1174)
69-1165	garnet-gneiss interbanded with 1183
69-1166	basic pod in garnet gneiss
69-1167	interlocking basic lenticles (in 951)
69-1168	metadolerite (in 740)
69-1169	granitic gneiss
69-1170	augen gneiss (host to 745, 791, 1178)
69-1171	basic
69-1172	amphibolite (finer phase of dyke: 754, 1399)
69-1173	concordant basic (in 1186)
69-1174	discordant metadolerite (in 956)
69-1175	metadolerite (in 1180)
69-1176	metadolerite
69-1177	transposed basic lenticle
69-1178	basic (in 1169, 1170)
69-1179	basic schlieren
69-1180	augen gneiss (host to 1175)
69-1181	concordant basic (in 1182)
69-1182	granitic gneiss (host to 1181)
69-1183	garnet-gneiss interbanded with 1165
69-1184	hybrid (?) mafic with hornblende pegmatite
69-1185	hornblende pegmatite
69-1186	granitic gneiss (host to 1173)
69-1187	fine margin to (744) metadolerite
69-1188	granitic gneiss (host to 748)
69-1346	basic
69-1347	reaction zone
69-1348	garnet-gneiss
69-1349	reaction zone
69-1350	reaction zone
69-1351	basic
69-1352	pyroxenite interbanded with acid gneiss and pegmatites (in 780)
69-1353	crenulated folded basic lenticle
69-1354	basic
69-1355	agmatitic garnet gneiss charnockite (host to 1370)
69-1356	"garnet pegmatite" transecting 1355, 1370
69-1357	reaction zone
69-1358	selvedge to coarse feldspar pegmatite
69-1359	basic (in 1360)
69-1360	garnet-gneiss (host to 1359)
69-1361	selvedge to coarse feldspar pegmatite
69-1362	garnet gneiss
69-1363	banded charnockite (host to 1364)
69-1364	agmatitic inclusions (in 1363)
69-1365	folded basic
69-1366	basic pod (in 1367)
69-1367	banded charnockite (host to 1366; near 777)
69-1368	reaction zone
69-1369	basic
69-1370	basic (in 1355)
69-1371	basic
69-1372	massive charnockite
69-1373	reaction zone
69-1374	basic
69-1375	garnet gneiss
69-1376	basic in garnet gneiss
69-1377	selvedge to pegmatite
69-1378	ga-charnockite
69-1379	ga-charnockite (host to 1380)
69-1380	amphibolite (in 1379)
69-1381	ga-charnockite (host to 1501)
69-1382	augen gneiss
69-1383	basic
69-1384	basic
69-1385	augen gneiss with hornblende pegmatite
69-1386	basic
69-1387	granitic gneiss
69-1388	core of basic dyke (1389)
69-1389	migmatitic margin of basic dyke (1388)
69-1390	aplitic band in granitic gneiss
69-1391	biotite-pegmatite in granitic gneiss
69-1392	"hybrid" basic xenolith in granitic gneiss
69-1393	"hybrid" basic xenolith
69-1394	pegmatitic veins in basic grading into host
69-1395	augen gneiss (host to 1396)
69-1396	basic (in 1395)
69-1397	concordant basic (in 1395)
69-1398	aplite
69-1399	core of dyke (754,1172)
69-1400	amphibolite
69-1501	amphibolite contacting pegmatite (1213) (in 1381)
69-1502	basic (in 1503)
69-1503	massive charnockite (host to 1502,4,5,6)
69-1504	discordant basic (in 1503)
69-1505	concordant basic (in 1503)
69-1506	discordant basic (in 1503)
69-1507	granitic gneiss
69-1508	basic
69-1509	pegmatitic granitic gneiss
69-1510	granitic gneiss
69-1511	basic
70-1201	reaction zone
70-1202	graphitic schist adjacent 939, 941, 942
70-1212	coarse feldspar pegmatite (in 944, 792)
70-1213	coarse feldspar pegmatite (in 1381, 1501)
70-1310	metadolerite (in 740)
70-1311	metadolerite (in 740)
70-1312	metadolerite

TABLE A.2 - PETROGRAPHIC SUMMARY

CAT.NO.	ROCK TYPE	LOCN.	METAMORPHIC STATUS	QZ	PL	KF	OP	CP	GA	HB	BI	OPQ	SI	OL	SP	COMMENTS
69-739	meta-ign	MC	s.r.pyx.gran.	-	M	-	M	M	-	-	m	T	-	M	m	R.IG.: 1^{o}ol(OD)/1^{o}op(Z,minor OD,EL)/1^{o}cp(EL,OD&Z)
69-740	charnock	"	"	M	D	D	m	-	-	m	T	T	-	-	-	
69-741	ga-contact	FB	"	M	M	M	M	-	m	-	M	T	-	-	-	Some development of op/pl/ga haloes
69-742	mafic gran.	"	hnb.gran.	-	D	-	M	M	-	M	T	T	-	-	-	Some pyx-rich patches/sulphides
69-743	"	"	pyx.gran.	m	D	-	M	M	-	-	-	m	-	-	-	Sulphides/abundant opaques
69-744	meta-ign	CC	s.r.pyx.gran.	-	D	-	M	M	-	m	m	T	-	-	-	R.IG.: SO/1^{o}cp(SL&EL)
69-745	"	KP	"	-	D	-	M	M	-	M	m	T	-	-	-	R.IG.: SO/1^{o}cp(OD,SL,EL&HG)/1^{o}op(minor OD).
69-746	charnock	SB	s.r.hnb.gran	M	M	M	m	m	M	m	-	T	-	-	-	Lamellar op/cp intergrowths
69-747	mafic gran	"	"	-	D	-	m	M	-	D	T	T	-	-	-	
69-748	"	PB	"	T	D	-	M	M	-	M	-	m	-	-	-	Relatively abundant apatite/sulphides
69-749	meta-ign	FP	s.r.pyx.gran	-	D	-	M	M	-	-	m	T	-	-	-	R.IG.: SO/1^{o}op(minor OD,EL)/1^{o}cp(EL)
69-750	charnock	CD	s.r.hnb.gran	M	D	M	m	-	-	m	T	T	-	-	-	Green hb/microxenolithic schlieren
69-751	meta-ign	"	"	-	D	-	M	M	-	M	-	m	-	-	-	R.IG.: SO/1^{o}cp(OD,SL,EL&Z)/green hb/abundant apt&opq
69-752	charnock	SB	i.r.gran.	M	m	D	T	-	T	T	-	m	-	-	-	Pegmatitic/dark brown-green hb
69-753	mafic gran	"	s.r.hnb.gran.	-	D	-	m	M	-	D	T	T	-	-	-	Brown hb usually opq-free/sulphides
69-754	amphib	KP	amphib	m	D	-	-	-	-	D	T	T	-	-	-	Brown-green hb usually opq-free/qz-pl-kf veinlets
69-755	mafic gran	FB	pyx.gran.	m	D	-	M	M	-	-	T	m	-	-	-	Abundant opq.
69-756	ultramafic	"	"	T	m	-	D	D	-	T	T	T	-	-	-	
69-757	charnock	CC	s.r.pyx.gran.	M	D	M	m	-	-	M	m	m	-	-	-	Hb-rich microxenolithic schlieren
69-775	amphib	SB	amphib.	-	D	-	-	m	-	D	m	T	-	-	-	Brown hb
69-776	ga-contact	FB	pyx.gran.	M	D	-	M	-	m	-	T	m	-	-	-	Some development of op/pl/ga haloes
69-777	calc-gneiss	"	amphib.	-	m	-	-	D	-	D	-	-	-	-	-	Pale green hb
69-778	mafic gran.	"	pyx.gran.	T	D	-	M	M	-	-	T	T	-	-	-	
69-779	"	"	"	T	D	-	M	M	-	-	T	m	-	-	-	Sulphides
69-780	ga-gneiss	"	granulite	M	m	D	-	-	M	-	m	T	-	-	T	Sulphides
69-781	charnock	SB	s.r.hnb.gran.	M	m	D	T	T	m	m	-	m	-	-	-	
69-782	amphib	PB	amphib	T	D	-	-	-	-	D	-	T	-	-	-	Abundant apatite/green hb
69-783	charnock	WP	s.r.hnb.gran.	M	M	D	m	-	-	m	T	T	-	-	-	Brown hb
69-784	"	SB	pyx.gran.	M	M	D	m	-	T	-	-	T	-	-	-	
69-785	ultramafic	FB	s.r.pyx.gran.	m	M	-	D	D	-	m	m	T	-	-	-	(Some coarse op&cp prisms with exsolution lamellae/
69-786	"	"	"	T	M	-	D	D	-	T	m	T	-	-	-	(brown hb/deep red to pale yellow bi
69-787	charnock	"	pyx.gran.	M	M	M	T	-	-	-	T	T	-	-	-	
69-788	ultramafic	"	i.r.gran.	-	-	-	M	M	-	M	M	m	-	-	-	Brown-green hb/red-brown to pale yellow bi
69-789	charnock	WP	s.r.pyx.gran.	M	D	M	m	-	-	m	m	m	-	-	-	
69-790a	mafic gran	CC	s.r.hnb.gran.	T	D	-	M	M	-	M	m	m	-	-	-	(Two xenoliths from same outcrop/
69-790b	"	"	i.r.pyx.gran.	T	D	-	M	M	-	m	M	m	-	-	-	(abundant apatite
69-790c	charnock	"	s.r.gran.	M	M	M	m	-	-	m	-	-	-	-	-	Host gneiss to xenoliths
69-791	mafic gran	KP	s.r.hnb.gran.	T	D	-	M	-	-	D	m	m	-	-	-	
69-792	"	FB	pyx.gran.	T	D	-	M	M	-	T	T	m	-	-	-	Poor subophitic relict texture
69-793	"	WP	s.r.gran.	-	D	-	m	m	-	D	m	-	-	-	-	Deep brown hb, relatively opq-free/qz-kf vein/abundant apt
69-794	amphib	SB	amphib	T	M	-	-	M	-	D	T	m	-	-	-	
69-933	charnock	"	s.r.hnb.gran.	M	m	D	T	T	m	T	-	m	-	-	-	
69-934	"	"	"	M	m	D	-	T	T	T	-	m	-	-	-	Deep brown hb
69-935	"	"	"	M	m	D	T	T	T	m	T	m	-	-	-	
69-936	"	"	"	M	m	D	T	T	T	m	-	m	-	-	-	
69-937	mafic gran	"	i.r.gran.	T	D	-	M	M	-	M	M	T	-	-	-	
69-938	charnock	"	s.r.hnb.gran.	M	M	M	T	m	T	m	-	m	-	-	-	
69-939	calc-gneiss	"	—	D	-	-	-	D	-	-	-	T	-	-	-	Graphite opq
69-940	"	"	—	M	M	-	-	D	-	-	m	-	-	-	-	
69-941	ga-gneiss	SB	granulite	M	-	D	-	-	m	-	T	T	T	-	-	
69-942	"	"	"	M	m	D	-	-	m	-	M	T	m	-	-	
69-943	"	FB	"	M	m	D	-	-	m	-	m	T	-	-	-	
69-944	"	"	"	M	M	m	-	-	M	-	T	T	T	-	T	Red-brown to pale yellow bi
69-945	gran	PB	amphib.	M	M	M	-	-	-	m	m	T	-	-	-	Green hb
69-946	"	WP	"	M	M	M	-	-	-	m	m	T	-	-	-	Green hb with blue-green rim

TABLE A.2 (contd.) - PETROGRAPHIC SUMMARY

CAT.NO.	ROCK TYPE	LOCN.	METAMORPHIC STATUS	QZ	PL	KF	OP	CP	GA	HB	BI	OPQ	SI	OL	SP	COMMENTS
69-947	gran.	WP	amphib.	M	M	M	-	-	-	m	m	m	-	-	-	Blue-green hb/sulphides
69-948	ga-gneiss	FB	granulite	M	M	M	-	-	M	-	t	t	t	-	t	
69-949	"	"	"	M	M	D	-	-	m	-	t	t	t	-	t	
69-950	ga-contact	"	pyx.gran.	-	D	-	M	-	M	-	t	m	-	-	-	ga-rich op-free zones/sulphide-rich/red-brown to yellow bi
69-951	charnock	"	s.r.hnb.gran.	M	D	M	m	-	-	t	t	m	-	-	-	
69-952	ga-gneiss	"	granulite	M	m	M	-	-	M	-	m	t	t	-	-	
69-953	charnock	MC	s.r.hnb.gran.	M	D	M	m	-	-	m	t	t	-	-	-	
69-954	"	"	"	M	D	M	m	-	-	m	m	t	-	-	-	
69-955	"	"	"	M	D	M	m	-	-	m	m	t	-	-	-	
69-956	"	CC	s.r.pyx.gran.	M	D	M	m	t	-	t	-	t	-	-	-	Op-cp-pl microxenoliths
69-1165	ga-gneiss	FB	granulite	M	M	D	-	-	M	-	m	t	-	-	-	
69-1166	mafic gran	"	pyx.gran.	t	D	-	M	M	-	-	t	m	-	-	-	Sulphides abundant
69-1167	"	"	s.r.hnb.gran.	-	D	-	m	M	-	M	-	m	-	-	-	Abundant opaques
69-1168	meta-ign	MC	pyx.gran.	-	D	-	M	M	-	t	t	t	-	-	-	R.IG.: SO/1°cp(SL,EL&Z)/abundant apt
69-1169	gran	KP	amphib	M	M	D	-	-	-	m	m	t	-	-	-	Green hb with blue-green rims
69-1170	"	"	"	M	M	D	-	-	-	-	t	t	-	-	-	
69-1171	amphib	"	"	t	D	-	-	m	-	D	t	t	-	-	-	Brown hb
69-1172	"	"	"	t	D	-	-	-	-	D	m	t	-	-	-	Brown-green hb
69-1173	"	WB	"	t	D	-	-	-	-	D	m	t	-	-	-	Green hb/interlocking pl laths moulded by hb
69-1174	meta-ign	CC	s.r.pyx.gran.	-	D	-	M	M	-	m	m	t	-	-	-	R.IG.: SO/1°cp(OD,SL,EL&Z)
69-1175	"	PB	s.r.hnb.gran.	-	D	-	M	M	M	m	m	m	-	-	-	R.IG.: SO/1°cp(OD,SL,&Z)/1°op(SL&Z)
69-1176	"	CD	i.r.hnb.gran.	-	D	-	M	M	-	m	M	m	-	-	-	R.IG.: SO/1°cp(OD,SL&EL)/1°op
69-1177	gran	KP	amphib	M	M	D	-	-	-	m	m	t	-	-	-	Green hb with blue-green rims
69-1178	amphib	"	"	-	M	-	-	-	-	D	t	m	-	-	-	Subophitic hb-pl/brown-green hb mostly opq-free
69-1179	gran	PB	"	M	M	D	-	-	-	m	m	t	-	-	-	Green hb/coarse pegmatitic vein
69-1180	"	"	"	M	M	D	-	-	-	t	t	m	-	-	-	Sulphides/green-brown hb
69-1181	amphib	SC	"	-	M	-	-	-	-	M	-	t	-	-	-	Subophitic/blue-green & pale green hb
69-1182	gran	"	"	M	M	D	-	-	-	m	m	m	-	-	-	Deep blue-green hb/abundant apt
69-1183	ga-gneiss	FB	hnb.gran.	M	M	M	-	-	m	-	-	-	-	-	-	
69-1184	gran	KP	amphib.	M	M	M	-	-	-	M	-	t	-	-	-	Brown-green hb
69-1185	"	PB	"	M	M	D	-	-	-	m	m	t	-	-	-	Green-hb
69-1186	"	WB	"	M	M	D	-	-	-	-	m	t	-	-	-	Epidote
69-1187	mafic gran	CC	s.r.hnb.gran.	-	D	-	M	M	-	M	m	t	-	-	-	
69-1188	gran	PB	amphib.	M	M	M	-	-	-	m	m	m	-	-	-	Green hb/epidote
69-1346	mafic gran	FB	pyx.gran.	m	D	-	M	m	-	-	t	m	-	-	-	Trace ga in rock analysed/cp-qz stable/qz-pl vein
69-1347	ga-contact	"	granulite	M	M	D	-	-	M	-	m	t	t	-	-	
69-1348	ga-gneiss	"	"	M	M	M	-	-	M	-	m	t	t	-	-	
69-1349	ga-contact	"	pyx.gran.	M	M	-	M	-	m	-	t	m	-	-	-	Op/pl/ga haloes associated with qz veins/opq-rich
69-1350	"	"	granulite	M	M	M	-	-	m	-	m	m	-	-	-	Abundant apatite
69-1351	mafic gran	"	pyx.hnb.gran.	-	D	-	M	M	-	m	m	m	-	-	-	Hb-rich patches at expense of cp
69-1352	ultramafic	"	i.r.gran.	-	-	-	M	M	-	M	m	m	-	-	-	abundant opq/brown hb
69-1353	mafic gran	"	s.r.hnb.gran.	m	D	-	M	M	-	m	-	m	-	-	-	Sulphides
69-1354	"	"	s.r.pyx.hnb. granulite	t	D	-	M	M	-	m	t	t	-	-	-	Hb patchy: hb locally at expense of cp; hb occurs only where qz absent
69-1355	ga-contact	"	pyx.gran.	M	M	M	M	-	m	-	t	t	t	-	-	Ga-op-qz-rich bands
69-1356	ga-gneiss	"	granulite	M	M	M	-	-	m	-	-	t	t	-	-	
69-1357	ga-contact	"	pyx.gran.	M	D	M	M	-	m	-	t	t	t	-	-	Well developed op/pl/ga haloes near qz-kf vein
69-1358	ultramafic	"	s.r.pyx.gran.	-	M	-	D	D	-	t	m	t	-	-	-	
69-1359	mafic gran	"	pyx.gran.	t	D	-	M	M	-	-	t	m	t	-	-	Sulphides
69-1360	ga-gneiss	"	granulite	M	M	M	-	-	m	-	m	t	t	-	-	
69-1361	"	"	"	M	M	M	-	-	M	-	M	t	t	-	-	Selvedge to qz-pl-kf pegmatite
69-1362	"	"	"	M	m	D	-	-	m	-	m	t	t	t	-	
69-1363	charnock	FB	pyx.gran.	M	M	M	m	-	-	-	t	t	-	-	-	

TABLE A.2 (contd.) - PETROGRAPHIC SUMMARY

CAT.NO.	ROCK TYPE	LOCN.	METAMORPHIC STATUS	QZ	PL	KF	OP	CP	GA	HB	BI	OPQ	SI	OL	SP	COMMENTS
69-1364a	charnock	FB	pyx.gran.	M	M	M	m	-	-	-	T	T	-	-	-	Acid host to basic bands
69-1364b	mafic gran	"	s.r.hnb.gran.	T	D	-	M	M	-	m	T	T	-	-	-	Basic bands: pyx-rich+qz/pl-rich/hb-rich & no qz
69-1365	"	"	s.r.pyx.gran.	T	D	-	M	M	-	m	T	T	-	-	-	Hb coexists with qz
69-1366	"	"	pyx.gran.	m	D	-	M	M	-	-	-	m	-	-	-	Sulphides/moderate apatite only
69-1367	charnock	"	"	M	M	M	m	-	m	-	T	T	-	-	-	Ga-op-rich band in slide atypical/few ga in rock analysed
69-1368	ga-contact	"	"	M	D	M	M	m	-	-	T	m	-	-	-	Few ga in rock analysed/cp+qz stable in qz-poor zones
69-1369	mafic gran	"	i.r.pyx.gran.	-	D	-	M	M	-	D	T	T	-	-	-	Brown-green hb
69-1370	"	"	s.r.hnb.gran.	T	D	-	M	M	-	m	T	T	-	-	-	Qz veinlets but hb+no qz
69-1371	"	"	pyx.gran.	m	D	-	M	M	-	-	T	m	-	-	-	
69-1372	charnock	MC	s.r.hnb.gran.	M	M	M	m	-	-	m	T	m	-	-	-	
69-1373	ga-contact	CW	granulite	M	M	M	-	-	m	-	m	T	-	-	-	
69-1374	mafic gran	"	pyx.gran.	T	D	-	M	M	-	T	T	T	-	-	-	
69-1375	ga-gneiss	"	granulite	M	M	M	-	-	m	-	m	T	-	-	-	
69-1376	mafic gran	TC	pyx.hnb.gran.	T	D	-	M	m	-	m	T	m	-	-	-	Hb-cp-rich patches with qz/op-rich patches/qz-kf-pl vein
69-1377	ga-contact	SB	i.r.gran.	T	D	-	T	-	m	D	T	T	-	-	-	Abundant apt & zircon/cp-kf-qz pegmatite contact
69-1378	charnock	"	s.r.pyx.gran.	M	M	M	m	T	m	T	T	m	-	-	-	
69-1379	"	"	s.r.hnb.gran.	M	M	D	m	m	m	T	T	m	-	-	-	
69-1380	mafic gran	"	i.r.gran.	-	D	-	m	M	-	M	T	T	-	-	-	Brown hb
69-1381	charnock	"	s.r.hnb.gran.	M	M	D	T	m	T	m	-	m	-	-	-	Sulphides
69-1382	gran	MG	amphib.	M	M	D	-	-	-	-	m	T	-	-	-	Green hb
69-1383	meta-ign	MQ	"	-	D	-	-	m	-	D	m	m	-	-	-	R.IG.: SO/1°cp(OD)/pale green & blue-green hb
69-1384	"	"	"	-	D	-	-	m	-	D	T	m	-	-	-	R.IG.: SO/1°cp(OD)/brown hb with green rims
691385	gran	"	"	M	M	D	-	-	-	m	m	T	-	-	-	Blue-green hb/pegmatitic vein qz-pl-kf
69-1386	meta-ign	"	"	-	M	-	-	-	-	D	M	m	-	-	-	R.IG.: SO/1°cp(OD)/brown-green hb with green rims
69-1387	gran	UP	"	M	m	D	-	-	-	T	m	T	-	-	-	Blue-green hb
69-1388	amphib	KP	"	T	D	-	-	-	-	D	m	T	-	-	-	Brown hb
69-1389	"	"	"	m	D	-	-	-	-	D	m	m	-	-	-	Migmatite/qz-kf-pl veins with green-hb-apt-rich selvedges
69-1390	gran	"	"	M	m	D	-	-	-	T	m	T	-	-	-	
69-1391	"	"	"	M	D	m	-	-	-	-	m	-	-	-	-	
69-1392	"	"	"	M	M	D	-	-	-	m	M	T	-	-	-	Green hb with blue-green rims/abundant apatite
69-1393	"	"	"	M	M	D	-	-	-	m	m	T	-	-	-	Green hb + blue-green rims
69-1394	"	"	"	M	M	D	-	-	-	m	m	T	-	-	-	Green to blue-green hb
69-1395	"	PW	"	M	M	M	-	-	-	M	m	T	-	-	-	Blue-green hb
69-1396	meta-ign	"	hnb.gran.	-	D	-	M	M	-	M	-	m	-	-	-	R.IG.: SO/1°cp(EL)/most hb (green) nucleating on opq
69-1397	mafic gran	"	s.r.hnb.gran.	-	D	-	M	M	-	M	m	m	-	-	-	R.IG.: SO/1°cp(EL)/most hb&bi nucleating on opq
69-1398	gran	KP	amphib.	M	T	D	-	-	-	T	T	m	-	-	-	
69-1399	amphib	"	"	m	D	-	-	-	-	D	T	m	-	-	-	Brown-green hb
69-1400	"	"	"	m	D	-	-	-	-	D	T	T	-	-	-	Brown-green hb with green rims
69-1501	"	SB	"	T	D	-	-	M	-	D	-	T	-	-	-	pyxs opq-rich/brown hb relatively opq-free/qz-pl-kf vein
69-1502	mafic gran	BI	s.r.pyx.gran.	T	D	-	M	M	-	m	m	T	-	-	-	
69-1503	charnock	"	"	M	M	M	m	-	-	m	m	m	-	-	-	
69-1504	mafic gran	"	"	T	D	-	M	M	-	-	m	m	-	-	-	
69-1505	"	"	s.r.hnb.gran.	m	D	-	M	M	-	m	m	m	-	-	-	
69-1506	"	"	"	m	D	-	M	M	-	M	-	m	-	-	-	
69-1507	gran	BB	amphib.	M	m	D	-	-	-	-	m	T	-	-	-	Accesory allanite - anomalous colours
69-1508	amphib	"	"	m	D	-	-	-	-	D	m	T	-	-	-	Abundant apatite
69-1509	gran	"	"	M	M	D	-	-	-	-	T	-	-	-	-	
69-1510	"	NPL	"	M	M	D	-	-	-	-	m	T	-	-	-	Minor epidote/allanite
69-1511	amphib	"	"	m	D	-	-	-	-	D	-	T	-	-	-	Brown hb with green rims
												CAR-BON-ATE				
70-1201	ga-contact	FB	s.r.pyx.gran.	m	D	-	M	-	M	-	m	m	-	-	-	Coarse sporadic ga/some very coarse op/pl/ga haloes
70-1202	graph	SB	—	D	-	-	-	-	-	-	-	M	D	-	-	Graphite is opq phase/carbonate is calcite
70-1310	meta-ign	MC	s.r. pyx.gran.	-	M	-	M	M	-	-	m	T	-	M	T	R.IG.: 1°ol(OD)/1°op(Z, minor OD&EL)/1°cp(EL,OD,Z&HG)
70-1311	"	"	"	-	M	-	M	M	-	-	m	T	-	M	m	R.IG.: 1°ol(OD)/1°op(Z, minor OD&EL)/1°cp(EL,OD&Z)
70-1312	"	"	"	-	M	-	M	M	-	—	m	T	-	m	T	R.IG.: 1°ol(OD)/1°op(Z, minor OD&EL)/1°cp(EL,OD&Z)

EXPLANATORY NOTES FOLLOW OVERLEAF

TABLE A.2 - PETROGRAPHIC SUMMARY

ABBREVIATIONS USED

(1) LOCATIONS - LOCN.

MC: Memory Cove
FB: Fishery Bay
CC: Cape Catastrophe
KP: Kirton Point
SB: Sleaford Bay
PB: Point Boston
FP: Fisherman's Point
CD: Cape Donnington
WP: West Point
WB: Wanna Beach
SC: Spalding Cove
CW: Cape Wiles
TC: Theakstone's Crevasse
MG: Mount Gawler
MQ: Main quarry west of Port Lincoln
UP: Uranium prospect
PW: Point Warna
BI: Boston Island
BB: Bessa Blox Quarry north of Port Lincoln
NPL: North Port Lincoln

For detailed grid-reference see ANU catalogue cards.

(2) ROCK TYPE

mafic gran = mafic granulite
ultramafic = ultramafic granulite
meta-ign = meta-igneous
amphib = amphibolite
ga-gneiss = garnet gneiss
charnock = charnockitic gneiss
ga-contact = garnet contact zone
gran = granitic gneiss
calc-gneiss = calc-silicate gneiss
graph = graphitic schist

(3) METAMORPHIC STATUS

pyx.gran.: pyroxene granulite
hnb.gran.: hornblende granulite
s.r.gran.: slightly rehydrated (secondary hydrous minerals minor (<10%)
i.r.gran.: intensely rehydrated (secondary hydrous minerals major (>10%)
amphib.: amphibolite

NOTES:

(1) hnb.gran implies discrete hb grains not rimming op/cp.
(2) s.r. and i.r. gran are additionally designated pyx. or hnb. gran if this can be ascertained.
(3) garnet gneisses are designated simply as granulite because they are associated with both pyx.gran and hnb.gran.

(4) MINERALS

QZ: quartz
PL: plagioclase
KF: K-feldspar
OP: orthopyroxene
CP: clinopyroxene
GA: garnet
HB: hornblende
BI: biotite
SI: sillimanite
OL: olivine
SP: green spinel
OPQ: opaques, usually magnetite-ilmenite and/or sulphides.
PYX: pyroxenes (op & cp)
APT: apatite

(5) PRIMARY IGNEOUS FEATURES

R.IG.: relict igneous textures
SO: subophitic
1^{o}: primary
SL: Schiller opaque lamellae
EL: pyroxene exsolution lamellae
OD: opaque granule dustings
Z: zoned
HG: hourglass structure

(6) MINERAL PROPORTIONS

D: dominant > 30%
M: major 10-30%
m: minor 1-10%
T: trace, accessory < 1%

APPENDIX B

SAMPLE PREPARATION AND ANALYSIS

B.1 SAMPLE PREPARATION

B.1.1 Rock Crushing

Larger sample weights were used for coarser-grained rocks: ½-1 kg for fine-grained rocks; 1-2 kg for medium-grained rocks; and 1-3 kg for coarse-grained rocks. Obviously weathered portions of the samples were removed in a mechanical wedge splitter. The samples were then crushed to chips of less than 1 cm in a Sturtevant jaw crusher (manganese steel jaws: 2% Mn, 1% C, 0.3% Si). An Agate and General Stonecutters agate cone grinder reduced samples to granules less than 2mm. Quartering on paper sheets reduced the samples to 150-200 g, which was finally crushed in an agate Siebtechnik swing mill. Three samples (69-741, 69-1361 and 70-1201) were crushed in a tungsten carbide Siebtechnik swing mill, resulting in cobalt and tungsten contamination.

Fine biotite flakes were observed in some pressed powder XRF pills, so small quantities of these samples were recrushed in a tungsten carbide ball mill. Comparison of measured trace element contents (except cobalt) of a few XRF pills showing more obvious biotite flakes, with recrushed samples, showed no significant differences. Hence the additional crushing was unwarranted. Comparison of cobalt in samples recrushed in tungsten carbide for XRF with the corresponding samples crushed in agate for emission spectroscopy indicated 30 to 60 ppm cobalt contamination from the tungsten carbide.

B.1.2 Mineral Separation

The rocks were jaw-crushed then passed through a Van Gelder roll mill with sieving after each pass to prevent overgrinding. Biotite passed through the rollers with minimum crushing and was easily removed in coarser fractions, which were utilised for H_2O, F, Na_2O and FeO determinations. The sieve fractions collected for separation were -80+100 mesh (biotite only), -100+120 mesh and -120+150 mesh.

TABLE B.2

MASS SPECTROMETER ISOTOPES AND PRECISION

ISOTOPE	RANGE OF STANDARD ERRORS
Lu175 (Internal Standard)	
Lu176 (Internal Standard)	
Cs133	4.8-17.8%
Ba135	3.8-10.6%
Ba137	3.2-10.1%
La139	2.4- 7.0%
Ce140	3.0- 7.1%
Pr141	2.5- 6.1%
Nd143	2.3- 6.1%
Nd146	2.2- 6.5%
Sm147	3.0- 7.5%
Sm149	2.1- 6.8%
Eu151	2.7- 7.1%
Eu153	2.0- 6.6%
Gd158	2.6- 8.7%
Tb159	2.5- 7.0%
Dy163	3.0- 6.4%
Ho165	2.1- 8.2%
Er166	2.2- 5.5%
Er167	2.3- 8.0%
Yb171	3.7- 8.5%
Yb172	2.0- 9.0%
Yb174	2.6- 6.6%
Hf177	4.3- 9.5%
Hf178	3.0-10.4%
Hf179	3.7-12.6%
Th232	3.0-12.0%
U238	2.6-14.5%

TABLE B.3

GAMMA-SPECTROMETRY PRECISION

Values obtained on Standard Rocks

	% K_2O	ppm U	ppm Th
AGV-1	2.91 (2.92)*	1.9	6.4
BCR-1	1.71 (1.71)*	1.7 (1.8)*	5.7 (6)*
GSP-1	5.31 (5.53)*	1.9 (1.7)**	108 (90)**
G-2	4.51 (4.48)**	2.1 (2.1)**	26 (24)**

	Observed Duplicate Agreement	Theoretical Coefficient*** of Variation	Average*** Background	Lower Limit of Detection***
%K > 0.1%	< ±1%	< ±1.7%	0.76% K	0.014% K
%K < 0.1%	< ±5%	< ±3.4%	0.76% K	0.014% K
ppm U > 0.5	< ±10%	< ±10%	4.3 ppm U	0.3 ppm U
ppm U < 0.5	< ±20%	< ±20%	4.3 ppm U	0.3 ppm U
ppm Th > 0.5	< ±10%	< ±12%	9.8 ppm Th	0.1 ppm Th
ppm Th < 0.5	< ±20%	< ±40%	9.8 ppm Th	0.1 ppm Th

* Standard values preferred by ANU Geology Department, 1971-2.

** Unpublished Data: B.W. Chappell (1968-9) ANU Geology Department

*** From Gill (1972) (C.V. = $100/\sqrt{}$(nett corrected counts).

Magnetic opaques were removed with a hand magnet, and initial separation carried out in a Carpco electromagnetic roll separator. The minerals were separated by a combination of isodynamic separator and heavy liquids (Clerici's Solution, methylene iodide and tetrabromoethane). Final handpicking under binocular microscope was necessary in some cases to produce the required degree of purity (greater than 99% pure). The mineral separates were thoroughly cleaned in an ultrasonic bath for about half an hour with two changes of distilled water and two changes of reagent acetone.

B.2 MASS SPECTROMETER ANALYTICAL TECHNIQUE

Selected samples were analysed for REE, U, Th, Hf, Ba and Cs in an AEI MS7 spark source mass spectrometer using lutetium internal standard and the methods of Taylor (1965 and 1971). The photoplates were read on a Jarrell-Ash microphotometer using a slit height of 1.2 mm and a slit width of 10 microns with a drive rate of 1.0 mm/min. The mass numbers read are shown in table B.2. Hf178 and Yb171 were read to correct the Lu176 standard for Hf176 and Yb176 interference. Cesium was only read when free from obvious overlap interference from the carbon doublet. Two photoplates were run for each sample yielding a minimum of four, and usually six to ten, separate determinations for each isotope.

The precision of individual isotopes is generally better than 10% (usually 2-6%) as shown in table B.2. Precision is expressed as standard error, where:

$$\text{Std Error} = \frac{100\ (\text{Standard Deviation})}{(\text{Average})\sqrt{(\text{Number of Determinations})}}$$

B.3 GAMMA-SPECTROMETER TECHNIQUE

The methods used are similar to those of Heier & Rogers (1963), Heier & Adams (1965) and Adams & Gasparini (1970). Rocks with low Th and U were measured for these elements and K by gamma-ray spectrometry, where sufficient sample was available. About half a kilogram of coarsely crushed rock powder was pressed into Perspex canisters without tapping down, and sealed with tape to allow equilibration with

radiogenic radon gas (about three weeks). The samples were analysed by a 5 x 4" NaI (Tl) crystal with a 400 channel RIDL model 24-2 pulse height analyser, using approximately 30 channels per sample. The energy peaks used were: 1.47 MeV K40 peak for potassium; 1.76 MeV Bi214 peak for uranium; and 2.62 MeV T1208 peak for thorium. Synthetic Atomic Energy Commission standards were used for calibration, and pure NaCl for backgrounds which were taken every eight days. No absorption corrections were made. The samples were run in duplicate and counted for 20 hours or more. Standard rocks were also run and results obtained are shown in Table B.3.

The precision of analysis was approached from observed agreement between duplicates and theoretical variation expected from counting statistics (Gill, 1972: analyses over same period). These are summarised in Table B.3 together with average backgrounds and lower limits of detection (Gill, 1972). There is good agreement between predicted and observed precision in most cases.

B.4 X-RAY FLUORESCENCE SPECTROGRAPHIC TECHNIQUE

The X-ray fluorescence spectrographic (XRF) techniques used are described by Norrish & Chappell (1967), Norrish & Hutton (1969) and Chappell *et al.*, (1969). Major elements were determined on lithium borate-lanthanum oxide fused glass discs; and trace elements on pressed powders with direct measurement of mass absorption coefficients to overcome the most serious matrix effects. Rb and Sr mass absorption coefficients were used for wavelengths 0.7-1.0Å; Zn for 1.0-1.744Å; and Fe for greater than 1.744Å (the iron Kα absorption edge). Rb and Sr mass absorption coefficients of pure rock powder were measured in duplicate (duplicate agreement usually $<\pm\frac{1}{2}\%$ and all $<\pm1\%$); and Fe and Zn mass absorption coefficients were calculated from measurement in quadruplicate of 1:1 cellulose-rock mixes (standard error less than ±1%). Major element matrix corrections have been applied using the method of Norrish & Hutton (1969). Trace element spectral interferences of both peaks and backgrounds have been corrected following Norrish & Chappell (1967) and Chappell (1971). The analytical lines, X-ray tube, crystal,

TABLE B.4.1.

XRF OPERATING CONDITIONS

Element	Tube	Line	Crystal	Collimator: Coarse or Fine	Detector: Flow/ Scintillation	Time (Secs) on Peak or Background	Mass Absorption Coefficient	Lower Limits of Detection* percent		Worst Observed Duplicate Agreement	
SiO_2	Cr	K_α	PE	C	F	200	Matrix Corrections Computed	0.05		±1%	
TiO_2	Cr	K_α	LiF(200)	C	F	80		0.003		±1%	
Al_2O_3	Cr	K_α	PE	C	F	200		0.02		±1%	
Fe_2O_3**	W/Cr	K_α	LiF(200)	C	F	80		0.01		±1%	
MnO	W	K_α	LiF(200)	C	F	80		0.003		±1%	
MgO	Cr	K_α	ADP	C	F	400		0.09		±2%***	
CaO	Cr	K_α	LiF(200)	C	F	80		0.002		±1%	
K_2O	Cr	K_α	LiF(200)	C	F	80		0.002		±1%	
P_2O_5	Cr	K_α	Ge	C	F	200		0.006		±1%	
SO_3	Cr	K_α	Ge	C	F	200		0.01		±2%	
								p.p.m. Acid	Basic	Mean of 30 duplicates	Standard Error of mean
Rb	Mo	K_α	LiF(200)	F	S	400	Rb	0.6	0.8	±1.2%	0.2
Sr	Mo	K_α	LiF(200)	C	S	200	Sr	0.6	0.8	±0.26%	0.03
Y	Mo	K_α	LiF(200)	C	S	400	Sr	0.3	0.7	±0.8%	0.2
Pb	Mo	$L_{\beta 1}$	LiF(200)	F	S	400	Rb	2.0	2.6	±6.8%	0.9
Th	Mo	L_{α_1}	LiF(200)	F	S	400	Rb	1.9	2.3	±5.5%	0.8
U	Mo	L_{α_1}	LiF(220)	F	S	800	Rb	1.9	1.7	±7.3%	1.4
Ga	Mo	K_α	LiF(200)	C	S	400	Zn	1.3	1.6	±2.4%	0.4
Zr	Ag	K_α	LiF(200)	C	S	200	Sr	2.2	3.1	±1.6%	0.4
Nb	Ag	K_α	LiF(200)	F	S	400	Sr	1.5	0.8	±4.4%	1.3
Co	Au	K_α	LiF(200)	C	S	400	Zn	2.5	2.8	±4.7%	0.9
Ni	Au	K_α	LiF(200)	C	S	400	Zn	0.6	1.3	±1.6%	0.3
Cu	Au	K_α	LiF(200)	C	S	400	Zn	0.7	0.8	±1.3%	0.2
Zn	Au	K_α	LiF(200)	C	S	400	Zn	0.9	1.1	±0.8%	0.2
V	W	K_α	LiF(220)	F	F	400	Fe	0.5	1.4	±0.8%	0.1
Cr	W	K_α	LiF(200)	F	F	200	Fe	0.7	1.1	±0.9%	0.1
Ba	W	L_{β_1}	LiF(220)	C	F	400	Fe	3.9	2.4	±1.9%	0.5
La	W	L_{α_1}	LiF(200)	C	F	400	Fe	1.6	2.0	±3.2%	0.8
Ce	W	L_{β_1}	LiF(200)	F	F	400	Fe	7	8	±3.9%	0.7
Pr	W	L_{α_1}	LiF(220)	C	F	80	Fe	2	3	±9.5%	2.2
Nd	W	$L_{\beta 1}$	LiF(220)	C	F	80	Fe	9	6	±7.4%	1.8

* based on counting statistics
** Total Fe as Fe_2O_3
*** Standard error of 4 determinations

TABLE B.4.2

"PREFERRED" MAJOR ELEMENT VALUES USED

Element	W-1	GSP-1	AGV-1	BCR-1	PCC-1
SiO_2	52.61	67.29	59.02	54.20	41.43
TiO_2	1.07	0.66	1.06	2.25	0.006
Al_2O_3	14.94	15.00	17.02	13.48	0.62
Fe_2O_3*	11.12	4.27	6.74	13.42	8.21
MnO	0.17	0.04	0.10	0.19	0.13
MgO	6.52	0.97	1.52	3.45	43.48
CaO	10.96	1.99	4.90	6.99	0.53
K_2O	0.66	5.53	2.92	1.71	---
Na_2O	2.16	2.88	4.33	3.31	---
P_2O_5	0.14	0.29	0.51	0.38	---
S**	0.05	0.12	0.03	0.14	0.03
Loss	0.22	0.57	1.69	0.64	4.74

* Total Fe as Fe_2O_3

** Values Obtained

COMPARISON OF "PREFERRED" AND MEASURED TRACE ELEMENTS

	BCR-1		W-1		PCC-1	
Element	Preferred	Obtained	Preferred	Obtained	Preferred	Obtained
Ba	700	697	165	160		
Rb	47.5	46.6	21.6	21.1		
Sr	335	330	185	189		
Pb	15	19	8	10		
Th	6	6	2.3	3		
U	1.8	---	0.55	---		
Zr	180	188	94	92		
Nb	13	11	9	6		
Y	40	33	26	20		
La	24	27	10	10		
Ce	52	52	23	19		
Pr	7	7.1	3.6	2.6		
Nd	29	24	15	12		
V	360	362	245	234		
Cr	14	12	115	91		
Ni	10	5	75	66	2500	2415
Cu	16	11	115	102	8	4
Zn	120	126	83	90	42	44
Ga	21	21	17	17		

collimator, detector, total duplicate counting time on peak for major, and peak or background for trace, mass absorption coefficient and theoretical 3σ lower limits of detection (LLD) based on counting statistics for granitic and basic rocks analysed, together with observed duplicate agreement are listed in table B.4.1. Duplicate agreements tabulated do not include samples near LLD, where poorer precision was observed. The samples were measured relative to a synthetic standard which was calibrated against natural rock standards using "preferred" values selected from superior analytical data. Table B.4.2 summarises "preferred" major and trace element values, and trace element values obtained for standards during analysis.

B.5 EMISSION SPECTROGRAPHIC TECHNIQUE

The small amounts of pure mineral separates remaining after major element analysis precluded use of XRF for trace elements. The minerals were analysed for "involatile" and alkali trace elements listed in table B.5.1. In addition, all rocks analysed for trace elements by XRF were run for "involatile" elements for comparative study of XRF and emission spectrograph techniques. Selected rocks were analysed for alkali elements by emission spectrograph. The emission spectrograph techniques used follow those of Ahrens & Taylor (1961) and Taylor et al., (1970). Jarrell-Ash emission spectrograph (model 71-100) and microphotometer (model 23-100) instrument conditions are summarised in table B.5.2 and analytical lines listed in table B.5.1. The palladium internal standard used for the "involatile" elements was prepared from Johnson Matthey Specpure $Pd(NH_3)_4(NO_3)_2$ thoroughly mixed with National Carbon Spectroscopic Powder Grade SP-2 in Spex 8000 and Turbula mixing mills. The Pd-C standard (about 280 ppm Pd) was mixed 3 parts by weight to 1 part of sample in a Spex 5000 mill. Johnson Matthey Specpure Na_2CO_3 was used as internal standard for alkali elements and was mixed 1 part by weight to 1 part of sample. The photoplates were read on a Jarrell-Ash microphotometer and results processed by a computerised version of the method of Ahrens & Taylor (1961: chapter 11). Standard rocks were

TABLE B.5.1

EMISSION-SPECTROSCOPE LINES AND PRECISION

"INVOLATILE" ELEMENTS

Element	Wavelength Å	Mean Triplicate Agreement	Standard Deviation of Mean	Standard Error of Mean
Pd	3460.8	(internal) (standard)	----	----
Cu	3274.0	±7.9%	3.8%	0.6
Y	3327.9	±7.0%	6.1%	1.5
Ni(High Ni)	3391.1	±5.7%	4.8%	0.7
Ni	3414.8			
Co	3453.5	±7.6%	4.6%	0.7
Sc	4246.8	±5.9%	2.8%	0.4
Cr	4254.3	±5.2%	3.7%	0.6
Cr(High Cr)	4344.5			
La	4333.7	±19%	4%	2.5
V	4379.2	±5.6%	3.2%	0.5
Sr	4607.3	±4.6%	4.0%	1.2
Ba	4554.0	±5.3%	2.9%	0.4
Ba	4934.1			

ALKALI ELEMENTS

Element	Wavelength Å	Mean Duplicate Agreement	Standard Deviation of Mean	Standard Error of Mean
Na*	6154.2	(internal) (standard)	----	----
Li	6707.8	±3.4%	3.1%	0.6
Li(High Li)	8126.5	----	----	----
Rb	7800.2	±8.0%	4.0%	0.7
Rb	7947.6			
Cs	8521.1	±8.1%	5.6%	1.1

(*Correction made for Na in rock)

TABLE B.5.2

JARRELL-ASH SPECTROGRAPH OPERATING CONDITIONS

Factor	"Involatile" Elements	Alkali Elements
Wavelength Setting	approx. 00624	approx. 01245
Wavelength Range	2450-5000Å	6100-8600Å
Slit Width	10 microns	30 microns
Slit Height	10.5 mm	11 mm
Anode (Sample)	National L4261	National L4260
Cathode	National L3863 ⅛"	National L3863 ⅛"
Current	10 amps DC	8 amps DC
Preburn	10 sec	5 sec
Exposure	2½ min	3 min
Photoplates	2 Ilford N30	2 Kodak IN
Filter	None	Corning 3486 with Cutoff at 5100Å to exclude second order UV lines
Step Sector	8 Step Sector with 2:1 ratio	

JARRELL-ASH MICROPHOTOMETER

Slit height	7 mm
Slit width	7 microns
Drive Speed	0.5 mm/min

TABLE B.5.3

STANDARD VALUES USED FOR EMISSION SPECTROSCOPY

	G1	G2	GSP1	AGV1	BCR1	DTS1	T1	S1	PCC1	W1	Concentration Ranges: Standardised	Concentration Ranges: Utilised & Extrapolated	Notes
Co	--	--	--	--	--	143	14	18	115	48	14---143	9---130	
Ni	--	--	--	16	--	1650	11	--	2500	75	11---2500	5---1330	Zr correction gave 2 ppm
Cu	12	10	32	--	--	7	48	21	9	115	7---115	2---350	Background bad <10 ppm. Ti correction gave 1 ppm.
Sc	--	--	6	11.5	31.5	3.5	11	13	8	34	6---34	3---160	
V	--	35	52	115	380	11	85	88	29	245	35---380	16---1070	
Cr	--	--	12	10	--	4000	21	55	2800	115	10---4000	9---4530	
Ba	1050	1850	1250	1220	700	0	620	320	1.0	165	55---1850	4---2400	Absorbs > 2000 ppm
Sr	250	480	240	660	335	0.5	375	220	1.0	185	62---660	10---800	Absorbs > 1000 ppm
Y	--	--	27	--	41	--	--	450	--	26	26---450	18---760	
La	100	80	175	--	--	--	--	225	--	--	80---225	80---140	
						Lunar 12070	Lunar 10084						
Li	24	32	32	--	15	16	12.5	120	--	10	24---120	2---80	Absorbs > 80 ppm on low Li line
Rb	220	170	255	68	48	6.4	2.7	145	--	22	2.7-500	1.5-880	Absorbs > 300 ppm
Cs	1.5	1.3	1.0	1.3	--	--	--	1.0	--	1.0	1.0-1.5	0.8-7	

Mixes of PCC-1:W-1 (1:3); DTS-1:W1 (2:1) and K-feldspars 70-1212, 70-1213 were used for calibration.

arced in quadruplicate and samples in triplicate for "involatile" element determination; and standards in triplicate and samples in duplicate for alkalis.

Table B.5.3 lists the standards and trace element values used, the standardised range of working curves and the extrapolated range. The likely error inherent in extrapolated values will be higher, especially for elements suffering from self-absorption at high concentrations (Ba, Rb, Sr and Li), or from bad background effects at low concentrations (Cu, Co, Sc and Cr). The precision of the technique is limited by precision of sample and standard determination, and the accuracy of standard trace element contents. The precision of triplicate and duplicate determinations was better than ±10% in most cases but poorer precision was observed for very high or very low concentrations, and for some elements (viz. Cs and La). The observed precision is summarised in table B.5.3.

B.6 CHEMICAL TECHNIQUES

B.6.1 Sodium

The samples were dissolved in reagent HF/H_2SO_4 in Pt dishes. The excess HF was volatilised and solutions made up to 250 ml with 500 ppm lithium internal standard. The samples were measured in a Baird-Atomic double beam flame photometer using a low temperature propane flame to minimise inter-element interference. The samples were bracketed with two standard solutions covering a small concentration range. Errors due to flame, atomiser and electronics fluctuations were minimised by constant monitoring of Li internal standard.

Eight to twelve determinations of each solution resulted in standard errors of: less than 0.5% for greater than 2% Na_2O; less than 1% for up to 2% Na_2O; and less than 4% for less than 0.1% Na_2O. Agreement between duplicates was within error of solution measurements.

B.6.2 Ferrous Iron

The samples were dissolved in HF in the presence of excess NH_4VO_3. The excess metavanadate was back-titrated using $Fe(NH_4)_2(SO_4)_2$ solution standardised against BDH standard ceric sulphate. The agreement of duplicate FeO determinations was within ±1% relative.

B.6.3 Water/Carbon Dioxide.

H_2O- was determined by weight loss after 2 hours at 110°C. H_2O+ and CO_2 were determined after H_2O- by heating samples at 1100°C in a gas stream (nitrogen for rocks, and air for minerals) and collecting H_2O in P_2O_5, and CO_2 in "carbasorb" soda asbestos microabsorption tubes. Samples were heated for ½ hour, except biotites which were heated for 1 to 1½ hours. Air stream was used for minerals to minimise effects of ferrous iron reduction of H_2O to H_2 but problems were still encountered with biotite, and biotite waters recorded may be low. The standard errors for ten determinations on a standard rock run to check system efficiency were 1.7% for H_2O and 9% for CO_2.

B.6.4 Fluorine

The samples were fused with Na_2CO_3 and fusion cakes dissolved in water. Fluoride ions were complexed with $La(NO_3)_2$ solution and alizarin complexan after interfering ions had first been precipitated. Absorbance was measured at 620 millimicrons in a Unicam spectrophotometer. Good agreement was observed between "preferred" and measured F values for G-2 but low values were measured for GSP-1 (about 30% low) and fluorines reported may be low.

B.7 AGREEMENT BETWEEN ANALYTICAL TECHNIQUES

The agreement of trace element data obtained from XRF, MS7, emission (ES) and gamma (GS) spectroscopy techniques was satisfactory. Least squares linear regression on y (ES, GS or MS7 ppm or %) versus x (XRF ppm or %) is set out in the form $y = mx + b$ with correlation coefficient "r" (see table B.7.1). For a 99.99% level of confidence "r"

TABLE B.7.1

CORRELATION BETWEEN ANALYTICAL TECHNIQUES

Element	Technique for y (x is XRF)	r	m	b
Co ppm	ES	0.935	1.415	1.14
Ni ppm	ES	0.998	1.185	3.91
Cu ppm	ES	0.989	1.198	1.19
V ppm	ES	0.981	1.086	2.11
Cr ppm	ES	0.997	0.999	6.74
Rb ppm	ES	0.973	1.111	-0.140
Ba ppm	ES	0.989	1.016	7.59
Ba ppm	MS7	0.932	1.042	45.2
La ppm	MS7	0.965	0.984	-0.644
Ce ppm	MS7	0.938	1.058	-2.50
Pr ppm	MS7	0.982	1.293	0.165
Nd ppm	MS7	0.980	1.314	-0.458
K%	GS	0.997	0.958	-0.009

XRF-ES Comparisons are for 60 samples

XRF-MS7 " " " 16 "

XRF-GS " " " 25 "

TABLE B.7.2

Uranium and Thorium

	XRF	MS7	GS
U	< 2	0.7	0.7
Th	49	39	51
U	< 2	0.2	0.1
Th	< 2	0.2	~0
U	< 2	0.4	0.4
Th	< 2	1.0	0.9
U	< 2	0.1	0.2
Th	< 2	0.3	0.2
U	< 2	0.3	0.4
Th	< 2	0.5	0.6
U	< 2	2.8	2.5
Th	13	15	13.5
U	< 2	0.3	0.5
Th	7.7	5.1	6.2
U	< 2	0.5	0.7
Th	11	7	10.6
U	< 2	0.4	0.3
Th	3.2	2.5	2.9

	MS7	Isotope Dilution
U	0.4	0.20
Th	0.5	0.34
U	1.2	1.3
Th	8	10

Light REE

	XRF	MS7	XRF	MS7
La	60	68	34	33
Ce	135	143	81	69
Pr	13	20	8	12
Nd	45	67	35	45
La	23	20	57	50
Ce	41	35	115	125
Pr	4	4	12	15
Nd	10	14	44	53
La	7	8	55	63
Ce	18	20	128	185
Pr	< 2	2.5	15	19
Nd	9	10	50	72
La	5	5.5	17	17
Ce	11	17	28	28
Pr	2	2.1	2	2.8
Nd	8	8.9	6	8.5
La	34	30	9	9.7
Ce	66	64	27	36
Pr	6	8	4	6
Nd	16	28	21	26
La	53	37	57	56
Ce	112	90	118	114
Pr	11	13	12	16
Nd	40	47	45	57
La	9	9.7	69	62
Ce	38	31	116	117
Pr	5	6	14	18
Nd	18	24	49	64
La	61	47	40	26
Ce	109	95	53	47
Pr	11	13	5	7
Nd	38	42	19	22

Barium

XRF	MS7	ES
734	775	830
43	66	56
91	126	100
420	500	480
737	676	620
464	392	420
664	---	680
960	980	960
603	786	620
858	703	850
10	13	16
863	924	910
100	151	130
1154	1240	1150
846	925	890
557	650	610

TABLE C.1

BASIC GNEISSES : MAJOR ELEMENT DATA

	AMPHIBOLITES				"PYROXENITES" OR PICRITIC THOLEIITES					
	69-1501	69-775	69-782	69-794	69-739	69-756	69-786	69-785	69-1352	69-788
SiO_2	47.88	49.41	54.55	44.54	47.19	52.21	52.00	53.33	44.76	43.34
TiO_2	0.71	0.93	1.27	3.62	0.48	0.37	0.46	0.45	2.21	2.22
Al_2O_3	15.17	14.89	13.69	12.59	8.19	2.87	5.83	5.95	7.20	6.03
Fe_2O_3	2.10	2.18	3.26	2.83	1.97	0.30	1.31	1.59	3.78	5.19
FeO	8.66	8.54	8.23	13.85	8.82	9.33	13.69	13.39	12.70	11.87
MnO	0.19	0.17	0.18	0.21	0.18	0.21	0.28	0.27	0.25	0.24
MgO	7.90	6.83	4.18	5.04	23.94	20.20	15.79	17.62	16.76	16.30
CaO	11.92	11.08	7.52	9.63	6.38	12.97	6.32	3.85	7.84	8.02
Na_2O	2.91	3.28	2.94	2.33	0.96	0.38	1.20	1.16	0.97	0.55
K_2O	0.92	1.13	2.60	3.08	0.48	0.06	0.68	0.67	1.79	2.53
P_2O_5	0.05	0.11	0.31	0.46	0.08	0.07	0.15	0.11	0.11	0.29
H_2O+	1.15	1.08	1.05	0.89	0.69	0.14	0.58	0.74	0.76	1.61
H_2O-	0.19	0.13	0.01	0.12	0.07	0.17	0.20	0.14	0.07	0.20
CO_2	0.21	0.12	0.24	0.09	0.31	0.75	0.60	0.52	0.09	0.88
S	0.06	0.01	0.02	0.01	0.06	0.32	0.06	0.06	0.02	0.21
$Cr_2O_3 + V_2O_5$	0.07	0.08	0.12*	0.15*	Cr_2O_3+NiO 0.62	0.30	0.20	0.26	0.26	0.33**
TOTAL	100.09	99.97	100.25	99.44	100.42	100.65	99.35	100.11	99.57	99.92
O = S	0.03	0.01	0.01	0.01	0.03	0.16	0.03	0.03	0.01	0.11
CORRECTED TOTAL	100.06	99.96	100.24	99.43	100.39	100.49	99.32	100.08	99.56	99.81
Molar MgO/(MgO+FeO)	0.619	0.588	0.475	0.393	0.829	0.794	0.673	0.701	0.702	0.710
Molar $Fe_2O_3/(Fe_2O_3$ +FeO)	0.10	0.10	0.15	0.08	0.09	0.01	0.04	0.05	0.12	0.16
W+%Na_2O/K_2O	3.2	2.9	7.1	0.76	2.0	6.3	1.8	1.7	0.54	0.22

* Includes Rb_2O + BaO
** Includes BaO

69-739 is tabulated separately so that the sequence 69-756 to 69-788 is not disrupted.

TABLE C.1 (Cont'd)

BASIC GNEISSES : MAJOR ELEMENT DATA

LOSS-FREE MAJORS

	AMPHIBOLITES				"PYROXENITES" OR PICRITIC THOLEIITES					
	69-1501	69-775	69-782	69-794	69-739	69-756	69-786	69-785	69-1352	69-788
SiO_2	48.63	50.08	55.27	45.04	47.70	52.77	52.73	54.09	45.18	44.54
TiO_2	0.72	0.94	1.29	3.66	0.49	0.37	0.47	0.46	2.23	2.28
Al_2O_3	15.41	15.09	13.87	12.73	8.28	2.90	5.91	6.03	7.27	6.20
Fe_2O_3	2.13	2.21	3.30	2.86	1.99	0.30	1.33	1.61	3.82	5.33
FeO	8.80	8.66	8.34	14.01	8.92	9.43	13.88	13.58	12.82	12.20
MnO	0.19	0.17	0.18	0.21	0.18	0.21	0.28	0.27	0.25	0.25
MgO	8.02	6.92	4.24	5.10	24.20	20.42	16.01	17.87	16.92	16.75
CaO	12.11	11.23	7.62	9.74	6.45	13.11	6.41	3.90	7.91	8.24
Na_2O	2.96	3.32	2.98	2.36	0.97	0.38	1.22	1.18	0.98	0.57
K_2O	0.93	1.15	2.63	3.11	0.49	0.06	0.69	0.68	1.81	2.60
P_2O_5	0.05	0.11	0.31	0.47	0.08	0.07	0.15	0.11	0.11	0.30
S	0.06	0.01	0.02	0.01	0.06	0.32	0.06	0.06	0.02	0.22
Total Fe as FeO	10.72	10.65	11.31	16.58	10.71	9.70	15.08	15.03	16.26	17.00
W+%Na_2O + K_2O	3.89	4.47	5.61	5.47	1.46	0.44	1.91	1.86	2.79	3.17

69-739 is tabulated separately so that the sequence 69-756 to 69-788 is not disrupted

TABLE C.1

BASIC GNEISSES : MAJOR ELEMENT DATA

HORNBLENDE GRANULITES & PARTLY REHYDRATED PYROXENE GRANULITES

	69-744	69-1167	69-742	69-753	69-1396	69-790	69-937	69-1354	69-1175	69-748	69-1397
SiO_2	49.40	48.49	48.41	48.60	48.26	52.05	49.77	52.27	47.36	49.93	48.34
TiO_2	0.67	0.80	0.81	0.86	1.15	1.18	1.26	1.43	1.59	2.29	2.54
Al_2O_3	16.04	16.26	15.41	14.94	15.01	14.28	13.91	15.63	15.84	12.95	13.87
Fe_2O_3	1.28	3.41	1.87	2.01	0.76	1.58	2.00	1.20	3.14	3.83	2.01
FeO	9.59	6.18	8.79	9.20	11.49	8.57	10.60	10.97	10.93	12.68	13.07
MnO	0.19	0.21	0.18	0.19	0.21	0.18	0.17	0.19	0.22	0.24	0.25
MgO	8.37	6.34	9.63	7.23	8.44	5.68	6.64	5.39	7.03	4.46	5.85
CaO	11.60	12.94	10.84	12.00	11.45	8.73	10.34	8.58	9.66	8.80	9.66
Na_2O	1.81	2.99	1.76	2.94	1.85	2.81	3.26	2.99	2.10	2.46	2.38
K_2O	0.46	0.85	0.50	0.85	0.35	3.84	1.24	0.48	1.07	1.34	0.89
P_2O_5	0.10	0.03	0.08	0.06	0.10	0.16	0.16	0.47	0.24	0.32	0.39
H_2O+	0.37	1.01	0.69	1.05	0.52	0.68	1.00	0.26	0.86	0.96	0.69
H_2O-	0.05	0.11	0.13	0.08	0.10	0.11	0.08	0.07	0.05	0.06	0.08
CO_2	0.42	0.67	0.48	0.35	0.34	0.14	0.11	0.37	0.28	0.33	0.49
S	0.08	0.05	0.05	0.11	0.12	0.06	0.01	0.12	0.12	0.14	0.17
$Cr_2O_3 + V_2O_5$	0.09*	0.12	0.11	0.08	0.08	0.15**	0.08	0.06	0.04*	0.08	0.08
TOTAL	100.52	100.46	99.74	100.55	100.23	100.20	100.63	100.48	100.53	100.87	100.76
O = S	0.04	0.03	0.02	0.06	0.06	0.03	0.01	0.06	0.06	0.07	0.09
CORRECTED TOTAL	100.48	100.43	99.72	100.49	100.17	100.17	100.62	100.42	100.47	100.80	100.67
Molar MgO/(MgO+FeO)	0.609	0.646	0.661	0.583	0.567	0.542	0.527	0.467	0.534	0.385	0.444
Molar $Fe_2O_3/(Fe_2O_3 + FeO)$	0.06	0.20	0.09	0.09	0.03	0.08	0.08	0.05	0.11	0.12	0.07
W+%Na_2O/K_2O	3.9	3.5	3.5	3.5	5.3	0.73	2.6	6.2	2.0	1.8	2.7

* Cr_2O_3 + NiO; ** includes Rb_2O + BaO

TABLE C.1 (Cont'd)

BASIC GNEISSES : MAJOR ELEMENT DATA

HORNBLENDE GRANULITES & PARTLY REHYDRATED PYROXENE GRANULITES

LOSS-FREE MAJORS

	69-744	69-1167	69-742	69-753	69-1396	69-790	69-937	69-1354	69-1175	69-748	69-1397
SiO_2	49.81	49.37	49.05	49.33	48.73	52.53	50.37	52.64	47.93	50.61	48.95
TiO_2	0.68	0.81	0.82	0.87	1.16	1.19	1.28	1.44	1.61	2.32	2.57
Al_2O_3	16.17	16.56	15.61	15.16	15.16	14.41	14.08	15.74	16.03	13.13	14.05
Fe_2O_3	1.29	3.47	1.89	2.04	0.77	1.59	2.02	1.21	3.18	3.88	2.04
FeO	9.67	6.29	8.91	9.34	11.60	8.65	10.73	11.05	11.06	12.85	13.24
MnO	0.19	0.21	0.18	0.19	0.21	0.18	0.17	0.19	0.22	0.24	0.25
MgO	8.44	6.46	9.76	7.34	8.52	5.73	6.72	5.43	7.11	4.52	5.92
CaO	11.70	13.18	10.98	12.18	11.56	8.81	10.46	8.64	9.78	8.92	9.78
Na_2O	1.83	3.04	1.78	2.98	1.87	2.84	3.30	3.01	2.13	2.49	2.41
K_2O	0.46	0.87	0.51	0.86	0.35	3.88	1.25	0.48	1.08	1.36	0.90
P_2O_5	0.10	0.03	0.08	0.06	0.10	0.16	0.16	0.47	0.24	0.32	0.39
S	0.08	0.05	0.05	0.11	0.12	0.06	0.01	0.12	0.12	0.14	0.17
total Fe as FeO	10.83	9.41	10.61	11.18	12.29	10.08	12.55	12.14	13.92	16.34	15.07
W+%Na_2O + K_2O	2.29	3.91	2.29	3.84	2.22	6.72	4.55	3.49	3.21	3.85	3.31

TABLE C.1 (Cont'd)

BASIC GNEISSES : MAJOR ELEMENT DATA

PYROXENE GRANULITES

	69-1351*	69-1359	69-1371	69-1166	69-1366	69-1374	69-1346	69-743
SiO_2	49.88	51.30	49.95	49.47	47.86	49.93	49.49	47.97
TiO_2	1.02	1.14	1.30	1.33	1.56	1.64	2.62	2.69
Al_2O_3	13.70	14.05	13.81	13.56	15.98	13.86	14.36	12.91
Fe_2O_3	3.08	2.90	4.25	3.70	0.87	0.76	4.35	5.76
FeO	9.71	10.46	9.72	10.61	13.11	12.90	12.01	11.21
MnO	0.23	0.22	0.23	0.24	0.21	0.22	0.26	0.27
MgO	7.12	7.37	6.81	6.77	6.91	6.94	6.06	6.05
CaO	11.71	10.66	10.96	10.72	10.26	11.01	8.76	10.13
Na_2O	2.62	0.78	2.37	2.52	1.54	1.91	0.84	1.52
K_2O	0.28	0.18	0.15	0.27	0.34	0.45	0.33	0.29
P_2O_5	0.11	0.10	0.16	0.16	0.108	0.10	0.40	0.35
H_2O+	0.42	0.25	0.16	0.22	0.16	0.19	0.10	0.14
H_2O-	0.04	0.06	0.05	0.05	0.05	0.14	0.05	0.04
CO_2	0.49	0.15	0.32	0.64	0.31	0.44	0.50	0.76
S	0.12	0.13	0.12	0.40	0.03	0.14	0.18	0.17
$Cr_2O_3 + V_2O_5$	0.06	0.05	0.06	0.07	0.07	0.07	0.08	0.08
TOTAL	100.59	99.80	100.42	100.73	100.34	100.70	100.39	100.34
O = S	0.06	0.07	0.06	0.20	0.02	0.07	0.09	0.09
CORRECTED TOTAL	100.53	99.73	100.36	100.53	100.32	100.63	100.30	100.25
Molar MgO/(MgO + FeO)	0.566	0.557	0.555	0.532	0.484	0.489	0.473	0.490
Molar $Fe_2O_3/(Fe_2O_3 + FeO)$	0.13	0.11	0.16	0.14	0.03	0.03	0.14	0.19
W+%Na_2O/K_2O	9.4	4.3	16	9.3	4.5	4.2	2.6	5.2

* 69-1351 has minor hornblendic patches

TABLE C.1 (Cont'd)

BASIC GNEISSES : MAJOR ELEMENT DATA

PYROXENE GRANULITES

LOSS-FREE MAJORS

	69-1351*	69-1359	69-1371	69-1166	69-1366	69-1374	69-1346	69-743
SiO_2	50.35	51.54	50.21	49.92	48.11	50.31	49.81	48.43
TiO_2	1.03	1.15	1.31	1.34	1.57	1.65	2.64	2.72
Al_2O_3	13.83	14.11	13.88	13.68	16.06	13.97	14.45	13.03
Fe_2O_3	3.11	2.91	4.27	3.73	0.87	0.77	4.38	5.81
FeO	9.80	10.51	9.77	10.71	13.18	13.00	12.09	11.32
MnO	0.23	0.22	0.23	0.24	0.21	0.22	0.26	0.27
MgO	7.19	7.40	6.85	6.83	6.95	6.99	6.10	6.11
CaO	11.82	10.71	11.02	10.82	10.31	11.09	8.82	10.23
Na_2O	2.64	0.78	2.38	2.54	1.55	1.92	0.85	1.53
K_2O	0.28	0.18	0.15	0.27	0.34	0.45	0.33	0.29
P_2O_5	0.11	0.10	0.16	0.16	1.09	0.10	0.40	0.35
S	0.12	0.13	0.12	0.40	0.03	0.14	0.18	0.17
total Fe as FeO	12.60	13.13	13.61	14.07	13.96	13.69	16.03	16.55
W+%Na_2O + K_2O	2.92	0.96	2.53	2.81	1.89	2.37	1.18	1.82

* 69-1351 has minor hornblendic patches

TABLE C.1 (Cont'd)

BASIC GNEISSES : MAJOR ELEMENT DATA

CALC-SILICATES

	69-939	69-777
SiO_2	60.49	48.64
TiO_2	0.02	0.15
Al_2O_3	0.27	9.39
Fe_2O_3	0.68	1.15
FeO	5.55	2.78
MnO	0.66	0.43
MgO	11.47	14.01
CaO	20.47	21.02
Na_2O	0.13	0.56
K_2O	0.11	0.76
P_2O_5	0.20	0.02
H_2O+	0.17	0.83
H_2O-	0.07	0.04
CO_2	0.46	0.59
S	0.01	0.01
BaO + SrO	-	0.11
TOTAL	100.77	100.47
O = S	0.01	0.01
CORRECTED TOTAL	100.76	100.46
Molar MgO/(MgO + FeO)	0.786	0.900
Molar $Fe_2O_3/(Fe_2O_3$ + FeO)	0.05	0.16
W+%Na_2O/K_2O	1.2	0.77

TABLE C.2 BASIC GNEISSES : TRACE ELEMENT DATA

PYROXENE GRANULITES

	69-1351	69-1359	69-1371	69-1166	69-1366	69-1374	69-1346	69-743
Rb	2.3	3.4	2.7	5.5	4.2	10	11	5.0
Ba	43	18	24	84	91	131	64	56
Sr	71	30	73	135	93	110	52	59
Ga	14	15	15	16	22	20	19	17
Th	∿0*	4.1*	1.0*	0.7*	0.9*	1.4*	1.0*	<2.3
U	0.1*	0.9*	0.6*	0.6*	0.4*	0.5*	0.8*	<1.7
Pb	∿4	∿6	10	13	10	9	10	6
Zr	55	65	86	93	83	107	169	170
Nb	3.1	4.0	9.3	4.7	9.3	6.0	18	16
Hf	2.1	-	-	-	2.2	-	-	-
La	5	20	11	14	55	12	34	21
Ce	∿11	59	24	30	128	29	85	50
Pr	<3	7	<3	∿3	15	∿5	11	∿5
Nd	∿8	24	∿7	14	50	13	45	21
Y	19	25	24	25	36	21	49	51
Sc	51	46	41	39	35	35	46	44
V	234	276	274	295	266	318	363	365
Cr	136	134	91	94	171	66	110	119
Co	60*	35	55*	31	27	34	24	31
Ni	60	58	55	58	57	62	41	41
Cu	37	38	35	119	∿2	61	32	40
Zn	89	128	108	109	128	96	167	162
Li	-	-	-	7	6	-	16	-
K/Rb	1011	440	461	408	672	382	249	482
Zr/Nb	18	16	9.2	20	8.9	18	9.4	11
Zr/Hf	26	-	-	-	38	-	-	-
				LOSS-FREE TRACE DATA				
Rb	2.3	3.4	2.7	5.5	4.2	10	11	5.0
Ba	43	18	24	85	92	132	64	57
Sr	72	30	73	136	94	111	52	60
Pb	4	6	10	13	10	9	10	6
La	5	20	11	14	55	12	34	21
Ce	11	59	24	30	129	29	86	51
Y	19	25	24	25	36	21	49	52
Sc	52	46	41	39	41	35	46	44
V	236	277	276	298	267	320	365	369
Cr	137	135	92	95	172	67	111	120
Co	61	35	55	31	27	34	24	31
Ni	61	58	55	59	57	63	41	41
Cu	37	38	35	120	2	61	32	40
Zn	90	129	109	110	129	97	168	164
Zr	56	65	87	94	83	108	170	172

TABLE C.2 (Cont'd)

BASIC GNEISSES : TRACE ELEMENT DATA

HORNBLENDE GRANULITES & PARTLY REHYDRATED PYROXENE GRANULITES

	69-744	69-1167	69-742	69-753	69-1396	69-790	69-937	69-1354	69-1175	69-748	69-1397
Rb	8.7	15	12	11	8.9	273	30	2.7	45	57	30
Ba	134	87	99	33	85	432	42	127	241	276	267
Sr	148	162	58	112	165	142	132	109	175	156	162
Ga	12	43	14	14	16	17	16	19	19	18	19
Th	<2.3	<2.3	<2.3	<2.3	0.6*	∿6	<2.3	1.4*	<2.3	∿7	∿3
U	<1.7	<1.7	<1.7	<1.7	0.2*	<1.7	<1.7	0.5*	<1.7	∿2	<1.7
Pb	10	10	∿6	12	7	18	18	11	15	13	∿8
Zr	42	20	46	50	54	107	74	62	102	198	174
Nb	10	<0.8	7.6	3.2	5.8	8.0	4.0	8.5	6	14	13
Hf	-	-	-	-	-	-	-	-	-	-	-
La	5	7	6	5	5	25	13	29	10	28	21
Ce	16	12	19	12	19	53	23	71	29	57	49
Pr	∿3	<3	<3	<3	<3	∿5	∿3	10	∿3	∿6	∿3
Nd	∿8	∿7	11	∿8	∿7	21	15	31	∿12	31	21
Y	16	9	16	17	16	35	45	23	23	41	38
Sc	36	48	30	33	32	30	44	33	36	34	31
V	205	337	195	256	270	220	321	233	234	369	340
Cr	485	404	507	266	202	227	149	114	121	75	162
Co	60*	50	49*	39	42	27	34	27	45	28	36
Ni	156	108	162	74	163	56	56	62	139	42	79
Cu	79	5	7	46	128	88	5*	37	116	227	86
Zn	76	113	124	81	104	125	116	146	108	141	140
Li	31					47					
K/Rb	439	470	346	641	326	117	343	1476	197	195	246
Zr/Nb	4.2	-	6.1	16	9.3	13	19	7.3	17	14	13
Zr/Hf	-	-	-	-	-	-	-	-	-	-	-
					CS	3.5					

TABLE C.2 (Cont'd)

BASIC GNEISSES : TRACE ELEMENT DATA

HORNBLENDE GRANULITES & PARTLY REHYDRATED PYROXENE GRANULITES

LOSS-FREE TRACE DATA

	69-744	69-1167	69-742	69-753	69-1396	69-790	69-937	69-1354	69-1175	69-748	69-1397
Rb	8.7	15	12	11	8.9	276	30	2.7	45	58	30
Ba	135	89	100	33	86	436	42	128	244	280	270
Sr	149	165	59	114	167	143	134	110	177	158	164
Pb	10	10	6	12	7	18	18	11	15	13	8
La	5	7	6	5	5	25	13	29	10	28	21
Ce	16	12	19	12	19	54	23	72	29	58	50
Y	16	9	16	17	16	35	45	23	23	41	38
Sc	36	48	30	33	32	30	44	33	36	34	31
V	207	343	198	260	273	222	325	235	237	374	344
Cr	489	411	514	270	204	229	151	115	123	76	164
Co	61	51	50	39	42	27	34	27	45	28	36
Ni	157	110	164	75	165	57	57	62	141	42	80
Cu	80	5	7	46	129	89	5	37	117	230	87
Zn	77	115	126	82	105	126	117	147	109	143	142
Zr	42	20	47	51	55	108	75	62	103	201	176

TABLE C.2 (Cont'd)

BASIC GNEISSES : TRACE ELEMENT DATA

	AMPHIBOLITES				PYROXENITES					
LOSS-FREE TRACE DATA										
	69-1501	69-775	69-782	69-794	69-739	69-756	69-786	69-785	69-1352	69-788
Rb	11	36	88	159	15	0.95	32	37	45	108
Ba	32	101	673	706	128	26	181	178	223	757
Sr	119	181	181	60	77	76	81	86	97	136
Pb	15	12	21	29	4	8	6	11	16	9
La	3	7	9	64	8	9	10	9	20	35
Ce	8	18	27	130	14	38	26	19	47	83
Y	14	27	37	79	12	16	19	12	20	18
Sc	34	40	36	32	24	46	31	32	29	25
V	231	256	200	258	140	180	140	110	241	215
Cr	237	261	19	84	3421	1858	1042	1302	1053	1053
Co	44	36	37	30	101	62	71	89	91	76
Ni	80	69	36	48	1059	230	437	571	839	808
Cu	19	5	64	0	45	95	27	21	1	196
Zn	73	85	118	252	75	80	249	218	144	144
Zr	34	63	202	248	59	38	70	85	125	151

TABLE C.2 (Cont'd)

BASIC GNEISSES : TRACE ELEMENT DATA

	AMPHIBOLITES				PYROXENITES						CALC-SILICATES	
	69-1501	69-775	69-782	69-794	69-739	69-756	69-786	69-785	69-1352	69-788	69-939	69-777
Rb	11	36	87	157	15	0.95	32	37	45	105	0.7	20
Ba	32	100	664	698	127	26*	178	175	221	737	∿8	670
Sr	117	179	179	59	76	75	80	85	96	132	38	324
Ga	13	15	15	24	8	5	10	9	11	10	<1.3	12
Th	1.1*	<2.3	9.3	5.7	∿2.5	0.4*	<2.3	<2.3	1.1*	3*	0.6*	<2.3
U	0.4*	<1.7	2.1	2	<1.7	0.2*	<1.7	<1.7	0.4*	0.9*	0.8*	<1.7
Pb	15	12	21	29	∿4	8	∿6	11	16	9	19	14
Zr	34	62	199	245	58	38	69	84	124	147	4	69
Nb	1.4	3.7	14	22	2	<0.8	5	5	30	36	<1.5	2
Hf	-	1.7	4.3	-	-	1.0	-	-	-	2.8	-	-
La	∿3	7	9	63	8	9	10	9	20	34	8	68
Ce	∿8	18	27	129	14	38	∿26	19	47	81	14	109
Pr	<3	<3	∿4	13	<3	5	∿3	<3	∿4	8	<2	8
Nd	<6	9	21	53	<6	18	15	13	17	35	<9	26
Y	14	27	37	78	12	16	19	12	20	18	5	7
Sc	34	40	36	32	24	46	31	32	29	25	n.d.*	n.d.*
V	227	253	197	255	138	178	138	108	239	209	6	7
Cr	233	257	19	83	3384	1838	1027	1284	1043	1024	<0.7	<1.1
Co	44	36	37*	30	100*	76*	70*	88*	90*	100*	<2.5	4
Ni	79	68	36	48	1048	228	431	563	831	786	<0.6	<1.3
Cu	19	5	63	<0.8	45	94	27	21	<1	191	<0.7	<0.8
Zn	72	84	116	249	74	79	245	215	143	140	22	85
Li	10	6	30	12	-	-	-	-	-	18		
Cs	-	-	-	-	-	-	-	-	-	4.6		
K/Rb	694	261	248	163	266	524	176	150	330	200	1302	303
Zr/Nb	24	17	14	11	29	-	14	17	4.1	4.1	-	35
Zr/HF	-	36	46	-	-	-	-	-	-	-	-	-

TABLE C.3

ACID GNEISSES : MAJOR ELEMENT DATA

	Garnet-symplectite Charnockites				High-potassium Garnet-free Charnockites			
	69-746	69-1381	69-938	69-1378	69-789	69-1372	69-954	69-956
SiO_2	67.17	69.48	69.71	73.12	64.88	65.76	66.05	66.52
TiO_2	0.68	0.71	0.63	0.49	0.88	0.85	0.85	0.81
Al_2O_3	13.62	12.39	12.63	12.64	15.56	14.84	15.06	14.99
Fe_2O_3	2.15	1.76	1.55	1.11	1.33	1.21	1.36	1.07
**FeO	4.92	5.08	4.22	3.22	4.47	4.18	4.06	4.20
MnO	0.13	0.12	0.08	0.07	0.09	0.08	0.08	0.08
MgO	0.33	0.27	0.28	0.18	1.37	1.41	1.27	1.18
CaO	3.10	2.82	2.61	1.98	3.96	3.49	3.49	3.40
Na_2O	2.98	2.54	2.70	3.01	2.92	2.93	2.91	2.95
K_2O	4.10	4.14	4.60	3.98	4.33	4.42	4.53	4.54
P_2O_5	0.17	0.21	0.19	0.11	0.25	0.24	0.29	0.24
H_2O+	0.33	0.29	0.27	0.18	0.29	0.20	0.27	0.14
H_2O-	0.09	0.14	0.11	0.07	0.10	0.13	0.06	0.07
CO_2	0.10	0.15	0.11	0.12	0.16	0.08	0.11	0.12
S	0.02	0.04	0.02	0.01	0.03	0.03	0.02	0.02
$BaO + ZrO_2$	0.19	0.19	0.19	0.16	0.14	0.13	0.13	0.13
TOTAL	100.08	100.33	99.90	100.45	100.77	99.98	100.54	100.46
O = S	0.01	0.02	0.01	-	0.01	0.01	0.01	0.01
CORRECTED TOTAL	100.07	100.31	99.89	100.45	100.76	99.97	100.53	100.45
** total Fe as FeO	6.85	6.66	5.61	4.22	5.67	5.27	5.28	5.16
Molar MgO/(FeO + MgO)	0.107	0.087	0.106	0.091	0.353	0.375	0.358	0.334
Molar $Fe_2O_3/(FeO + Fe_2O_3)$	0.16	0.13	0.14	0.13	0.12	0.12	0.13	0.10
W+%Na_2O/K_2O	0.73	0.61	0.59	0.76	0.67	0.66	0.64	0.65

TABLE C.3 (Cont'd)

ACID GNEISSES : MAJOR ELEMENT DATA

	Compositionally Banded Charnockites				Garnet Gneisses					
	69-1367	69-787	69-951	69-1363	69-948	69-944	69-942	69-1355*	69-1375	69-1348
SiO_2	67.20	68.58	69.68	73.34	66.18	67.20	67.66	68.95	68.45	70.67
TiO_2	0.45	0.41	0.43	0.29	0.53	0.54	0.59	0.57	0.72	0.41
Al_2O_3	17.03	15.71	15.08	14.01	15.24	15.19	17.77	13.94	14.74	14.20
Fe_2O_3	0.14	1.61	1.15	1.07	0.07	0.49	0.48	0.72	0.02	0.21
** FeO	2.71	2.51	2.51	1.31	8.02	5.51	2.05	4.23	4.62	3.73
MnO	0.03	0.07	0.07	0.03	0.18	0.08	0.02	0.05	0.06	0.05
MgO	1.30	1.15	1.17	0.49	3.17	2.89	1.30	1.67	1.97	2.28
CaO	4.31	3.86	3.91	2.98	1.43	1.93	0.38	2.56	1.98	1.68
Na_2O	4.60	4.57	3.84	3.60	1.75	2.42	1.73	3.17	2.85	3.47
K_2O	1.37	1.29	1.88	2.50	1.82	2.74	6.33	3.48	3.74	2.57
P_2O_5	0.05	0.13	0.18	0.07	0.04	0.03	0.13	0.25	0.09	0.04
H_2O+	0.52	0.27	0.27	0.39	0.49	0.38	1.30	0.35	0.58	0.33
H_2O-	0.15	0.07	0.06	0.07	0.07	0.02	0.19	0.07	0.05	0.05
CO_2	0.41	0.11	0.12	0.18	0.51	0.41	0.07	0.17	0.13	0.06
S	0.04	0.01	0.01	0.00	0.21	0.15	0.01	0.03	0.04	0.01
BaO + ZrO_2	0.11	0.09	0.13	0.11	0.08	0.06	0.13	0.11	0.12	0.10
TOTAL	100.42	100.44	100.49	100.44	99.79	100.04	100.14	100.32	100.16	99.86
O = S	0.02	-	-	-	0.11	0.08	-	0.02	0.02	-
CORRECTED TOTAL	100.40	100.44	100.49	100.44	99.68	99.96	100.14	100.30	100.14	99.86
** total Fe as FeO	2.84	3.96	3.55	2.27	8.08	5.95	2.48	4.88	4.64	3.92
Molar MgO/(FeO + MgO)	0.461	0.449	0.454	0.400	0.413	0.483	0.531	0.413	0.432	0.521
Molar $Fe_2O_3/(FeO+Fe_2O_3)$	0.02	0.22	0.17	0.27	0.004	0.04	0.10	0.07	0.002	0.02
W+%Na_2O/K_2O	3.4	3.5	2.0	1.4	0.96	0.88	0.27	0.91	0.76	1.4

* 69-1355 is a migmatitic garnetiferous charnockite transitional to the banded charnockites and garnet gneisses

TABLE C.4

ACID GNEISSES : TRACE ELEMENT DATA

	Garnet-symplectite Charnockites				High-potassium Garnet-free Charnockites			
	69-746	69-1381	69-938	69-1378	69-789	69-1372	69-954	69-956
Rb	90	87	103	82	161	192	198	200
Ba	960	1019	1154	776	894	858	850	856
Sr	135	135	147	109	198	176	175	173
Ga	22	19	21	19	19	17	18	18
Th	10.6*	12	6.2*	10.7	11*	13.5*	20	18
U	0.7*	<1.9	0.5*	0.4*	1.7*	2.5*	∿2	2.1*
Pb	25	24	28	28	27	27	27	28
Zr	568	566	447	546	277	264	266	266
Nb	15	18	15	14	15	14	15	15
Hf	8.3*	-	11.7*	-	-	9.7*	-	4.6*
La	57	67	57	50	52	53	56	51
Ce	118	139	115	103	114	112	115	109
Pr	12	14	12	12	11	11	12	11
Nd	45	50	44	37	41	40	43	38
Y	66	83	49	51	37	35	36	36
Sc	11	10	10	5	14	14	15	13
V	5	4	∿2	∿1	48	44	44	40
Cr	<0.7	<0.7	<0.7	∿2	23	24	22	21
Co	6	<2.5	<2.5	<2.5	8	15	8	10
Ni	<0.6	∿1	∿1	<0.6	11	9	10	17
Cu	3	6	4	∿1	23	25	23	26
Zn	79	88	85	58	78	71	69	71
Cs	-	-	-	-	1.7	1.9	2.0	2.1
Li	6	4	2	6	32	26	27	14
K/Rb	378	395	371	403	223	191	190	188
K/Ba	35.5	33.7	33.1	42.6	40.2	42.8	44.2	44.0
K/Cs x 10^{-3}	-	-	-	-	21.1	19.3	18.8	17.9
Rb/Cs	-	-	-	-	95	101	99	95
Ba/Rb	10.7	11.7	11.2	9.4	5.6	4.5	4.3	4.3
Ba/Sr	7.1	7.5	7.8	7.1	4.5	4.9	4.9	4.9
Zr/Nb	37.9	31.4	29.8	39.0	18.5	18.9	17.7	17.7
Zr/Hf	68	-	38	-	-	27	-	58
Th/U	15.1	-	12.4	26.8	6.5	5.4	∿10	8.6

TABLE C.4 (Cont'd)

ACID GNEISSES : TRACE ELEMENT DATA

	Compositionally Banded Charnockites				Garnet Gneisses					
	69-1367	69-787	69-951	69-1363	69-948	69-944	69-942	69-1355	69-1375	69-1348
Rb	20	13	33	47	25	39	234	71	95	66
Ba	420	603	663	692	464	912	873	747	734	567
Sr	339	286	186	173	115	208	191	181	134	71
Ga	19	19	16	15	15	13	24	17	17	14
Th	0.2*	0.6*	<1.9	10.5*	3.1*	4.7	38	6.6*	51*	2.9*
U	0.2*	0.3*	<1.9	0.3*	0.5*	<1.9	9.7	0.5*	0.7*	0.3*
Pb	17	10	11	17	15	14	47	19	14	9
Zr	100	188	155	199	436	223	219	254	262	135
Nb	3.8	5.3	6.1	2.9	5.3	27	23	7.7	27	13
Hf	2.1	2.8	-	-	18.5	-	3.5*	-	4.4	3.4
La	17	23	26	33	34	41	59	30	60	30
Ce	28	41	46	58	66	75	116	64	135	53
Pr	∿2	∿4	∿4	∿5	6	6	14	6	13	5
Nd	<9	10	∿10	∿15	16	24	49	23	45	∿19
Y	6	14	11	4	65	36	35	16	29	25
Sc	3	11	6	<3	27	22	7	9	11	7
V	42	40	44	17	105	96	55	53	72	71
Cr	13	9	12	6	168	153	67	52	58	122
Co	10	9	10	8	23	27	<2.5	10	15*	15*
Ni	9	5	4	3	115	70	12	19	18	33
Cu	3	4*	n.d*	4*	48	38	11	8	26	25
Zn	38	68	46	34	96	77	43	68	59	56
Cs	0.2*	0.1*	-	-	0.2*	-	1.6	-	-	0.6
Li	16	5	5	15	5	6	40	9	8	11

(Cs value for 69-942 is the average of mass spectrometer and emission spectroscope values)

TABLE C.4 (Cont'd)

ACID GNEISSES : TRACE ELEMENT DATA

	Compositionally Banded Charnockites				Garnet Gneisses					
	69-1367	69-787	69-951	69-1363	69-948	69-944	69-942	69-1355	69-1375	69-1348
K/Rb	569	824	473	442	604	583	225	407	327	323
K/Ba	27	18	24	30	33	25	60	39	42	38
K/Cs x 10^{-3}	57	107	-	-	76	-	32	-	-	36
Rb/Cs	100	130	-	-	125	-	146	-	-	110
Ba/Rb	21	46	20	15	19	23	3.7	10.5	7.7	8.6
Ba/Sr	1.2	2.1	3.6	4.0	4.0	4.4	4.6	4.1	5.5	8.0
Zr/Nb	26.3	35.5	25.4	68.6	82.3	8.3	9.5	33.0	9.7	10.4
Zr/Hf	48	67	-	-	24	-	63	-	60	40
Th/U	1.0	2.0	-	35	6.2	-	3.9	13.2	73	9.7

TABLE C.5

REACTION ZONE GNEISSES AND REACTANT ACID AND BASIC GNEISSES

	Series (1)			Series (2)			
	69-1374	69-1373	69-1375	69-1366	69-1368	69-1357	69-1367
SiO_2	49.93	67.91	68.45	47.86	55.71	64.88	67.20
TiO_2	1.64	0.79	0.72	1.56	1.47	0.65	0.45
Al_2O_3	13.86	14.75	14.74	15.98	14.56	14.80	17.03
Fe_2O_3	0.76	0.11	0.02	0.87	0.74	0.13	0.14
FeO	12.90	5.23	4.62	13.11	11.53	6.54	2.71
MnO	0.22	0.08	0.06	0.21	0.19	0.10	0.03
MgO	6.94	2.08	1.97	6.91	5.04	3.31	1.30
CaO	11.01	2.16	1.98	10.26	7.44	4.37	4.31
Na_2O	1.91	2.70	2.85	1.54	1.88	2.80	4.60
K_2O	0.45	3.61	3.74	0.34	0.29	1.05	1.37
P_2O_5	0.10	0.09	0.09	1.08	0.35	0.05	0.05
H_2O+	0.19	0.55	0.58	0.16	0.33	0.51	0.52
H_2O-	0.14	0.04	0.05	0.05	0.08	0.13	0.15
CO_2	0.44	0.11	0.13	0.31	0.60	0.87	0.41
S	0.14	0.05	0.04	0.03	0.18	0.16	0.04
* TOTAL	100.56	100.23	100.02	100.25	100.30	100.27	100.29
total Fe as FeO	12.58	5.33	4.64	13.89	12.20	6.66	2.84
Molar $Fe_2O_3/(Fe_2O_3 + FeO)$	0.03	0.009	0.002	0.03	0.03	0.009	0.02
$W+\%Na_2O/K_2O$	4.2	0.75	0.76	4.5	6.5	2.7	3.4

(* Total corrected for O = S)

TABLE C.5 (Cont'd)

REACTION ZONE GNEISSES AND REACTANT ACID AND BASIC GNEISSES

	Series (1)			Series (2)			
	69-1374	69-1373	69-1375	69-1366	69-1368	69-1357	69-1367
Rb	10	132	95	4.2	3.2	22	20
Ba	131	601	734	91	80	748	420
Sr	110	149	134	93	87	161	339
Ga	20	16	17	22	19	15	19
Th	1.4*	70*	51	0.9*	<2.3	∿2	0.2*
U	0.5*	0.8*	<1.9	0.4*	<1.7	<1.9	0.2*
Pb	9	26	14	10	∿5	9	17
Zr	107	270	262	83	71	208	100
Nb	6.0	22	27	9.3	10	8.6	3.8
Hf	-	-	4.4	2.2	-	-	2.1
La	12	86	60	55	20	21	17
Ce	29	188	135	128	46	35	28
Pr	∿5	21	13	15	∿4	∿3	∿2
Nd	∿13	68	45	50	21	12	<9
Y	21	42	29	36	25	31	6
Sc	35	13	11	41	34	19	3
V	318	77	72	266	242	125	42
Cr	66	68	58	171	81	153	13
Co	34	14*	15*	27	30	29	10
Ni	62	28	18	57	57	62	9
Cu	61	30	26	∿2	55	52	3
Zn	96	51	59	128	130	76	38
Li	-	-	-	6	9	9	16
K/Rb	382	227	327	672	752	396	569
Zr/Nb	18	12	9.7	8.9	7.1	24	26
Zr/Hf	-	-	60	38	-	-	48

TABLE C.5 (Cont'd)

REACTION ZONE GNEISSES AND REACTANT ACID AND BASIC GNEISSES

	Series (3)						
	69-1346	69-1349	70-1201	69-1347	69-1350	69-1348	(original) 69-1349
SiO_2	49.49	50.5	51.01	52.69	58.90	70.67	57.46
TiO_2	2.62	2.1	1.47	1.03	0.74	0.41	1.93
Al_2O_3	14.36	15.9	17.62	19.82	21.03	14.20	14.78
Fe_2O_3	4.35	4.5	1.23	0.39	0.22	0.21	4.17
FeO	12.01	8.9	12.21	9.85	3.64	3.73	8.24
MnO	0.26	0.2	0.15	0.16	0.04	0.05	0.20
MgO	6.06	3.9	7.16	5.51	2.14	2.28	3.65
CaO	8.76	5.8	2.73	2.11	3.34	1.68	5.42
Na_2O	0.84	3.0	3.43	3.05	6.40	3.47	2.79
K_2O	0.33	0.3	1.34	3.86	2.24	2.57	0.27
P_2O_5	0.40	0.3	0.07	0.05	0.03	0.04	0.25
H_2O+	0.10	-	0.59	0.75	0.41	0.33	0.17
H_2O-	0.05	-	0.08	0.09	0.06	0.05	0.04
CO_2	0.50	-	0.31	0.45	0.12	0.06	0.29
S	0.18	-	0.04	0.14	0.01	0.01	0.18
*TOTAL	100.22	-	99.42	99.88	99.32	99.76	99.75
total Fe as FeO	15.94	13.0	13.32	10.20	3.84	3.92	11.9
Molar $Fe_2O_3/(Fe_2O_3 + FeO)$	0.14	0.19	0.04	0.02	0.03	0.02	0.19
W+%Na_2O/K_2O	2.6	10	2.6	0.79	2.9	1.4	10

(* Total corrected for O = S)

TABLE C.5 (cont'd)

REACTION ZONE GNEISSES AND REACTANT ACID AND BASIC GNEISSES

	69-950	69-741	69-1361	69-1356	69-1377
SiO_2	41.92	57.81	69.45	68.57	51.79
TiO_2	2.45	1.38	0.47	1.14	0.80
Al_2O_3	18.70	14.71	14.44	14.15	20.66
Fe_2O_3	2.92	0.43	0.25	0.65	1.79
FeO	17.47	10.73	5.04	4.38	6.96
MnO	0.31	0.16	0.10	0.05	0.20
MgO	8.10	5.02	2.27	1.76	2.15
CaO	4.82	5.74	1.99	3.31	8.51
Na_2O	1.45	2.65	3.58	3.65	5.07
K_2O	0.25	0.62	1.52	1.76	1.05
P_2O_5	0.05	0.10	0.03	0.16	0.17
H_2O+	0.52	0.27	0.50	0.38	0.74
H_2O-	0.10	0.05	0.06	0.03	0.21
CO_2	1.02	0.64	0.08	0.26	0.12
S	0.20	0.23	0.01	0.02	0.02
*TOTAL	100.18	100.41	99.79	100.26	100.23
total Fe as FeO	20.10	11.12	5.27	4.97	8.57
Molar $Fe_2O_3/(Fe_2O_3 + FeO)$	0.07	0.02	0.02	0.06	0.10
W+%Na_2O/K_2O	5.8	4.3	2.4	2.1	4.8

(*Total corrected for O = S)

TABLE C.5 (Cont'd)

REACTION ZONE GNEISSES AND REACTANT ACID AND BASIC GNEISSES

	Series (3)						(original)					
	69-1346	69-1349	70-1201	69-1347	69-1350	69-1348	69-1349	69-950	69-741	69-1361	69-1356	69-1377
Rb	11	1.6	35	120	85	66	1.5	11	18	65	30	24
Ba	64	66	259	952	446	567	61	42	201	446	243	76
Sr	52	48	46	118	228	71	45	44	94	193	163	172
Ga	19	17	20	20	21	14	16	14	17	16	17	14
Th	1.0*	6.4	5.3	16*	2.3*	2.9*	5.9	<2.3	<1.9	7.0	9.5	41
U	0.8*		<1.7	1.0*	0.5*	0.3*	<1.9	<1.7	<1.9	<1.9	<1.9	3.4
Pb	10	∿5	12	13	50	9	∿5	7	9	37	20	28
Zr	169	156	151	217	351	135	145	117	113	204	290	1015
Nb	18	12	21	16	22	13	11	24	16	7.4	15	27
Hf	-	-	-	-	-	3.4	-	-	-	-	-	-
La	34	35	26	52	39	30	32	12	14	56	22	121
Ce	85	70	53	96	64	53	65	22	28	93	43	264
Pr	11	11	∿4	9	∿4	5	10	∿3	∿3	6	∿3	29
Nd	45	27	14	27	13	19	25	∿8	17	25	16	107
Y	49	48	29	44	30	25	45	65	25	34	13	146
Sc	46	38	29	23	9	7	35	45	26	14	6	11
V	363	246	250	226	88	71	228	360	210	79	85	78
Cr	110	30	82	310	249	122	28	∿6	148	139	67	n.d.
Co	49*	48*	-	38	16*	15*	45*	47*	-	-	11	9
Ni	41	55	57	114	58	33	51	47	72	42	13	19
Cu	32	30	16	44	<1	25	28	40	77	19	6*	∿2*
Zn	167	122	155	157	63	56	113	177	122	66	58	127
Li	16	10	15	22	18	11	9	-	-	-	-	-
K/Rb	249	1494	318	267	219	323	1494	189	286	194	487	363
Zr/Nb	9.4	13	7.2	14	16	10	13	4.9	7.1	28	19	38
Zr/Hf	-	-	-	-	-	40	-	-	-	-	-	-

APPENDIX TABLE C.6

MASS SPECTROMETER DATA

ACID GNEISSES

	69-746	69-938	69-956	69-1372	69-787	69-1367	69-942	69-948	69-1348	69-1375
La	56	50	47	37	20	15	62	30	26	68
Ce	114	125	95	90	35	28	117	64	47	143
Pr	16	15	13	13	4.3	2.8	18	8.0	6.7	20
Nd	57	53	42	45	14	8.5	64	28	22	67
Sm	12	12	7.9	9.1	2.6	1.6	12	7.7	4.0	11
Eu	2.8	3.5	1.6	2.1	0.78	0.97	1.9	1.6	1.1	1.4
Gd	12	11	7.4	8.5	3.0	1.7	10.6	10.2	4.3	9.2
Tb	1.8	1.7	1.1	1.3	0.46	0.29	1.3	1.9	0.76	1.2
Dy	13	13	7.7	10.2	3.1	2.0	8.7	15	5.3	8.8
Ho	2.8	2.5	1.4	1.7	0.53	0.26	1.3	3.3	1.0	1.1
Er	7.1	6.2	3.4	4.6	1.4	0.67	2.9	10.3	2.7	2.7
Yb	6.6	5.8	3.4	4.2	1.3	0.68	2.0	9.7	2.8	1.7

BASIC GNEISSES

	69-756	69-775	69-782	69-788	69-1351	69-1366
La	9.7	7.9	9.7	33	5.5	63
Ce	31	20	36	69	17	185
Pr	5.8	2.5	6.2	12	2.1	19
Nd	24	10.3	26	45	8.9	72
Sm	5.0	3.1	6.1	9.3	2.8	10.9
Eu	0.88	1.04	1.6	2.8	1.1	2.0
Gd	3.8	3.7	6.8	8.5	2.8	9.7
Tb	0.48	0.65	1.3	1.5	0.54	1.2
Dy	3.2	5.4	8.9	6.8	4.4	10.2
Ho	0.65	1.08	1.8	1.05	0.92	1.7
Er	1.6	2.7	5.1	2.4	2.6	4.5
Yb	1.4	2.7	4.8	2.2	2.3	3.9

APPENDIX 0.7

C.I.P.W. NORMS OF BASIC ROCKS

(Norms marked * or ** have Fe_2O_3/FeO adjusted to 0.2, and those marked ** have K_2O set to 0.6% as well.)

C.I.P.W. NORMS, WEIGHT PERCENTAGES.

	69-1351		69-1359		69-1371		69-1166	
QUARTZ	* .00	.22	* 9.14	11.13	* .89	2.82	* .48	2.99
ORTHOCLASE	1.65	1.69	1.07	1.09	.89	.91	1.67	1.64
ALBITE	22.16	22.59	4.94	6.78	20.05	20.51	21.27	21.84
ANORTHITE	24.78	24.26	34.50	35.24	24.59	24.20	24.65	24.81
DIOPSIDE	24.30	24.57	14.08	14.26	20.44	20.71	19.09	19.41
HYPERSTHENE	16.48	18.71	28.10	24.89	23.80	20.33	23.61	19.08
OLIVINE	3.80	.00	.00	.00	.00	.00	.00	.00
FE3O4	3.07	3.13	3.23	3.30	3.33	3.40	3.41	3.51
ILMENITE	1.94	1.97	2.18	2.22	2.47	2.52	2.51	2.59
APATITE	.26	.27	.24	.24	.38	.39	.38	.39
FES	.45	.46	.49	.50	.45	.46	1.49	1.53
CALCITE	1.11	1.14	.34	.35	.73	.74	1.48	1.49

C.I.P.W. NORMS, WEIGHT PERCENTAGES.

	69-1366		69-1374		69-1346		69-743	
QUARTZ	* 2.43	4.67	* 2.21	3.47	* 10.64	14.16	* 5.28	8.77
ORTHOCLASE	2.00	2.05	2.69	2.72	1.98	2.02	1.93	1.96
ALBITE	12.99	13.30	16.08	16.50	17.40	17.87	13.88	13.38
ANORTHITE	35.69	34.43	27.77	28.61	34.40	35.72	27.58	28.64
DIOPSIDE	5.12	5.19	19.12	19.41	2.70	2.74	13.03	13.23
HYPERSTHENE	31.94	28.40	24.02	20.00	31.68	25.68	27.18	21.34
FE3O4	3.40	3.49	3.32	3.41	3.91	4.04	4.03	4.19
ILMENITE	2.95	3.02	3.10	3.18	4.97	5.16	5.11	5.32
APATITE	2.58	2.61	.24	.24	.95	.98	.82	.86
FES	.11	.11	.52	.53	.67	.70	.64	.66
CALCITE	.70	.72	1.00	1.02	1.14	1.18	1.73	1.80

C.I.P.W. NORMS, WEIGHT PERCENTAGES.

	69-744		69-1167		69-742		69-753	
ORTHOCLASE	* 2.23	2.26	* 5.07	5.14	* 2.99	3.03	* 5.05	5.14
ALBITE	15.30	15.49	21.96	22.58	15.07	15.29	21.75	23.48
ANORTHITE	34.48	34.91	28.70	29.09	33.06	33.55	26.21	25.64
NEPHELINE	.00	.00	2.43	1.79	.00	.00	1.78	.96
DIOPSIDE	18.53	18.67	25.93	26.09	14.43	14.56	24.32	24.56
HYPERSTHENE	20.47	22.42	.00	.00	22.89	25.20	.00	.00
OLIVINE	4.33	1.53	11.19	9.60	5.92	2.64	14.17	12.19
FE3O4	2.65	2.68	2.29	2.33	2.60	2.64	2.72	2.77
ILMENITE	1.28	1.29	1.53	1.55	1.56	1.58	1.64	1.67
APATITE	.24	.24	.07	.07	.19	.19	.14	.15
FES	.00	.00	.19	.19	.19	.19	.41	.42
CALCITE	.00	.00	1.54	1.56	1.10	1.12	.80	.81

C.I.P.W. NORMS, WEIGHT PERCENTAGES.

	69-1396		69-790		69-937		69-1354	
QUARTZ	* .00	.00	** 5.30	.00	* .00	.00	* 4.33	6.38
ORTHOCLASE	2.07	2.12	3.69	22.85	7.36	7.51	2.83	2.89
ALBITE	15.70	16.02	24.75	21.48	26.30	28.27	25.23	25.82
ANORTHITE	31.70	32.36	25.59	16.12	19.76	20.16	27.74	28.38
NEPHELINE	.00	.00	.00	1.34	.77	.00	.00	.00
DIOPSIDE	18.37	18.60	14.40	21.89	24.82	25.10	7.73	7.83
HYPERSTHENE	20.46	23.67	20.42	.00	.00	.59	24.07	20.46
OLIVINE	5.04	.44	.00	11.83	14.85	12.11	.00	.00
FE3O4	3.00	3.06	2.56	2.31	3.06	3.12	2.95	3.02
ILMENITE	2.19	2.24	2.33	2.26	2.41	2.45	2.71	2.77
APATITE	.24	.24	.39	.38	.38	.39	1.11	1.14
FES	.45	.46	.23	.23	.04	.04	.45	.46
CALCITE	.78	.79	.33	.32	.25	.26	.84	.86

C.I.P.W. NORMS, WEIGHT PERCENTAGES.

	69-1175		69-748		69-1397		69-1501	
QUARTZ	* .00	.00	* 2.11	5.31	* .35	3.43	* .00	.00
ORTHOCLASE	6.38	6.53	7.94	8.22	5.26	5.45	5.61	5.69
ALBITE	17.93	18.35	20.87	21.60	20.13	20.87	18.32	19.87
ANORTHITE	30.91	31.63	20.39	21.10	24.52	25.42	25.95	26.32
NEPHELINE	.00	.00	.00	.00	.00	.00	3.60	2.74
DIOPSIDE	13.12	13.30	16.17	16.51	14.79	15.09	24.42	24.63
HYPERSTHENE	13.60	17.29	21.96	16.54	23.83	18.21	.00	.00
OLIVINE	11.04	5.71	.00	.00	.00	.00	15.39	13.75
FE3O4	3.41	3.49	3.97	4.11	3.65	3.79	2.63	2.66
ILMENITE	3.05	3.12	4.36	4.51	4.82	5.00	1.37	1.39
APATITE	.57	.59	.76	.79	.92	.96	.12	.12
FES	.00	.00	.53	.54	.64	.66	.13	.13
CALCITE	.00	.00	.75	.78	1.09	1.13	.58	.59

C.I.P.W. NORMS, WEIGHT PERCENTAGES.

	69-775		69-782		69-794		69-739	
QUARTZ	* .00	.00	** 10.77	5.66	** .00	.00	* .00	.00
ORTHOCLASE	6.77	6.87	3.66	15.52	3.70	18.81	2.88	2.91
ALBITE	23.82	25.58	25.68	25.12	20.57	10.18	8.23	8.32
ANORTHITE	22.88	23.23	23.11	10.44	23.09	15.08	16.85	17.03
NEPHELINE	2.33	1.61	.00	.00	.00	5.38	.00	.00
DIOPSIDE	25.74	25.95	9.82	14.45	19.28	25.02	11.71	11.80
HYPERSTHENE	.00	.00	20.25	14.03	17.11	.00	23.94	25.65
OLIVINE	13.47	11.69	.00	.00	3.48	13.36	32.64	30.49
FE3O4	2.62	2.66	2.83	4.77	4.21	4.17	2.64	2.67
ILMENITE	1.79	1.82	2.49	2.44	7.17	4.89	.92	.93
APATITE	.26	.27	.76	.74	1.14	1.11	.19	.19
FES	.04	.04	.08	.08	.04	.04	.00	.00
CALCITE	.28	.28	.56	.55	.21	.21	.00	.00

C.I.P.W. NORMS, WEIGHT PERCENTAGES.

	69-756		69-786		69-785		69-1352	
QUARTZ	* .11	1.44	* 1.02	2.13	* 2.42	3.53	** .00	.00
ORTHOCLASE	.35	.36	4.11	4.16	4.02	4.07	3.65	10.78
ALBITE	3.20	3.26	10.38	10.51	9.97	10.10	8.45	8.34
ANORTHITE	5.93	6.02	8.70	8.81	9.19	9.31	15.93	10.17
DIOPSIDE	42.20	42.47	18.12	18.30	7.66	7.73	20.53	23.06
HYPERSTHENE	42.10	40.05	52.68	51.03	61.92	60.36	22.60	8.94
OLIVINE	.00	.00	.00	.00	.00	.00	22.27	28.62
FE3O4	2.35	2.39	3.73	3.78	3.70	3.75	4.08	3.57
ILMENITE	.70	.71	.89	.90	.87	.88	3.32	4.27
APATITE	.17	.17	.36	.37	.26	.27	.27	.26
FES	1.19	1.21	.00	.00	.00	.00	.00	.00
CALCITE	1.70	1.73	.00	.00	.00	.00	.00	.00

	69-788	
ORTHOCLASE	** 3.71	18.29
ALBITE	4.87	4.76
ANORTHITE	12.77	4.66
DIOPSIDE	17.01	21.15
HYPERSTHENE	35.98	14.81
OLIVINE	13.37	21.77
FE3O4	4.25	3.69
ILMENITE	4.41	4.31
APATITE	.72	.70
FES	.82	.80
CALCITE	2.09	2.05

APPENDIX C.8

C.I.P.W. NORMS OF ACID GNEISSES

	69-1367	69-787	69-951	69-1363	69-948	69-944	69-942	69-1355	69-1348
		C.I.P.W. NORMS. WEIGHT PERCENTAGES.							
QUARTZ	23.54	26.51	29.47	35.95	36.91	31.70	30.54	27.61	31.37
CORUND	1.22	.34	.33	.55	9.15	5.78	7.97	1.30	2.91
O-CLAS	8.12	7.62	11.10	14.79	10.86	16.25	37.96	20.60	15.28
ALBITE	39.06	38.66	32.48	30.50	14.95	20.55	14.86	26.87	29.54
ANORTH	18.53	17.60	17.46	13.21	3.64	6.81	.60	10.01	7.74
HYPERS	7.27	5.55	5.95	2.32	21.69	15.60	5.71	10.38	11.80
FE304	.20	2.33	1.67	1.55	.10	.71	.71	1.05	0.31
ILMENI	.86	.78	.82	.55	.63	1.03	1.14	1.08	0.78
APATIT	.12	.31	.43	.17	.10	.07	.31	.59	0.10
FES	.15	.04	.04	.00	.79	.56	.04	.11	0.04
CALCIT	.94	.25	.27	.41	1.17	.94	.16	.39	0.14

	69-746	69-1381	69-938	69-1378	69-789	69-1372	69-954	69-956	69-1375
		C.I.P.W. NORMS. WEIGHT PERCENTAGES.							
QUARTZ	25.45	30.74	29.40	34.54	19.39	21.01	21.25	21.45	27.86
CORUND	.00	.00	.00	.32	.00	.00	.00	.00	2.94
O-CLAS	24.35	24.53	27.36	23.51	25.52	26.24	26.74	26.79	22.23
ALBITE	25.35	21.55	23.00	25.46	24.64	24.91	24.60	24.93	24.25
ANORTH	11.74	10.21	8.81	8.34	16.52	14.35	14.64	14.23	8.46
DIOPSI	1.72	1.31	1.99	.00	.37	.80	.04	.24	0.0
HYPERS	6.25	6.76	5.19	4.72	8.90	8.45	8.12	8.36	12.20
FE304	3.13	2.56	2.26	1.61	1.92	1.76	1.97	1.55	6.03
ILMENI	1.30	1.35	1.20	.93	1.67	1.62	1.61	1.54	1.38
APATIT	.40	.50	.45	.26	.59	.57	.69	.57	0.21
FES	.08	.15	.08	.04	.11	.11	.07	.07	0.15
CALCIT	.23	.34	.25	.27	.36	.18	.25	.27	0.30

APPENDIX D

REE DATA

REE are normalised to chondritic abundances and North American composite shale abundances (table D). The chondritic abundances used produced the smoothest REE patterns.

"Complete" REE patterns (La, Ce, Pr, Nd, Sm, Eu, Gd, Tb, Dy, Ho, Er and Yb) and "partial" REE patterns (La, Ce, Pr, Nd and Y) were determined. Y is plotted beyond Lu in some of the more fractionated "complete" REE patterns, and closely follows Ho values (figures 3.11 and 3.12). This is consistent with recent determinations of ionic radii of the REE (Whittaker and Muntus, 1970): Y^{3+} and Ho^{3+} have identical sixfold co-ordination ionic radii of 0.98Å, while those adjacent to Ho have slightly different radii (Dy^{3+} 0.99Å; Er^{3+} 0.97Å). Accordingly, Y is plotted at the Ho position for partial REE patterns.

Most comparative REE studies use chondrite-normalised or shale-normalised REE plots, and REE fractionation is considered relative to chondritic or sedimentary abundances. Therefore, it is logical to use chondrite-normalised or shale-normalised La/Yb ratios (instead of ppm La/ppm Yb ratios) as an index of fractionation. This procedure has been adopted and is especially useful for indicating divergences from sedimentary REE patterns (shale-normalised La/Yb=1.0). The size of Eu anomalies is usually reported as Eu/Eu*, where Eu* is the value of Eu interpolated between Sm and Gd on a chondrite-normalised REE plot. The Eu/Eu* normally used in the literature is here termed "chondrite-normalised Eu/Eu*". The "shale-normalised Eu/Eu*" is also used.

TABLE D

	CHONDRITE		NORTH AMERICAN SHALE
	(1)	(2)	(3)
La	0.325	--	39
Ce	0.798	--	76
Pr	--	0.12	10.3
Nd	0.567	--	37
Sm	0.186	--	7.0
Eu	0.0692	--	2.0
Gd	0.255	--	6.1
Tb	--	0.049	1.30
Dy	0.305	--	--
Ho	--	0.073	1.40
Er	--	--	4.0
Tm	--	0.033	0.58
Yb	0.231	--	3.4
Lu	0.0349	--	0.6
Y	--	1.8	35

(1) Hubbard & Wiesman, 1971: pers. comm. to S.R. Taylor, A.N.U.

(2) & (3) Haskin et al., 1966

APPENDIX E

THE ORIGIN OF PRECAMBRIAN GRAPHITE

Thermodynamic restrictions preclude the reduction of carbonates to carbon. In addition, the reduction of carbon dioxide to carbon can only occur in very special circumstances in the presence of metallic iron or atomic hydrogen (Rankama, 1963; Schwarcz, 1969). Therefore, it is highly unlikely that the graphite commonly occurring in Precambrian rocks is of metamorphic origin.

$^{12}C/^{13}C$ isotopic ratios together with strong evidence for one fossil (Corycium enigmaticum) in Precambrian graphite were used to conclude biogenic origin (Rankama, 1963). The use of isotope ratios was criticised on the grounds that isotopic fractionation during metamorphic decarbonation reactions may produce organic $^{12}C/^{13}C$ ratios (Rankama, 1963; Schwarcz, 1969). However, $^{12}C/^{13}C$ ratios in Precambrian graphites consistently fall within the modern biogenic range, and available data show no significant changes in the isotopic composition of biogenic carbon since early Palaeozoic. This strongly suggests a biogenic (and hence sedimentary) origin for Precambrian graphite.

If the graphite is not biogenic, the only possible source remaining is from igneous rocks. The amount of graphite in igneous rocks is quite small and concentration by sedimentary processes is required to explain the amount observed in Precambrian rocks.

The available evidence strongly favours a sedimentary origin for Precambrian graphite, and the presence of graphite in Eyre Peninsula rocks may be used as evidence for a sedimentary origin.

APPENDIX F

CORRELATION MATRIX FOR THE BASIC ROCKS

The correlation coefficient matrix for all Eyre Peninsula basic rocks (on a loss-free basis) is given in table F. Throughout this section "correlates with" will be taken to mean "significant positive correlation" (above 99.5% confidence level). Ba, La, Ce, Y, Sc, V, Co, Zr, Nb, Th, Pb, P and Ti are significantly mutually correlated. P_2O_5 correlates with La and Ce but not significantly with Y indicating the inclusion of light REE in apatite. La, Ce and Y show highly significant mutual correlations emphasising the general coherence of REE+Y group. La, Ce and Y also correlate highly significantly with Zr, Nb and Th (all three of which also show significant mutual correlations) indicating the incorporation of REE, Y, Zr, Nb and Th in zircon. (Note that Zr correlates more significantly with Y (= heavy REE) than La and Ce (= light REE) reflecting the enrichment in zircon of heavy REE.) Pb correlation with La and Ce could be explained by entry of Pb into apatite; but Pb correlates even more significantly with Y which has much less tendency to enter apatite than La and Ce. Hence the entry of Pb into apatite seems unlikely. Pb correlation with Zr, Th, La, Ce and Y (Y > La, Ce) could be explained by incorporation in zircon, but Pb^{2+} (1.20Å) entry into zircon (Zr^{4+}: 0.8Å) is highly unfavourable on crystal chemical grounds. It is impossible to explain the correlation of Pb with La, Ce, Y, Th, Zr other than by parallel enrichment or depletion during magma genesis or fractionation. Pb, Y, Zr and Th correlation with Na_2O can be explained in the same manner. The correlations between TiO_2, Fe_2O_3, FeO and V indicates incorporation in magnetite/ilmenite opaques. The mutual correlation exhibited by the group Zr, Nb, La, Ce, Y, Ti, P, Ba and Pb together with K can be explained as variation of "incompatible" element content either due to magma source abundance or percent melting at the source. The negative correlation of Ti with Si may be due to a similar effect, or may be due to early opaque precipitation resulting in

APPENDIX F

CORRELATION COEFFICIENT MATRIX

FOR BASIC ROCKS

99.9% confidence level = 0.57

99.5% confidence level = 0.45

	SiO_2	TiO_2	Al_2O_3	Fe_2O_3	FeO	MnO	MgO	CaO	Na_2O	K_2O	P_2O_5	S	Rb	Ba	Sr	Pb	La	Ce	Y	Sc	V	Cr	Co	Ni	Cu	Zn	Zr	Nb	Th	Ga
SiO_2																														
TiO_2	-0.536																													
Al_2O_3	0.043	0.56																												
Fe_2O_3	-0.374	0.548	-0.031																											
FeO	-0.268	0.555	-0.408	0.030																										
MnO	-0.112	0.371	-0.449	0.439	0.643																									
MgO	-0.145	-0.336	-0.858	-0.144	0.163	0.209																								
CaO	-0.183	-0.080	0.409	-0.084	-0.407	-0.360	-0.368																							
Na_2O	0.256	-0.112	0.722	-0.106	-0.496	-0.487	-0.689	0.205																						
K_2O	-0.140	0.355	-0.056	0.170	0.008	-0.199	-0.122	-0.294	0.207																					
P_2O_5	-0.173	0.511	0.160	0.044	0.453	0.132	-0.277	-0.158	-0.064	0.085																				
S	-0.001	0.098	-0.278	0.211	0.134	0.396	0.132	0.241	-0.348	-0.339	-0.061																			
Rb	-0.041	0.297	-0.085	0.078	0.045	-0.139	-0.096	-0.293	0.108	0.931	0.081	-0.225																		
Ba	-0.206	0.480	-0.225	0.263	0.245	0.036	0.006	-0.397	-0.058	0.839	0.246	-0.124	0.740																	
Sr	0.104	-0.105	0.369	-0.105	-0.293	-0.315	-0.331	0.079	0.583	0.319	-0.075	-0.111	0.194	0.237																
Pb	0.016	0.277	0.303	0.021	-0.103	-0.291	-0.417	-0.140	0.586	0.641	0.133	-0.363	0.508	0.448	0.357															
La	-0.078	0.334	0.298	0.033	0.052	0.036	-0.314	-0.214	0.348	0.244	0.451	-0.170	0.207	0.211	0.053	0.609														
Ce	-0.054	0.321	0.283	0.017	0.055	0.050	-0.299	-0.198	0.295	0.203	0.470	-0.128	0.172	0.190	0.032	0.565	0.993													
Y	0.058	0.330	0.405	0.091	-0.068	-0.032	-0.467	-0.143	0.521	0.238	0.267	-0.207	0.189	0.140	0.130	0.691	0.932	0.884												
Sc	0.113	0.024	0.001	0.187	-0.030	0.093	-0.166	0.506	-0.215	-0.368	0.047	0.257	-0.298	-0.354	-0.295	-0.391	-0.487	-0.483	-0.401											
V	-0.286	0.589	0.282	0.422	0.213	0.176	-0.486	0.443	-0.013	-0.105	0.230	0.266	-0.106	-0.115	0.016	-0.165	-0.201	-0.207	-0.112	0.565										
Cr	-0.102	-0.365	-0.702	-0.177	-0.027	0.015	0.928	-0.368	-0.530	-0.102	-0.258	0.046	-0.068	-0.010	-0.260	-0.345	-0.215	-0.214	-0.333	-0.239	-0.498									
Co	-0.202	-0.323	-0.734	0.015	0.112	0.233	0.835	-0.356	-0.577	-0.078	-0.376	-0.044	-0.102	0.056	-0.243	-0.415	-0.453	-0.461	-0.571	-0.102	-0.440	0.795								
Ni	-0.343	-0.131	-0.703	0.077	0.189	0.224	0.881	-0.555	-0.550	0.097	-0.200	-0.053	0.043	0.216	-0.165	-0.250	-0.140	-0.148	-0.322	-0.405	-0.451	0.842	0.872							
Cu	-0.075	0.185	-0.191	0.210	0.197	0.212	0.050	-0.014	-0.203	0.156	-0.016	0.570	0.201	0.347	0.368	-0.158	-0.132	-0.117	-0.182	-0.113	0.205	0.011	-0.001	0.082						
Zn	-0.002	0.445	-0.306	0.168	0.639	0.586	0.039	-0.597	-0.208	0.274	0.323	-0.160	0.306	0.399	-0.324	0.224	0.328	0.311	0.275	-0.163	-0.067	-0.065	0.017	0.106	-0.142					
Zr	0.114	0.144	0.332	0.068	-0.159	0.021	-0.318	-0.230	0.504	0.184	0.102	-0.162	0.109	0.129	0.245	0.609	0.874	0.863	0.926	0.576	-0.303	-0.200	-0.391	-0.139	-0.078	0.168				
Nb	-0.430	0.630	-0.083	0.495	0.292	0.323	-0.044	-0.359	-0.063	0.471	0.304	-0.055	0.324	0.583	0.054	0.408	0.609	0.609	0.502	-0.460	-0.033	-0.107	-0.022	0.266	0.173	0.379	0.545			
Th	0.217	-0.015	0.382	-0.022	-0.327	-0.150	-0.323	-0.183	0.568	0.221	0.019	-0.222	0.150	0.118	0.306	0.609	0.822	0.812	0.873	-0.588	-0.376	-0.170	-0.393	-0.157	-0.063	0.044	0.969	0.432		
Ga	-0.149	0.302	0.531	0.165	-0.130	-0.066	-0.564	0.340	0.344	0.090	0.247	-0.175	0.063	0.092	0.231	0.162	0.116	0.085	0.093	0.375	0.561	-0.470	-0.437	-0.446	-0.159	0.089	-0.020	-0.165	-0.018	

depletion of Ti in later Si - richer differentiates. K correlates highly significantly with Rb, Ba and slightly less significantly with Pb; Rb, Ba, Pb show significant mutual correlation. The coherence of the group indicates concentration in mantle melts during magma genesis or concentration in melts during fractionation. Enhanced correlation may have resulted from coherent alteration of K, Rb and Ba during metamorphism. Mg correlates highly significantly with Cr, Co and Ni (which show mutual correlation) indicating concentration of these elements in the more pyroxene and/or olivine-rich pyroxenites or picritic basalts. The significant negative correlations of Al with Mg, Cr, Co, Ni, Fe and Mn is due to fractionation of these elements in low-Al phases (pyroxenes and olivines) during magma genesis or magma differentiation. Na is concentrated in the melt with Al and crystallised almost entirely as plagioclase resulting in significant positive Na-Al correlation. The correlation between Ca and Al is much lower because Ca occurs in clinopyroxene in addition to plagioclase. Copper correlates only with sulphur, apparently indicating occurrence of copper as sulphides. However, copper sulphides are of minor importance and pyrrhotite is the main sulphide phase. The correlation is explained by the parallel enrichment of copper and sulphur observed during fractionation of tholeiites.